LOYOLA UNIVERSITY CHICAGO 1870 AD MAJOREM DEI GLORIAM
eCOMMONS

Loyola University Chicago
Loyola eCommons

Dissertations | Theses and Dissertations

2011

Molecular Expression of Neuroprotective and Neurodestructive Signaling Systems Following Axotomy-Induced Target Disconnection: Relevance to ALS

Melissa Marie Haulcomb
Loyola University Chicago

Recommended Citation

Haulcomb, Melissa Marie, "Molecular Expression of Neuroprotective and Neurodestructive Signaling Systems Following Axotomy-Induced Target Disconnection: Relevance to ALS" (2011). *Dissertations*. Paper 17.
http://ecommons.luc.edu/luc_diss/17

This Dissertation is brought to you for free and open access by the Theses and Dissertations at Loyola eCommons. It has been accepted for inclusion in Dissertations by an authorized administrator of Loyola eCommons. For more information, please contact ecommons@luc.edu.

This work is licensed under a Creative Commons Attribution-Noncommercial-No Derivative Works 3.0 License.
Copyright © 2011 Melissa Marie Haulcomb

LOYOLA UNIVERSITY CHICAGO

MOLECULAR EXPRESSION OF NEUROPROTECTIVE AND NEURODESTRUCTIVE SIGNALING SYSTEMS FOLLOWING AXOTOMY-INDUCED TARGET DISCONNECTION: RELEVANCE TO ALS

A DISSERTATION SUBMITTED TO

THE FACULTY OF THE GRADUATE SCHOOL

IN CANDIDACY FOR THE DEGREE OF

DOCTOR OF PHILOSOPHY

NEUROSCIENCE PROGRAM

BY

MELISSA MARIE HAULCOMB

CHICAGO, IL

DECEMBER 2011

Copyright by Melissa Marie Haulcomb, 2011
All rights reserved.

ACKNOWLEDGEMENTS

I want to express my appreciation and gratitude for all the individuals who have assisted me throughout my graduate education. First, I would like to sincerely thank my advisor, Dr. Kathryn J. Jones, for her mentorship and guidance during my training as a scientist. Dr. Jones is a distinguished neuroimmunologist and she has inspired me to pursue my goal of being a career neuroscientist. I will continue to strive to achieve the level of dedication she has to advancing medical research. The time spent in her laboratory during my graduate student years taught me many things, but, one of the most important aspects I will take away from my three years experience is the ability to critically analyze data and interpret the results into conclusions. I also would like to thank Dr. Virginia M. Sanders for her mentorship and valuable insights as an immunologist. Additionally, I wish to express appreciation to my dissertation committee members Drs. Edward J. Neafsey, Lydia L. DonCarlos, and Evan Stubbs, Jr. for their dedication to assisting me with my project from beginning to end. I am thankful for the many hours spent discussing my work, their critical review of the data and conclusions as well as their invaluable knowledge that has helped shaped my dissertation work into what it is today. I would also specifically like to thank someone whom I consider an honorary committee member, Dr. Nichole A. Mesnard. Nichole was a senior graduate student when I joined the lab in 2008, and has been like a co-mentor to me. As my

project has stemmed from her dissertation work; she has assisted me not only with the project development but also with instruction on crucial laboratory techniques. She additionally played a major role in interpretation of the results. I would also like to thank many members of the Jones lab, past and present, for their technical and moral support throughout this process. The lab members I would like to thank are thus follows: Drs. Todd Brown, Junpin Xin, Derek Wainwright, Eileen Foecking, Keith Fargo, Gina Monaco, as well as Tom Alexander, Linda Poggensee, Lisa Tanzer, Christine Politis, and Richard Batka. I would also like to thank all of the staff, students and faculty of the Biomedical Sciences Graduate Programs who have assisted me throughout my student years at Loyola University Chicago.

Lastly, I would like to express my appreciation and gratitude for my family. I would like to thank my mother and father for all of their support throughout my undergraduate and graduate student years. I credit both of my parents with providing me with the skills and the drive to succeed in life and I thank them for stressing importance of education and hard work. I would like to express gratitude to my mother who passed on to me her passion for the medical sciences, although our cell-specific fascination differs greatly, neurons vs. pathogenic bacteria. We have shared a particularly close relationship throughout my adult life that I am truly grateful for. I would like to thank my father for all his support during my student years and recently for the memorable, family times which have helped to balance the demands of graduate

student life. While my father does not have a strong biology background, his engineering and business background provided him with the ability to understand the majority of my dissertation project. I would like to convey my gratitude for all of his help during the editing stage of this dissertation and for providing voluble feedback based on his unique, non-neuroscience perspective. Last but not least, I would like to thank my wonderful husband, Brandon, for standing by me throughout my graduate student years. I wish to express immense appreciation for the sacrifices endured in order to put my education first during the last few years which has allowed me to achieve necessary requirements for my chosen career. I could not ask for a more supportive friend and partner during some of the most challenging times of my life thus far. I credit Brandon with giving me strength, confidence, and help during graduate school. I am truly grateful to have such a wonderful family.

To my parents, Thomas and Debra Quaka
To my husband, Brandon Haulcomb

TABLE OF CONTENTS

LIST OF TABLES

LIST OF FIGURES

LIST OF ABBREVIATIONS

α-MN	alpha motoneuron(s)
AC	adenylyl cyclase
Ach	acetylcholine
ADAM10	disintegrin and malloproteinase domain-containing protein 10
ALS	amyotrophic lateral sclerosis
ANS	autonomic nervous system
ANOVA	analysis of variance
ASK1	apoptosis signal-regulating kinase 1
ATP	adenosine triphosphate
Ax	axotomized, injured facial motor nucleus
BB	balance beam
BBB	blood-brain barrier
BLAST	basic local alignment search tool
C	control, uninjured facial motor nucleus
cAMP	cyclic adenosine monophosphate
Caspase-3	cysteine-dependent aspartate-directed protease 3
Caspase-8	cysteine-dependent aspartate-directed protease 8
CD68	cluster of differentiation 68

cDNA	complementary deoxyribonucleic acid
ChAT	choline acetyltranferase
CNS	central nervous system
CRMP4	collapsin response mediator protein 4
C_T	threshold cycle
CX3CL1	fractalkine
CX3CR1	fractalkine receptor
DA	dorsal accessory
Daxx	death associated protein-6
DEPC	diethylprocarbonate
DI	deionized
DI	dorsal intermediate
DISC	death-inducing signaling complex
DL	dorsolateral
DM	dorsomedial
DNA	deoxyribonucleic acid
DNase	deoxyribonuclease
Doa	days of age
Dpo	days post-operative

EMG	electromyography
ER	extension reflex
ERK 1/2	extracellular signal-related kinase 1/2
Etk-1	endothelial/epithelial tyrosine kinase-1
ETOH	ethanol
FADD	fas-associated death domain
fALS	familial amyotrophic lateral sclerosis
Fas	fas receptor
FasL	fas ligand
FMN	facial motoneuron(s)
FPG	fast disease progression group
GAPDH	glyceraldehydes-3-phosphate dehydrogenase
GAP-43	growth-associated protein of 43 kilodaltons
GFAP	glial fibrillary associated protein
GPCR	g-protein-coupled receptor
HAc	glacial acetic acid
IACUC	institutional animal care and use committee
INF-γ	interferon-gamma
IL-1	Interleukin-1
IL-1β	interleukin-1 beta
IL-6	interleukin-6

iNOS	inducible nitric oxide synthase
kDa	kilodalton
KO	knock-out
LMD	laser microdissection
MAPK	mitogen-activated protein kinase
MG	medial gastrocnemius
MM	molecular marker
MN	motoneuron(s)
mRNA	messenger ribonucleic acid
NaAc	sodium acetate
NeuN	neuronal nuclei marker
NCBI	national center for biotechnology information
NMJ	neuromuscular junction(s)
nNOS	neuronal nitric oxide synthase
NO	nitric oxide
OF-CRB	open field complete rearing behavior
OF-EB	open field exploratory behavior
OF-GA	open field gait analysis
OF-TE	open field tail elevation
PAC1-R	pituitary adenylate cyclase-activating polypeptide receptor 1
PACAP	pituitary adenylate cyclase-activating polypeptide

PBS	phosphate buffered saline
PCR	polymerase chain reaction
PEN	polyethylene
PFA	paraformaldehyde
PGE	paw-trip endurance
PKA	protein kinase A
PKB	protein kinase B
PNS	peripheral nervous system
RAG-2 KO	recombinase-activating gene-2 knock out
RDLN	retrodorsal lateral nucleus
RFU	relative fluorescent units
RIP1	receptor interacting protein-1
RNA	ribonucleic acid
ROS	reactive oxygen species
RT-PCR	reverse-transcription polymerase chain reaction
sALS	sporadic amyotrophic lateral sclerosis
Scid	severe combined immunodeficient
SPG	slow disease progression group
SEM	standard error of the mean
shRNA	short hairpin ribonucleic acid
siRNA	small interfering ribonucleic acid

SOD1	Cu/Zn superoxide dismutase 1
SOD1	$SOD1^{G93A}$ transgenic mouse/mice
SODD	silencer of death domains
solTNFα	soluble tumor necrosis factor alpha
SMF	stylomastoid foramen
T_A	annealing temperature
TA	tibialis anterior
TACE	tumor necrosis factor alpha converting enzyme
TBE	tris borate ethylenediaminetetraacetic acid
T_m	melting temperature
tmTNFα	transmembrane tumor necrosis factor alpha
TNFα	tumor necrosis factor alpha
TNFR1	tumor necrosis factor receptor 1
TNFR2	tumor necrosis factor receptor 2
TRADD	tumor necrosis factor receptor 1-associated death domain
UV	ultraviolet
VI	ventral intermediate
VL	ventrolateral
VM	ventromedial
WT	wild-type mouse/mice

CHAPTER I

INTRODUCTION

Amyotrophic Lateral Sclerosis (ALS) is the most common adult motoneuron (MN) degenerative disease. The disease is fatal within approximately 3-5 years after clinical onset. Discovery of a small portion of familial cases with a mutation in the gene that encodes for Cu/Zn superoxide dismutase 1 (SOD1) led to the development of a transgenic mouse model for the disease in 1994 (Gurney et al., 1994). Pre-symptomatic SOD1 mice appear normal and show no clinical symptoms well into adulthood, however once symptom onset has occurred they display many of the pathological hallmarks of ALS patients (Chiu et al., 1995). It has been well-documented that the initial pathological event during the SOD1 pre-symptomatic stage is loss of neuromuscular junctions (NMJ), axonal retraction and compensatory sprouting in the lower limbs (Fischer et al., 2004; Schaefer et al., 2005). These findings and others has led to development of the die-back theory of ALS, where disconnection from target and the inability to maintain target connection leads to MN degeneration (Dadon-Nachum et al., 2011).

The facial nerve injury model has proven to be a valuable tool used in our laboratory as well as others, to investigate the mechanisms of MN survival and degeneration in wild-type (WT) and immunodeficient mice. Recently, we have utilized this injury model to investigate the mechanisms of MN survival in the pre-symptomatic

SOD1 mouse. Our lab has shown that following a facial nerve axotomy, pre-symptomatic SOD1 mice display enhanced facial MN (FMN) cell loss in the facial motor nucleus, compared to WT mice. The inability to retain WT FMN survival levels suggests that the mechanisms involved in MN degeneration are already present at the pre-symptomatic stage. Expression of MN regenerative genes as well as genes specific to the neuropil were previously analyzed following axotomy in both WT and pre-symptomatic SOD1 mice. Surprisingly, MN regenerative genes were expressed to a similar extent in SOD1 MN with respect to WT. Differences were seen among genes expressed by the neuropil, namely glial fibrillary acidic protein (GFAP), specific to the astrocytic response, and constitutive expression of tumor necrosis factor-α (TNFα; Mesnard et al., 2011). These results suggest that the SOD1 MN within the pre-symptomatic stage are capable of a "WT-like" molecular response to target disconnection, including upregulation of survival and regenerative genes. However, different molecular responses related to the neuropil and the presence of a pro-inflammatory microenvironment may explain the enhanced FMN cell loss following axotomy.

The strengths of the facial nerve axotomy model have allowed us to begin initial investigation of dysregulation within the glial response, to identify mechanisms mediating MN degeneration and to determine potential factors involved in mediating neuroprotection. Experiments within this dissertation evaluated whether the axotomy-

induced molecular response in pre-symptomatic SOD1 mice, resembles the disease-induced molecular response within the facial nucleus in symptomatic SOD1 mice.

A. Central Hypothesis

The central hypothesis of the research presented in this dissertation is that the molecular response to axotomy in the pre-symptomatic SOD1 is similar to the molecular response to disease. To determine whether this central hypothesis can be supported, the research presented in this dissertation established four specific aims.

B. Specific Aim 1: Survival and Molecular Responses to Facial Nerve Axotomy

Aim #1 of this dissertation was to analyze the expression of genes involved in neuroprotective and neurodegenerative signaling systems as well as genes specific to the glial response, following a facial nerve axotomy in WT and pre-symptomatic SOD1 mice. The working hypothesis for this aim was that molecular expression within the axotomized SOD1 facial motor nuclei will display enhanced mRNA levels, compared to WT, for death receptor signaling systems and other genes that have been shown to be present within the CNS of ALS patients and symptomatic or end-stage SOD1 mice. Experiments performed specifically investigated the molecular changes induced by axotomy within the facial motor nucleus of WT and SOD1 mice for neurodegenerative genes of death receptor signal transduction and signaling systems involved neuroprotection and genes specific to the glial cell responses to CNS injury. Similarities and differences in the expression between WT and SOD1 axotomized facial nuclei help

to elucidate mechanisms involved in the enhanced FMN cell death after axotomy in the pre-symptomatic SOD1 mouse.

C. Specific Aim 2: Survival and Molecular Responses to Disease Progression

Aim #2 of this dissertation was to determine whether molecular response to axotomy within the pre-symptomatic SOD1 facial motor nucleus resemble the disease-induced molecular response within the facial motor nucleus. The working hypothesis for this aim was that the molecular response following facial nerve axotomy in pre-symptomatic SOD1 mice resembles the molecular response of disease progression and subsequent MN degeneration within the symptomatic SOD1 facial motor nucleus. It has been well established in the SOD1 mouse model that neuronal target disconnection precedes MN cell death in the spinal cord and brainstem during disease progression. The experiments in Aim2 examined the effects of disease on FMN survival and mRNA expression of glial-specific genes and genes involved in neuroprotective and neurodegenerative signaling systems within the neurodegenerating, disease-affected facial motor nucleus.

D. Specific Aim 3: Two Rates of Symptom Progression in SOD1 Mice

Aim #3 of this dissertation was to confirm that a group of symptomatic SOD1 mice displaying a faster rate of symptom progression also demonstrate a faster rate of disease progression within the facial motor nucleus. The working hypothesis for this aim was that the variability seen among motor scores during behavioral assessment is a

result of two different rates of symptom progression which correlates with evidence of increased disease progression rate within the SOD1 facial motor nucleus. Dramatic differences among severity of symptoms were apparent during behavioral assessment of motor function following symptom onset. The experiments analyzed FMN survival levels as well as differences in expression of genes involved in the response to target disconnection (axotomy/disease) between the two symptomatic groups.

E. Specific Aim 4: Molecular Expression in Facial Motor Subnuclei

Aim #4 of this dissertation was to analyze the axotomy-induced molecular expression of neuroprotective and neurodestructive signaling systems within the regenerative and degenerative subnuclei of the facial motor nucleus. The working hypothesis for this aim was that the regenerative, ventromedial (VM) subnucleus of the facial motor nucleus will display attenuated molecular expression of genes related to neurodegenerative signaling systems compared to the degenerative, ventrolateral (VL) subnucleus in both WT and SOD1 mice following axotomy. The experiments investigated differences between axotomy-induced mRNA expression within the WT VM and VL subnuclei, and separately, within the SOD1 VM and VL subnuclei. The purpose of these experiments was to provide additional information regarding axotomy-induced molecular responses of genes involved in neuroprotective and neurodestructive signaling systems among facial nuclei populations with inherent degenerative and regenerative characteristics.

The research presented within this dissertation addressed to the four aims stated above. The results support the conclusion that molecular response within the SOD1 facial nucleus is similar regardless of the method of MN injury (axotomy/disease) and therefore, allows for axotomy to be used in the pre-symptomatic mouse as a model of disease progression.

CHAPTER II

LITERATURE REVIEW

A. The Nervous System: A General Overview

The human brain, known as the organ of the mind, is the most complex tissue in the body. It is made up of cells called neurons which are specialized for sending and receiving signals (**Figure 1**). Four distinct parts make up the neuron: the cell body, the dendrites, the axon, and the presynaptic axon terminals. The cell body of the neuron, also called the soma or perikaryon, is the portion that surrounds the nucleus and contains many of the cell's organelles and is responsible for most of the neuronal housekeeping functions, including synthesis and protein processing. Dendrites are processes that arise from the cell body like tentacles of varying complexity and are responsible for receiving incoming signals. Portions of the membrane display receptors, proteins capable of binding and transmitting the incoming signals that arrive via proteins or chemical compounds termed neurotransmitters. This message is translated into a biochemical event and may or may not be transmitted as a signal down the third part of the neuron known as the axon. The axon projects away from the cell body and is the message sending portion of the neuron. Biochemical signals that reach a certain threshold are propagated down the axon as an electrical signal known as an action potential, and ultimately reach the fourth part of the neuron the presynaptic axon

terminals. The presynaptic axon terminals result in multiple endings designed for rapid communications and convert the electrical signal back into a biochemical signal. The junction between the presynaptic axon terminal and the target is called the synapse, where neurotransmitters can diffuse across to the adjacent cell and communicate the signals.

Subdivisions of the nervous system are somewhat arbitrary, since all elements of the nervous system work closely together without clear boundaries. However, traditional definitions provide a useful framework for understanding the brain and its connections. The central nervous system (CNS) consists of the brain and spinal cord which are contained within a specific environment that is separate from the rest of the body. The peripheral nervous system (PNS) consists of those parts of the nervous systems that lie outside the CNS, sending and receiving signals to and from the body. Sensory nerves carry messages from the periphery to the CNS and are called afferent nerves or signals. Peripheral motor nerves carry messages from the CNS to the peripheral tissues are termed efferent nerves or signals. Additionally, a third portion of the nervous system regulates and controls visceral functions such as digestion, heart rate, blood pressure, reproductive functions and is known as the autonomic nervous system (ANS). This system is anatomically part of the CNS and PNS, but is functionally distinct.

The human brain contains anywhere between 15-33 billion neurons, depending on age and gender (Pelvig et al., 2008). Neurons can vary greatly in their morphology throughout the nervous system. This dissertation will focus on a specific type of neuron, the motoneuron (MN). Two types of MN carry efferent signals that activate skeletal muscle; upper and lower MN (**Figure 2**). Upper MN originate in the motor cortex of the brain and send their axons, usually bundled together within a tract, down common pathways to synapse on lower MN in the brainstem or the spinal cord. Therefore, upper MN are mainly responsible for generating motor signals to lower MN via the neurotransmitter, glutamate, but do not directly stimulate the target musculature. Lower MN cell bodies reside within distinct anatomical groups referred to as a nucleus (localized within the brainstem) or ganglion (localized within the peripheral nervous system). Alpha MN (α-MN) are a type of lower MN that innervate extrafusal muscle fibers, the most numerous type of muscle fiber and those that are involved in skeletal muscle contraction. α-MN send their axons through the periphery, bundled together as "nerves" and using the neurotransmitter, acetylcholine, send their signals across the neuromuscular junction (NMJ). The NMJ is the space or synapse between the presynaptic terminals of the α-MN and the motor end plate, the highly-excitable region of muscle fiber plasma membrane. The motor end plate contains acetylcholine (ACh) receptors that generate an action potential in the muscle cell which serves as the signal

for muscle contraction once ACh crosses the NMJ and binds to them. A series of complex steps leads to the contraction of skeletal muscle and therefore movement.

While neurons are often considered the main component, they are not the only cells that make up the nervous system. Neuroglial cells, often simply called glia or glial cells, are more numerous than neurons (Pelvig et al., 2008). They are non-neuronal cells which lack axons, action potentials, and synaptic potentials but play important roles and diverse functions within the nervous system. While the Greek word "glia" implies that they are the glue of the nervous system they are much more than that. Glial cells are involved in nearly every function of the brain; they structurally support neurons, insulate axons with myelin, supply nutrients and oxygen, destroy pathogens and remove the debris of dead cells, modulate neurotransmission, etc. The main types of CNS glia are ependymal cells, oligodentrocytes, astrocytes and microglial cells. Within the PNS the main types of glial cells are satellite cells in autonomic and sensory ganglia, enteric glial cells and Schwann cells.

B. Amyotrophic Lateral Sclerosis

Amyotrophic Lateral Sclerosis (ALS), colloquially known as Lou Gehrig's disease, was first described by Jean-Martin Charcot in 1869. ALS refers to a form of MN disease which selectively targets both upper and lower MN. As mentioned previously, upper MN originate in the motor cortex and synapse on MN within brainstem nuclei or the spinal cord ventral horn. These lower MN comprise the majority of the peripheral nervous

system and innervate skeletal muscles to produce voluntary movement. “Amyotrophic” refers to the atrophy of the denervated skeletal muscles and “Lateral Sclerosis” refers to the hardening of the anterior and lateral corticospinal tracts observed during autopsy; a result of degenerating MN and gliosis, a proliferation of astrocytes (Rowland and Shneider, 2001). ALS is the most common MN degenerative disease with a prevalence of 3-5/100,000 (Naganska and Matyja, 2011). Typical age of onset occurs between 55-65 years of age however rare juvenile onset forms of the condition also exist. For reasons not currently known, the disease affects men more commonly than women with a male: female ratio of 1.5:1. ALS progresses rapidly, affecting voluntary muscle movement leading to respiratory failure and other pulmonary complications. Life expectancy after diagnosis is an average of 3-5 years (Wijesekera and Leigh, 2009). In the United States it is estimated that 20,000 people are affected with ALS and 5,000 new cases are diagnosed each year (Naganska and Matyja, 2011). The diagnosis of ALS is substantiated when patents present with signs of both upper and lower MN deficits, further investigation excludes other MN diseases, and the progression is consistent with that of ALS. Symptom onset is gradual and will often go unnoticed or patients attribute the symptoms to benign ailments or conditions. This, in addition to the clinical process of ruling out other MN diseases, neuropathies and neurological conditions, almost always results in a delay of diagnosis (Kraemer et al., 2010). The disease presents clinically as two forms; spinal onset of ALS (classical ‘Charcot ALS’) or bulbar onset ALS. Two thirds of

patients suffer from spinal onset ALS and will notice asymmetrical muscle weakness in the upper or lower limbs often of an insidious nature. Clinical examination will reveal focal muscle atrophy; in the lower limbs this includes proximal thigh and distal foot muscles. The upper limbs display atrophy of the hand musculature, forearms and shoulders. Spasticity and pathologically brisk tendon reflexes will also appear throughout the course of the disease. Patients experiencing bulbar onset ALS will frequently present with dysarthria of speech. Other symptoms include brisk jaw jerk, various facial weakness, fasciculations and atrophy of the tongue. Regardless of the type of onset, those affected with ALS will gradually develop both limb and bulbar symptoms within 1-2 years. Typical ALS cases will not exhibit sensory deficits. However, in non-typical cases, multi-system involvement can occur including dementia and Parkinsonism (Wijesekera and Leigh, 2009).

Treatment options for patients are limited. ALS is considered an incurable disease. More than 7,000 compounds have been suggested for treatment of ALS and approximately 100 reached clinical trials (Cozzolino et al., 2008; http://www.als.net). Riluzole, the active ingredient in Rilutek, was approved by the FDA December 12, 1995 for the treatment ALS (http://www.fda.gov). Riluzole (2-amino-6-(trifluoromethoxy)benzothiazole) has been shown to have neuroprotective and anticonvulsant actions attributed to its ability to reduce the K^+-evoked release of glutamate and aspartate from synaptic terminals (Martin et al., 1993). Riluzole is the

only approved drug for treatment of ALS. It is most effective early in the disease process however; it provides only limited therapeutic benefits of increased survival of 4 months (Traynor et al., 2003).

Although some genetic risk factors have been identified, the cause of ALS is still eludes scientists. Recent studies have attempted to determine environmental risk factors and found only smoking is associated with developing ALS (Sutedja et al., 2007; Kamel et al., 1999). Current theory suggests a complex genetic-environmental interaction leads to development of the disease.

In 1986 it was discovered that a small portion of ALS cases appeared to be inherited in an autosomal dominant fashion (Mulder et al., 1986). These cases are known as inherited familial ALS (fALS) and make up approximately 10% of all ALS cases while in 90% of cases the disease occurs randomly, considered sporadic ALS (sALS). In 1993 a landmark discovery was made identifying 11 missense mutations in the gene encoding for the anti-oxidant enzyme, Cu/Zn superoxide dismutase 1 (SOD1) in 13 fALS families (Rosen et al., 1993). Today 339 mutations related to ALS have been identified and among those more than 150 are mutations within the SOD1 gene. Surprisingly, cases caused by a mutation in the SOD1 gene makes up only 20% of fALS cases or 2% of all ALS cases (http://alsod.iop.kcl.ac.uk). Currently, ten known genes influence the development of ALS (Beleza-Meireles and Al-Chalabi, 2009). During normal biological processes, molecular oxygen acts as a strong oxidant and is capable of extracting

electrons from various molecules resulting in the production of the cytotoxic reactive oxygen radical, superoxide anion (O_2^-). SOD1 is in part responsible for detoxification and subsequent maintenance of intracellular O_2^- concentration in the low femtomolar range by catalyzing the dismutase of O_2^- into hydrogen peroxide (H_2O_2) and molecular oxygen (Martin, 2007). The concentration of SOD1 in brain is approximately 4.5 times higher than in erythrocytes (Kurobe et al., 1990). Upon examination of the mouse spinal cord and brainstem immunoreactivity for SOD1 was much greater in MN than several classes of other neurons. The highest concentration appeared to be localized to the cytoplasm of the perikarya of MN; however SOD1 was also identified in axons, dendrites, and glial cells (Pardo et al., 1995). Later studies have analyzed the intracellular distribution and found that while SOD1 is primarily localized to the cytoplasm. Although, a small portion of the protein can be found within the intermembrane space of the mitochondria as well (Okado-Matsumoto and Fridovich, 2001). SOD1 protein is a soluble metalloenzyme made up of 153 amino acids. The functional enzyme is a 32 kilodalton (kDa) homodimer, covalently linked and bound to one Cu and one Zn ion per subunit (Martin, 2007). While the Zn ion is responsible for stabilizing the structure of the two subunits, the Cu ion carries out the catalysis (Forman and Fridovich, 1973). As many as 7% of sALS cases have mutations that occur within the SOD1 gene (http://alsod.iop.kcl.ac.uk).

C. ALS Mouse Model: SOD1

Several transgenic rodent models have been developed based on mutations in the SOD1 gene. The mouse model that most resembles the pathological features observed in ALS patients is the G93A mouse model. Developed in 1994, the $SOD1^{G93A}$ mouse overexpresses a human, mutant protein with a Gly^{93}→Ala substitution within exon 4 (Gurney et al., 1994). For the reasons that the $SOD1^{G93A}$ mouse was the first ALS rodent model developed and the similarities between disease progression within the mouse and in fALS and sALS patients, the $SOD1^{G93A}$ mouse has been the most widely studied and is the mouse model used throughout this dissertation. From this point on the $SOD1^{G93A}$ transgenic mouse will be referred to as simply SOD1, unless clarification of specific transgenic model is necessary.

While the SOD1 mouse overexpresses the human mutant gene, this overexpression does not have any affects on its endogenous mouse SOD1 gene or the subsequent protein function (Borchelt et al., 1995). The overexpression of the human mutant gene brings about a toxic gain of function. This is supported by studies using SOD1 knock out (KO) mice that live well into adulthood and do not develop motor neuron disease suggesting that the toxicity of this mutation is not due to a reduction in the enzyme's ability to scavenge free radicals (Reaume et al., 1996). Mice that over-express the WT human SOD1 do not develop any symptoms of the disease (Dal Canto and Gurney, 1995; Bruijn et al., 2004). Additionally, analysis of mutant SOD1 enzyme

activity has been performed for all SOD1 transgenic models and variations within enzymatic activity have been found as complete inactivation (Borchelt et al., 1994). Mutant SOD1 enzymes across transgenic SOD1 mice have also varying degrees of stability, which can affect the ability to form stable dimers (Borchelt et al., 1995; Jonsson et al., 2006). The toxic gain of function of mutant SOD1 has not yet been identified.

While there are differences in disease onset and rate of disease progression among the different SOD1 mouse models, all develop MN disease. The pathological phenotype is similar; massive death of MN in the ventral horn and loss of myelinated axons in ventral motor roots ultimately leads to paralysis and muscle atrophy (Cozzolino et al., 2008). SOD1 mice show three distinct phases of disease; pre-symptomatic, symptomatic, and end-stage. These stages have been determined by approximating deficits in motor function and MN cell death within the spinal cord (Chiu et al., 1995). Reports of symptom onset and disease progression of $SOD1^{G93A}$ vary widely within the literature, often a result of different methods of behavioral assessment. Many early studies exhaustively documented the progression of the disease and their findings are typically used as reference. The first symptoms develop at approximately 90 days of age (doa) and consist of a slight tremor of the hind-limbs. This tremor becomes more pronounced, including both hind-limbs and sometimes the forelimbs. Proximal muscle weakness and atrophy begin to develop by 120 doa as evident by shortness of stride.

SOD1 mice reach end-stage disease by 136 doa, marked by severe paralysis. The mice are unable to lift their pelvis, generally do not respond to tapping on the cage, and are unable to groom themselves. MN cell death accompanies the progression of symptoms. At symptomatic stage, 90 doa, the decrease in the number of somatic MN in C7 and L3 segments reaches significance compared to aged-matched controls. The MN death continues into end-stage disease where the MN loss reaches 50% in the ventral horn of spinal cord. Previous studies within the brainstem showed MN in the hypoglossal motor nucleus revealed a trend for MN loss, however significance was not reached by end-stage disease (Chiu et al., 1995). Research has focused on the mechanisms of the MN cell death which may be dysregulated in ALS and the SOD1 mouse model.

D. Target Disconnection Theory of ALS: "Die-back"

One of the leading theories suggests that disease progression and subsequent MN degeneration that occurs the SOD1 mouse model and ALS patients is initiated by an unknown pathological event within the periphery resulting in functional loss of the NMJ. This target disconnection ultimately results in a "die-back" pathophysiology and over time the MN will degenerate. This theory is supported by a variety of studies. As mentioned previously, the first initial pathological event that has been documented within the pre-symptomatic SOD1 mouse is significant denervation (40%) of motor end-plates at 47 doa within the medial gastrocnemius (MG), soleus, and tibialis anterior (TA; Fischer et al., 2004; Durand et al., 2006). Electromyography (EMG) recordings revealed a

loss of motor units within the MG at approximately the same time (Hegedus et al., 2007). Motor nerve conduction tests a MN ability to transmit signals from the spinal cord to the muscle. This evaluates a motor unit, one MN, and the many muscle fibers it innervates via many NMJ. Results determined significant functional loss of TA as evident by the motor nerve conduction test and EMG recordings which revealed a loss of motor units at 56 doa (Mancuso et al., 2011). Also evident at 56 doa is a reduction of muscle mass and muscle fiber diameter within the biceps femoris (Marcuzzo et al., 2011). These results display a pattern of target disconnection within the early pre-symptomatic stage which is observed as loss of NMJ followed by a reduction in muscle mass. Additionally, compensatory sprouting of axons is observed at 60 doa which leads to reinnervation of lost NMJ (Schaefer et al., 2005; Frey et al., 2000). It has been suggested that within the later pre-symptomatic stage, the degree of target disconnection becomes overwhelming which leads to the “die-back” of the MN cell bodies within the spinal cord. By 90 doa, there is a significant reduction of synapse on MN within the lumbar spinal cord, evidence of neurodegeneration (Zang et al., 2005). Then between 90 – 100 doa, many studies report significant loss of MN within the lumbar spinal cord, decreased average body weight, and behavioral tests reveal appearance of motor symptoms (Mancuso et al., 2011; Fischer et al., 2004; Chiu et al., 1995).

E. Cranial Nerve VII: The Facial Nerve

In humans, acute lesions of the facial nerve, or cranial nerve VII, are the most common of the mononeuropathies that affect the cranial nerves. Bell's palsy and trauma are frequent causes of ipsilateral, same side, facial paralysis. This is in part due to its long, boney course through the cranium as well as its superficial location through the face to innervate the muscles of facial expression (Netter, 1987).

The facial motor nucleus, or referred to simply as facial nucleus, is located in the reticular formation of the lower pons where fibers from the motor cortex, namely the corticobulbar tract, synapse on MN of the facial nucleus. The facial nucleus sends efferent fibers to form the large *motor root* which loops around the abducens nucleus forming the genu of the facial nerve then course ventrolaterally en route to their exit from the brainstem. Prior to exiting, the *motor root* of the facial nerve is joined by the small *nervus intermedius*, also called the "sensory root" of the facial nerve. These fibers, from the superior salivatory nucleus, contain secretomotor fibers for salivary glands, lacrimal glands, as well as some pharyngeal and nasal mucosal glands. The *nervus intermedius* also carries parasympathetic efferent, vasodilator fibers for vessels in the areas supplied by the facial nerve. The facial nerve also contains afferents transmitting taste sensations from the tongue and palate, general sensations from the external acoustic meatus and the auricular concha, terminating in the spinal nucleus of the trigeminal nerve. The facial nerve, *motor root* and *nervus intermedius*, exit the

brainstem at the cerebellopontine angle and enter the internal acoustic meatus and travel through the facial canal which traverses through the petrous part of the temporal bone. The nerve travels through a treacherous course within the facial canal laterally, above and between the vestibule and cochlea then bends backwards, almost at a right angle, forming the facial geniculum. Finally, after curving inferiorly it reaches its exit from the facial canal at the stylomastoid foramen (SMF; Netter, 1991).

F. Facial Nerve Axotomy Injury Paradigm

Today, the facial nerve axotomy model represents one of the most widely used animal models to study MN regeneration and degeneration. In the mouse, the facial nerve axotomy is a relatively minor and easily replicated surgical procedure. It is performed by exposing the facial nerve as it exits the skull at the SMF and completely transecting the nerve prior to the distal branches which radiate rostrally within the face as the temporal, zygomatic, buccal, mandibular and cervical branches. Since the transection takes place in the periphery, there is no direct CNS trauma and no physical disruption of the blood-brain barrier (BBB; Moran and Graeber, 2004). Only the ipsilateral facial motor nucleus is affected by the axotomy, as there are no bilateral projections between the two nuclei. The contralateral nucleus can be used as an internal control because it remains uninjured (Cammermeyer, 1963). For descriptive purposes throughout this dissertation the ipsilateral facial motor nucleus affected by the axotomy, or injured by the axotomy will be referred to as the axotomized facial nucleus

(Ax). Additionally, the contralateral, uninjured facial motor nucleus will be referred to as the control facial nucleus (C). The facial nucleus contains a homogeneous population of MN which adds an additional level of control to this *in vivo* model. The mild and easily reproducible surgical procedure as well as the ability to make use of the contralateral, control nucleus, makes this a valuable injury model for studying MN survival and regeneration (Moran and Graeber, 2004).

The facial motor nucleus of the mouse contains approximately 2,000 MN and can be divided into seven subnuclei. Six of the seven subnuclei, are encompassed within the main body of the nucleus and are as follows; the dorsolateral (DL), dorsal intermediate (DI), dorsomedial (DM), ventral lateral (VL), ventral intermediate (VI), and ventromedial (VM) subnuclei (**Figure 3**). The seventh nucleus, the dorsal accessory (DA), is located directly dorsal to the rostral portion of the main nucleus. The musculotopic organization of the mouse facial motor nucleus was determined in 1982 by a series of experiments using the retrograde tracer horseradish peroxidase and its anatomical organization corresponds to functional and morphological arrangement of the subnuclei (**Table 1**). The VM and DM subnuclei, located medially, supply the posterior and anterior auricular musculature. The mentalis and associated portions of the platysma are innervated mainly by the VI subnuclei. The nasolabial musculature is represented by the lateral subnuclei, the VL and DL, which account for approximately 43% of all MN in the facial

motor nucleus. The DA contains MN innervating the stapedius muscle as well as the posterior belly of the digastric muscle (Ashwell, 1982).

G. Motoneuron Reactions After Facial Nerve Axotomy

Transection of the axon results in a process called Wallerian degeneration in which the separated portion undergoes degeneration. Within the cell body, the initial event is termed chromatolysis and is the disintegration, redistribution, and later, perceivable disappearance of the Nissl substance (Cammermeyer, 1963; Lieberman, 1971). Nissl bodies consist of parallel cisterns of granular endoplasmic reticulum and clusters of free ribosomes between lamellae. Within 24 hours of facial nerve transection, ultrastructural changes are present in the neuronal cytoplasm. Clusters of free ribosomes become evident throughout the cytoplasm, known as dispersion of Nissl granules, and this process reaches a maximum at four days. Within a nerve crush injury, a transection of axons occurs but the nerve sheath maintains intact, the new Nissl bodies reappear within one week, however after transection of the facial nerve, the endoplasmic reticulum remains dispersed and there are no further changes for several weeks. During that time the cell bodies were almost completely surrounded by glial cells. Prior to disintegration, the cytoplasm of the MN displayed extensive degeneration, closely packed mitochondria, an increase in neurofibrils, large amounts of free ribosomes, and multiple small vesicles with or without attached ribosomes. Ultimately the neurons are removed by phagocytic microglia between 16 and 30 days post-

axotomy (Torvik and Skjorten, 1971). Additionally, during the initial axon reaction is swelling of the entire cell body and dislocation of the cell nucleus and nucleolus closer to the cell membrane (Guntinas-Lichius et al., 1996; Brum, 1991). There is also an enlargement in the nucleolar volume which is associated with a dramatic increase in ribonucleic acid (RNA) and protein synthesis and enhanced nucleolar RNA synthesis (Lieberman, 1971). It has been proposed that the increase in RNA synthesis is due to axonal sprouting and the resulting expansion of the axonal membrane.

While changes in Nissl substance are present after facial nerve axotomy, facial methods of counting surviving MN after injury is still accomplished by staining cell bodies with a Nissl-stain, such as thionin or cresyl violet (Cammermeyer, 1963; Ashwell, 1982; Torvik and Skjorten, 1971; Guntinas-Lichius et al., 1996). It has been well-established that no changes in the control, uninjured facial motor nucleus take place after axotomy. Therefore, this non-operated side can be considered useful comparison for control purposes (Cammermeyer, 1963). Counting FMN using Nissl stain is still the gold standard in the facial nerve axotomy injury model. Retrograde tracing has technical limitations and in some instances application of the tracer itself can inadvertently produce injury. Additionally, immunohistochemical techniques that utilize antibodies to neuron-specific proteins can lead to identification problems because the targeted proteins themselves can be affected following injury. Facial nerve axotomy in adult mice results in an almost complete loss of expression of the cholinergic enzyme, choline

acetyltranferase (ChAT). This affect, not seen in young mice, could be mistakenly considered MN cell death (Kou et al., 1995). The neuronal nuclei (NeuN) antibody was identified in 1992 as a panneuronal marker against uncharacterized antigen/antigens and exhibits staining in the nuclei and diffuse cytoplasmic staining in neurons (Mullen et al., 1992). In mice and rats, facial nerve axotomy results in dramatic reduction of NeuN staining within the facial motor nucleus (McPhail et al., 2004). While these neuronal markers are widely used within the field of neuroscience, specific axotomy-induced changes in cellular protein prohibit their use in MN identification after facial nerve axotomy.

H. Glial Reactions After Facial Nerve Axotomy

It is well-understood that microglia are the first cells to respond to even minor pathological changes within the CNS (Kreutzberg, 1996). After facial nerve axotomy, microglia cells undergo mitosis and are the only proliferating cells within the axotomized nucleus and are distinct from circulating blood mononuclear cells. Even inducing death of FMN by toxic ricin injection, results in no perivascular infiltrates of mononuclear cells, but again, increased proliferation of endogenous microglia ensues (Graeber et al., 1988). In the facial nucleus, microglia begin to proliferate approximately 3 days after axotomy and reach a peak between four to six days (Tetzlaff et al., 1988b). It has been repeatedly shown, in a variety of axonal-lesion models that endogenous microglial cells become activated and rapidly proliferate between one and three days post injury (Dissing-Olesen

et al., 2007; Hailer et al., 1999). Using electron microscopy, during the initial stage of the axonal reaction, proliferating perineuronal microglia displace morphologically intact synaptic terminals from the injured MN cell body and dendrites (Blinzinger and Kreutzberg, 1968). This process is known as synaptic stripping and is considered part of the first stage of microglial activation. After completion of synaptic stripping, perineuronal microglia migrate to the nearby parenchyma or neuropil of the axotomized nucleus where they remain, although they appear to decrease in number (Jones et al., 1997). Upon death of FMN, microglia rapidly transform from activated to phagocytic cells, known as microglia-derived brain macrophages, and gradually remove the neuronal debris. This is known as the second stage of microglial activation and this transformation into potentially cytotoxic cells is under strict control within the healthy CNS (Kreutzberg, 1996). Studies using floro-gold labeled MN demonstrated that after transection of the vagus nerve, axotomized MN of the dorsal motor nucleus of the vagus, MN were phagocytosed by microglia or brain-derived macrophages (Rinaman et al., 1991).

In the rodent facial nucleus, local astrocytes normally express low levels of glial fibrillary acidic protein (GFAP). GFAP is the major protein constituent of glial filaments and is the cell-specific intermediate filament in astrocytes. In the rat, facial nerve axotomy elicits a significant increase in GFAP messenger RNA (mRNA) expression by resident reactive astrocytes as early as 24 hours after peripheral nerve injury. However,

increased protein immunoreactivity for GFAP was not seen until two days after axotomy. These astrocytes become reactive and transform into fibrous astrocytes and this is considered the first of two phases the astrocytic reaction. It was determined that the astrocyte reaction, just like the microglial reaction, occurred only within the axotomized nucleus, not the contralateral control nucleus. Within the facial nerve axotomy model, no evidence of astrocyte proliferation has been detected. It has also been shown that continued synthesis of GFAP is influenced by functional contact with target musculature. In the crush lesion, GFAP synthesis begins to return to normal as functional recovery is attained (Tetzlaff et al., 1988b). Additional studies support these findings as well as report no increase in GFAP occurs within the uninjured, contralateral control facial nucleus (Laskawi and Wolff, 1996). After microglia have completed synaptic stripping and have left their perineuronal positions and moved into the neuropil, the second phase of the astrocytic reaction begins (Graeber and Kreutzberg, 1988). Reactive astrocytes in the axotomized facial nucleus form very thin, sheet-like lamellar processes which become arranged in stacks and ultimately cover all surfaces of regenerating MN. This process, known as astrocytic ensheathment, begins two – three weeks post-operative is thought to insulate the MN from their synaptic inputs. Additionally, these astrocytic lamellar processes exhibited 5'-nucleotidase enzymatic activity, which is known to produce adenosine by hydrolyzing adenosine monophosphate (AMP). Adenosine is thought to inhibit synaptic transmission. This

further supports the theory that purpose of the second phase of the astrocytic reaction is synaptic insulation of the regenerating MN (Graeber and Kreutzberg, 1988).

I. Facial Motoneuron Survival Following Axotomy

The degree of neuronal cell death following facial nerve axotomy differs widely between species (Moran and Graeber, 2004). It has been well established that in the adult mouse, most FMN initially survive a facial nerve axotomy, however, agreement among researchers concludes that 28 days post operative (dpo) represents the first time-point at which maximal MN cell death occurs subsequent to peripheral nerve damage (Serpe et al., 1999; Lieberman, 1971).

FMN percent survival is measured by counting the number of FMN in the axotomized facial nucleus and comparing to the number of FMN within the control facial nucleus. It has been previously shown that at 28 dpo the percent of FMN survival in WT mice is approximately 86%, significantly decreased compared to 7 or 14 dpo (97% and 93%, respectively). All WT mice used within this dissertation were on the C57BL/6 background. They will be referred to as simply WT unless of a different background then the specific background strain will be identified. In 2000, our laboratory performed a facial nerve axotomy on severe combined immunodeficient (*Scid*) mice, an immunodeficient transgenic mouse which lacks functional B and T cells. The result was significantly lower FMN survival of 52% compared to the Balb/c WT, 86%. To verify these results, another immunodeficient mouse model was also used in the same study,

the recombinase-activating gene-2 KO (RAG-2 KO), which fail to develop mature B and T lymphocytes. After facial nerve axotomy, RAG-2 KO mice also displayed significantly less FMN survival of 64% compared to Balb/c WT (Serpe et al., 2000). The immunodeficient mice, both *Scid* and RAG-2 KO were reconstituted with WT splenocytes, which include cells of the acquired immune system, such as B and T cells. During reconstitution WT splenocytes are injected into the tail vein of the immunodeficient mouse and have been shown to migrate to, and segregate within, their respective compartments of the spleen and lymph node (Serpe et al., 1999). The previous decreases in FMN survival in the immunodeficient mice were reversed back to WT levels after having been reconstituted with WT splenocytes one week prior to facial nerve axotomy. These findings revealed the important role of the peripheral immune system in mediating neuroprotection after peripheral nerve injury (Serpe et al., 2000). Additionally, it was determined that the immune cell subset, within the splenocyte population, responsible for restoring the immune-mediated neuroprotection to the axotomized facial motor nucleus was the $CD4^+$ T cell. Therefore, reconstitution of RAG-2 KO with $CD4^+$ T cells one week prior to facial nerve axotomy rescued FMN survival back to WT levels. As a positive control, CD4 KO mice were also reconstituted with WT $CD4^+$ T cells and again, rescue of FMN survival occurred and FMN numbers were returned to 28 dpo WT levels (Serpe et al., 2003).

FMN survival levels at time-points extended past 28 dpo reveal continued decreases in MN numbers within the WT facial motor nucleus. Balb/c WT mice reveal a

significant decrease from 86% FMN survival at 28 dpo to 60% at 70 dpo (Serpe et al., 2000). Even further extended time-points within the C57BL/6 WT showed that FMN survivals decline to approximately 45% at 126 dpo and survival levels are maintained at 182 dpo (roughly 40%). Similar results were seen in immunodeficient mice (Beahrs, 2009). While *Scid* mice display dramatic FMN loss at 28 dpo compared to Balb/c WT, they present no significant difference in FMN survival at 70 dpo (52% and 45%, respectively). Reconstitution of *Scid* mice with WT splenocytes does rescue FMN survival at 28 dpo (83%) and even with this newly acquired immunity, *Scid* mice show significantly decreased FMN survival at 70 dpo (58%; Serpe et al., 2000). These findings have been replicated in the RAG-2 KO, however ultimately in both WT and immunodeficient mouse models, reconstituted or not, with time, FMN survival levels reach a plateau of approximately 40-50% (Serpe et al., 2000; Beahrs, 2009). Therefore, we hypothesize that within the facial motor nucleus there exists an immune-dependent MN subpopulation which persists for a limited time after peripheral nerve injury and is dependent upon a functional peripheral immune system. It is thought that this subpopulation is maintained indirectly by the $CD4^+$ T cell and delays neurodegeneration for the purpose of axonal regeneration and subsequent reconnection to target (Xin et al., 2011). Also evident is a second subpopulation of MN in the facial motor nucleus that make up the 40-50% of cells that are a resilient population and survive for long periods of time, regardless of immune-status or target reconnection (Jones et al., 2005).

The distribution of FMN survival across the six subnuclei allows us to investigate functional or topographical responses to nerve injury. Previous studies revealed an uneven distribution of FMN survival at 28 dpo, with the VL showing the lowest percent survival at 70% and the VM subnuclei maintaining the highest level of FMN survival at nearly 100% (Canh et al., 2006). Additionally in the RAG-2 KO, this same variance in numbers of surviving MN was seen, although percentage FMN survival was much lower. This distribution was also maintained after FMN rescue by reconstituting the RAG-2 KO mouse prior to facial nerve axotomy. This identification of differing populations of MN within the facial nucleus is important and provides two populations with intrinsic differences and/or surrounding environments that can be further studied (Canh et al., 2006).

J. SOD1 Facial Motoneuron Survival following Axotomy

Several investigators have utilized a variety of nerve injuries in $SOD1^{G93A}$ rodent models of ALS to determine MN responses to axonal damage. One study, using the SOD1 rat model performed a facial nerve transection as well as the more severe injury facial nerve avulsion, where the proximal end of the transected facial nerve is gently pulled or separated away from the brainstem during surgery. Both surgeries were conducted on pre-symptomatic rats, and FMN survival counts 14 dpo after axotomy showed no difference in FMN survival compared to controls. However, 14 dpo after facial nerve avulsion, revealed an even greater loss of MN at 35% FMN survival

compared to control rats, 77% (Ikeda et al., 2005). In the pre-symptomatic SOD1 mouse, sciatic nerve crush at 42 doa results in an acceleration in disease progression such that at 90 doa the injured mice showed deficits in muscle force, contractile characteristics, and MN survival that are only seen in uninjured, end-stage mice 130 doa (Sharp et al., 2005). Significant decrease in FMN survival numbers at 30 dpo were determined following a facial nerve transection with a 1 mm resection in pre-symptomatic SOD1 mice (Mariotti et al., 2002). In one of our previous studies, a facial nerve axotomy was performed on pre-symptomatic SOD1 mice and dramatic decreases in FMN survival at 28 dpo compared to WT (41% and 85%, respectively) were observed (Mesnard et al., 2011). Together this research employing nerve injuries within the pre-symptomatic stage of SOD1 models has revealed the vulnerability of SOD1 MN to stressful stimuli and the inability to retain WT survival levels. This apparent lack of neuroprotection after facial nerve injury and the possibility that axotomy may resemble the target disconnection that occurs prior to MN degeneration during disease, lead us to continue our investigation into the axotomy-induced FMN cell death in the pre-symptomatic SOD1 mouse.

Subsequent studies by our laboratory have advanced our understating of the susceptibility of MN within the SOD1 mouse model. After facial nerve axotomy the distribution of FMN survival was assessed among the subnuclei as was previously performed by our laboratory (Canh et al., 2006). VM and VL subnuclei of pre-

symptomatic SOD1 mice revealed a similar pattern of varying survival as seen previously; the “regenerative” VM subnuclei retained the highest percent FMN survival while the “degenerative” VL resulted in the lowest percent of FMN survival across the subnuclei (Mesnard, 2009). These results revealed that populations of MN within the SOD1 facial motor nucleus do retain a regenerative phenotype after injury in comparison to other MN populations within the nucleus. This distribution FMN survival was shown previously in WT and RAG-2 KO mice while the FMN levels within the subnuclei is closely aligned with that seen in the RAG-2 KO. While the SOD1 FMN loss is similar in magnitude and distribution when compared to the immunodeficient RAG-2 KO, there is no agreement within the literature of peripheral immune deficits within the pre-symptomatic SOD1 (Barbeito et al., 2010). However, our laboratory has been studying immune-mediated neuroprotection for the last decade and is well-aware of the complexity of the signaling between the peripheral immune system and the CNS which leads to the neuroprotection. For these reasons, our lab has focused on the SOD1 MN and neuropil response to injury to uncover mechanisms involved in MN cell death and consequently the lack of neuroprotection.

In an effort to delineate neuronal and/or neuropil contributions to MN survival after axotomy, our laboratory recently began using the technique of laser microdissection (LMD) to accurately dissect axotomized facial motor nuclei or subnuclei for collection of RNA and analysis of the mRNA expression in response to axotomy

(Mesnard et al., 2010; Mesnard et al., 2011). The measurable outcome of mRNA expression was chosen over protein for the following reasons: in comparison to protein expression, mRNA expression identifies the initial response of the cell to the injury, its quantification can be considered less variable than protein, and the majority of MN survival research within the facial motor nucleus past and present utilizes mRNA expression.

The three most recent studies from our lab utilized LMD of the axotomized facial motor nucleus and axotomized VM and VL facial motor subnuclei of WT and pre-symptomatic SOD1 mice. Among the genes assessed for mRNA expression were MN-specific genes involved in regeneration and survival, genes specific to the neuropil such as the astrocytic marker GFAP and tumor necrosis factor-alpha (TNFα), a pro-inflammatory cytokine. The mRNA expression was measured at four time-points after facial nerve axotomy. Surprisingly, axotomized SOD1 FMN displayed a pro-survival/regenerative response, similar to WT, despite the dramatic increase in FMN cell death after axotomy. However, differences were revealed during comparisons of neuropil-specific genes. In addition to differences in the axotomy-induced mRNA expression, the SOD1 control, uninjured facial nucleus revealed constitutive expression of TNFα (Mesnard et al., 2011). This constitutive expression was not seen within the WT control nucleus and is indicative of the presence of a pro-inflammatory microenvironment within the early pre-symptomatic stage. Therefore, the increased

susceptibility of pre-symptomatic SOD1 FMN cell death after axotomy may involve a dysregulated response within the neuropil. In addition, WT comparisons between the regenerative VM, maintaining almost 100% FMN survival after axotomy, and the degenerative VL, displaying the greatest cell loss among the six subnuclei at 70% FMN survival, were performed using the same experimental design. It was determined that regardless of neuronal fate after injury, both subnuclear populations responded with a similar survival/regenerative profile of mRNA expression. In addition, differences within mRNA expression specific to the neuropil were evident (Mesnard et al., 2010). The last comparison was made between the pre-symptomatic SOD1 VM and VL subnuclei after axotomy. Similar results from this study support the previous findings (Mesnard, 2009). In summary, we propose that MN fate is ultimately controlled or regulated by cells within the neuropil, we hypothesize that this lack of regulation by the neuropil may also result in the MN degeneration that occurs during disease progression.

In general the experiments detailed within this dissertation were aimed at verifying that axotomy-induced mRNA expression and FMN cell death in pre-symptomatic SOD1 mouse resembles disease-induced mRNA expression and FMN cell death that occurs during disease-progression. Additional genes were also assessed to provide further insight into the mechanisms of neurodegeneration.

K. Gene Expression Profiling

The remainder of this Chapter introduces the 21 genes used in the analysis of the mRNA expression following facial nerve axotomy in the WT and SOD1 facial motor nucleus as well as disease progression in the SOD1 facial nucleus. In general, each gene or category of genes will be identified and information if available will be presented; 1) information pertaining to its expression with regard to nerve injury, particularly facial nerve injury, 2) mRNA expression in WT and SOD1 whole facial motor nucleus following axotomy, if available, 3) mRNA expression in WT and SOD1 VM and VL subnuclei, if available, and 4) briefly, indications of differential gene or protein expression in the SOD1 mouse model or ALS patients within the literature. **Table 2** summarizes the genes, their function, mRNA expression after facial nerve axotomy, if known, and their expression or connection with ALS or SOD1 disease progression, if known. Every gene listed within **Table 2** and introduced in the subsequent section will be analyzed for mRNA expression in the experiments within this dissertation. Several genes have already been profiled in our laboratory using the LMD technique and reverse-transcription polymerase chain reaction (RT-PCR), however the time course will need to be extended from 28 to 56 dpo. Therefore, regardless of previous profiling, all genes discussed will be analyzed throughout Chapters IV – VII.

a. Neuroregenerative Genes: βII-Tubulin and GAP-43

The MN regenerative genes that were assessed include; βII-Tubulin and growth-associated protein of 43 kilodaltons (GAP-43). It has been well-established that successful regeneration following peripheral nerve injury is dependent on neuronal survival. Differential regulation of mRNA expression and protein synthesis occur after peripheral nerve injury and play a role in transitioning the neuron from a signaling mode, to a regenerative, developmental, growth mode (Hoffman and Cleveland, 1988; Lieberman, 1971; Fu and Gordon, 1997). It has been demonstrated by insitu hybridization and northern blot analyses that following facial nerve axotomy, in contrast to the decrease seen in mRNA for neurofilament, there is an increase in mRNA of cytoskeletal proteins actin, αI-Tubulin, and βII-Tubulin as well as the regenerative gene, GAP-43 (Tetzlaff et al., 1991). GAP-43 is a calmodulin-binding phosophoprotein located on the cytoplasmic side of the plasma membrane and is a major protein component of axonal growth cones. Similar increases in gene expression have been shown after facial nerve axotomy within the hamster for αI-Tubulin, βII-Tubulin, βIII-Tubulin, and in the rat (Tetzlaff et al., 1988a; Jones and Oblinger, 1994; Jones et al., 1999; Sharma et al., 2010). Specifically, the isotype βII-Tubulin has been shown to be particularly important in axonal elongation during development and regeneration after injury during assembly of the cytoskeleton and has been shown to be predominantly expressed by MN within the

facial motor nucleus (Hoffman and Cleveland, 1988; Moskowitz and Oblinger, 1995; Tetzlaff et al., 1991).

In comparison of βII-Tubulin and GAP-43 mRNA within the WT VM and VL after facial nerve axotomy, it was surprisingly expressed at higher levels throughout the time course and this same finding was seen in the pre-symptomatic SOD1 VM and VL following facial nerve axotomy (Mesnard et al., 2010; Mesnard, 2009).

The MN-specific regenerative genes, βII-Tubulin and GAP-43 were expressed to a similar extent in both the WT and SOD1 whole nucleus after axotomy (Mesnard et al., 2011).

Several studies have previously shown increased protein expression of GAP-43 on anterior horn cells within the lumbar segments of spinal cords of five sALS patients (Ikemoto et al., 1999). In support of the previous finding, a two – four-fold increase of mRNA expression for GAP-43, was shown by Northern Blot. This expression was within anterior horn cells of the lumbar spinal cord in 11 ALS patients, 10 of which were sALS (Parhad et al., 1992). These mRNA expression results were later verified by a study using the RT-PCR method of measuring the increased mRNA expression of GAP-43 in the spinal cord of five ALS patients compared to controls (Kage et al., 1998). These data suggest increased mRNA expression for GAP-43 is a marker of sALS disease progression. In the symptomatic SOD1 mouse model, increased immunoreactivity for GAP-43 around MN was seen at 105 – 126 doa, within the lumbar anterior horn (Miyazaki et al., 2009).

b. Neuroprotective Signaling Genes:

i. CX3CR1

It has been well-established that fractalkine (CX3CL1) and its receptor (CX3CR1) are important for signaling after neuronal injury and mediating neuroprotection. Within hours after injury CX3CL1 protein is increased on neurons. Membrane-bound or soluble CX3CL1, the latter cleaved from neuronal membranes via disintegrin and malloproteinase domain-containing protein 10 (ADAM10), results in signaling through its receptor CX3CR1 localized to microglia (Harrison et al., 1998; Hundhausen et al., 2003; Chapman et al., 2000). CX3CL1 binding to its G-protein-coupled receptor (GPCR), CX3CR1, triggering phosphatidylinositol-3 kinase (PI3K)-dependent Ca2+ influx and mitogen-activated protein kinase (MAPK) activation, subsequent cytoskeletal changes, actin rearrangements and ultimately, a migratory response. Additionally, downstream signaling leads to activation of Akt pathways and cell survival signals as well as attenuation of pro-inflammatory molecules such as interleukin-6 (IL-6), interleukin-1β (IL-1β), TNFα, and downregulation of inducible nitric oxide synthase (iNOS), making up CX3CR1's anti-inflammatory affects (**Figure 4**; Re and Przedborski, 2006; Maciejewski-Lenoir et al., 1999). Using insitu hybridization, it was determined that mRNA for CX3CR1 increased after facial nerve axotomy in C57BL/6 mice as early as 2 dpo and persisted through 14 dpo. By the time-point of 21 dpo, the mRNA expression for CX3CR1 was nearly equal to that of the contralateral, uninjured facial motor nucleus. The same study

also saw similar upregulation of CX3CR1 mRNA in the dorsal motor nucleus after vagus nerve axotomy as well as in the red nucleus after rubrospinal tractotomy, a central axotomy model as opposed to a peripheral axotomy model (Zujovic et al., 2005). Additionally, CX3CR1 mRNA was shown to be upregulated in the axotomized facial motor nucleus of the rat and the increase CX3CR1 mRNA expression was found to parallel the transient increase in microglial cell numbers (Harrison et al., 1998).

CX3CR1 expression has not been investigated in ALS patients or SOD1 mice. However, one study crossed the $SOD1^{G93A}$ transgenic mouse with $CX3CR1^{-/-}$ mice. These mice displayed a more rapid loss of hind-limb grip strength and decreased survival compared to $SOD1^{G93A}/CX3CR1^{+/-}$ mice (Cardona et al., 2006). These findings lend support to the neuroprotective role of CX3CR1 signaling in the SOD1 mouse in addition to that which has already been established in the WT.

ii. PAC1-R

Pituitary adenylate cyclase-activating polypeptide (PACAP) is a pleiotropic and mutifunctional peptide known to promote neurite outgrowth and cell survival. It is considered to be a potent neurotrophic and neuroprotective peptide in several conditions such as brain trauma, ischemia, and several neurodegeneration diseases and is believed to possess anti-inflammatory properties (Somogyvari-Vigh and Reglodi, 2004; Reglodi et al., 2011). In support of these findings, facial nerve crush axotomy in PACAP-deficient mice resulted in a significant delay of axon regeneration as well as an increase

in gene expression of pro-inflammatory cytokines such as TNFα and interferon-gamma (INF-γ; Armstrong et al., 2008). PACAP mRNA is upregulated has been well-established in a variety of axotomy models such as; sensory neurons of the dorsal root ganglia and the mesencephalic trigeminal nucleus, the sympathetic neurons of the cervical ganglia, and the facial motor nucleus (Zhang et al., 1995; Zhang et al., 1996; Larsen et al., 1997; Moller et al., 1997; Zhou et al., 1999; Sharma et al., 2010; Mesnard et al., 2010). While PACAP has been shown to bind to several receptors and exert its effects, one of these receptors, PACAP 1-Receptor (PAC1-R) is highly specific for PACAP. The neuroprotective affects of PACAP via signaling through the GPCR, PAC1-R, are thought to act through the activation of the adenylyl cyclase (AC) pathway. AC stimulation production of cyclic AMP (cAMP) leading to activation of protein kinase A (PKA) followed by phosphorylation of extracellular signal-related kinase 1/2 (ERK 1/2) which leads to a subsequent increase in expression of the gene c-*fos*. This downstream signaling pathway has been linked to PACAP's effects on cell survival and anti-inflammatory effects such as inhibition of apoptosis, and attenuation of TNFα and Interleukin-1 (IL-1; **Figure 5**; Vaudry et al., 2000).

While PACAP mRNA after axotomy is upregulated, paradoxically, expression of PAC1-R is downregulated after facial nerve axotomy in the rat. It was determined by insitu hybridization that PAC1-R mRNA expression in the uninjured and injured facial motor nucleus was localized to almost all MN and within hours of facial nerve axotomy

the mRNA expression decreased by approximately 50% compared that of the contralateral, control nucleus and by 30 dpo PAC1-R mRNA expression was 10-20% less than control levels (Zhou et al., 1999). The reason for this downregulation following injury is not currently understood. To date, PAC1-R has not been investigated in ALS patients or the SOD1 mouse.

iii. TNFR2

TNF receptor 2 (TNFR2) is a glycoprotein, preassembled as a trimer and is activated by the pro-inflammatory cytokine, TNFα (**Figure 6**). For additional information on TNFα, refer to Section K.e.i of this Chapter. TNFR2 is activated preferentially by transmembrane TNFα (tmTNFα) and is expressed within the CNS by microglia and endothelial cells (McCoy and Tansey, 2008). Like other members of the TNFR superfamily, TNFR2 does not contain a cytoplasmic death domain. Receptor activation in response to tmTNFα, leads to survival signals such as upregulation of anti-apoptotic molecules such as cellular inhibitors of apoptosis (c-IAP1 and -2), known to inhibit cysteine-dependent aspartate-directed protease 8 (Caspase-8) activity (**Figure 8**). In addition, endothelial/epithelial tyrosine kinase-1 (Etk-1), a TNFR2-specific kinase, leads to downstream activation of protein kinase B (PKB). PKB is a mediator of survival, cell adhesion and migration signals (Grivennikov et al., 2006). Although TNFR2 can promote cell survival it can also activate apoptotic signals. TNFR2 can enhance the association between TNFR1 and TNFα by a type of ligand passing mechanism. While TNFR2 is not

considered a death receptor it may play a role in promotion of death receptor signaling (McCoy and Tansey, 2008).

TNFR2 has been evaluated in the facial nerve axotomy model and this information is detailed in Section K.e.i of this Chapter.

TNFR2 mRNA and protein has been detected within the spinal cord within late symptomatic stage (Elliott, 2001; Hensley et al., 2002). Additionally, soluble forms of both TNFR1 and TNFR2 were found in ALS patient serum, which suggests a significant activation of the TNF system during the disease (Cereda et al., 2008).

TNFR2 and TNFR1 protein expression changes were evaluated after mouse sciatic nerve injury. For additional information on TNFR1 see Section K.e.i of this Chapter. While protein for both receptors was detectable at low levels within the spinal cord before injury, after injury TNFR1 increased by two-fold at 3 and 7 dpo, while TNFR2 was significantly increased at 1 dpo and reached a level of seven-fold by 3 and 7 dpo. Protein expression for both receptors remained elevated out through 28 dpo (George et al., 2005). While mRNA expression of TNFR1 or TNFR2 has not been investigated following facial nerve axotomy in the mouse, facial nerve axotomy in TNFR1 deficient or TNFR2 deficient mice do not show any significant decreases in FMN cell loss 29 dpo compared to WT. However, a combined TNFR1/TNFR2 deficient transgenic mouse revealed a massive reduction in FMN percent survival at 29 dpo (Bohatschek et al., 2004). Recently our lab assessed FMN survival in TNFR1 KO and TNFR2 KO. It was

determined that no differences in FMN survival was seen 28 dpo compared to WT. These results support the results of the study previously mentioned. Additionally, FMN survival was determined for the VM and VL subnuclei of the TNFR1 KO and TNFR2 KO. No differences were seen in the VM subnuclei compared to WT 28 dpo. However, in both receptor KO transgenic mice, VL FMN survival was rescued back to uninjured WT VL levels. This suggests that FMN cell loss seen within the degenerative VL subnucleus may be related to TNFR1 and TNFR2 signaling (Mesnard, 2009).

c. Glial-Specific Genes:

i. GFAP

The important role of the astrocyte response after facial nerve axotomy and the increase in mRNA expression of GFAP has already been discussed in detail, refer to Section H of this Chapter.

Upregulation of GFAP mRNA within the WT VM and VL after facial nerve axotomy, was similar between the subnuclei throughout the time course with peak expression displayed at 14 dpo which is consistent with previous findings (Graeber and Kreutzberg, 1988; Mesnard et al., 2010). Within the SOD1 VM and VL, GFAP was also upregulated however, no peak at 14 dpo was seen and expression was significantly higher within the VL compared to the VM at 7 and 28 dpo (Mesnard et al., 2010).

Within the whole facial motor nucleus, GFAP mRNA expression was found to be similar between WT and SOD1 after axotomy at all time-points except 14dpo, where the

WT showed expression at approximately 4000% higher than mRNA expression within the contralateral, uninjured control but in the SOD1 14 dpo axotomized nucleus, GFAP mRNA expression was drastically lower at approximately 1000% compared to control (Mesnard et al., 2011). This suppressed expression at 14 dpo helps to clarify the lack of peak mRNA expression within the SOD1 VM and VL.

GFAP mRNA and protein expression related to the SOD1 mouse model and ALS patients is incorporated with that of CD68 below.

ii. CD68

The response of microglia to facial nerve axotomy has also been described in Section H of this Chapter. It has been established that the glycoprotein, Cluster of Differentiation 68 (CD68) is a monocyte and macrophage specific marker, often referred to as macrosialin in the mouse, and ED1 in the rat, can be used within the CNS as a marker for microglia (Graeber et al., 1990; Lemstra et al., 2007; Holness and Simmons, 1993). After facial nerve axotomy in the rat, local microglia and perivascular cells as well as brain-derived macrophages newly express antigens of the myelomonocytic lineage, such as CD68. Therefore, unlike other brain injuries, such as cortical stab lesions which disturb the BBB, it is unlikely that a significant portion of the CD68 positive cells infiltrated the degenerating facial nucleus (Graeber et al., 1990).

CD68 or markers for microglia have not been previously evaluated facial motor nucleus or subnuclei with our laboratories technique of LMD followed by semi-

quantitative RT-PCR analysis of mRNA expression. CD68 was evaluated in experiments within this dissertation for WT and SOD1 whole nucleus and VM and VL subnuclei.

Additional reasons for selecting the gene CD68 as the marker for microglial reactivity, is the overwhelming use of this gene as a microglial marker within the SOD1 literature. Increased mRNA expression from lumbar spinal cords of $SOD1^{G93A}$ mice for both CD68 and GFAP was shown in comparison to WT controls within the pre-symptomatic stage and the symptomatic stage (Yoshihara et al., 2002; Chen et al., 2004). Additional studies using CD68 mRNA as a marker for microglia in SOD1 spinal cord identify upregulation anywhere from 42 throughout 126 doa (Beers et al., 2011; Malaspina and de Belleroche, 2004; Chen et al., 2004).

d. Neurodegenerative Gene: CRMP4

Collapsin response mediator protein 4 (CRMP4) is a member of a family of five developmentally regulated cytosolic phosphoproteins. CRMP4 protein has been found to be expressed in rat neurons during discrete periods of neuronal development (Wang and Strittmatter, 1996). Within the hippocampal dentate gyrus, CRMP4 is upregulated following transient global ischemia and was considered indicative of enhanced neurogenesis in the rat (Kee et al., 2001). Additionally, in another rat ischemia model, CRMP4-positive cells were found in immature neurons generated from neuronal precursors in the ischemic striatum (Liu et al., 2003). These studies suggest that CRMP4, normally only expressed during embryonic development within the brain, may be a

specific immature neuronal marker to be used in identifying proliferation of neuronal progenitors after brain injury such as ischemia. However, more detailed analysis has shown that the two splice variants of CRMP4, CRMP4a and CRPM4b, have different effects on cytoskeletal rearrangements and *in vitro* CRMP4b can inhibit neurite outgrowth in dorsal root ganglion neurons (Alabed et al., 2007). While initially considered a marker of neuroregeneration because of its role, neurite outgrowth in some neuronal populations following injury, additional studies do not support this theory. Overexpression of CRMP4a in cultured WT MN leads to inhibition of neurite outgrowth followed by cell death. This finding was verified *in vivo* by adeno-associated virus-mediated overexpression of CRMP4a in MN and this led to significant muscle denervation as well as reduction in MN cell numbers (Duplan et al., 2010). These findings suggest that CRMP4 and/or its splice variant, CRMP4a, do not play a neuroprotective role in MN.

The regulation of CRMP4 mRNA expression by peripheral nerve injury has not been investigated to date and because of the role of CRMP4a in inhibition of neurite outgrowth and MN cell death it is important to determine its expression after facial nerve axotomy. The primer set developed for use in the experiments within this dissertation was specific for the mRNA CRMP4 itself and will not reflect specific levels of the splice variants.

While the role of CRMP4a and CRMP4b in the adult, injured brain is not clear-cut, increased expression of CRMP4a was recently observed in a subpopulation SOD1 lumbar MN. At 45 doa, no difference in CRMP4a protein expression was detected, but by 60 doa, there was a 2.5-fold increase in protein and this increase peaked at 90 doa, among 25% of lumbar MN. While the percentage of MN expressing CRMP4a is relatively low, it is suggested that the expression within the pre-symptomatic stage may be specific to a particular subpopulation affected early by the disease. An additional *in vitro* study was performed in SOD1 MN that supports the neurodegenerative properties of CRMP4a in MN. Cultured SOD1 MN were treated with CRMP4a-specific short hairpin RNA (shRNA). Silencing of CRMP4a protected SOD1 MN from prevented NO-induced cell death (Duplan et al., 2010).

e. Death Receptor Signaling System Genes:

i. TNFR1 receptor signaling genes: TNFα, TNFR1, TRADD, TRAF2, SODD

The pro-inflammatory cytokine, TNFα, is known to be synthesized within the CNS by microglia, astrocytes, and some neurons as tmTNFα which is inserted into the membrane as a homotrimer. The matrix metalloprotease, TNFα converting enzyme (TACE), is responsible for cleaving tmTNFα into soluble TNFα (solTNFα), a circulating trimer. Previous data from our lab has shown TNFα mRNA is constitutively expressed in the facial motor nucleus of pre-symptomatic SOD1 mice (Mesnard et al., 2011). Two different membrane glycoprotein receptors, TNFR1 and TNFR2, bind both forms of TNFα

(McCoy and Tansey, 2008). Receptor activation can be classified in two ways depending upon where the ligand is expressed. *Cis* activation occurs when a transmembrane ligand on the same cell binds and activates a receptor also expressed on the same cell. *Trans* receptor activation can occur through binding of a transmembrane ligand expressed on a different cell or a soluble ligand (Haase et al., 2008). TNFR1 has a higher affinity for solTNFα and is ubiquitously expressed. Activation of TNFR1 requires that the receptor is preassembled as a trimer prior to binding of solTNFα or tmTNFα (McCoy and Tansey, 2008). TNFR1 is a member of the TNFR superfamily, while TNFR1 is classified as a death receptor. Death receptors contain a specific 80-amino acid sequence within the cytoplasmic tail, the death domain (Haase et al., 2008). After ligand binding the silencer of death domains (SODD) dissociates allowing subsequent association of the adaptor protein, TNFR1-association death domain (TRADD). TRADD is responsible for recruitment of other adaptor proteins such as receptor interacting protein-1 (RIP1) and formation of complex I (**Figure 7**). It is suggested that SODD plays an important regulatory role in TNFR1 signaling.

It is thought that complex I transmits the activation signal to the pro-apoptotic, death-inducing signaling complex (DISC) consisting of TRADD, RIP1, and Fas-associated death domain protein (FADD; Grivennikov et al., 2006). DISC also contains a homodimer of procaspase-8, which are proteolytically activated by each other within the confined space of DISC. The result is an active caspase-8 dimer (**Figures 7** and **8**). Caspase-8 is

considered an initiator caspase; when it is activated it binds to the inactive procapsase-3 dimer within the cytosol. The initiator caspase proteolytically activates the procaspase-3 dimer, resulting in an active effector cysteine-dependent aspartate-directed protease-3 (Caspase-3; Boatright and Salvesen, 2003). The effector caspase is responsible for the subsequent apoptotic cascade. While TNFR1 signaling is generally thought of as pro-apoptotic, it may also activate transcription of survival signals. It is suggested that activation of DISC takes time and is only achieved if the survival signals initially upregulated during TNFR1 activation, remain below a threshold (Grivennikov et al., 2006).

TRAF2 interacts with TNFR1 or TNFR2 and can lead to a cell survival signal or a cell death signal. TRAF2 is expressed in MN within the CNS and displays increased expression in neurodegenerative diseases (Culpan et al., 2009). It is not clear whether the increased expression is destructive or protective.

It is well-established that TNFα mRNA and protein expression is greatly increased in the SOD1 mouse model and in ALS patients (Cereda et al., 2008; McCoy and Tansey, 2008; Mesnard et al., 2011; Hensley et al., 2003; Veglianese et al., 2006). TNFR1 mRNA and protein has been detected within the spinal cord within the symptomatic stage (Elliott, 2001; Hensley et al., 2002). No differences in mRNA expression for TRADD in SOD1 symptomatic spinal cord were found (Hensley et al., 2002). Constitutive expression of mRNA for the ligand TNFα was previously shown in the pre-symptomatic

SOD1 mouse as well as sustained upregulation after axotomy at 28 dpo. While increased expression of the pro-inflammatory cytokine mRNA in pre-symptomatic SOD1 facial nucleus suggests the presence of a pro-inflammatory microenvironment prior to nerve injury, induction of TNFα mRNA was seen after axotomy in the WT facial motor nucleus. While this induction was no longer present at 28 dpo, the findings suggest that TNFα plays a role in signaling after axonal injury to MN (Mesnard et al., 2011). It is thought that TNFR1 signaling plays a role in the disease, however, those mechanisms have yet to be elucidated.

ii. Fas receptor signaling genes: FasL, Fas, Daxx, ASK1, nNOS

Fas receptor (Fas), another member of the TNFR superfamily and classified as a death receptor, is ubiquitously expressed and uses a similar downstream pathway for Caspase-8 activation. However, after Fas activation, DISC is formed while FADD interacts directly with the receptor (**Figure 9**). There are a few instances of Fas initiating survival signals, but in general Fas is implicated solely in death signaling. Like TNFR1, the outcome of receptor activation is thought to be a function of the thresholds for survival and death signals (Grivennikov et al., 2006). Within the CNS, Fas ligand (FasL) is expressed on both neurons and glial cells (Beer et al., 2000). Traditionally, constitutive expression of FasL within the brain is thought to play an important role in limiting inflammatory responses and maintenance of the relative immune suppression of the CNS (Choi and Benveniste, 2004). This ligand is expressed in an active membrane-bound

form and cleaved to an active soluble form. Recently, FasL has been investigated in the pre-symptomatic SOD1 mouse model which was found to exhibit two-fold higher FasL-positive MN in the lumbar spinal cord at 75 doa using immunohistochemical techniques (Raoul et al., 2006).

Basal expression of Fas within the healthy CNS are so low that they thought to be relatively nonfunctional, however inducible expression of Fas can lead to direct or bystander damage to neurons and/or glia (Tan et al., 2001). Fas expression and increased levels of activated Caspase-8 have been reported in response to brain ischemia. Cortical neurons and MN are the only types of neuronal culture systems sensitive to Fas activation. Exogenous activation of Fas induced death through Caspase-8 in 50% of cultured MN after 48 hours, suggesting transcriptional events may be involved. Raoul et al. (2002), discovered a novel, MN-specific pathway downstream of Fas involving transcription of neuronal nitric oxide synthase (nNOS) (**Figure 9**). In response to Fas activation, death associated protein-6 (Daxx), a Fas-associated protein, binds to Fas and recruits apoptosis signal-regulating kinase-1 (ASK1). ASK1 phosphorylates p38, phosphorylated p38 leads to transcription of nNOS and subsequent increased production of nitric oxide (NO) which can spontaneously react with superoxide anion to form peroxynitrite (Raoul et al., 2002). Peroxynitrite can be responsible for irreversible damage to complexes I and II of the respiratory chain, ensuing inhibition of ATP synthesis and eventual release of cytochrome c from the

mitochondria. Cytochrome-c can activate Caspase-3 leading to apoptosis. Peroxynitrite itself at high enough concentrations within the cell can cause lipid peroxidation, protein oxidation and nitration, inactivation of enzymes and necrotic cell death (Novo and Parola, 2008).

Cell-type dependent differences in Fas signaling have been reported extensively in non-neuronal cells. Fas activation in type I cells leads to DISC formation, activation of Caspase-8 followed by activation of Caspase-3, and subsequent apoptosis, independent of mitochondrial function. Fas activation in type II cells involves Caspase-8; however Caspase-3 is activated as a result of cytochrome c release from the mitochondria. The discovery of the MN-specific Fas signaling pathway has lead to development of a third classification, type III cells. MN-death induced by Fas activation involves both the FADD/Caspase-8 and the Daxx/Ask1/p38/nNOS pathways. Blocking either of these pathways separately in cultured MN after treatment with Fas agonist produced no or minimal protection against cell death. However, blocking the pathways with both Caspase-8 and nNOS inhibitors provided complete protection of Fas-induced cell death. Unlike in MN, blocking only Caspase-8 provided complete protection of Fas-induced cell death in cortical neuron culture. Fas activation in type III cells or MN requires co-activation of Caspase-8 and p38 with subsequent nNOS transcription in order to induce cell death. This additional level of control of the Fas pathway may be a way to protect

these essentially irreplaceable neurons from the common Fas-induced cell death (Raoul et al., 2002).

Discovery of the novel Fas pathway in MN lead to investigation of Fas involvement in the MN degenerative disease, ALS. SOD1 MN cultured from three SOD1 ALS mouse models showed a 10- to 100-fold increased sensitivity to Fas-induced cell death compared to WT MN. In addition, exogenous NO produces no cell death in WT MN, therefore NO alone is not sufficient to trigger MN death. SOD1 MN culture subjected to exogenous NO triggers as much as 50% cell death (Raoul et al., 2002). Further investigation using SOD1 MN cultures revealed a NO-triggered feedback loop not present in WT MN. In response to exogenous NO, SOD1 MN upregulate membrane-bound FasL which is able to activate Fas via *cis* receptor activation (**Figure 10**). In addition, ASK1 has been shown to be solely responsible for activation of p38 in response to Fas-induced MN cell death (Raoul et al., 2002).

Further support for this feedback loop was found in pre-symptomatic spinal cords of both $SOD1^{G93A}$ and $SOD1^{G85R}$ mice, with two-fold higher FasL-positive MN as well as an increase in Daxx. SOD1 mice crossbred with transgenic mice expressing a dominant negative form of Daxx, lead to a 36% reduction in FasL-positive MN. Increased levels of ASK1 and increased activation of p38 have been found in spinal cords of SOD1 mice (Hu et al., 2003). The NO trigger for this feedback loop, NO, is produced by MN, microglia, and activated astrocytes. Evidence has lead to a proposed model in which

chronic cycling of a Fas feedback loop in SOD1 mice, leads to accumulation of signaling molecules overtime and eventually leading to MN-specific degeneration (Raoul et al., 2006).

Treatments against the Fas feedback loop *in vivo* have provided further support for this model. SOD1 mice were treated with Fas small interfering RNA (siRNA) at the beginning of the symptomatic stage for four weeks. Results of the treatment were dramatic; 52% reduction of Fas-positive MN in spinal cord, reduction of nNOS and activated p38, and complete blocking of activated Caspase-8, compared to non-specific siRNA-treated SOD1 mice. In addition, increased survival of spinal MN and axons, delay of motor deficit onset by 21 days and increased survival of Fas siRNA treated mice by 18 days (Locatelli et al., 2007). Treatment of pre-symptomatic SOD1 mice for 10 days with a new, highly selective and specific nNOS inhibitor, AR-R 17,477, prolonged survival for 22 days (Facchinetti et al., 1999). Lithium, a well-known anti-apoptotic agent, has been found to delay ALS progression in human patients. (Shin et al., 2007) used a combinatorial treatment of Lithium and Neu2000 in pre-symptomatic mice. Neu2000 is a novel antioxidant and alone treatment in pre-symptomatic SOD1 mice resulted in a decrease of reactive oxygen species (ROS) in the spinal cord. Lithium treatment alone completely blocked upregulation of Fas and several downstream mediators. When the treatments were combined in pre-symptomatic SOD1 mice, the beneficial effects were additive. Improvements were seen in motor strength and coordination, delay of

symptom onset by 23 days, and extended survival of the mice by 18 days. The dual treatment showed its greatest additive effect on MN survival, at near end-stage disease 74% of MN in the spinal cord of control mice underwent degeneration. SOD1 mice treated with Lithium or Neu2000 alone showed significantly reduced MN cell loss (57 and 58%) but in combination degeneration was reduced to only 17%. This combinatorial treatment strategy is thought to block the NO and Caspase-8 pathways of Fas-induced MN death, further providing support for the Fas pathways implicated in SOD1 MN degeneration (Shin et al., 2007).

To date, genes or proteins involved in the Fas pathway have not been evaluated in the facial nerve axotomy model.

iii. Shared factors genes:

a. FADD. FADD is considered a promiscuous adapter protein capable of binding to the DD of Fas or TNFR1 via recruitment by TRADD. Once bound, it is capable of recruiting other signaling molecules, mainly Caspase-8 (Choi and Benveniste, 2004; **Figures 7** and **9**). For additional details about downstream signaling, refer to Section K.e.i and ii within this Chapter. While FADD has not been evaluated in the facial nerve axotomy model, FADD mRNA expression is increased within the symptomatic SOD1 spinal cord.

b. Caspase-3. Details on Caspase-3 can be found throughout Section e and **Figures 7, 8, 9** and **10.** Caspase-3 mRNA has been shown to be upregulated in the adult

rat facial motor nucleus after facial nerve axotomy within 24 hours and was still increased compared to uninjured control nucleus at the last time-point of 14 dpo. Although a dramatic increase in Caspase-3 mRNA was established after axotomy, no activated form of Caspase-3 was found (Vanderluit et al., 2000). Increased Caspase-3 mRNA has been shown in SOD1 spinal cord during the symptomatic stage and additionally, it has been localized to SOD1 MN and glial cells within the lumbar spinal cord (Hensley et al., 2002; Ando et al., 2003).

c. Caspase-8. Details on Caspase-8 can be found throughout Section e and **Figures 7, 8, 9** and **10.** Caspase-8 mRNA is upregulated to a greater degree in the WT VL compared to the VM and was similar to results from the SOD1 where expression was significantly upregulated in the VL subnucleus compared to the VM (Mesnard et al., 2010; Mesnard et al., 2011). Within the whole facial motor nucleus axotomy also results in upregulation of Caspase-8 mRNA, however percent expression levels compared to control nucleus, across the time course are relatively similar except for 14 dpo, where SOD1 expression is significantly less (Mesnard et al., 2011). Increased Caspase-8 mRNA has been shown in SOD1 spinal cord during the symptomatic stage (Hensley et al., 2002).

L. Significance

ALS is the most common adult MN degenerative disease and with a mean survival of only 3-5 years after onset, it is rapid and fatal. Since 90% of cases are

sporadic there is no forewarning of the disease which blindsides patients and their families. With no suitable treatments to significantly extend the lives of patients more than 4 months, it is overwhelmingly clear that new, novel research approaches must be considered to improve our understanding of disease mechanisms and determine checkpoints for therapeutic intervention.

Based on the literature, an axonal die-back process likely leads to the MN degeneration see during SOD1 disease progression. While the initial pathological event that results in the target disconnection is unknown, understanding the mechanism of MN degeneration and the lack of neuroprotection are important. We have shown that facial nerve axotomy in the pre-symptomatic SOD1 mouse results in dramatic FMN loss. Therefore, regardless of how the SOD1 MN are disconnected from target, they are unable to maintain WT survival levels. Facial nerve axotomy in the pre-symptomatic SOD1 mouse will help elucidate mechanisms important in disease progression. The experiments performed throughout this dissertation support that facial nerve axotomy in the pre-symptomatic SOD1 mouse can be used as a model for SOD1 disease progression.

Use of a simple facial nerve axotomy in the pre-symptomatic stage results in a standardized time course to study molecular mechanisms involved in neurodegeneration following target disconnection which is considered to the initial event leading to MN death seen during disease. This model will also be useful for

assessment of therapeutic compounds and treatments for ALS. Their effects on the molecular expression and FMN survival will provide specific information on their mechanism of actions and beneficial properties. Finally, the development of the facial nerve axotomy model in the pre-symptomatic SOD1 mouse, experiments performed within the dissertation have already revealed the strengths of this model in uncovering and identifying several potentially dysregulated molecular mechanisms initiated by target disconnection that are not seen in the WT.

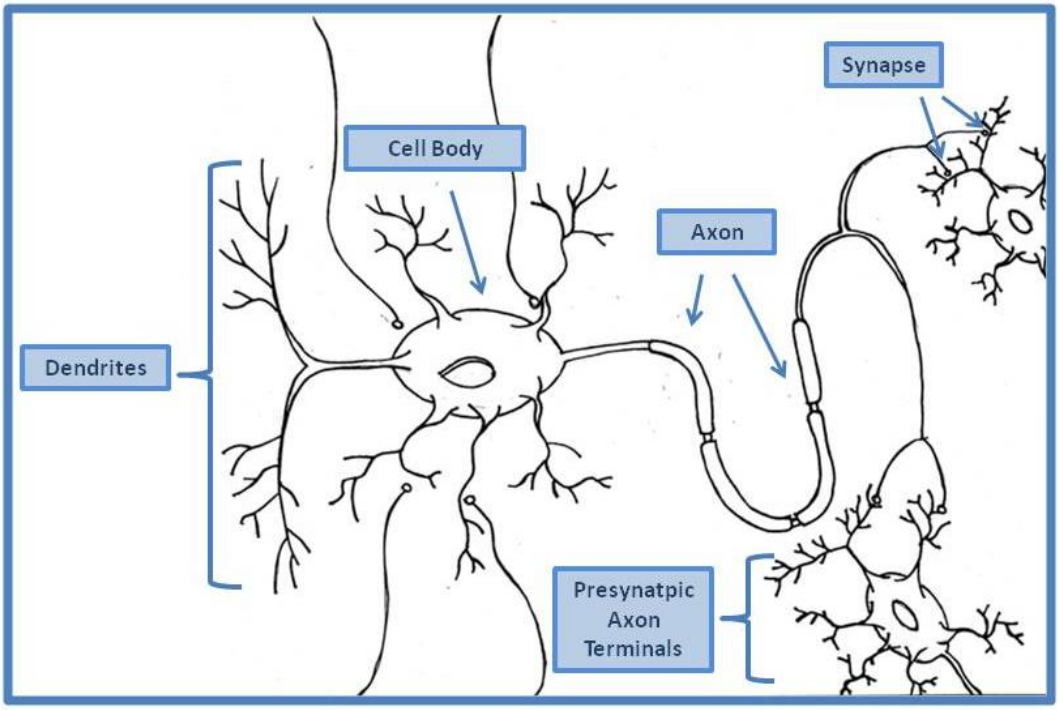

Figure 1. General illustration of a neuron.

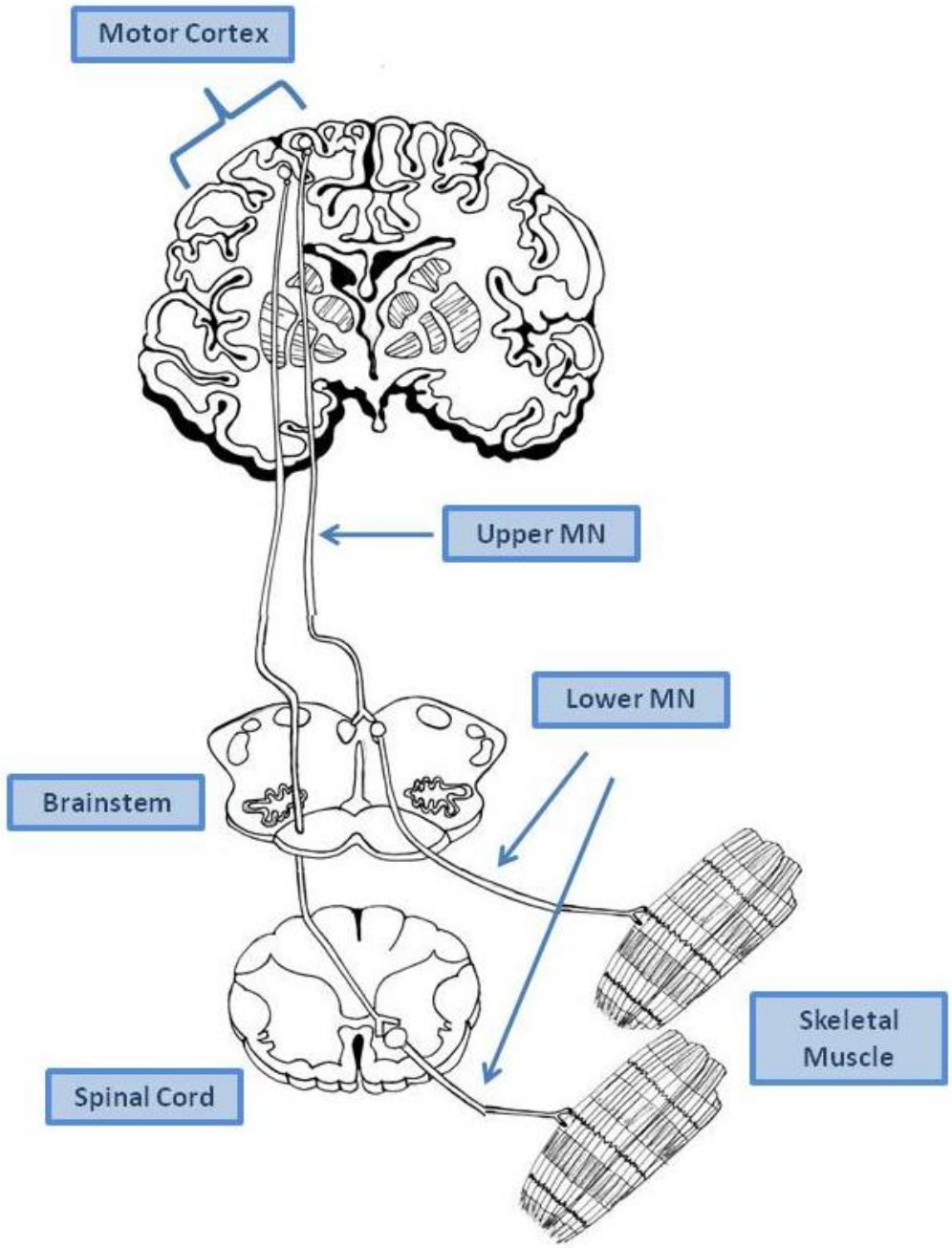

Figure 2. Illustration of general motor pathways involved in transmitting motor signals from the motor cortex of the brain to the target skeletal musculature.

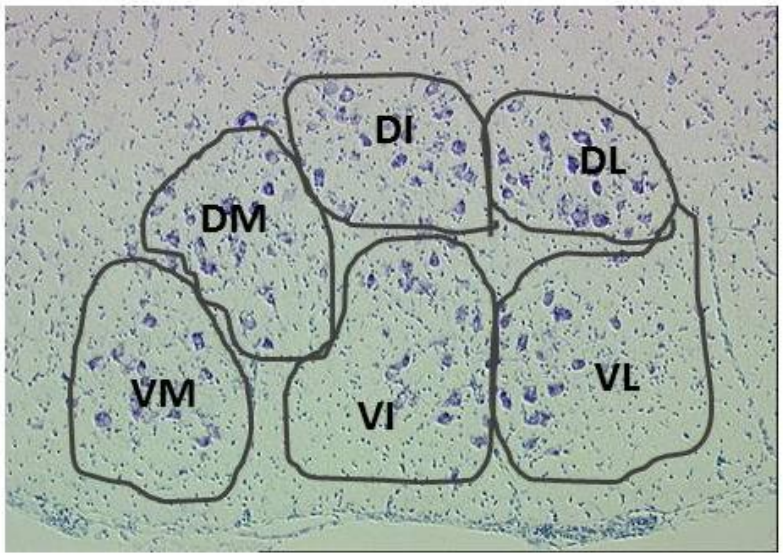

Figure 3. Distribution six of facial motor subnuclei. Representative photomicrograph of thionin-stained facial motor nucleus superimposed with a template to identify the facial motor nucleus subnuclei. Adapted from Ashwell, 1982. Original magnification 20X.

Subnuclei of the Facial Motor Nucleus	Subnuclei Abbreviation	Innervated Muslces of Facial Expression
Dorsomedial	DM	Anterior auricular musculature
Ventromedial	VM	Posterior auricular musculature, lateral portion innervating mentalis and associated protions of platysma
Dorsal Intermediate	DI	Stapedius muscle, posterior belly of digastrics muscle, orbicularis oculi muscle; with ventral portion innervating mentalis and associated protions of platysma
Ventral Intermediate	VI	Mentalis and associated protions of platysma
Dorsolateral	DL	Nasolabial musculature
Ventrolateral	VL	Nasolabial musculature

Table 1. Facial motor subnuclei musculotopic organization. The six facial motor subnuclei, abbreviations, and the muscles they innervate in the mouse (Ashwell, 1982).

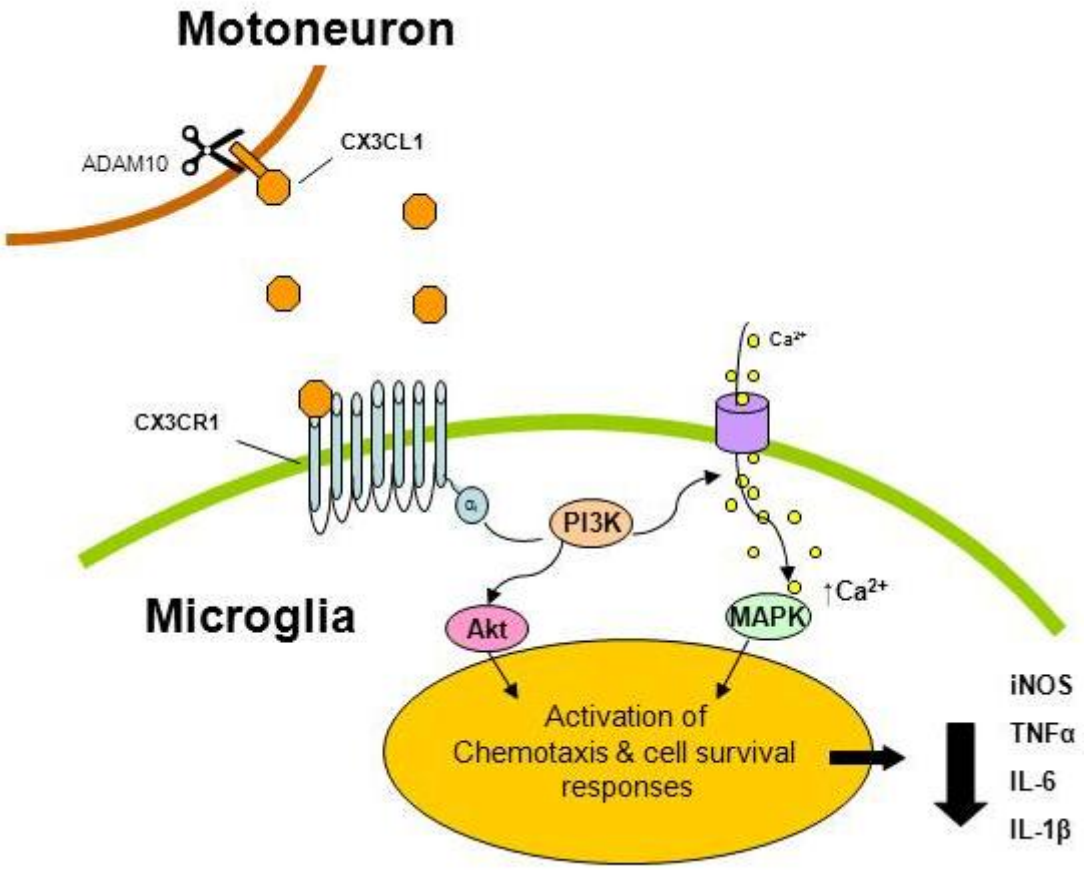

Figure 4. Schematic of CX3CR1 signaling cascade. Adapted from Re and Przedborski, 2006.

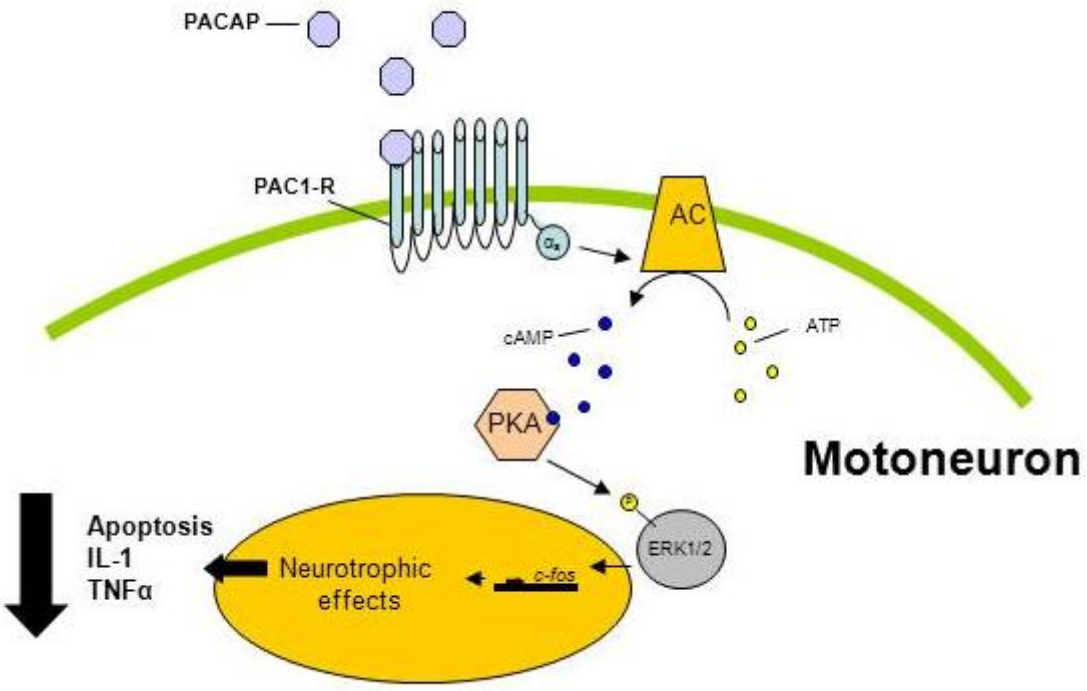

Figure 5. Schematic of PAC1-R signaling cascade. Adapted from Vaudry et al., 2000.

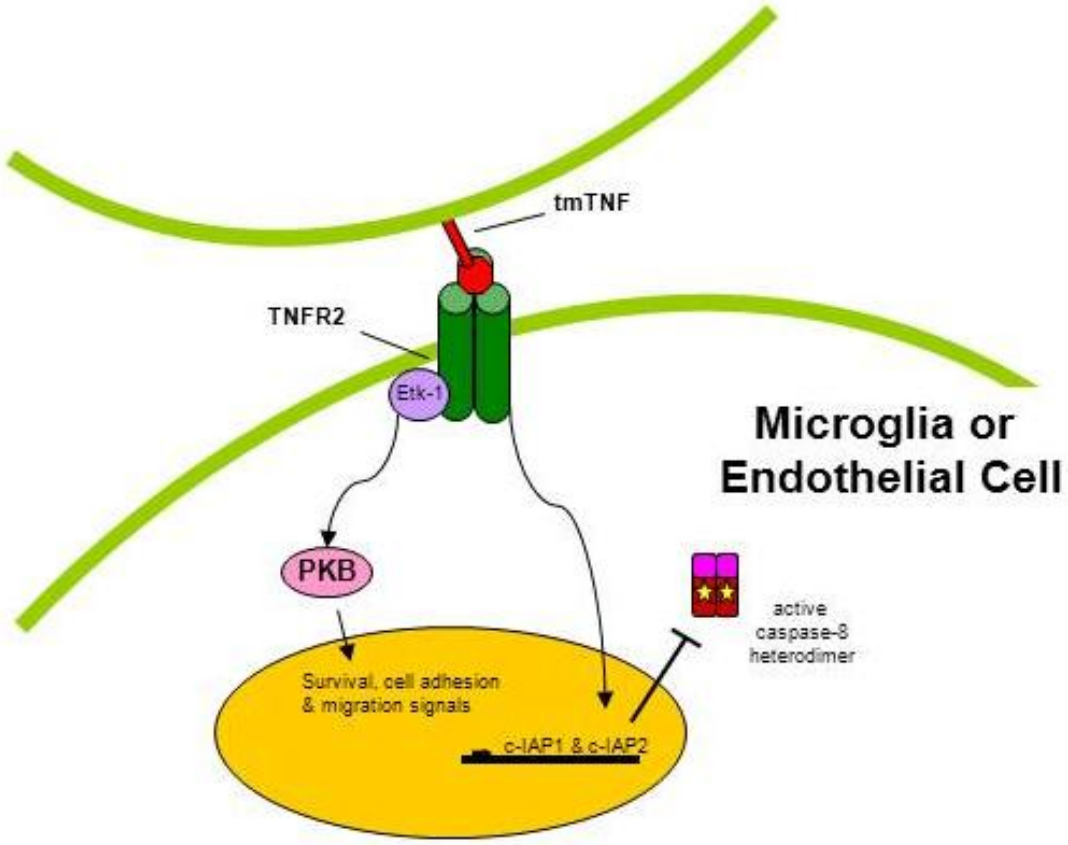

Figure 6. Schematic of TNFR2 downstream signaling cascade. Adapted from Grivennikov and Kuprash 2006; McCoy and Tansey, 2008.

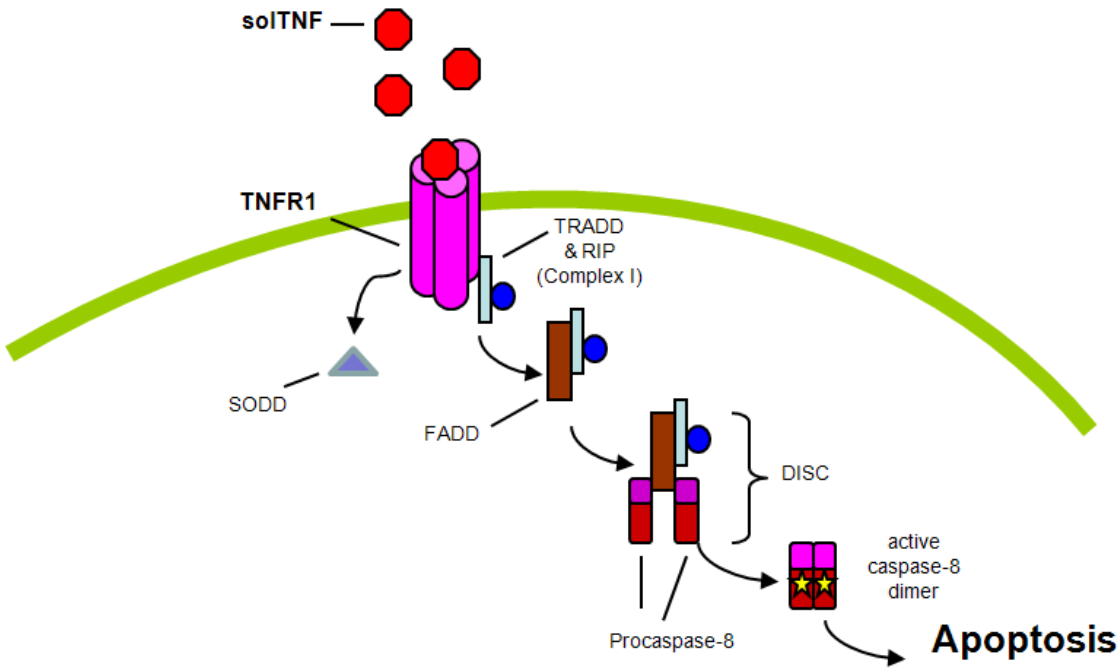

Figure 7. Schematic of TNFR1 downstream signaling cascade. Adapted from Grivennikov and Kuprash 2006.

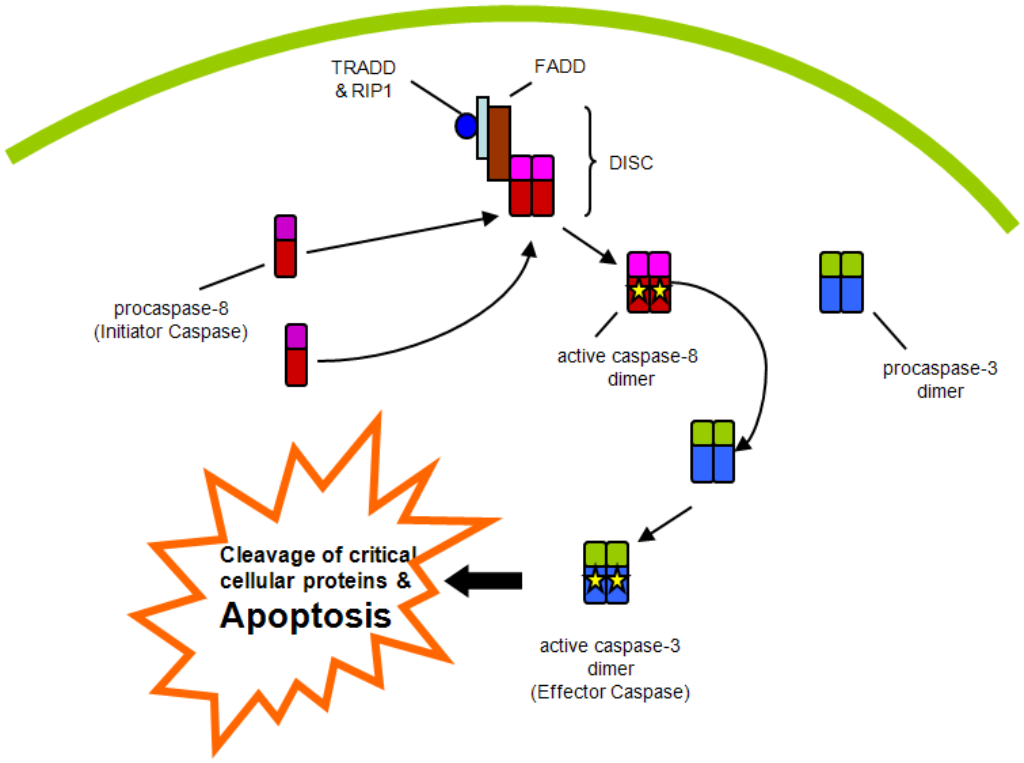

Figure 8. Schematic of Caspase activation. Adapted from Boatright and Salvensen 2003.

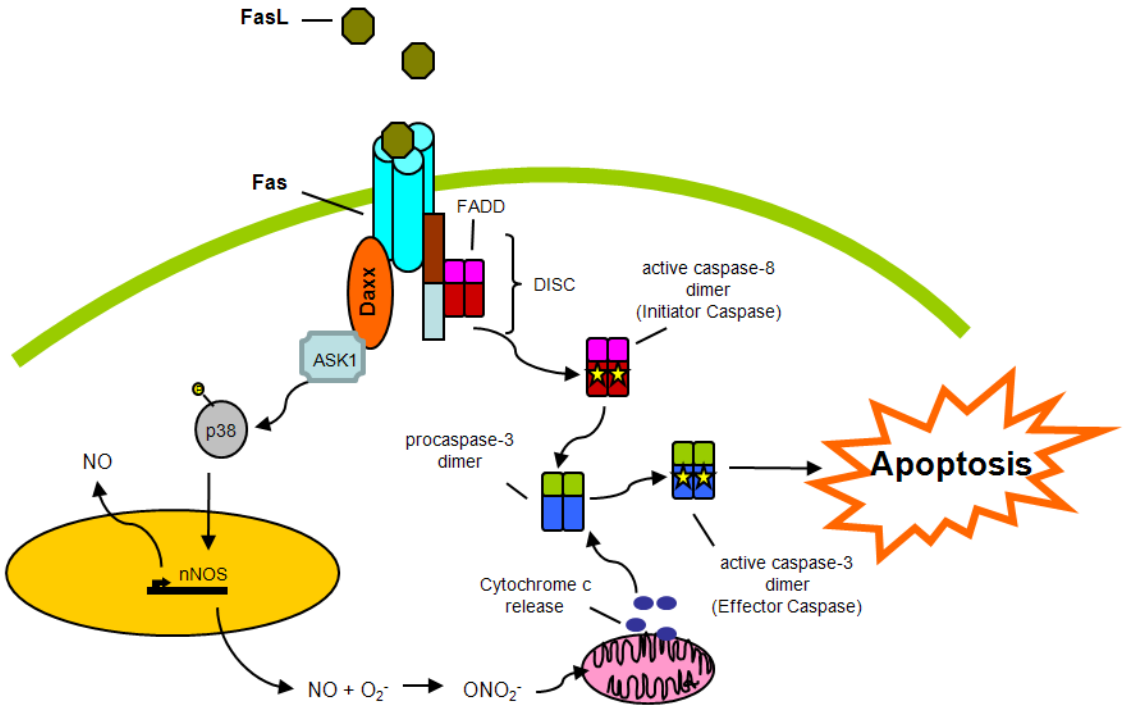

Figure 9. Schematic of Fas downstream signaling. Adapted from Grivennikov and Kuprash 2006; Boatright and Salvensen 2003; and Raoul and Estevez 2002.

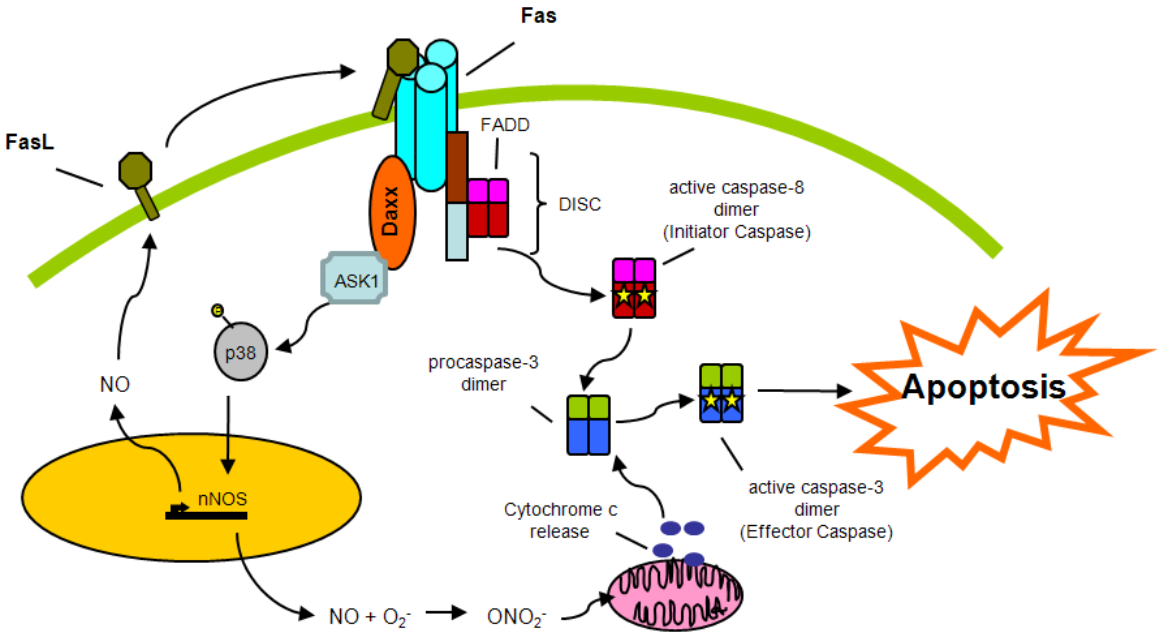

Figure 10. Schematic of SOD1 MN-specific Fas feedback loop. Adapted from Grivennikov and Kuprash 2006; Boatright and Salvensen 2003; and Raoul and Buhler 2006.

Gene	General Function	Expression after Axotomy	Increased Expression in SOD1 Mouse and/or ALS Patients
TNFR1 Death Receptor Signaling			
TNFR1	Death Receptor	Unknown	Increased in ALS patients & SOD1 mouse
TNFα	Pro-inflammatory cytokine, ligand for TNFR1 & TNFR2	Induction of mRNA	Increased in ALS patients & SOD1 mouse
TRADD	Adapter protein of TNFR1	Unknown	Baseline expression in SOD1 mouse
TRAF2	Associated factor of TNFR1	Unknown	Unknown
SODD	Regulatory Fas	Unknown	Unknown
Fas Death Receptor Signaling			
Fas	Death Receptor	Unknown	Increased in SOD1 mouse
FasL	Ligand for Fas	Unknown	Increased in SOD1 mouse
Daxx	Adapter protein of Fas	Unknown	Increased in SOD1 mouse
ASK1	Kinase downstream of Fas	Unknown	Unknown
nNOS	Downstream of Fas, enzyme, NO production	Unknown	Increased in ALS patients & SOD1 mouse
Shared Factors of TNFR1 & Fas Death Receptors			
FADD	Adapter protein for TNFR1 or Fas	Unknown	Increased in SOD1 mouse
Caspase-8	Initiator Caspase, downstream of TNFR1 and Fas signaling	Increased mRNA	Increased in SOD1 mouse
Caspase-3	Effector Caspase, downstream of TNFR1 and Fas	Increased mRNA in Rat	Increased in SOD1 mouse
Neurodegenerative Signaling Gene			
CRMP4	Inhibition of neurite outgrowth and cell death in MN	Unknown	Silencing CRMP4a mRNA is protective in SOD1 MN
Neuroprotective Signaling			
TNFR2	Receptor localized to microglia, mediates cell survival	Unknown	Increased in ALS patients & SOD1 mouse
PAC1-R	Receptor mediates neuroprotection	Decreased mRNA in Rat	Unknown
CX3CR1	Receptor mediates microglia chemotaxis	Increased mRNA	$SOD1^{G93A}$/$CX3CR1^{-/-}$ transgenic mice show decreased survival
Neuroregenerative, MN-Specific Genes			
GAP-43	Component of axonal growth cones during regeneration	Increased mRNA	Increased in ALS patients & SOD1 mouse
βII-Tubulin	Cytoskeletal protein, axonal elongation and regeneration	Increased mRNA	Unknown
Glial-Specific Genes			
GFAP	Cytoarchitecture of Astrocytes, marker for activated Astrocytes	Increased mRNA	Increased in ALS patients & SOD1 mouse
CD68	Monocyte/macrophage marker for activated Microglia	Unknown	Increased in ALS patients & SOD1 mouse

Table 2. Genes differentially regulated by axotomy or ALS/SOD1 disease progression.

CHAPTER III

MATERIALS AND METHODS

A. Animals

Rodents used in the experiments described in this dissertation were mice purchased from Jackson Labs (Bar Harbor, ME) at seven weeks of age. The WT mouse strain used for the experiments in this dissertation was the C57BL/6 (stock #000664). The C57BL/6 WT mouse was the first to have its genome sequenced and is the most widely used inbred strain (http://jaxmice.jax.org; Waterston et al., 2002). For the past decade our laboratory has been using the C57BL/6 WT mouse in researching the mechanism of neuroprotection following peripheral nerve injury (Canh et al., 2006; Hashiguchi et al., 1992; Serpe et al., 2005; Beahrs et al., 2010; Xin et al., 2011). In a recent study, we observed regenerative and degenerative molecular phenotypes of MN and neuropil in the facial motor nucleus after axotomy using laser microdissection to obtain RNA followed by quantification of mRNA expression (LMD; Mesnard et al., 2010). Therefore, it was important to continue using the C57BL/6 WT, as results from experiments in this dissertation contribute to the overall understanding of how molecular mechanisms mediate neuroprotection or neurodegeneration after nerve injury. The ALS mouse model used was the $SOD1^{G93A}$ mouse (stock #002726) on a non-uniform background consisting of a mixture of SJL and C57BL/6J called a hybrid

background (Leitner et al., Jackson Labs). The B6SJL SOD1^{G93A} was the first ALS mouse model developed and therefore has been the most widely used and well-characterized (Gurney et al., 1994). In order to ensure that differences in mRNA expression were not due to strain, B6SJLF1/J WT (stock #100012) were assessed for mRNA expression at two time-points. The mRNA expression within the control nucleus and percent change following axotomy were compared between the two WT strains at 7 and 28 dpo (data not shown). No strain difference in mRNA expression within the facial nucleus before or following axotomy has been shown previously in our laboratory (Mesnard et al., 2011). For the remainder of this dissertation, C57BL/6 WT mice will be simply referred to as WT, unless specific background strain differs, then the strain will be indicated.

All mice used in this dissertation were female mice. Our laboratory has consistently used female mice mainly because of the research focus of neuroprotective effects of the immune system. Mice are social animals and prefer group housing. However, males in small cages can often display aggressive behavior. Fighting between two males could potentially disrupt surgical wounds and increase inflammation. Potential infections or inflammatory responses due to fighting could distort results. Additionally, many of our previous experiments required reconstitution or adoptive transfer of immune cells from one mouse to another. It has been well established that the male specific H-Y antigen can cause to an immune response of the syngeneic transfer and can lead to rejection (Gordon et al., 1975). Therefore, female mice have

always been used in our laboratory (Canh et al., 2006; Hashiguchi et al., 1992; Serpe et al., 2005; Beahrs et al., 2010; Xin et al., 2011).

All manipulations and housing were performed in accordance with institutional and the National Institutes of Health guidelines on the care and use of laboratory animals for research purposes and approved by the Institutional Animal Care and Use Committee (IACUC). Mice were housed under a 12 hour light/dark cycle in autoclaved microisolator cages under social conditions (three – four mice per cage) and provided autoclaved pellets and autoclaved drinking water at libitum. The facility that housed the mice was equipped with a laminar flow system in order to maintain a pathogen-free environment. All mice were permitted one week to acclimate to the environment prior to any manipulations or surgical procedures.

B. Surgical Procedures

Surgical procedures were performed using aseptic technique and completed in accordance with the National Institutes of Health guidelines on care and use of laboratory animals for research purposes and approved by the IACUC. All mice were 8 weeks of age at time of surgery and all surgeries took place approximately 6 hours into the daily light cycle. Prior to all surgical procedures, mice were fully anesthetized with 3% isoflurane inhalation and maintained at 2% isoflurane throughout the procedure. Mice were monitored while under anesthesia by assessing reflexes such as toe-pinch and eye blink and visually observing respiration rate. The skin behind the right ear was

prepared for surgery by removing fur with a straight razor and sterilizing the area with 70% ethanol (ETOH). A 5 mm incision was made behind the right ear and the muscles gently separated with forceps to expose the facial nerve. The right facial nerve was exposed at the level of the SMF and the facial nerve was completely transected with iridectomy scissors proximal to the bifurcation of the posterior and anterior auricular branches, as described previously (Whitehouse et al., 1985; Powrie and Mason, 1989). The proximal and distal facial nerve stumps were carefully positioned apart to discourage reconnection. Following the surgery, the separated muscles were re-apposed and the skin was sealed with a wound clip. Maximum duration of procedure was 15 minutes. Mice were monitored after surgery and were considered recovered from anesthesia when they could walk with a normal gait. Successful transections were verified by complete, unilateral loss of vibrissae movement and eye blink reflex on the ipsilateral side. The left facial nerve remained intact and served as an internal control for comparison purposes. Additional post-operative monitoring was performed by daily visual inspection. Wound clips were removed 7-10 days following surgery.

C. Animal Euthanasia and Brain Harvest

At the time of euthanasia mice were again assessed for vibrissae movement and eye blink reflex on the ipsilateral side to verify maintenance of the facial nerve transection. Euthanasia time-points varied by experiment and were as follows; 3, 7, 14, 28 and 56 dpo. The mice were euthanized by CO_2 asphyxiation in an isolated chamber

followed by cervical dislocation. After which the brains were immediately removed from the skull and rapidly frozen in a bi-phasic solution containing *n*-butyl bromide (62.5%) and 2-methyl-butane (37.5%) for five minutes at -30^{o}C. Brains were individually stored at -80^{o}C until cryosectioned.

D. Cryosectioning

Prior to cryosectioning brains were allowed to warm from -80^{o}C to -20^{o}C for one hour to reach optimal temperature. The cryostat used was a Leica CM1850UV which uses an ultraviolet (UV) light as an additional measure to minimize contamination. The brains were mounted and embedded on frozen brain chucks using an OTC compound and allowed to solidify at -20^{o}C for 15 minutes. Twenty five µm coronal sections were collected throughout the rostral-caudal extent of the facial motor nucleus. Precise location and symmetry between the control and axotomized nuclei were verified by presence of the nucleus ambigiouus rostral to both facial nuclei and the internal genu of the facial nerves at the caudal end of the facial nuclei. Tissue sections were thaw-mounted onto Superfrost Plus glass slides (Fisher) for thionin staining or glass polyethylene (PEN) foil-membrane slides (Leica) for LMD. All slide-mounted tissue sections were stored at -80^{o}C in slide boxes until fixation and staining.

E. Thionin Staining and FMN Counts

Slide-mounted tissue sections intended for FMN survival counts were removed from -80^{o}C storage and allowed to acclimate to room temperature for one hour. The

tissue sections were then fixed in freshly prepared 4% paraformaldehyde (PFA) in phosphate buffered saline (0.01 M PBS; pH 7.4) for 15 minutes. The slides were rinsed twice for 5 minutes with deionized (DI) water then stained with 1X working thionin solution for 7 minutes. The 1X working thionin solution was prepared by combining 200 mL of NaAc/HAc working buffer at pH 3.5 (20 mL 1M sodium acetate (NaAc) and 180 mL 1M glacial acetic acid (HAc)), 560 mL of DI water, and 38 mL of 10% thionin in DI water. Tissue sections were rinsed for 30 seconds in DI water then dehydrated in a graded ETOH series for 30 seconds each (50%, 70%, 95%, 100%, respectively). The tissue sections were cleared overnight in Hemo-de followed by coverslipping using Permount mounting media. Two days of drying took place before slides labels were covered and coded by another investigator unaware of group divisions. This technique allows for analysis of FMN survival to occur under “blind” conditions.

Light microscopy and the Neurolucida Tracing System were used to visualize MN and trace the sections. MN within the facial motor nucleus were identified by their morphology, displaying a clear nucleus and nucleolus, and were demarcated with a symbol using the tracing system. Subnuclei MN were not counted in any of the experiments within this dissertation. All sections were counted for the each animal to determine the number of FMN within the control nucleus compared to the axotomized nucleus for two time-points, 28 and 56 dpo or 84 and 112 doa, respectively.

Percent of FMN survival for the facial nucleus was calculated by dividing the total number of MN remaining in the axotomized nucleus by the total number of MN in the WT 28 dpo (84 doa) control nucleus, then multiplying by 100. This was done because at the 56 dpo time-point, or 112 doa, the SOD1 mice are well within the symptomatic stage and display MN cell loss within the control nucleus. Using total numbers of MN from a control facial nucleus with MN loss to calculate percent FMN survival would not accurately portray the FMN loss due to axotomy. Therefore, MN numbers from the WT 28 dpo (84 doa) control nucleus were used and, for consistency purposes, the WT 56 dpo percent FMN survival was calculated in the same manner as the SOD1 28 and 56 dpo. At 84 doa there are no differences in the number of FMN between WT and SOD1 mice. This data as well as further analysis of FMN loss which occurs during SOD1 disease progression can be found in Chapter V.

Average number of FMN per section was determined for the uninjured control facial motor nucleus and was calculated by counting the total number of MN within the control nucleus and dividing by the number of sections counted for that mouse.

To compensate for double counting MN in adjacent sections, the Abercrombie correction factor [$N = (n \times T) \div (T + D)$], where N is the actual number of cells, n is the number of nuclear profiles, T is the section thickness (25 µm), and D is the average diameter of nuclei (5 µm) was used (Coggeshall, 1992).

F. Laser Microdissection

The technique LMD was used to accurately collect tissue from the facial motor nuclei. A Leica AS LMD microscope equipped with a UV laser controlled manually was used to perform two different dissections previously described in detail (Mesnard et al., 2010). The first involved dissecting the whole facial nucleus, both control and axotomized; while the second involved dissecting out the VM and VL facial subnuclei of both control and axotomized nuclei. The two subnuclei were identified by utilizing a template adopted from Ashwell, 1982 and modified by our laboratory (Canh et al., 2006). Slide-mounted tissue sections intended for RNA analysis were removed from -80^{o}C storage and allowed to warm within their sealed slide boxes to -20^{o}C for one hour. Each PEN foil-membrane slide contained 8-10 coronal sections and great care was taken throughout the procedure to minimize contamination or RNA degradation. Each side was removed from the slide box at -20^{o}C, rapidly fixed and stained with thionin for histological identification of specific regions. The slides were fixed in 100% ETOH for one minute, washed twice for 15 seconds in 0.01% diethylprocarbonate (DEPC)-treated DI water then stained for 35 seconds in a 2X working thionin solution. The 2X working thionin solution was prepared by combining 200 mL of NaAc/HAc working buffer at pH 3.5 (20 mL 1M NaAc and 180 mL 1M HAc), 522 mL of 0.01% DEPC-treated DI water, and 76 mL of 10% thionin in 0.01% DEPC-treated DI water. Tissue sections were again rinsed twice for 15 seconds in 0.01% DEPC-treated DI water then dehydrated in a graded ETOH

series prepared with 0.01% DEPC-treated DI water for 30 seconds each (70%, 90%, 100%, respectively). The tissue sections were placed in a covered container to dry for three minutes. Once dry, the slide was placed inverted on the LMD microscope stage for dissection and collection. The process of tissue collection occurs as follows; the tissue section and PEN foil membrane on the slide are cut with the UV laser and immediately the sample falls into one of the designated collection tube caps. Prior to the ETOH fix and thionin staining, the collection caps were each filled with 65 µL of extraction buffer (PicoPure RNA Isolation Kit; Arcturus). LMD tissue samples of the whole facial nucleus resulted in two collection tubes per mouse (control and axotomized), while samples of the VM and VL facial subnuclei resulted in four collection tubes per mouse (control and axotomized sample for each of the two subnuclei).

G. RNA Isolation and Semi-Quantitative Real-Time RT-PCR

Total cellular RNA was isolated from LMD samples of the whole facial motor nucleus or the VM and VL facial subnuclei using the PicoPure RNA Isolation Kit (Arcturus) including a deoxyribonuclease (DNase) treatment step (Qiagen). Total RNA quantification was determined using a NanoDrop 1000 spectrophotometer and the concentrations were standardized for reverse-transcription. Total RNA concentrations for whole nucleus samples averaged 110 ng while VM and VL samples averaged 28 ng. RNA samples for each time-point were standardized together relative to the lowest sample concentration. Complementary deoxyribonucleic acid (cDNA) was obtained

using Superscript First Strand Synthesis System for RT-PCR (Invitrogen) according to the manufacturer's instructions.

Polymerase chain reaction (PCR) primer sets used for amplifying target deoxyribonucleic acid (DNA) sequences were designed from published mouse sequences using Oligo Primer Analysis software version 6.54 (Molecular Biology Insights). The primer sets consisted 16-25 nucleotides each and produced amplicon lengths between 78 and 121 base-pair (bp; **Table 3**). Primers were designed and selected for duplex stability, internal stability, and low complementarity. In general, primers are stable at their 5'-termini, i.e. GC-rich, but somewhat unstable at their 3'-ends function well in PCR. These primers are less likely to initiate false priming on the 3'-end and will require complete annealing along the target sequence in order to prime efficiently. In addition, the optimal annealing temperature (T_A) range is usually broad with unstable 3'-end primers, which is beneficial when selecting parameters for RT-PCR. Formation of primer-dimer artifacts can lead to non-specific DNA synthesis due to an unbalanced primer ratio. Therefore, the 3'-terminal end of a primer should be free of significant complementarity and is analyzed within the Oligo Primer Analysis software for its statistical likelihood of forming primer-dimers (Molecular Biology Insights Handbook). After several primer sets were selected, each individual primer's nucleotide sequence was then examined for regions of local similarity to those within sequence databases using Basic Local Alignment Search Tool (BLAST) provided by the National

Center for Biotechnology Information (NCBI). BLAST compares the nucleotide sequence of interest with all published sequences with NCBI databases and calculates the statistical significance of matches. BLASTing a primer sequence provides a measure of its ability to form a stable duplex with the specific site on the target DNA as well as reveals any false priming sites on the target DNA. Only primer sequences which met all criteria were selected for RT-PCR. Primer sets were custom ordered from BioSynthesis, Inc. However one gene of interest, nNOS did not yield acceptable primer sets when designed with the Oligo Primer Analysis software and was purchased from SuperArray Biosciences (**Table 3**). GAPDH control for nNOS was also purchased from SuperArray Biosciences.

Semi-quantitative real-time RT-PCR was performed using the iCycler iQ detection system (Bio-Rad; Fargo et al., 2008; Sharma et al., 2010; Mesnard et al., 2010). A reaction volume of 25 µL contained 1X SYBR Green PCR Master Mix (Applied Biosystems), 1 µL fluorescein, and 200 nM forward and reverse primers. RT-PCR cycle parameters used are as follows; 10 minute, 95^{o}C denaturing step, followed by three steps, 30 seconds each, repeated for 45 cycles of denaturing at 95^{o}C, annealing at the predetermined annealing temperature (T_A) for the respective primer set, and extension at 65^{o}C. The T_A for each primer set (**Table 3**) was determined experimentally using either whole mouse brain cDNA or mouse spleen cDNA as the template over a temperature gradient based on the T_A estimated by the design software. Immediately after conclusion of the amplification protocol, a melt curve analysis was performed to

verify specificity of the amplified product. The melting temperature (T_m) for each primer set was compared to the experimentally determined value (**Table 3**).

After completion of the PCR run, the threshold cycle (C_T) was determined for each well within the 96-plate. This was accomplished by first manually setting the baseline cycles according to the linear amplification curves. The first baseline cycle was selected as the cycle immediately following the stabilization of relative fluorescence units (RFU) and the last baseline cycle was 2 cycle values before the earliest visible amplification. Next, the threshold value was defined by visualizing the logarithmic amplification curves and placing the threshold line above background signal but within the lower third of the linear phase of the amplification plot. All cDNA samples were run in triplicates and an average C_T was calculated. Relative mRNA expression levels were analyzed using the comparative C_T method also known as the $2^{-\Delta\Delta CT}$, in which the C_T value for a target gene is normalized to the C_T value for the endogenous housekeeping gene or internal standard. The result is the C_T difference or the ΔC_T for a single sample. Next, the difference between two ΔC_T's of a control and axotomized sample yields the $\Delta\Delta C_T$. Since the C_T is determined from a logarithmic scale, $\Delta\Delta C_T$ must be converted to a linear form using the following formula, $2^{-\Delta\Delta CT}$. The housekeeping gene used for all PCR amplification protocols was glyceraldehyde 3-phosphate dehydrogenase (GAPDH) which has been well-established in the as an internal standard for the facial nerve axotomy model for the reason that expression levels do not change with axotomy (Raivich et al.,

1998; Livak and Schmittgen, 2001; Li et al., 2000; Wainwright et al., 2009). For the purposes of determining mRNA expression levels after axotomy, the results are calculated as the percent change relative to the control using the following formula, by $(2^{-\Delta\Delta Ct} -1) * 100$ (Fargo et al., 2008; Mesnard et al., 2010).

H. Electrophoresis

Gel electrophoresis was used identify PCR amplified products for genes induced by axotomy, with below detectable levels of mRNA expression in the uninjured control, namely the gene TNFα. In addition, efficacy of all primer sets used within this dissertation amplicons of their PCR product were analyzed by gel electrophoresis to confirm amplicon size and to identify any non-specific amplification. None of the primer sets revealed any non-specific amplification products and all were confirmed to be appropriate size (data not shown). of a The samples used in the electrophoresis consisted of 12 µL of PCR amplified products extracted from the wells of the 96-well PCR plate and 3 µL nucleic acid sample loading buffer (Bio-Rad). The samples were loaded into wells of Criterion precast 10% Tris Borate Ethylenediaminetetraacetic acid (TBE) gels (Bio-Rad) along with a single 100 bp molecular weight marker (Bio-Rad) and a GAPDH sample as a positive control. Separation of the PCR products was accomplished using a Criterion cell vertical electrophoresis system (Bio-Rad) for 90 minutes at 100 V using 1X TBE running buffer, prepared from 10X TBE nucleic acid electrophoresis buffer (Bio-Rad) and contained 100 µL of SYBR Green I nucleic acid gel stain (Invitrogen). Gels

were scanned on a STORM 860 PhosphorImager (Molecular Dynamics) using Image Quant Software for visualization.

I. Behavioral Assessment

SOD1 mice were evaluated for symptom onset by a series of seven behavioral tests assessing general motor function. Reports of symptom onset vary with the type of motor or behavioral assessments used, even among the B6SJL SOD1^{G93A} model. Therefore, it was necessary to design a behavioral analysis protocol which will provide us with a measure of symptom onset. Development of this protocol has important implications for our laboratories' future research.

Behavioral testing took place three times per week within the animal housing room approximately six hours into the daily light cycle. Behavioral testing began at 70 doa and ended on the day of euthanasia, 112 doa, resulting in 15 time-points. The order in which the mice were tested was rotated, both the order of the cages and the mice within the cages. All behavioral equipment was sterilized after each cage of mice (three per cage) were tested, Versi-Dry bench paper (Fisher) was replaced if soiled by a mouse or after each cage, and gloves were changed after handling each mouse. Individual test scores for each mouse per test were recorded per time-point. A score of zero indicated normal function and higher scores indicated a loss of motor function for the particular task. WT control groups were also tested for baseline motor function. All observations and subsequent scoring are detailed within **Figures 13, 14, 15, 16, 17, 18** and **19**.

The extension reflex (ER) test assesses the ability to engage extensor/anti-gravity muscles in response to suspension by tail (**Figure 13**). Each mouse was suspended by the tail for 5 seconds. Observations on fore- and hind-limb extensions and equivalent test score are listed in **Figure 13** (Feng et al., 2008).

The paw-grip endurance (PGE) test is a measure of appendicular muscular endurance (**Figure 14**; Combs and D'Alecy, 1987, Feng et al., 2008). The lid of the mouse cage is held flat or horizontal and the mouse is lowered onto the lid. Once the mouse grips the lid with all four paws the lid is rotated to a vertical position for five seconds. Capabilities for this task and the corresponding test scores are reported in **Figure 14**.

The balance beam (BB) test is a general test of overall muscle strength and requires suitable vestibular and proprioceptive functioning (**Figure 15**; Feeney et al., 1982; Combs and D'Alecy, 1987; Feng et al., 2008). This test not only assesses the ability of the mouse to remain on the beam but also lift itself onto the beam. The mouse is carried over to the middle of the beam while suspended by its tail. Near the beam the mouse is lowered to a level so that the body of the mouse is level with the height of the beam. The mouse reaches for the beam with the forepaws and once the beam is gripped the suspension level of the mouse by the tail is reduced, requiring the mouse to pull itself onto the beam using the forelimbs followed by engaging of the hind-limbs to lift its body onto the beam. Once on the beam the mouse must remain, balancing on the beam without falling off for five seconds. All mice tested automatically began walking

once on the beam. Test scores are listed in **Figure 15**. Mice unable to lift their body onto the beam were physically placed onto the beam to assess the second part of the test, the ability to balance on the beam itself; however the test score reflected the inability to complete the first task.

For the remaining behavioral tests, mice were placed in a transparent rat box with clean Versi-Dry bench paper lining the bottom. Four behavioral assessments took place in box, the open field tail elevation (OF-TE) test (**Figure 17**), the open field exploratory behavior (OF-EB) test (**Figure 16**), the open field complete rearing behavior (OF-CRB) test (**Figure 18**), and the open field gait analysis (OF-GA) test (**Figure 19**). Mice remained within the box for a maximum of two minutes or until all four test scores could be determined. The minimum amount of time in the box was one minute, regardless of how fast the mouse completed all four tasks. The OF-TE test assesses the level of elevation of the tail during forward movement. Normally, mice hold their tail straight or slightly elevated while moving. This action uses muscles at the base of the tail innervated by coccygeal MN (Shinohara, 1999). Holding the tail at a position less than horizontal during normal forward movement resulted in a test score greater than zero. See **Figure 17** for observations and subsequent test scores.

OF-EB test is routinely used as a measure of anxiety and it is based upon a rodent's natural tendency to move along side walls when anxious (Schneider et al., 2005). Anxiety itself can also be considered a feature of sickness behavior. The criteria

for maintaining a score of zero did not necessarily require the mice to enter the center of the field, but required them to explore all four corners within two minutes. Therefore, the OF-EB test assessed whether mice displayed anxiety or sickness behavior that resulted in them not exploring the four corners of the box. Test scores for exploring specific numbers of corners are listed in the table in **Figure 16**.

The OF-CRB test evaluates the weight bearing ability of the hind-limbs during rearing behavior (**Figure 18**). Fortunately, rearing or standing upright on the hind-limbs at the walls of the open field box was a frequent and consistent behavior of all mice tested. It was a rare occurrence when mice did not perform this behavior at least twice within two minutes. Ability of mice to completely extend the hind legs while stretching up in a rearing position at the wall was easily observed and recorded. Their determination to perform this behavior was so great that even a severe loss of motor control and inability to bear weight on the hind-limbs did not deter them from attempting it. **Figure 18** lists the test scores corresponding observations.

The OF-GA test assesses gait, motility and posture (**Figure 19**). Mice were observed during forward movement for hind-limb gait, stride, and hind foot placement. Gross, abnormal movements were recorded, such as circumduction of the hind-limbs. Any impairment in forward movement by motor control was also recorded. Observations and their equivalent test scores are listed in **Figure 19**.

The sum of all seven test scores for one mouse per time-point was called the motor score. The motor scores of all mice per time-point were averaged and plotted to show the loss of motor control over time. Symptom onset was determined to be the time-point in which the averaged motor scores were statistically higher than the previous. Once symptom onset was determined for the entire group of SOD1 mice, each individual mouse's motor score per time-point was averaged from symptom onset until 112 doa. This average motor score during the symptomatic stage was used to split the SOD1 mice into two different disease progression groups, a slow disease progression group (SPG) and a fast disease progression group (FPG). The rates of disease progression or the rate of increasing motor scores over time for the SPG and FPG was plotted.

J. Statistical Analysis

The relative mRNA expression was statistically compared using a two-way analysis of variance (ANOVA; group x time), followed by the Student-Newman-Keuls multiple comparison post-hoc test, with significance at $p \leq 0.05$ (GB-Stat School Pak; Sharma et al., 2010).

Statistical analysis of the FMN survival used a two-way ANOVA (group x time), followed by the Student-Newman-Keuls multiple comparison post-hoc test, with significance at $p \leq 0.05$ (GB-Stat School Pak).

Symptom onset was determined by statistically comparing average motor scores between two sequential time-points using a repeated measures ANOVA, then the

Student-Newman-Keuls multiple comparison post-hoc test, with significance at $p \leq 0.05$ (GB-Stat School Pak). The group of symptomatic SOD1 mice were divided into the two disease progression groups (SPG and FPG) by using a median-split of all individual motor scores averaged throughout the symptomatic stage.

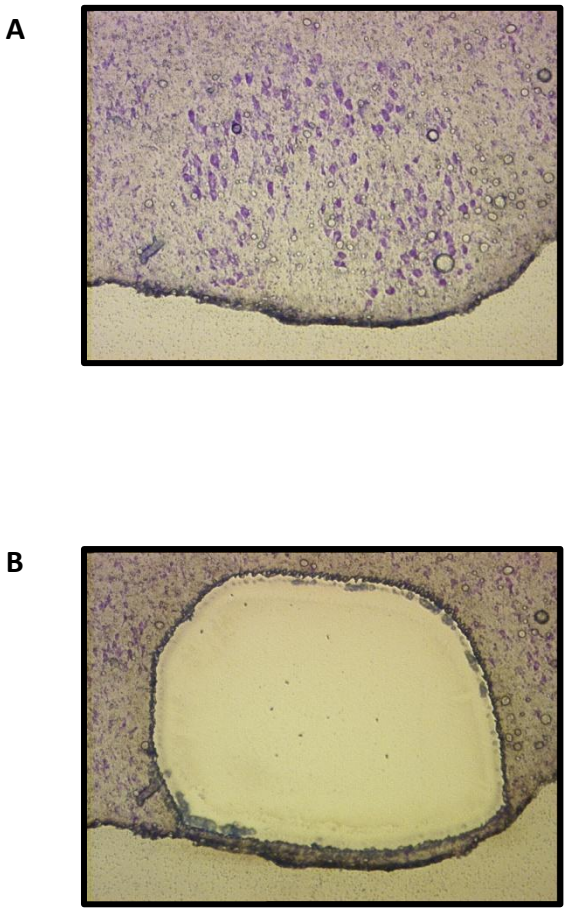

Figure 11. LMD of whole facial motor nuclei. Representative photomicrographs depicting thionin-stained coronal sections for LMD of the axotomized facial motor nuclei. **A**, Coronal section displaying facial axotomized motor nucleus. **B**, Near complete LMD of axotomized facial motor nucleus. Original magnification 20x.

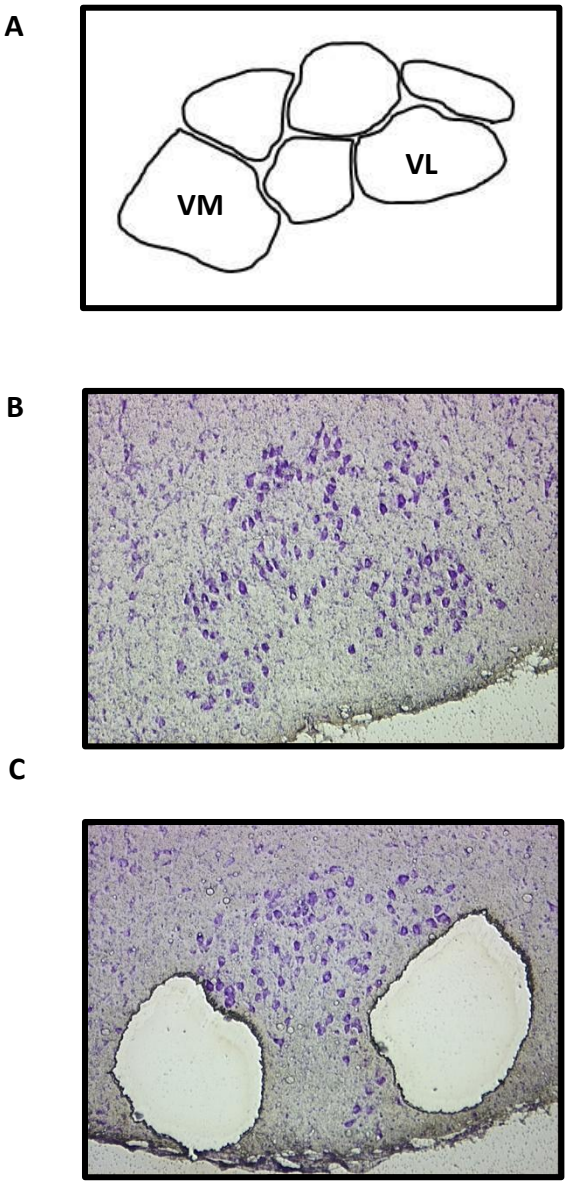

Figure 12. LMD of VM and VL subnuclei. Representative photomicrographs depicting thionin-stained coronal sections for LMD of the VM and VL subnuclei. **A**, Template of facial motor subnuclei. **B**, Coronal section displaying facial axotomized motor nucleus. **C**, Complete LMD of axotomized VM and VL subnuclei. Original magnification 20x.

Extension Reflex (ER) Test

Test Score	**Observations**, 5 sec duration
0	normal forelimb and hind-limb stretching
1	normal forelimb stretching, only partial hind-limb extension
2	partial forelimb stretching and partial hind-limb extension
5	partial forelimb stretching and no hind-limb extension
7	no forelimb stretching and no hind-limb extension

Equipment

- None

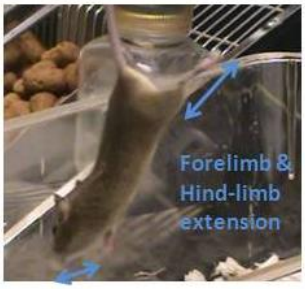

Figure 13. ER test, one of seven behavioral assessment tests used to determine SOD1 symptom onset and as a measure of motor symptoms severity.

Paw Grip Endurance (PGE) Test

Test Score	**Observations**, 5 sec duration
0	grasping screen with forepaws and hind -paws for more than 5 sec
1	grasping screen with forepaws and hind -paws temporarily (intentional drop)
2	grasping screen with forepaws and hind -paws for less than 5 sec
4	grasping screen with forepaws only for less than 5 sec
5	falling instantaneously

Equipment

- Mouse Cage Lid

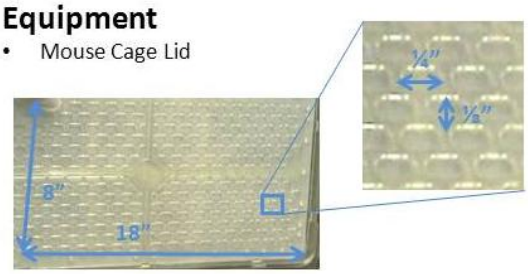

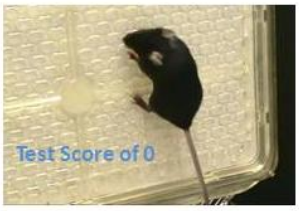

Figure 14. PGE test, one of seven behavioral assessment tests used to determine SOD1 symptom onset and as a measure of motor symptoms severity.

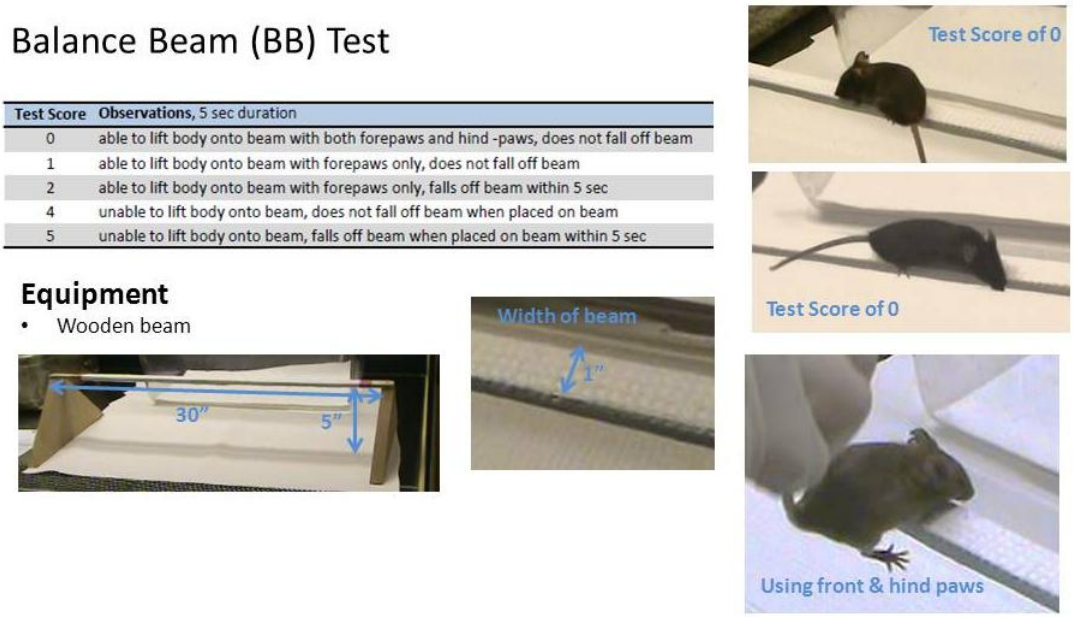

Figure 15. BB test, one of seven behavioral assessment tests used to determine SOD1 symptom onset and as a measure of motor symptoms severity.

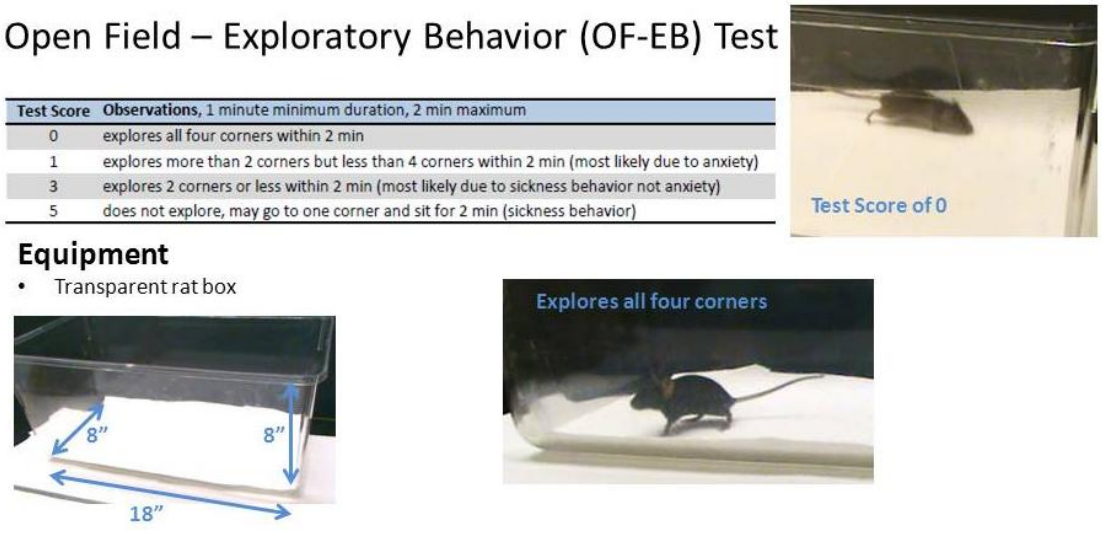

Figure 16. OF-EB test, one of seven behavioral assessment tests used to determine SOD1 symptom onset and as a measure of motor symptoms severity.

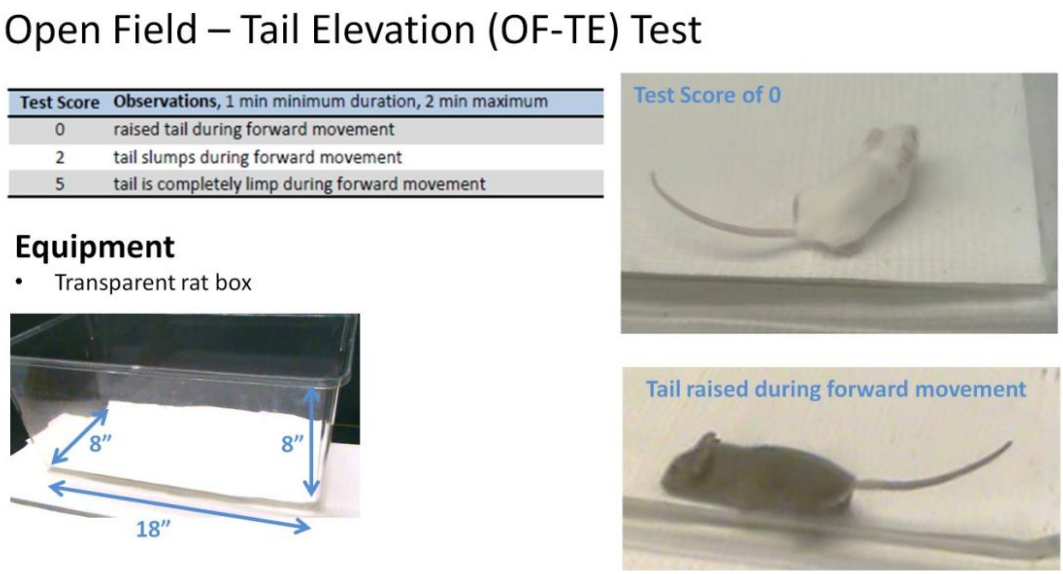

Figure 17. OF-TE test, one of seven behavioral assessment tests used to determine SOD1 symptom onset and as a measure of motor symptoms severity.

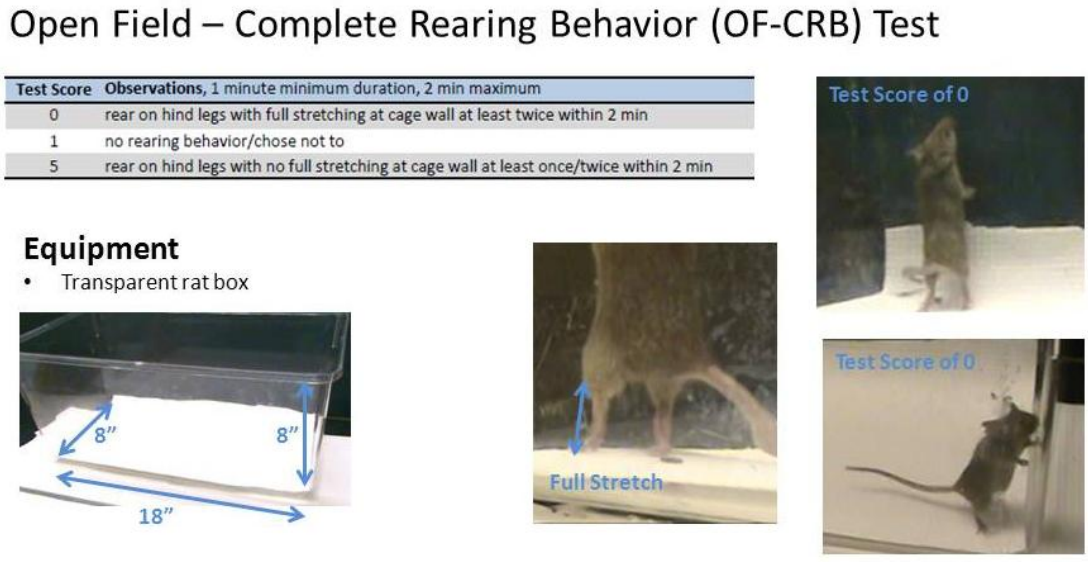

Figure 18. OF-CRB test, one of seven behavioral assessment tests used to determine SOD1 symptom onset and as a measure of motor symptoms severity.

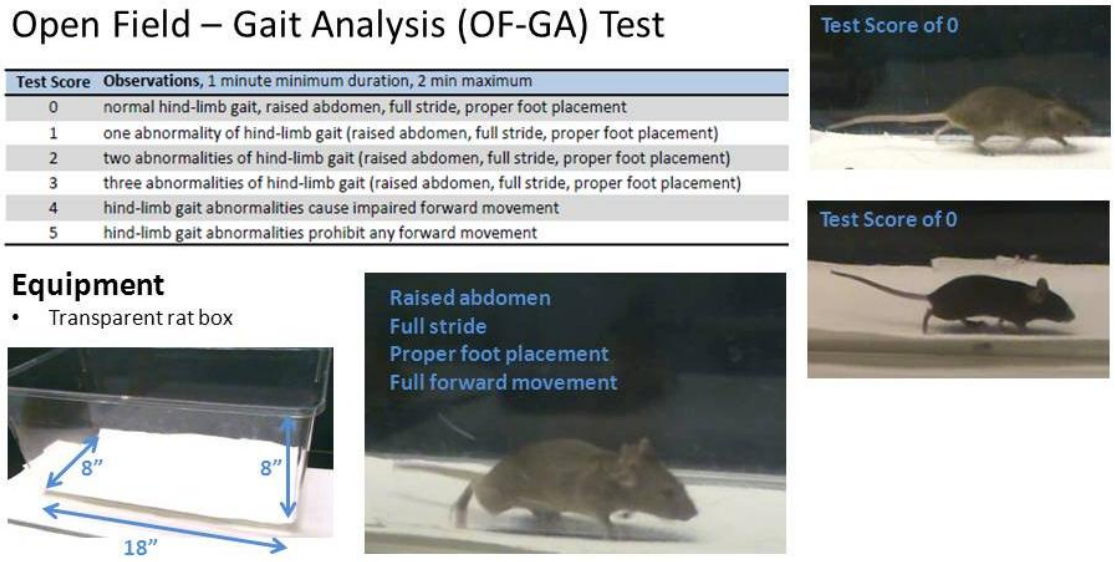

Figure 19. OF-GA test, one of seven behavioral assessment tests used to determine SOD1 symptom onset and as a measure of motor symptoms severity.

Gene	Primer Sequence	Accession Number	T_A (°C)	T_m (°C)	Amplicon Length (bp)
ASK1	F 5′-CATTTGAGTCTGAGCCAACACT-3′ R 5′-GGCTACTCAGCTTCACTCCAACT-3′	BC133697	55	82	120
βII-Tubulin	F 5'-TGGCAACAAATATGTACCTC-3' R 5'-GAATGGTCCCGACCTC-3'	NM009450	54	84	79
Caspase-3	F 5′-TGGAAAGCCGAAACTCTT-3′ R 5′-CGGTATCTTCTGGCAAGC-3′	BC038825	55	85	109
Caspase-8	F 5'-CGGTGAAGAACTGCGTTTC-3' R 5'-CGCCAGTCAGGATGCTAAG-3'	AF067834	53	81	123
CD68	F 5′-CCCAAATTCAAATCCGAATCC-3′ R 5′-GGTACCGTCACAACCTCC-3′	BC021637	51	80	110
CRMP4	F 5′-GCTGATATTTACATGGAGGATGG-3′ R 5′-TGGCCTCGATGGTCTTCACAC-3′	AF501324	53	79	85
CX3CR1	F 5′-CTACTTCCGCATCATCCAGAC-3′ R 5′-AGAGGAAGAAGGCAAAGACCAC-3′	AF074912	55	84	98
Daxx	F 5′-TGCAACATCCTCTCCAGGGTTC-3′ R 5′-GTGCAGAGCTCGTTAATGTACAC-3′	BC128373	55	83	80
FADD	F 5′-TGTCTGAGGCCAAGATGGAT-3′ R 5′-TTCTCAGCATTCTTCCAGACTTTCA-3′	BC021400	55	82	97
Fas	F 5′-ACCGGAAAAGAAAGTGCTG-3′ R 5′-GCAATTCTCGGGATGTATTTAC-3′	BC061160	53	79	121
FasL	F 5′-GAAGAGGTTGAACTACTGCAC-3′ R 5′-TGACATATAAATGGTCAGCACT-3′	BC052866	55	82	98
GAP-43	F 5'-CCTAAGGAAAGTGCCCCACAG-3' R 5'-CAGGTGGGGGCAACGTGG-3'	BC028288	54	84	102
GAPDH	F 5′-GAACATCATCCCTGCATCCA-3′ R 5′-CCAGTGAGCTTCCCGTTCA-3′	M32599	50-57	81	78
GAPDH	unknown unknown	NM008084.2	55	85	140
GFAP	F 5'-AGAACAACCTGGCTGCGTAT-3' R 5'-TCTCCTCCTCCAGCGATTC-3'	AF332062	55	84	93
nNOS	unknown unknown	NM008712.2	55	86	167
PAC1-R	F 5′-GGGCTTTGTGGTGGCTGTACTCT-3′ R 5′-CCGGTGCTTGAAGTCCATAGTGA-3′	BC067039	55	82	118
SODD	F 5′-CAGTGACAAGATTCTTTCCGGTT-3′ R 5′-GCAGCAGCCTACAGACACC-3′	AF332863	53	81	115
TNFα	F 5'-ATTCACTGGAGCCTCGAATG-3' R 5'-AGGAAGGCCTGAGATCTTATC-3'	X02611	53	82	102
TNFR1	F 5′-TGCCATGCAGGGTTCTTTCTG-3′ R 5′-TTTGCAAGCGGAGGAGGTAGG-3′	M60468	55	83	104
TNFR2	F 5′-GAGTGGCCAGTTCAAGAG-3′ R 5′-GGCCTGCACACATCAGT-3′	M60469	55	84	100
TRADD	F 5′-CGTAACTGTCGGGCACT-3′ R 5′-GCCTGCTCGTATAGCCCATC-3′	BC138642	53	84	80
TRAF2	F 5′-CTGTCCCAATGATGGATGCAC-3′ R 5′-TACATGCAGGACACTCCG-3′	L35303	55	83	120

Table 3: Primers designed for RT-PCR. Primer sets for nNOS and its control, GAPDH, were purchased from SuperArray Biosciences, therefore the primer sequence is proprietary information.

CHAPTER IV

FACIAL NERVE AXOTOMY DIFFERENTIALLY REGULATES MOLECULAR EXPRESSION WITHIN THE FACIAL MOTOR NUCLEUS

A. Abstract

Previous research in our laboratory has shown that following axotomy, WT and SOD1 mice display similar mRNA expression of MN survival and regeneration genes, however, differences were observed among mRNA expression for genes specific to the neuropil, such as a decreased astrocytic response, as evident by reduced GFAP expression. Additionally TNFα was shown to be constitutively expressed within the control, uninjured nucleus as early as 59 doa. These results suggest that SOD1 MN respond to nerve injury in a conventional manner, upregulating regenerative gens, however, differences in neuropil mRNA expression suggests that this alternative response of the neuropil to the axotomy injury and may play a role in the enhanced FMN loss seen in the pre-symptomatic SOD1 at 28 dpo (Mesnard et al., 2011). The SOD1 molecular response to axotomy was assessed further with genes involved in death receptor systems, neuroprotective signaling, neurodegenerative signaling, and genes specific to the glial response. Both WT and SOD1 mice revealed a transient increase in death receptor gene expression, however this expression appeared to have been regulated and was returned to baseline by 56 dpo. The pre-symptomatic SOD1 axotomy-

induced response to death receptors suggests a dysregulation of these genes after target disconnection. This suggests that axotomy may resemble the target disconnection that occurs during disease, but more importantly the axotomy-induced molecular response may resemble the disease-induced molecular response. Data presented within this dissertation supports this resemblance.

B. Introduction

ALS is the most common, adult MN degenerative disease. The disease rapidly progresses with a mean survival of only three – five years after onset of clinical symptoms. The development of the SOD1 mouse model for ALS in 1994, has lead to significant advances understand the progression of fALS as well investigation of potential disease mechanisms. While the SOD1 mouse appears to develop normally well into adult hood, before symptoms become apparent, research has identified an initial pathological event early in the lifespan of the mouse. This initial event is loss of neuromuscular junctions of the lower limbs as early as 47 doa (Fischer et al., 2004). This phenomenon has been termed the die-back theory of ALS, where loss of the neuromuscular junction or target, results in compensatory sprouting of MN axons but ultimately neurodegeneration due to overwhelming target disconnection (Dadon-Nachum et al., 2011). While significant loss of MN does occur within the symptomatic stage, it is thought that the inability for the MN to maintain target connection, specifically life sustaining musculature, ultimately results in fatality.

Our laboratory has been using the facial nerve axotomy injury model to study WT MN survival mechanisms for decades. Since the facial nerve axotomy is a neuronal target disconnection injury, it was performed in the pre-symptomatic SOD1 mouse to determine the percent FMN survival after axotomy. The result was a dramatic decrease in FMN survival levels 28 dpo compared to WT (41 and 85%, respectively; Mesnard et al., 2011). This dramatic decrease in FMN survival is also seen after axotomy in immunodeficient mouse models (Serpe et al., 2000).

LMD was utilized to investigate the molecular response of WT and SOD1 FMN and neuropil to the facial nerve axotomy. Surprisingly, WT and SOD1 MN responded in a similar manner, upregulating regenerative genes to a similar extent. Differences, however, were seen in genes specific to the neuropil, suggesting that the target disconnect resulting in a dysregulated response of the neuropil which may play a role in the enhanced FMN loss after axotomy (Mesnard et al., 2011).

The experiments within this Chapter were performed to provide a better understanding of the enhanced FMN cell loss that occurs in pre-symptomatic SOD1 mice following axotomy. mRNA expression changes in response to target disconnection were assessed in WT and SOD1 mice through an extended time course and the genes chosen were those which have been implicated in MN degeneration that occurs in SOD1 mice or ALS patients. Death receptors, their ligands, and downstream signaling factors that have been suggested as mechanisms within the disease such as those involved in the

TNFR1 and Fas pathway were investigated. In addition to the molecular expression of systems involved in neurodegeneration, several genes associated with neuroprotective signaling systems were also were assessed. Many of the protective signaling systems are also important in neuron-glial and glial-glial functional communication. The details of the genes used within this dissertation can be found in **Table 2**. Additional information of all 21 genes assessed is provided within Chapter II Section K. Investigating the axotomy-induced molecular response of these systems within the WT facial motor nucleus will provide an understanding of the normal, characteristic response to axotomy. Once the molecular expression patterns are determined for WT, investigation of the molecular expression response of the SOD1 can be analyzed and compared for similarities and differences within the molecular response.

Additionally, FMN survival was investigated at the extended time-point of 56 dpo to determine whether axotomy-induced FMN loss continues or resembles the lack of neuroprotection of immune-deficient mice previously identified by our laboratory.

Aim #1 of this dissertation was to analyze the expression of genes involved in neuroprotective and neurodegenerative signaling systems as well as genes specific to the glial response, following a facial nerve axotomy in WT and pre-symptomatic SOD1 mice. The working hypothesis for this aim was that molecular expression within the axotomized SOD1 facial motor nuclei will display enhanced mRNA levels, compared to WT, for death receptor signaling systems and other genes that have been shown to be

present within the CNS of ALS patients and symptomatic or end-stage SOD1 mice. Experiments performed specifically investigated the molecular changes induced by axotomy within the facial motor nucleus of WT and SOD1 mice for neurodegenerative genes of death receptor signal transduction and signaling systems involved neuroprotection and genes specific to the glial cell responses to CNS injury. Similarities and differences in the expression between WT and SOD1 axotomized facial nuclei help to elucidate mechanisms involved in the enhanced FMN cell death after axotomy in the pre-symptomatic SOD1 mouse.

C. Materials and Methods

Animals and Surgical Procedures

Mice were obtained and housed as previously described in Chapter III Section A. All mice received a right facial nerve transection axotomy described In Chapter III Section B. Also refer to experimental designs illustrated in **Figures 20** and **23** of this Chapter.

Tissue Preparation

Refer to Chapter III Sections C and D as well as **Figures 20** and **23** of this Chapter for details.

FMN Survival Counts

The experimental design for the FMN survival experiment is illustrated in **Figure 20**. For specific details, refer to Chapter III Section E.

Laser microdissection

Details are described in Chapter III Section F and the experimental design illustrated in **Figure 23** of this Chapter.

RNA Isolation and Real-Time RT-PCR

Percent change of mRNA expression was assessed at 3, 7, 14, 28 and 56 dpo for the following genes: CX3CR1, TNFR1, TNFR2, Fas, FasL, Caspase-3, PAC1-R, CRMP4, ASK1, Daxx, FADD, TRAF2, TRADD, SODD, CD68, and nNOS. Genes TNFα, Caspase-8, GFAP, GAP-43, and βII-Tubulin were previously analyzed by our laboratory for the time-points: 3, 7, 14, and 28 dpo. For this dissertation the time course was extended to 56 dpo, and therefore the time-point of 28 dpo was replicated for conformation and comparison and the 56 dpo time-point was additionally assessed. However, the gene Caspase-8 does not include the fourth data point of WT 56 dpo. Due to failure of amplification during the real-time PCR run and insufficient volume of remaining WT 56 dpo samples, the time-point could not be included in the analysis.

For specific details refer to Chapter III Section G and the experimental design illustrated in **Figure 23** of this Chapter.

Electrophoresis

Gel electrophoresis was used to determine the presence of the axotomy or disease-induced gene TNFα for the time-points of 28 and 56 dpo. Refer to Chapter III Section H for further information.

Statistical Analysis

Details of statistical analysis for FMN percent survival following axotomy and axotomy-induced percent change mRNA expression can be located in Chapter III Section J.

D. Results

Facial Nerve Axotomy in Pre-Symptomatic SOD1 Mice Results in a Dramatic Reduction in FMN Survival Which is Maintained with Time and Resembles that of Immunodeficient Mice

It has previously been shown that pre-symptomatic SOD1 mice are more susceptible to axotomy-induced death compared to WT 28 dpo. The results from the experiment confirm previous findings that at 28 dpo WT mice FMN survival in the entire facial motor nucleus was 81 ± 8% relative to the contralateral, control facial motor nucleus (**Figures 21A** and **22**; Serpe et al., 1999; Serpe et al., 2000; Canh et al., 2006). In contrast, FMN survival in the entire facial motor nucleus of pre-symptomatic SOD1 mice at 28 dpo was 48 ± 8%, relative to contralateral, control facial motor nucleus (**Figures 21B** and **22**). This enhanced axotomy-induced MN loss at 28 dpo is in agreement with the literature (Mariotti et al., 2002; Mesnard et al., 2011).

WT and SOD1 axotomy-induced FMN cell survival was assessed at a second time-point of 56 dpo. WT FMN survival in the facial motor nucleus significantly declined further to 43 ± 13% (**Figures 21C** and **22**), this is also in accordance with previous

published results from our laboratory at a 70 dpo (Serpe et al., 2000). Finally, SOD1 FMN percent survival was assessed within the entire facial motor nucleus at 56 dpo and found to be 42 ±4% (**Figures 21D** and **22**). There were no significant differences found between FMN survival levels SOD1 56 dpo, WT 56 dpo or SOD1 28 dpo. The lack of significance between SOD1 FMN percent survival levels at 28 and 56 dpo is in accordance that the dramatic loss of FMN levels 28 dpo in immunodeficient RAG2-KO and *Scid* mice (Serpe et al., 2000; Beahrs, 2009). Therefore, the dramatic loss of FMN survival after axotomy in pre-symptomatic SOD1 mice suggests lack of immune-mediated neuroprotection.

The Initial Molecular Response to Axotomy in WT and SOD1 is Similar; However in SOD1 Mice a Delayed Response to Axotomy Results in Upregulation of Death Receptor Signaling Systems

This dissertation analyzed mRNA expression of genes involved in neurodegeneration, specifically death receptor signaling systems, the Fas receptor and TNFR1. Additional genes were assessed that are known to play a role in functional communication between neuron-glial and glial-glial and are thought be neuroprotective. Details of all 21 genes analyzed can be found in **Table 2**. A summary of axotomy-induced mRNA expression results from this Chapter can be found in **Table 4**.

TNFR1 mRNA expression in the WT facial motor nucleus is significantly upregulated at 3 (70 ± 15%), 7 (96 ± 18%), 14 (86 ± 5%) and 28 (65 ±11%) dpo, relative

to the contralateral, uninjured control facial motor nuclei (**Figure 24A**). No difference was seen between 56 dpo (9 ± 12%) and control facial motor nucleus, however a significant decrease between the two time-points 28 and 56 dpo could account for the TNFR1 mRNA expression returning to baseline, i.e. control levels (**Figure 24A**). TNFR1 mRNA expression in the SOD1 facial motor nucleus is significantly upregulated at all time-points investigated, 3 (78 ± 21%), 7 (94 ± 8%), 14 (97 ± 11%), 28 (82 ± 11%), and 56 (58 ± 7%) dpo, relative to the control (**Figure 24B**).

The SOD1 TNFR1 mRNA expression appears to resemble the WT expression pattern throughout 28 dpo, however by 56 dpo SOD1 is significantly upregulated compared to WT (**Figure 24C**). Therefore in WT and SOD1 facial motor nuclei are similar in their initial and delayed response to axotomy for the death receptor mRNA TNFR1 mRNA in that it is upregulated to a similar extent and sustained (**Figure 24C**). However at 56 dpo, the TNFR1 mRNA in the SOD1 axotomized facial motor nuclei is still significantly upregulated relative to control and does not significantly differ from the previous, 28 dpo time-point (**Figure 24B**). While in the WT axotomized facial motor nucleus, the TNFR1 expression has returned to baseline and a significant decrease from the previous time-point of 28 dpo is apparent (**Figure 24A**). These results lead to a significant difference between the sustained upregulation of TNFR1 in the SOD1 facial nucleus and the WT at 56 dpo (**Figure 24C**).

The WT and SOD1 axotomy-induced response relative to **TNFα** mRNA was previously investigated in our laboratory, however it was only assessed out until 28 dpo. At 28 dpo, axotomized WT facial motor nucleus did not display any measurable amplicon for TNFα in accordance with previous findings and lack of any measureable PCR amplicon was also shown at 56 dpo in both control and axotomized WT facial motor nucleus (**Figure 25A upper panel**). As was previously shown, SOD1 control and axotomized nuclei display amplicons for TNFα mRNA which are still present at 56 dpo (**Figure 25A lower panel**; Mesnard et al., 2011). Note that amplicon band density is not representative of mRNA quantity for the reason that PCR product shown on the gel was post-linear phase of amplification.

The axotomized SOD1 facial motor nuclei, displays a sustained upregulation (554 ± 91%) of TNFα mRNA expression relative to control at 28 dpo followed by a slight, but non-significant decrease in TNFα mRNA expression (348 ± 84%) at 56 dpo. Both time-points were significantly different relative to control nucleus, but not between the two time-points (**Figure 25B**).

It was unexpected to find that **Fas** mRNA expression in the WT facial motor nucleus is significantly upregulated at 3 (37 ± 10%), 14 (33 ± 13%), and 28 (43 ±20%) dpo, relative to the contralateral, uninjured control facial motor nuclei (**Figure 26A**). No difference was seen between 7 (13 ± 14%) and 56 dpo (48 ± 25%) and WT control facial motor nucleus. After target disconnection in the WT, there is a transient upregulation of

Fas mRNA which returns to baseline at 7 dpo then displays a second and delayed upregulation before returning to baseline by 56 dpo (**Figure 26A**).

Fas mRNA expression in the SOD1 facial motor nucleus is significantly upregulated at 3 (59 ± 16%), 7 (57 ± 13%), 28 (125 ± 13%), and 56 (201 ± 51%) dpo, relative to the control (**Figure 26B**). The SOD1 Fas mRNA expression appears to have a resemblance to the WT expression pattern after axotomy. The initial, small transient upregulation seen in the WT from zero to 7 dpo is present after axotomy in the SOD1 facial nucleus, however it is delayed to 14 dpo (48 ± 25%) where no significant difference exits relative to control (**Figure 26A** and **B)**. The result of the increased interval of the initial transient response in the SOD1 reveals a significant difference between SOD1 compared to WT at 7 dpo (**Figure 26C**). While the second upregulation of Fas mRNA in the WT remains at low levels and returns to baseline by 56 dpo, the second upregulation of Fas receptor mRNA in the SOD1 axotomized nucleus is greatly increased, as demonstrated by the significance between 14 dpo and 28 dpo (**Figure 26B**). Compared to WT, the Fas mRNA expression within the delayed response to axotomy is significantly upregulated at 28 and 56 dpo (**Figure 26C**).

FasL mRNA expression in the WT axotomized facial motor nucleus is unchanged compared to control at 3 dpo (1 ± 47%) but is significantly upregulated at 7 dpo (111 ± 50%). This upregulation is transient because WT FasL mRNA expression returns to baseline at 14 dpo (13 ± 70%; **Figure 27A**). The high variability of WT data points during

the initial, transient upregulation does not allow for detection of potential significant differences between the time-points, however a similar initial transient upregulation pattern occurs in the SOD1 facial nucleus after axotomy (**Figure 27B**), suggesting that increasing number of WT samples would most likely decrease variability and reveal a more significant pattern of transient upregulation between 3, 7 and 14 dpo.

Following the initial upregulation of FasL mRNA in WT, the delayed response to axotomy is down regulated, as shown by the 28 dpo (-57 ± 25%) which is significantly different that control mRNA expression. However, this second change in mRNA expression relative to control could be considered regulated as across time the expression returns to baseline by 56 dpo (1 ± 12%) and while 56 dpo is not significantly different than control, it is significant from 28 dpo (**Figure 27A**).

FasL mRNA expression after axotomy in the SOD1 facial nucleus does not differ from control at 3 dpo (10 ± 32%) but displays a significant upregulation at 7 (183 ± 25%), 14 (80 ± 37%), 28 (221 ± 60%), and 56 (102 ± 14%) dpo (**Figure 27B**). The decreased variability among the SOD1 data sets, in comparison with those of the WT, as well as the enhanced upregulation results in significance between subsequent time-points (3 to 7, 7 to 14, 14 to 28 and 28 to 56 dpo; respectively; **Figure 27B**).

Again, similarities in the axotomy-induced mRNA expression pattern of WT and SOD1 facial motor nuclei is seen for the fourth component of the two death receptors investigated thus far. No differences between WT and SOD1 apparent during the initial,

transient upregulation which occurs between 3 and 14 dpo (**Figure 27C**). After 14 dpo, considerable differences between SOD1 and WT are revealed throughout the remaining delayed response to axotomy. While the WT axotomized nucleus displayed a small down regulation between 14 and 56 dpo, SOD1 axotomized nucleus shows a significant upregulation from 14 to 28 dpo followed by a significant decrease from 28 to 56 dpo, but not substantial enough to reach baseline (**Figure 27B**).

Following axotomy in WT mice, mRNA expression for **TRADD** displays an initial transient downregulation at 3 (-17 ± 5%) and 7 (-24.55 ± 9%) dpo, which is significant relative to TRADD mRNA in the control facial motor nucleus (**Figure 28A**). No difference exists between WT TRADD mRNA expression and control levels for 14 (-5 ± 7%) and 28 (-10 ± 10%) dpo, however 56 dpo (-7 ± 2%) displays less variability and differs significantly relative to control (**Figure 28A**). It is unclear whether the significance of the 56 dpo time-point is suggestive of sustained downregulation throughout the entire time course. Potentially this sustained downregulation may be obscured by the variability of the 14 and 28 dpo time-points.

The SOD1 axotomized facial motor nucleus displays a similar pattern of WT TRADD mRNA expression after target disconnection with no significant differences between any of the time-points (**Figure 28C**). After axotomy, SOD1 facial nuclei displays a transient downregulation of TRADD mRNA that is significant from control at 7 dpo (-22 ± 9%; **Figure 28B**). The remaining SOD1 time-points 3 (-5 ± 7%), 14 (-12 ± 9%), 28 (-4 ±

19%) and 56 (7 ± 17%) dpo do not significantly differ from control facial nucleus (**Figure 28B**). It is not clear why high variability plagues the SOD1 28 and 56 dpo time-points relative to previous data points and those of the WT time-course (**Figure 28**).

WT axotomized facial motor nuclei display an increase of **FADD** mRNA expression at 3 (39 ± 14%), and 7 (12 ± 13%) dpo relative to control nucleus FADD expression (**Figure 29A**). The FADD mRNA upregulation appears to be another initial, transient response to axotomy because throughout the remainder of the time-course FADD mRNA expression has returned to basal levels and shows no difference from control; 14 (13 ± 13%), 28 (-16 ± 15%) and 56 (9 ± 5%) dpo, respectively (**Figure 29A**).

SOD1 FADD mRNA expression within the axotomized facial motor nucleus also displays a significant, initial transient upregulation at 3 (39 ± 8%) and 7 (26 ± 11%) dpo relative to control that returns to baseline at 14 dpo (10 ± 11%; **Figure 29B**). While no significant differences are seen comparing SOD1 axotomized facial nuclei to WT for the time-points of 3, 7 and 14 dpo, a delayed response to axotomy within the SOD1 facial nucleus results in significant difference at 28 and 56 dpo (**Figure 29C**). The increased, delayed regulation of FADD mRNA that occurs at 28 dpo (75 ± 12%) and out to 56 dpo (73 ± 24%) is nearly two-fold compared to the initial transient upregulation seen in both WT and SOD1 mice (**Figures 29A** and **29B**). This second upregulation leads to a significant difference between 28 dpo and the previous time-point of 14 dpo (**Figure 29B**).

Daxx mRNA is upregulated in WT facial motor nuclei after axotomy at 7 (19 ± 6%) and 14 (43 ± 15%) dpo, relative to control (**Figure 30A**). No difference is seen between WT axotomized and control nucleus for 3 dpo (15 ± 13% dpo) or the remaining time-points after the initial transient upregulation, 14 (43 ± 15%), 28 (20 ± 11%) and 56 (-3 ± 12%) dpo (**Figure 30A**).

Like WT, SOD1 axotomized facial motor nuclei do not display a difference in Daxx mRNA expression at 3 dpo (6 ± 10%), but do display significance with respect to the control nucleus for the remaining points in the time course; 7 (13 ± 6%), 14 (25 ± 7%), 28 (13 ± 5%) and 56 (48 ± 18%) dpo (**Figure 30B**). SOD1 axotomized facial motor nuclei mRNA expression is significantly upregulated at 56 dpo compared to WT (**Figure 30C**). The return of Daxx's mRNA to baseline in the WT by 14 dpo suggests the initial transient upregulation is a normal response to target disconnection but is regulated and returns to baseline. Within the axotomized, SOD1 facial motor nuclei, Daxx mRNA expression is initially a comparable response to that seen in the WT facial nucleus, however the prolonged and enhanced upregulation and failure to return the expression to baseline levels is suggestive of dysregulation.

In WT axotomized facial motor nuclei, ASK1 mRNA is unchanged relative to control facial motor nuclei for all time-points; 3 (16 ± 11%), 7 (3 ± 10%), 14 (-5 ± 9%), 28 (-3 ± 12%) and 56 (1 ± 8%) dpo (**Figure 31A**). SOD1 axotomized facial motor nuclei does not display any change in ASK1 mRNA expression at 3 dpo (14 ± 17%), however a short,

transient downregulation occurs at 7 dpo (-25 ± 8%) that is significantly different than control, however this reduction in mRNA expression returns to basal levels at 14 dpo (9 ± 11%; **Figure 31B**). The return to basal mRNA expression at 14 dpo results in a significant difference between mRNA expression levels at 7 and 14 dpo (**Figure 31B**). The delayed response to axotomy in the SOD1 facial nuclei is an increasing upregulation at 28 (33 ± 15%) and 56 (59 ± 20%) dpo, both of which show significantly increased ASK1 mRNA expression relative to SOD1 control facial nuclei (**Figure 31B**). During comparison of SOD1 axotomized mRNA expression relative to WT expression, significant differences were apparent during the initial transient downregulation within the SOD1 nucleus and again during the delayed response to axotomy at 56 dpo (**Figure 31C**).

The mRNA expression of **nNOS** within the WT facial motor nucleus after axotomy is no different relative to the uninjured, control facial motor nucleus for the entire time course; 3 (-12 ± 12%), 7 (-12 ± 20%), 14 (-5 ± 8%), 28 (-23 ± 14%) and 56 (5 ± 5%) dpo (**Figure 32A**).

Initially there is no change in nNOS mRNA expression within the SOD1 axotomized facial motor nucleus relative to control at 3 (9 ± 15%) and 7 (-16 ± 12%) dpo (**Figure 32B**). A significant upregulation between 7 dpo and 14 dpo (65 ± 18%) reveals a delayed response to axotomy in the SOD1 facial motor nucleus (**Figure 32B**). In addition to the upregulated 14 dpo time-point, 28 (109 ± 16%) and 56 (104 ± 20%) dpo reveal sustained upregulation of nNOS mRNA and these data are significantly different relative

to SOD1 control facial nuclei and WT axotomized facial motor nuclei (**Figures 32B** and **32C**). Since it has been established that activation of the Fas-pathway in MN results in increased transcription of nNOS, the possibility that increased FMN loss after axotomy in SOD1 mice may be a result of Fas-induced cell death cannot be discounted.

In WT facial motor nuclei, axotomy results in a large, significant upregulation of **Caspase-3** mRNA expression relative to control nucleus at 3 (384 ± 98%), 7 (379 ± 65%), 14 (443 ± 58%) and 28 (139 ± 29%) dpo (**Figure 33A**). The upregulation begins to subside after 14 dpo and there is a significant drop in Caspase-3 mRNA expression between 14 and 28 dpo as well as between 28 and 56 dpo (25 ± 38%) and by 56 dpo the expression reaches basal levels and is no different than WT control mRNA expression (**Figure 33A**). In SOD1 axotomized facial motor nuclei Caspase-3 mRNA is also significantly upregulated at 3 (259 ± 38%), 7 (367 ± 53%), 14 (331 ± 40%), 28 (164 ± 37%), and continued at 56 dpo (111 ± 46%; **Figure 33B**). As seen in WT axotomized facial nuclei, in the SOD1 nuclei there is a significant decreases between the 14 and 28 dpo, however between 28 and 56 dpo there is no difference and the upregulation is sustained out to 56 dpo relative to control (**Figure 33B**). During comparison of Capase-3 mRNA expression after axotomy in SOD1 relative to WT, no significant differences were seen suggesting upregulation of Caspase-3 mRNA is a normal, characteristic response to facial nerve axotomy (**Figure 33C**).

The WT and SOD1 axotomy-induced mRNA expression relative to **Caspase-8** mRNA was previously investigated in our laboratory, however it was only assessed out until 28 dpo.

WT axotomized facial motor nucleus displays a significantly increased mRNA expression relative to control at 28 dpo (122 ± 57%; **Figure 34A**). SOD1 facial motor nuclei also display a similar, significant increase expression of Caspase-8 mRNA at 28 dpo (213 ± 59%) relative to SOD1 control facial nuclei (**Figure 34B**). At 28 dpo no difference exists between Caspase-8 mRNA expression in SOD1 facial nuclei compared to WT (**Figure 34C**). The results of WT and SOD1 Caspase-8 mRNA expression at 28 dpo is consistent with previous findings from our laboratory (Mesnard et al., 2011). Due to errors during sample processing and insufficient sample volume Caspase-8 was not analyzed for WT 56 dpo within this dissertation, but will be analyzed in the future. SOD1 axotomy-induced upregulation of Caspase-8 mRNA was significantly reduced between the 28 and 56 (12 ± 19%) dpo time-points and at 56 dpo mRNA expression levels have returned to baseline relative to SOD1 control facial motor nuclei (**Figure 34B**). The extended time course for Caspase-8 reveals that while it is upregulated after axotomy in both WT and SOD1 facial nuclei, it has returned to basal expression levels within the SOD1 nuclei suggesting the response is regulated.

WT facial motor nuclei display an initial transient downregulation of TRAF2 mRNA at 3 (-15 ± 9%) and 7 (-26 ± 4%) dpo with significance between 7 dpo and control

nuclei expression (**Figure 35A**). The return to baseline expression results in a significant difference between WT 7 dpo and 14 dpo (-6 ± 5%; **Figure 35A**). For the remainder of the WT time course, TRAF2 mRNA expression is maintained at baseline levels and therefore, no differences between WT axotomized facial nuclei and control nuclei are present; 28 (-1 ± 15%) and 56 (6 ± 11%) dpo (**Figure 35A**).

SOD1 axotomized facial motor nuclei also display an initial, transient and significant downregulation of TRAF2 mRNA at 3 (-27 ± 8%) and 7 (-41 ± 9%) dpo (**Figure 35B**). A dramatic upregulation occurs after 7 dpo resulting in the return to baseline mRNA expression at 14 (-6 ± 9%) dpo, and a significant difference between the time-points 7 and 14 dpo (**Figure 35B**). After 14 dpo, expression of TRAF2 mRNA is maintained at baseline through 28 dpo (0 ± 11%; **Figure 35B**). However, there is a significant difference between 28 and 56 (55 ± 20%) dpo, and 56 dpo is also significantly different than SOD1 control facial nuclei mRNA levels (**Figure 35B**). No differences exist between SOD1 TRAF2 mRNA in response to axotomy and WT throughout the time course (**Figure 35**).

In WT axotomized facial motor nuclei, **SODD** mRNA is significantly downregulated at 3 (-50 ± 5%), 7 (-51 ± 6%), 14 (-24 ± 7%) and 28 (-24 ± 8%) dpo relative to control (**Figure 36A**). The initial downregulation of SODD mRNA expression in WT is considered a transient response because a significant difference between 7 and 14 dpo, where although SODD mRNA levels are still downregulated they are to a lesser extent

and maintained through 28 dpo before returning to baseline by 56 dpo (-9 ± 17%; **Figure 36A**).

In SOD1 facial motor nuclei there is also an initial, significant downregulation in response to axotomy at 3 (-34 ± 6%), 7 (-32 ± 7%) and 14 (-12 ± 6%) dpo, relative to SOD1 control facial nuclei (**Figure 36B**). In a similar pattern as seen in WT, a significant difference between 7 and 14 dpo leads to the termination of the transient downregulation (**Figure 36B**). The remaining SOD1 time course of SODD mRNA expression is not significantly different than SOD1 control facial nucleus expression levels, 28 (3 ± 13%) and 56 (-12 ± 21%) dpo (**Figure 36B**). Comparison of axotomized SOD1 facial motor nuclei expression of SODD mRNA with that of WT reveals a significant difference at 3 and 7 dpo resulting in a diminished transient downregulation in the SOD1 compared to the WT (**Figure 36C**).

In WT facial motor nucleus, axotomy results in a large upregulation of **TNFR2** mRNA that is sustained throughout the time course and significantly different than WT control, uninjured nucleus at all time-points; 3 (865 ± 242%), 7 (1606 ± 162%), 14 (1084 ± 214%), 28 (517 ± 93%) and 56 (115 ± 25%) dpo (**Figure 37A**). Throughout the WT time course of increased TNFR2 mRNA expression, significant differences can be seen between 3 and 7 dpo, 14 and 28 dpo, and also between 28 and 56 dpo (**Figure 37A**).

SOD1 axotomized facial motor nuclei also displays significant upregulation of TNFR2 mRNA throughout the time-course; 3 (1659 ± 388%), 7 (1479 ± 287%), 14 (721 ±

178%), 28 (502 ± 87%) and 56 (138 ± 14%) dpo (**Figure 37B**). Significant difference between 7 and 14 dpo as well as 28 and 56 dpo can also be seen (**Figure 37B**). The axotomy-induced upregulation of TNFR2 mRNA is similarly expressed between SOD1 and WT facial motor nuclei (**Figure 37C**).

PAC1-R is significantly different from WT control expression at the following time-points; 3 (-60 ± 10%), 7 (-65 ± 4%) and 14 (-46 ± 10%) dpo (**Figure 38A**). By 28 (-22 ± 13%) and 56 (15 ± 20%) dpo, WT mRNA expression of PAC1-R has returned to baseline (**Figure 38A**). PAC1-R mRNA expression within the axotomized SOD1 facial motor nuclei is also downregulated significantly at 3 (-52 ± 4%), 7 (-53 ± 7%) and 14 (-36 ± 7%) dpo, relative to SOD1 control nuclei (**Figure 38B**). There is a significant increase between 14 and 28 (7 ± 12%) dpo however no difference exists between 28 and 56 (15 ± 8%) dpo (**Figure 38B**). The axotomy-induced upregulation of PAC1-R mRNA is similarly expressed between SOD1 and WT facial motor nuclei (**Figure 38C**). Results suggest that like the WT, PAC1-R mRNA expression is regulated in SOD1 facial motor nucleus after neuronal target disconnection.

In WT facial motor nucleus, axotomy results in a large upregulation of **CX3CR1** mRNA that is sustained throughout the time course and significantly different than WT control nucleus at all time-points; 3 (391 ± 46%), 7 (624 ± 30%), 14 (461 ± 51%), 28 (275 ± 39%) and 56 (58 ± 14%) dpo (**Figure 39A**). Throughout the WT time course of increased

CX3CR1 mRNA expression, significant differences can be seen between every time-point and the preceding (**Figure 39A**).

SOD1 axotomized facial motor nuclei also displays significant upregulation of CX3CR1 mRNA throughout the time-course; 3 (614 ± 89%), 7 (516 ± 56%), 14 (308 ± 43%), 28 (270 ± 42%) and 56 (86 ± 17%) dpo (**Figure 39B**). Significant difference between 7 and 14 dpo, as well as 28 and 56 dpo can also be seen (**Figure 39B**). The axotomy-induced upregulation of CX3CR1 mRNA is similarly expressed between SOD1 and WT facial motor nuclei, however significant differences exist between SOD1 axotomized facial nuclei CX3CR1 mRNA expression at 3 and 14 dpo relative to WT CX3CR1 mRNA expression (**Figure 39C**).

WT expression of **CRMP4** mRNA in the axotomized facial motor nucleus differed significantly relative to WT control nucleus for the following time-points; 3 (-29 ± 4%), 7 (13 ± 2%), 14 (36 ± 12%), 28 (38 ± 13%) dpo then returned to baseline expression by 56 dpo (-18 ± 46%; **Figure 40A**). CRMP4 expression significantly differed between 7 and 14 dpo (**Figure 40A**). CRMP4 mRNA expression in SOD1 axotomized facial nucleus is as follows; 3 (1 ± 8%), 7 (5 ± 12%), 14 (27 ± 14%), 28 (28 ± 12%) and 56 (-1 ± 25%) dpo (**Figure 40B**). The only time-point significantly different than control SOD1 CRMP4 mRNA expression is 28 dpo (**Figure 40B**). Regarding SOD1 CRMP mRNA expression compared to that of WT, the only significant difference is revealed at 3 dpo (**Figure 40C**). Overall no

noteworthy differences are seen regarding mRNA expression of CRMP4 between WT and SOD1 facial motor nuclei in response to axotomy.

WT **GAP-43** was found to be significantly upregulated at 28 dpo (612 ± 193%) relative to control but not at 56 dpo (116 ± 68%; **Figure 41A**). SOD1 GAP-43 mRNA expression at 28 dpo (896 ± 197%) differs significantly from SOD1 control but does not differ from uninjured facial motor nucleus at 56 dpo (118 ± 47%; **Figure 41B**). There is no significant difference between SOD1 GAP-43 expression and WT (**Figure 41C**).

The cytoskeletal protein **βII-Tubulin** is also considered a regenerative gene and was previously shown to be upregulated after facial nerve axotomy to a similar extend tin WT and SOD1 mice. Extension of the time course from 28 to 56 dpo was analyzed to determine whether βII-Tubulin mRNA expression returned to baseline in WT and SOD1 axotomized facial motor nuclei. In WT axotomized facial motor nuclei there was no difference between the two time-points 28 (58 ± 48%) and 56 (16 ± 30%) dpo relative to WT control mRNA (**Figure 42A**). Within SOD1 axotomized facial motor nuclei, βII-Tubulin mRNA expression at 28 dpo (101 ± 33%) was significantly increase relative to control as well as significantly different than the 56 dpo (24 ± 11%) time-point (**Figure 42B**). Again, no difference was seen between this MN-regenerative gene in SOD1 axotomized facial motor nucleus and WT (**Figure 42C**).

GFAP mRNA expression following axotomy has been previously assessed in our laboratory and SOD1 axotomized facial motor nuclei displayed a greatly suppressed

upregulation compared to WT. Here, the original time course was extended from 28 to 56 dpo. At 28 dpo (660 ± 135%), WT axotomized facial nuclei display a significant difference from control nuclei and a significant difference between the two time-points 28 and 56 dpo (122 ± 73%; **Figure 43A**). At 56 dpo, WT facial motor nuclei do not display significantly different GFAP mRNA expression relative to control (**Figure 43A**). In SOD1 axotomized facial motor nuclei, both 28 (494 ± 125%) and 56 (298 ± 50%) dpo differ significantly than SOD1 control GFAP mRNA expression (**Figure 43B**). SOD1 axotomized facial motor nuclei GFAP expression is significantly higher at 56 dpo relative to WT (**Figure 43A**). While GFAP mRNA expression is significantly suppressed after facial nerve axotomy in SOD1 facial nucleus its upregulation is sustained for a longer period of time.

Following axotomy in WT facial motor nuclei, **CD68** mRNA is significantly upregulated relative to WT control at all time-points; 3 (549 ± 48%), 7 (1020 ± 111%), 14 (1151 ± 222%), 28 (605 ± 145%) and 56 (220 ± 53%) dpo (**Figure 44A**). Among the WT time-points significant differences are revealed between 7 and 14 dpo as well as 28 and 56 dpo (**Figure 44A**). Regarding the SOD1 time course for CD68 mRNA expression after axotomy, significant differences relative to SOD1 control expression is shown for all time-points; 3 (455 ± 155%), 7 (607 ± 105%), 14 (291 ± 61%), 28 (693 ± 157%) and 56 (184 ± 50%) dpo (**Figure 44B**). In SOD1 axotomized facial motor nuclei significant differences occur between 14 and 28 dpo as well as 28 and 56 dpo (**Figure 44B**). In comparison between SOD1 and WT significantly reduced mRNA expression is seen in the

SOD1 axotomized nucleus compare to WT at 7 and 14 dpo (**Figure 44C**). This result is consistent with the findings from GFAP mRNA expression and suggests a dysregulation exists within in the glial response to neuronal target disconnection which reveals itself as a suppression of the astrocyte and microglial response.

Figure 20. Experimental Design: Percent FMN survival in axotomized WT and SOD1 facial motor nuclei at 28 and 56 dpo

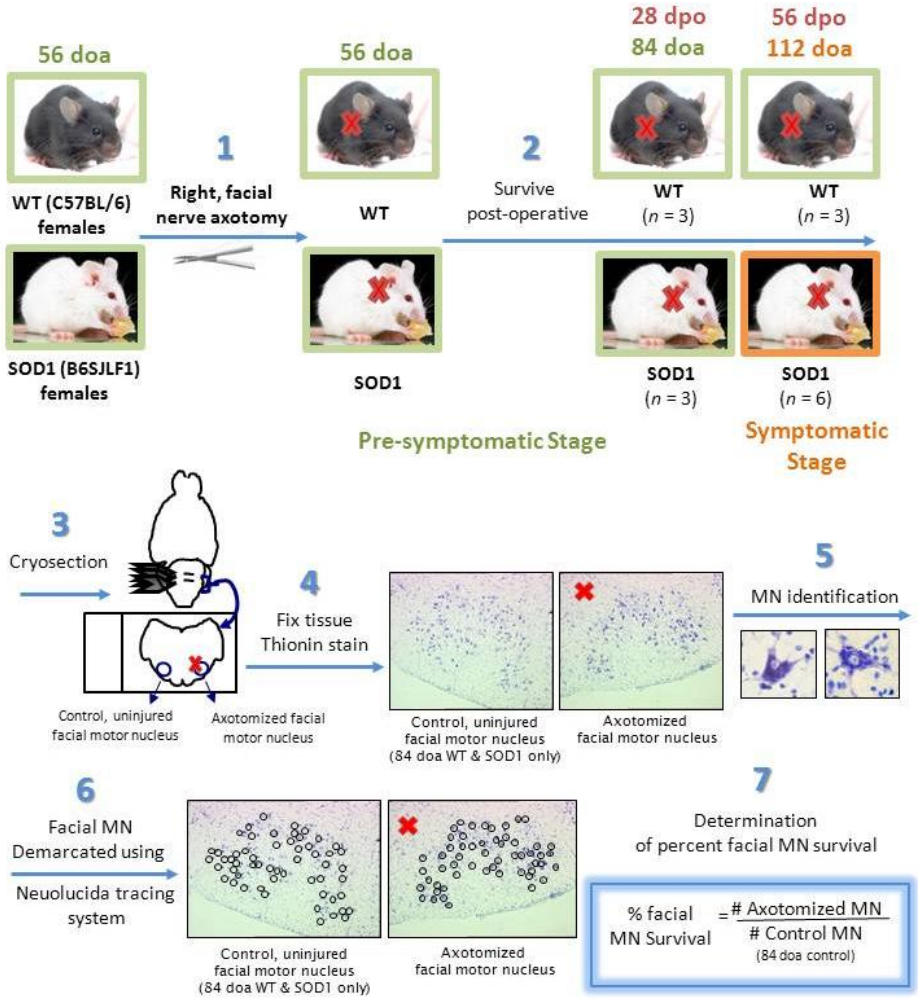

1. WT and SOD1 mice received a right facial nerve axotomy at 56 doa.
2. Mice were euthanized at 28 and 56 dpo.
3. Brains were removed and cryosectioned through the facial motor nucleus at 25 µm.
4. Sections were fixed with 4% PFA and stained with thionin.
5. FMN identified by morphology and a defined nucleus and nucleolus.
6. F MN were demarcated under light microscopy using the Neurolucida Tracing System and total number of MN per section were recorded for both control (left) and axotomized (right) facial motor nuclei.
7. The average percent of FMN survival was calculated by taking the total number of MN counted in the axotomized nucleus and dividing by the total number of MN counted in the WT 28 dpo (84 doa) control nucleus, then multiplying by 100. The percent of FMN survival for each mouse was averaged within a time-point (28 or 56 dpo) for the total percent of FMN survival

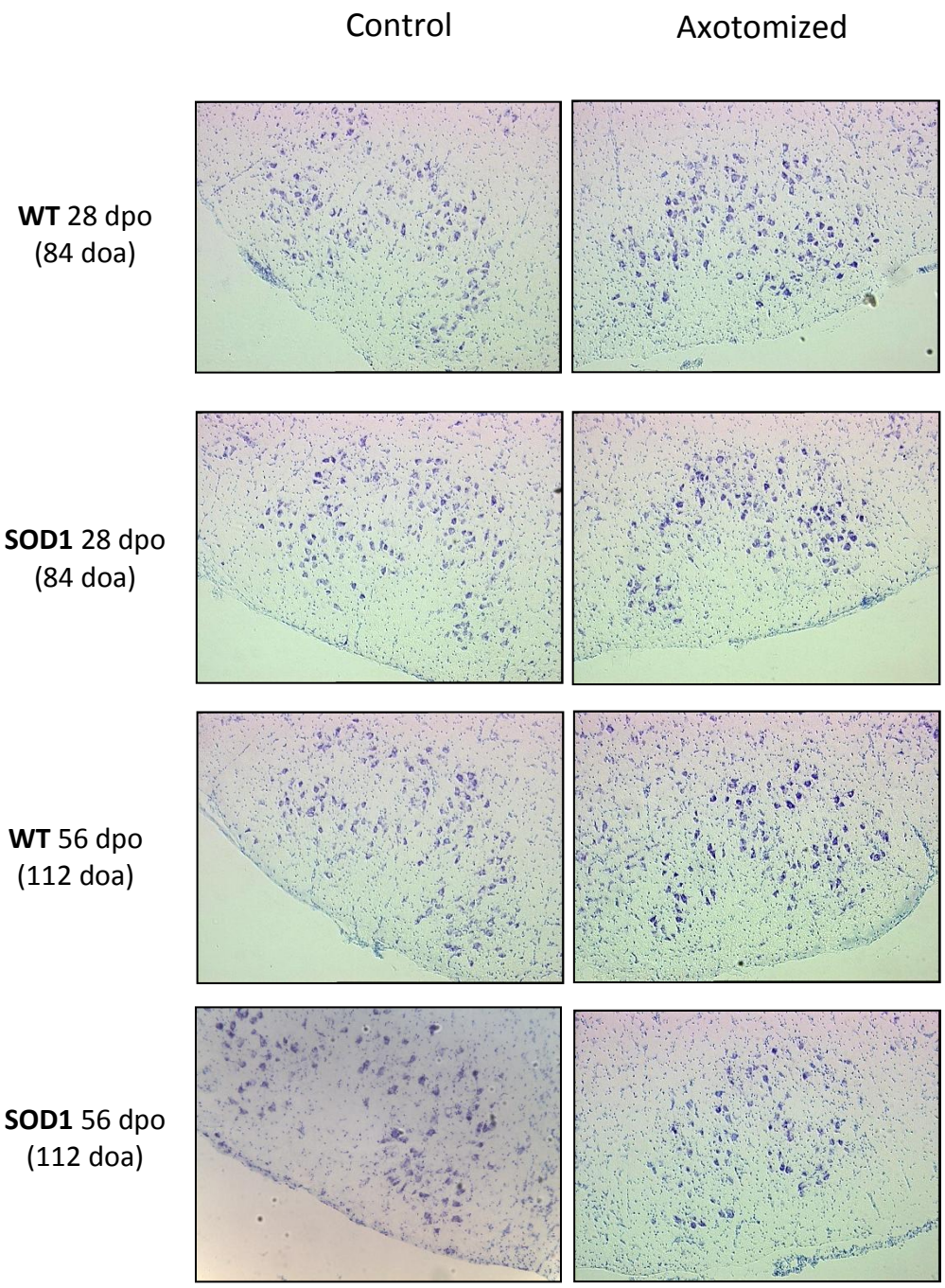

Figure 21. Representative photomicrographs of thionin-stained control and axotomized facial motor nuclei of WT and SOD1 mice at 28 and 56 dpo. Original magnification 20x.

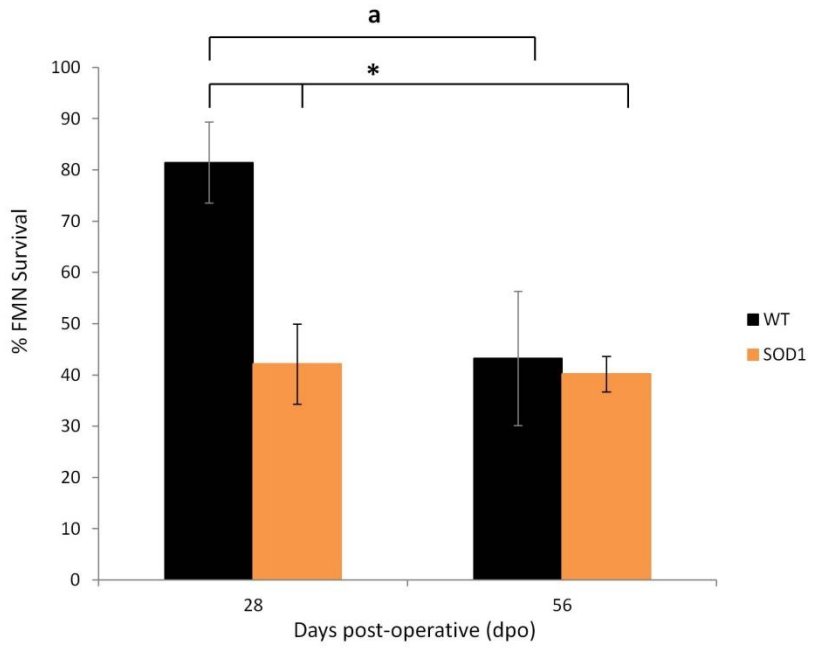

Figure 22. The average percent of FMN survival ± SEM in WT and SOD1 axotomized facial motor nuclei at 28 and 56 dpo relative to WT 28 dpo uninjured, control facial motor nucleus. **a** represents a significant difference between time among the same strain. ***** represents a significant difference between SOD1 relative to WT; $p \leq 0.05$.

Figure 23. Experimental Design: LMD of WT and SOD1 axotomized and control facial motor nuclei, real time RT-PCR and analysis of mRNA expression

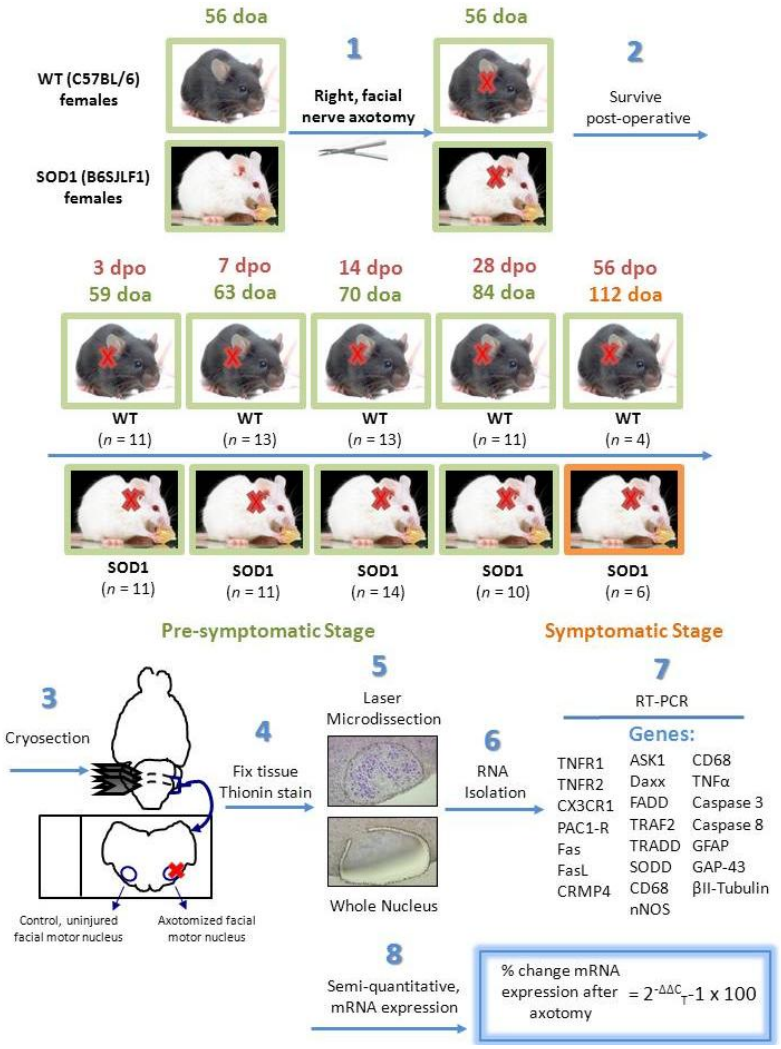

1. WT and SOD1 mice received a right facial nerve axotomy at 56 doa.
2. Mice were euthanized at 3, 7, 14, 28 and 56 dpo.
3. Brains were removed and cryosectioned through the facial motor nucleus at 25 µm.
4. Sections were fixed with 100% ETOH and stained with thionin.
5. Control and axotomized nuclei were separately collected by laser microdissected for each mouse.
6. RNA was isolated from control and axotomized facial motor nucleus samples.
7. Real-time, RT-PCR was performed for specific genes to profile the axotomy-induced molecular response in the SOD1 compared to the WT across time.
8. The semi-quantitative, percent change of mRNA expression of the axotomized nucleus relative to the uninjured, control nucleus was calculated using the $2^{-\Delta\Delta C}{}_{T}$ method.

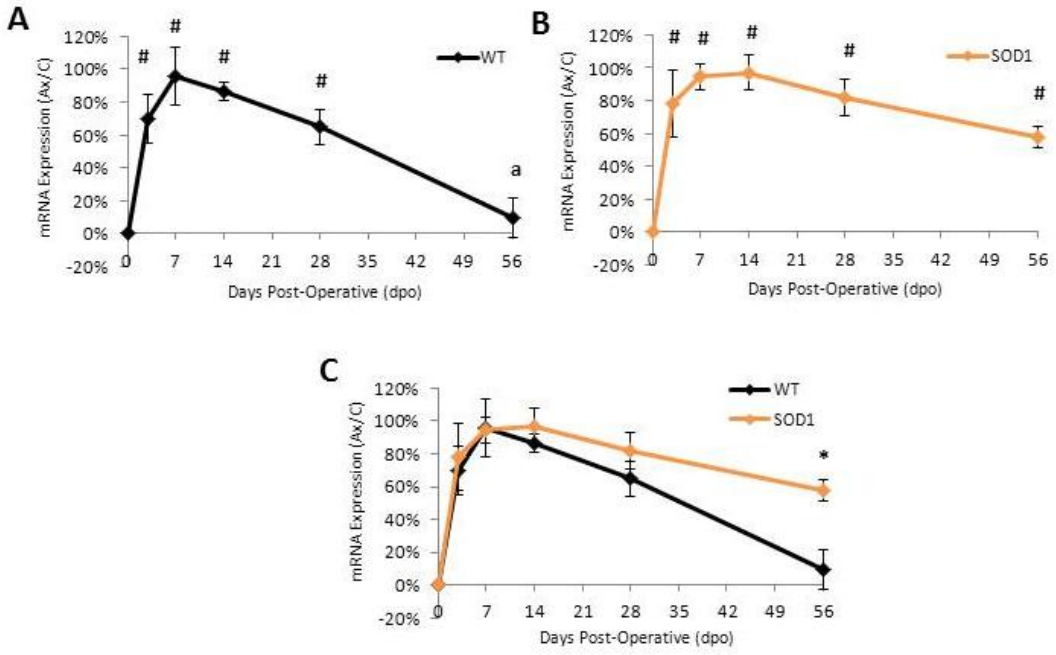

Figure 24. Percent change of **TNFR1** mRNA expression ± SEM in **WT** and **SOD1 axotomized** facial nuclei at 3, 7, 14, 28 and 56 dpo relative to control. **A**, WT. **B**, SOD1. **C**, WT vs. SOD1. **#** represents a significant difference relative to the control; ***** represents a significant difference relative to WT at $p \leq 0.05$.

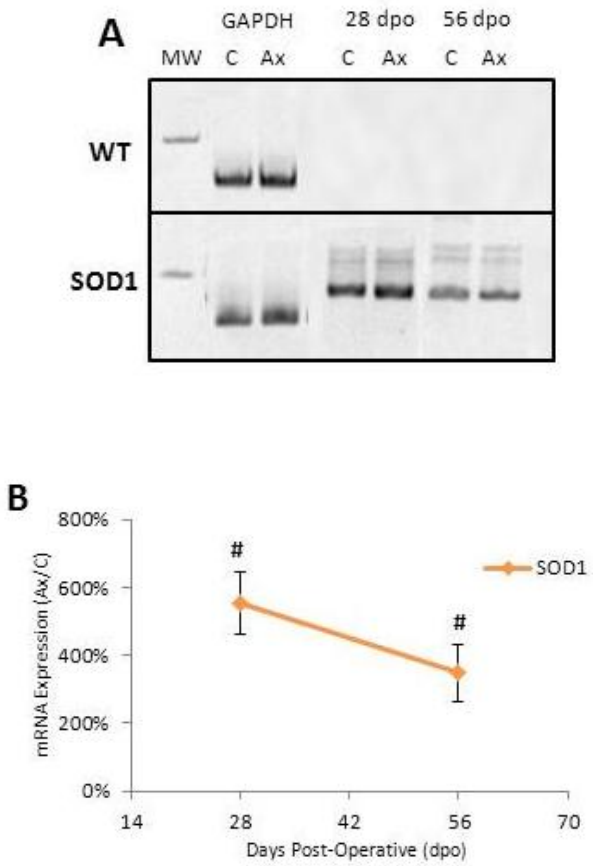

Figure 25. Change of **TNFα** mRNA expression in **WT** and **SOD1**, **control** (C) or **axotomized** (Ax) facial motor nuclei at 28 and 56 dpo. **A**, scanned image of TNFα gel electrophoresis, amplicon length of 102 base pairs (bp). Molecular marker (MM) band represents 100 bp. GAPDH, housekeeping gene, amplicon length of 78 bp. Upper panel displays WT and lower panel displays SOD1 facial nuclei. **B**, Percent change of **TNFα** mRNA expression ± SEM in **SOD1 axotomized** facial nuclei at 28 and 56 dpo relative to control. **#** represents a significant difference relative to the control at $p \leq 0.05$.

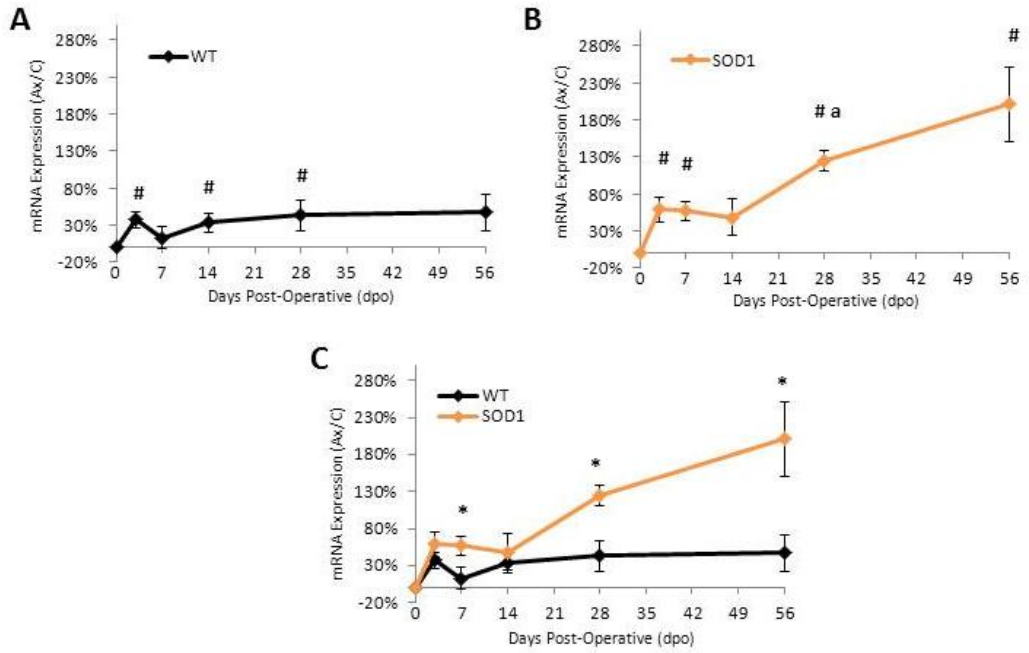

Figure 26. Percent change of **Fas** mRNA expression ± SEM in **WT** and **SOD1 axotomized** facial nuclei at 3, 7, 14, 28 and 56 dpo relative to control. **A**, WT. **B**, SOD1. **C**, WT vs. SOD1. **#** represents a significant difference relative to the control; **a** represents a significant difference relative to the previous time-point; ***** represents a significant difference relative to WT at $p \leq 0.05$.

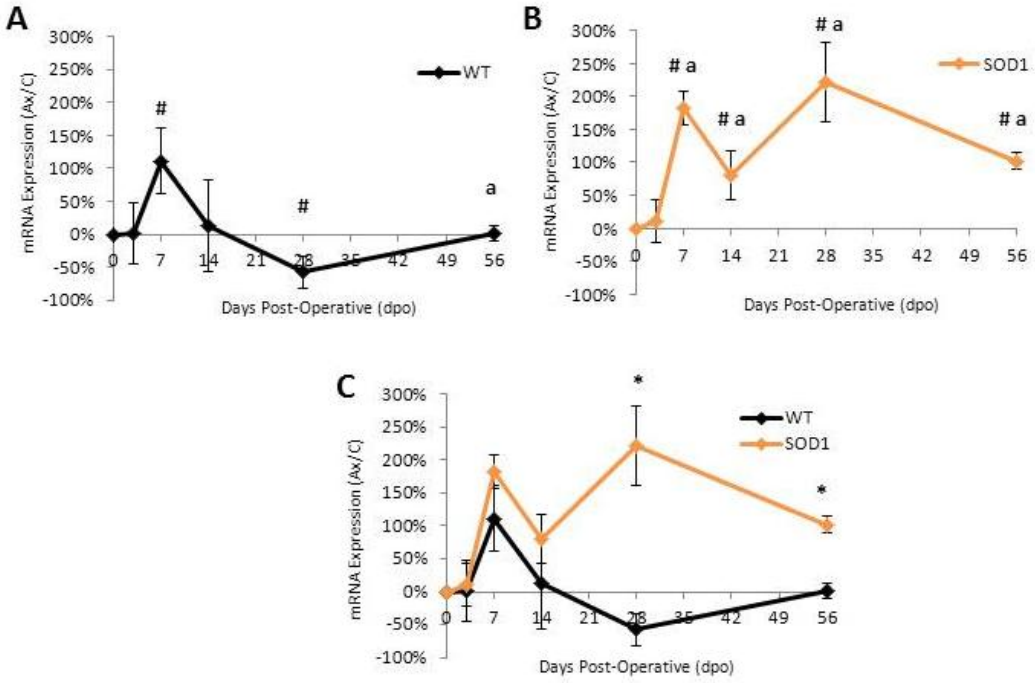

Figure 27. Percent change of **FasL** mRNA expression ± SEM in **WT** and **SOD1 axotomized** facial nuclei at 3, 7, 14, 28 and 56 dpo relative to control. **A**, WT. **B**, SOD1. **C**, WT vs. SOD1. **#** represents a significant difference relative to the control; **a** represents a significant difference relative to the previous time-point; ***** represents a significant difference relative to WT at $p \leq 0.05$.

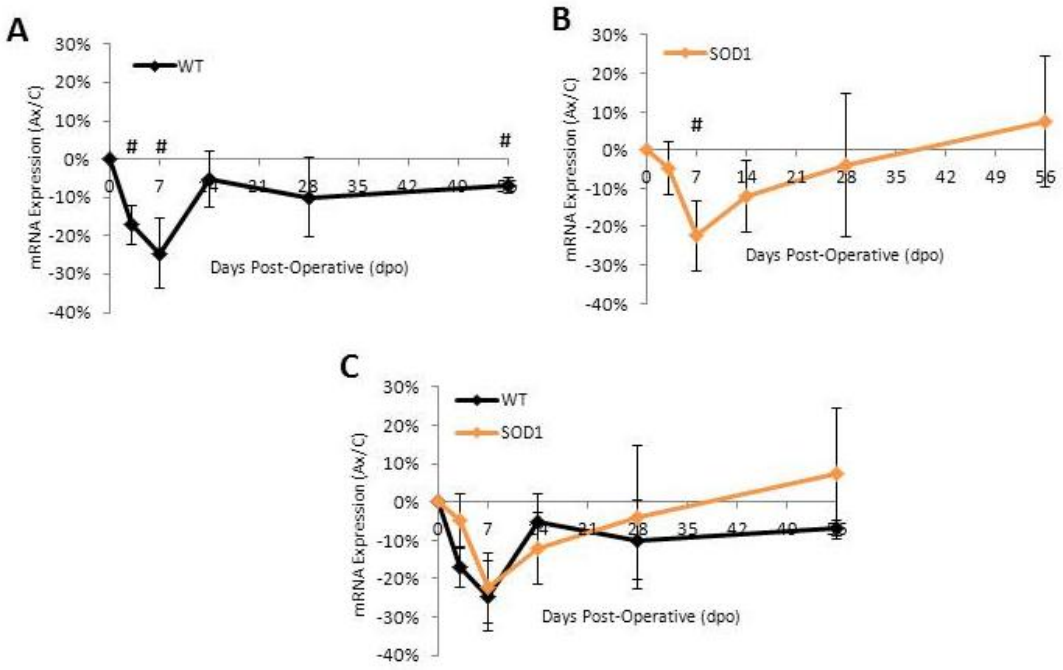

Figure 28. Percent change of **TRADD** mRNA expression ± SEM in **WT** and **SOD1 axotomized** facial nuclei at 3, 7, 14, 28 and 56 dpo relative to control. **A**, WT. **B**, SOD1. **C**, WT vs. SOD1. **#** represents a significant difference relative to the control at $p \leq 0.05$.

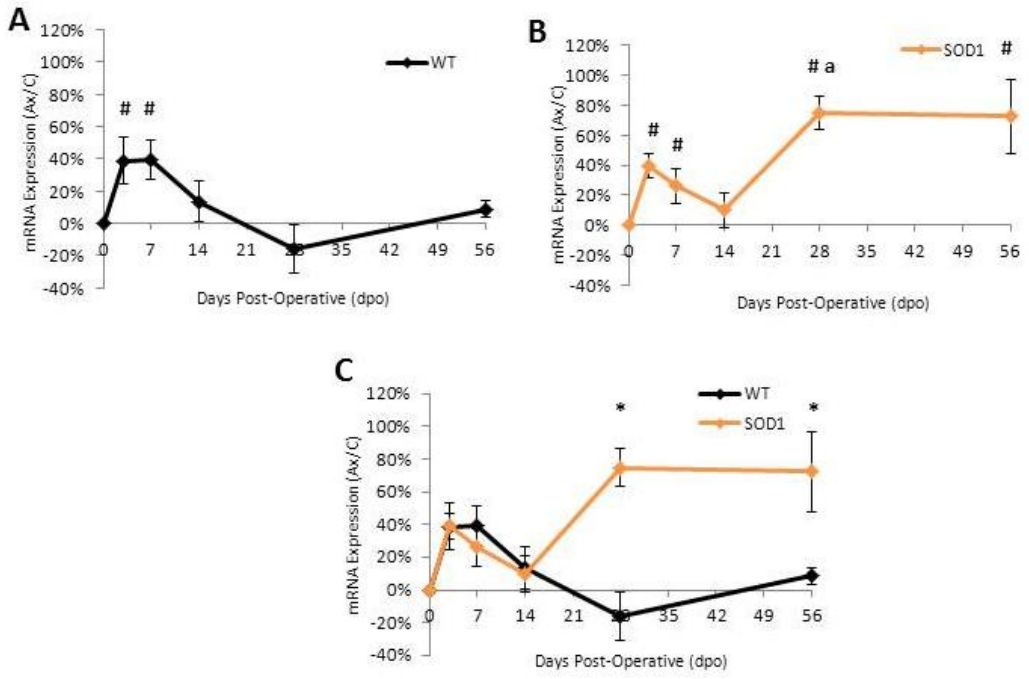

Figure 29. Percent change of **FADD** mRNA expression ± SEM in **WT** and **SOD1 axotomized** facial nuclei at 3, 7, 14, 28 and 56 dpo relative to control. **A**, WT. **B**, SOD1. **C**, WT vs. SOD1. **#** represents a significant difference relative to the control; **a** represents a significant difference relative to the previous time-point; ***** represents a significant difference relative to WT at $p \leq 0.05$.

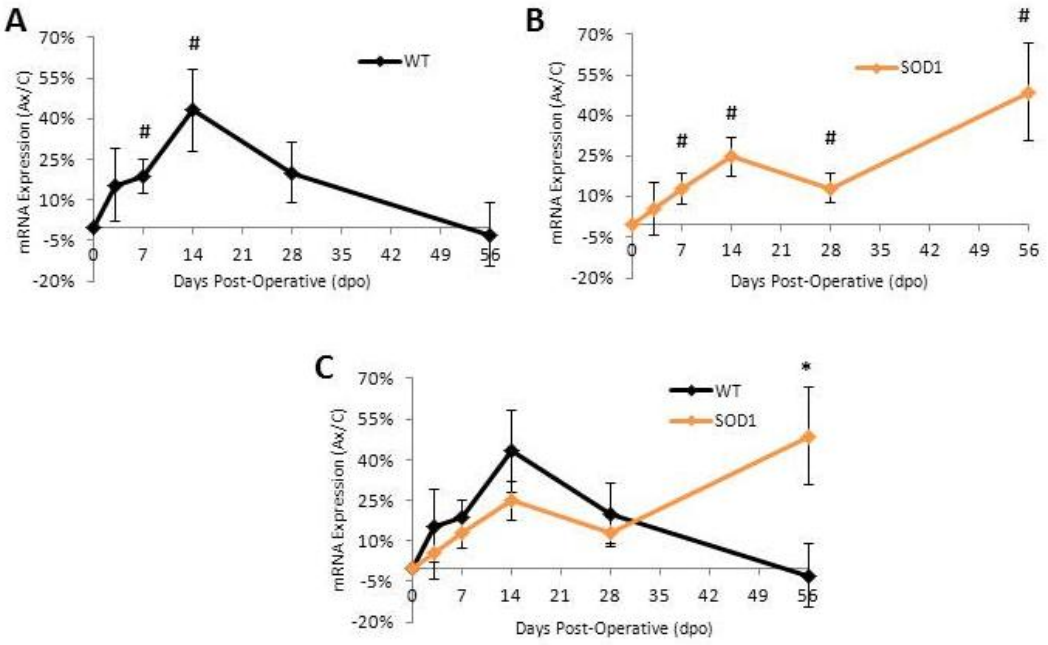

Figure 30. Percent change of **Daxx** mRNA expression ± SEM in **WT** and **SOD1 axotomized** facial nuclei at 3, 7, 14, 28 and 56 dpo relative to control. **A**, WT. **B**, SOD1. **C**, WT vs. SOD1. **#** represents a significant difference relative to the control; ***** represents a significant difference relative to WT at $p \leq 0.05$.

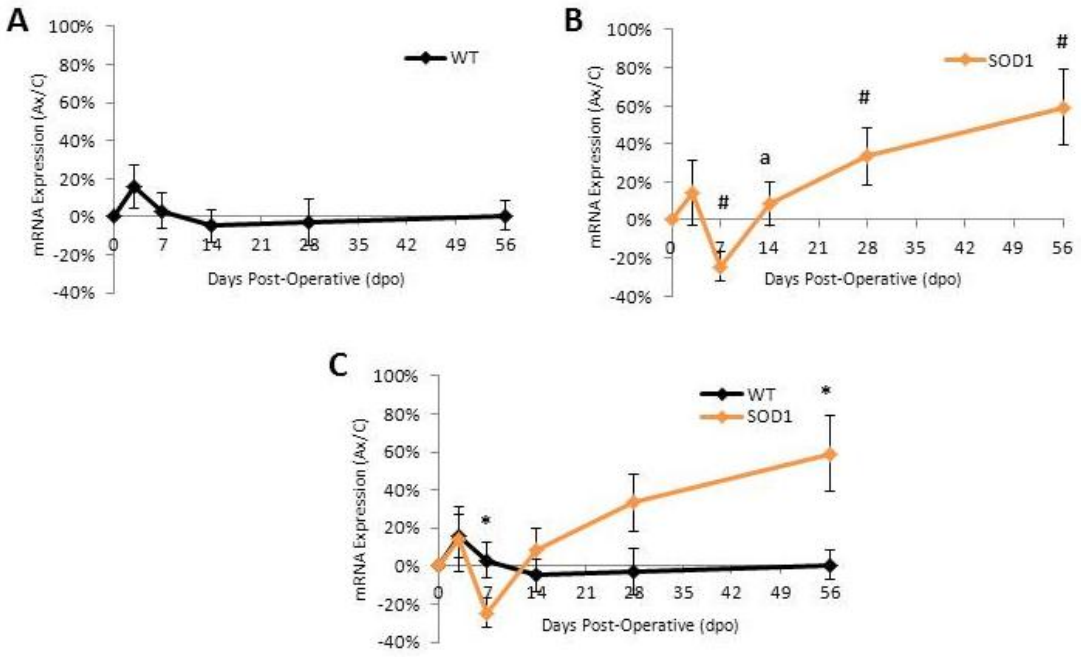

Figure 31. Percent change of **ASK1** mRNA expression ± SEM in **WT** and **SOD1 axotomized** facial nuclei at 3, 7, 14, 28 and 56 dpo relative to control. **A**, WT. **B**, SOD1. **C**, WT vs. SOD1. **#** represents a significant difference relative to the control; **a** represents a significant difference relative to the previous time-point; ***** represents a significant difference relative to WT at $p \leq 0.05$.

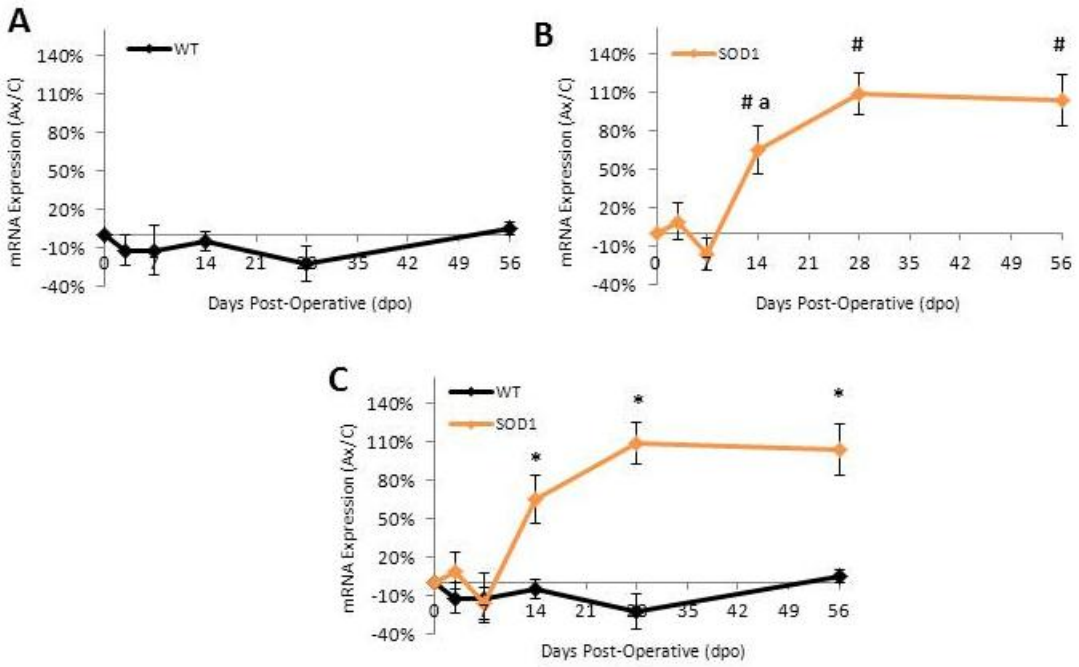

Figure 32. Percent change of **nNOS** mRNA expression ± SEM in **WT** and **SOD1 axotomized** facial nuclei at 3, 7, 14, 28 and 56 dpo relative to control. **A**, WT. **B**, SOD1. **C**, WT vs. SOD1. **#** represents a significant difference relative to the control; **a** represents a significant difference relative to the previous time-point; ***** represents a significant difference relative to WT at $p \leq 0.05$.

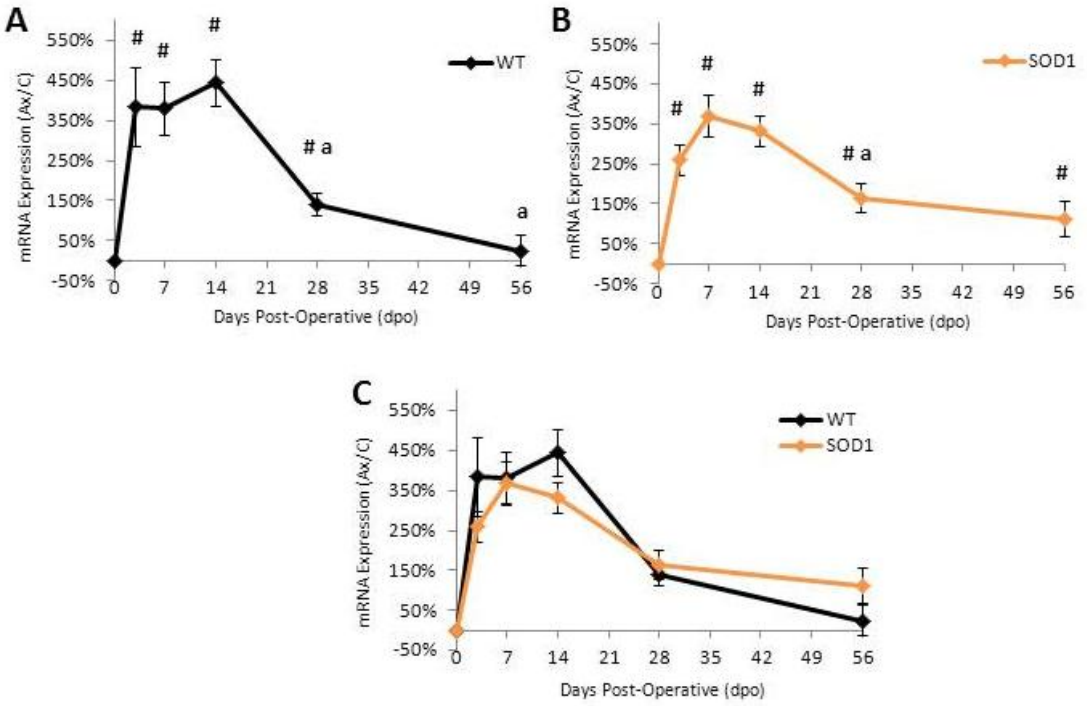

Figure 33. Percent change of **Caspase-3** mRNA expression ± SEM in **WT** and **SOD1 axotomized** facial nuclei at 3, 7, 14, 28 and 56 dpo relative to control. **A**, WT. **B**, SOD1. **C**, WT vs. SOD1. **#** represents a significant difference relative to the control; **a** represents a significant difference relative to the previous time-point at $p \leq 0.05$.

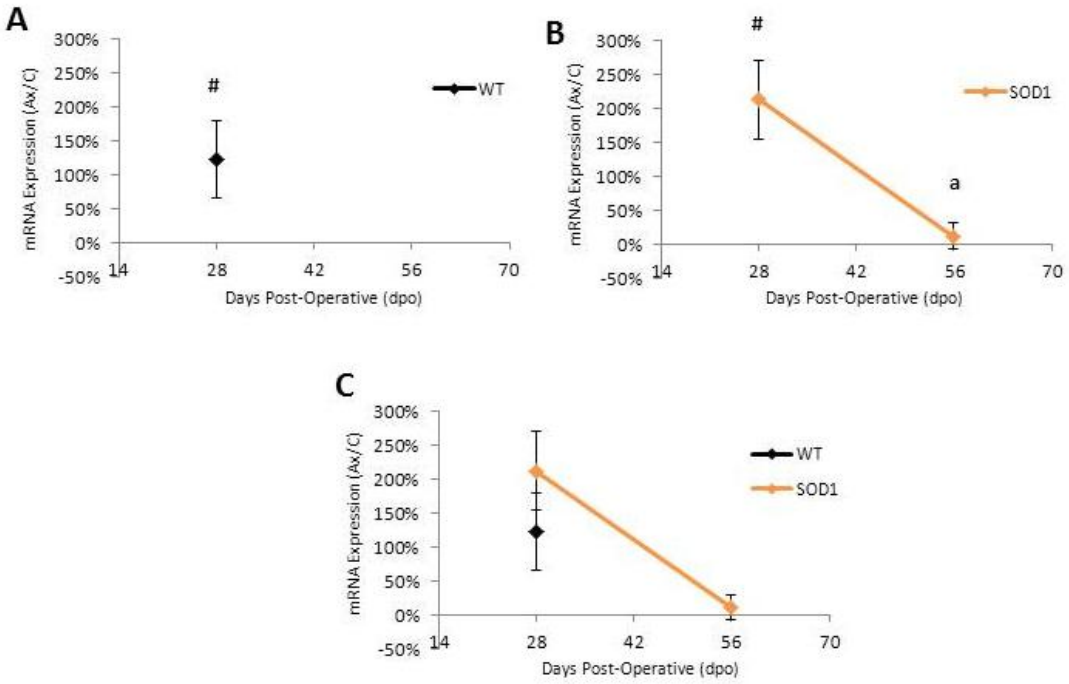

Figure 34. Percent change of **Caspase-8** mRNA expression ± SEM in **SOD1 axotomized** facial nuclei at 28 and 56 dpo and **WT axotomized** facial nuclei at 28 dpo relative to control. **A**, WT. **B**, SOD1. **C**, WT vs. SOD1. **#** represents a significant difference relative to the control; **a** represents a significant difference relative to the previous time-point at $p \leq 0.05$.

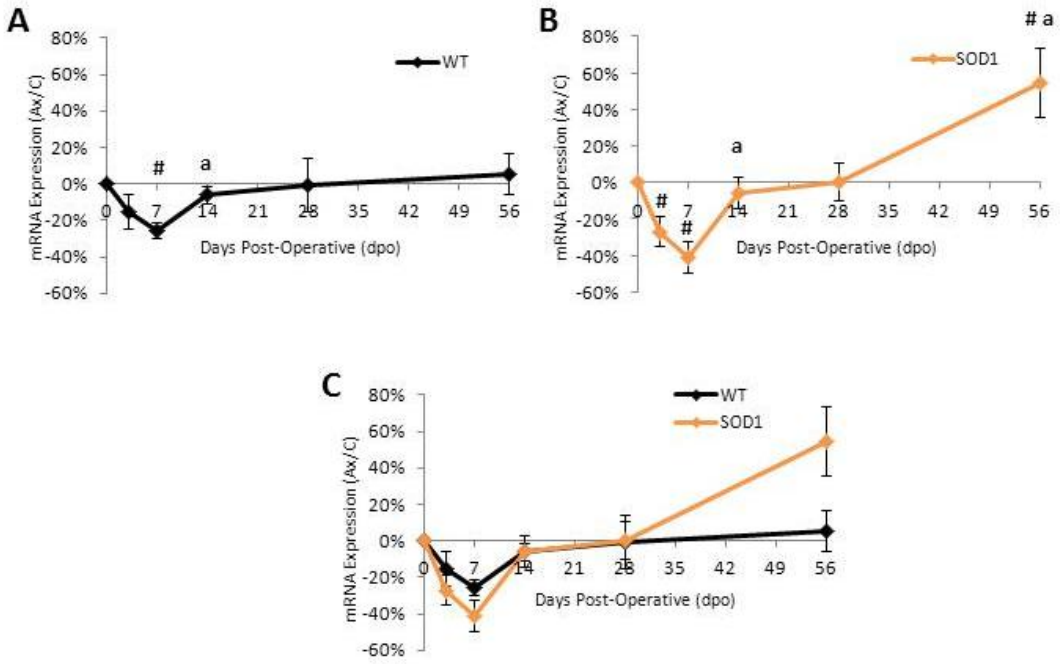

Figure 35. Percent change of **TRAF2** mRNA expression ± SEM in **WT** and **SOD1 axotomized** facial nuclei at 3, 7, 14, 28 and 56 dpo relative to control. **A**, WT. **B**, SOD1. **C**, WT vs. SOD1. **#** represents a significant difference relative to the control; **a** represents a significant difference relative to the previous time-point at $p \leq 0.05$.

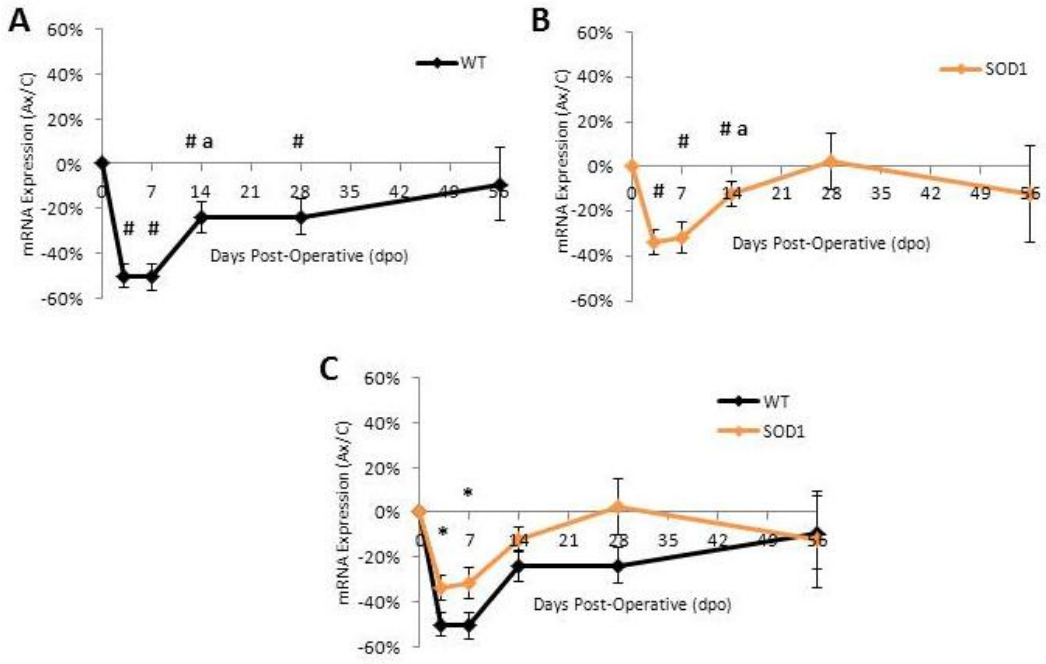

Figure 36. Percent change of **SODD** mRNA expression ± SEM in **WT** and **SOD1 axotomized** facial nuclei at 3, 7, 14, 28 and 56 dpo relative to control. **A**, WT. **B**, SOD1. **C**, WT vs. SOD1. **#** represents a significant difference relative to the control; **a** represents a significant difference relative to the previous time-point; ***** represents a significant difference relative to WT at $p \leq 0.05$.

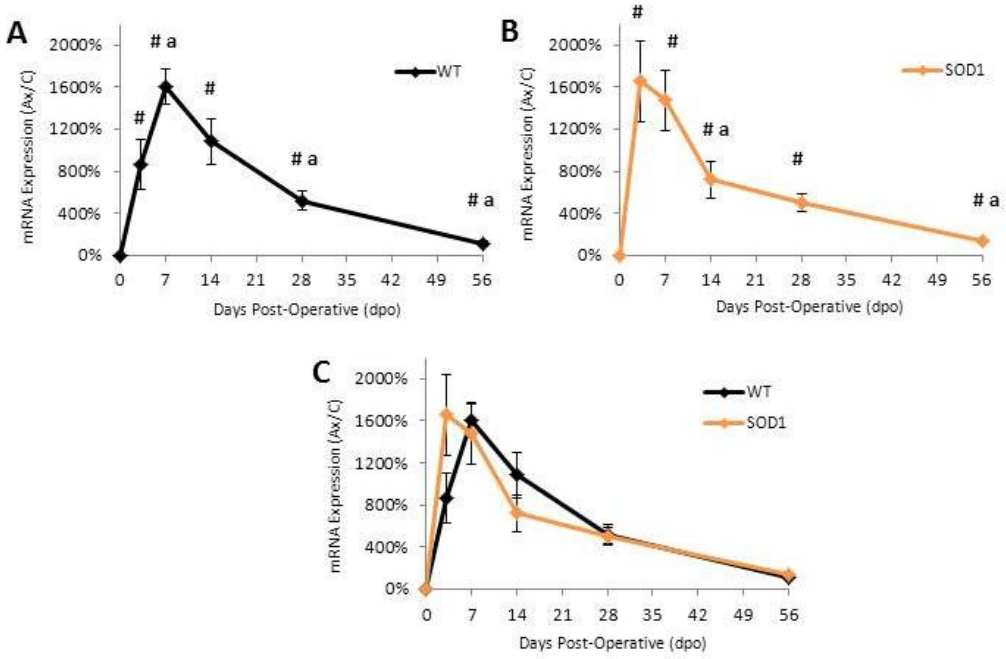

Figure 37. Percent change of **TNFR2** mRNA expression ± SEM in **WT** and **SOD1 axotomized** facial nuclei at 3, 7, 14, 28 and 56 dpo relative to control. **A**, WT. **B**, SOD1. **C**, WT vs. SOD1. **#** represents a significant difference relative to the control; **a** represents a significant difference relative to the previous time-point at $p \leq 0.05$.

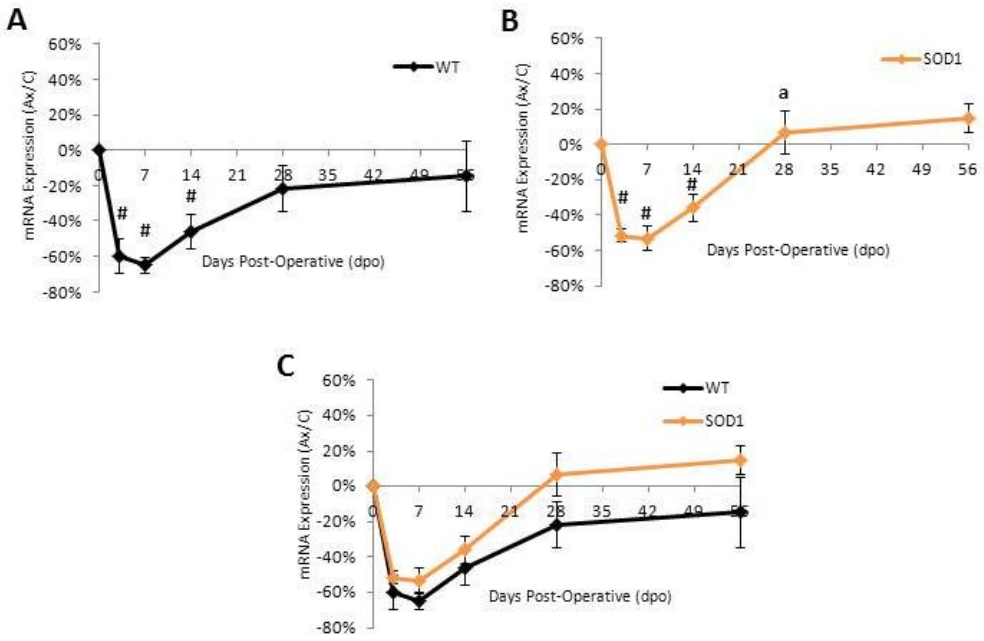

Figure 38. Percent change of **PAC1-R** mRNA expression ± SEM in **WT** and **SOD1 axotomized** facial nuclei at 3, 7, 14, 28 and 56 dpo relative to control. **A**, WT. **B**, SOD1. **C**, WT vs. SOD1. **#** represents a significant difference relative to the control; **a** represents a significant difference relative to the previous time-point at $p \leq 0.05$.

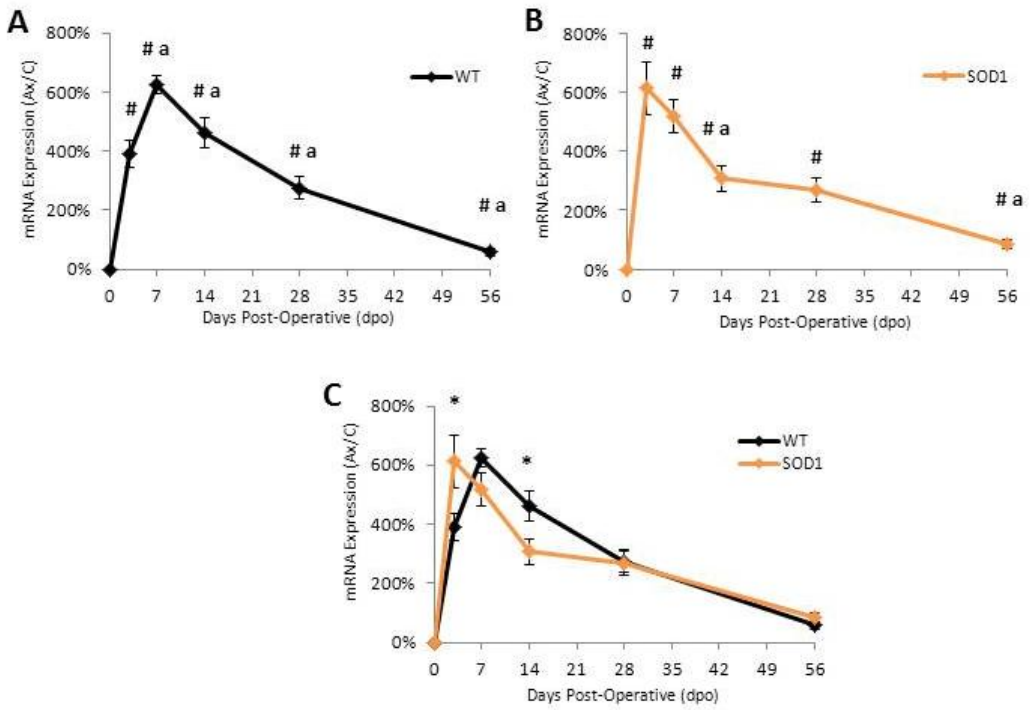

Figure 39. Percent change of **CX3CR1** mRNA expression ± SEM in **WT** and **SOD1 axotomized** facial nuclei at 3, 7, 14, 28, and 56 dpo relative to control. **A**, WT. **B**, SOD1. **C**, WT vs. SOD1. **#** represents a significant difference relative to the control; **a** represents a significant difference relative to the previous time-point; ***** represents a significant difference relative to WT at $p \leq 0.05$.

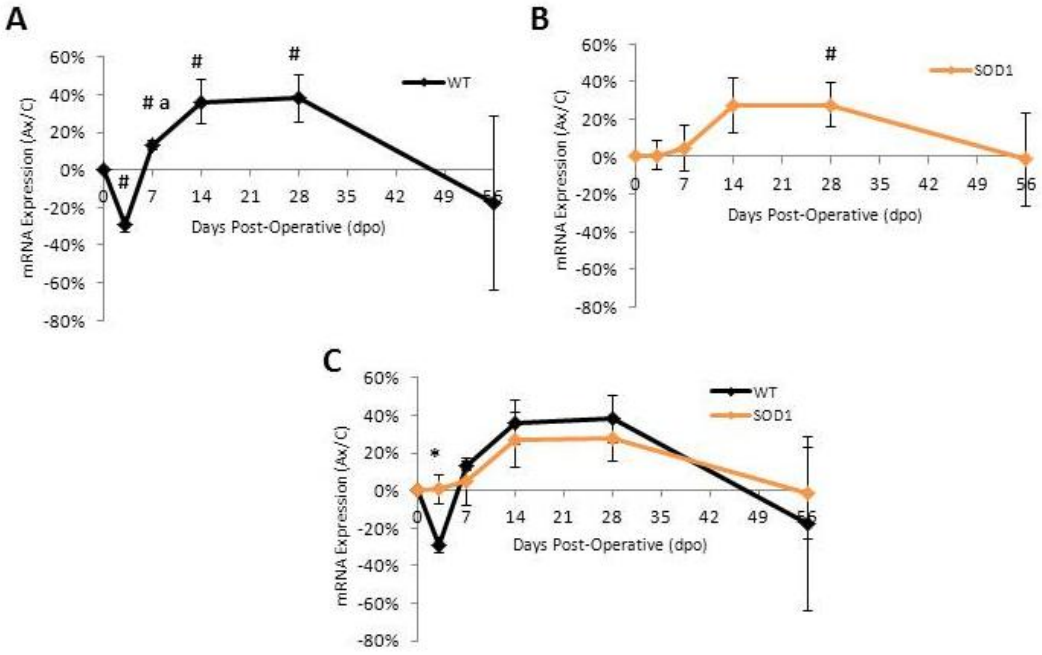

Figure 40. Percent change of **CRMP4** mRNA expression ± SEM in **WT** and **SOD1 axotomized** facial nuclei at 3, 7, 14, 28 and 56 dpo relative to control. **A**, WT. **B**, SOD1. **C**, WT vs. SOD1. **#** represents a significant difference relative to the control; **a** represents a significant difference relative to the previous time-point; ***** represents a significant difference relative to WT at $p \leq 0.05$.

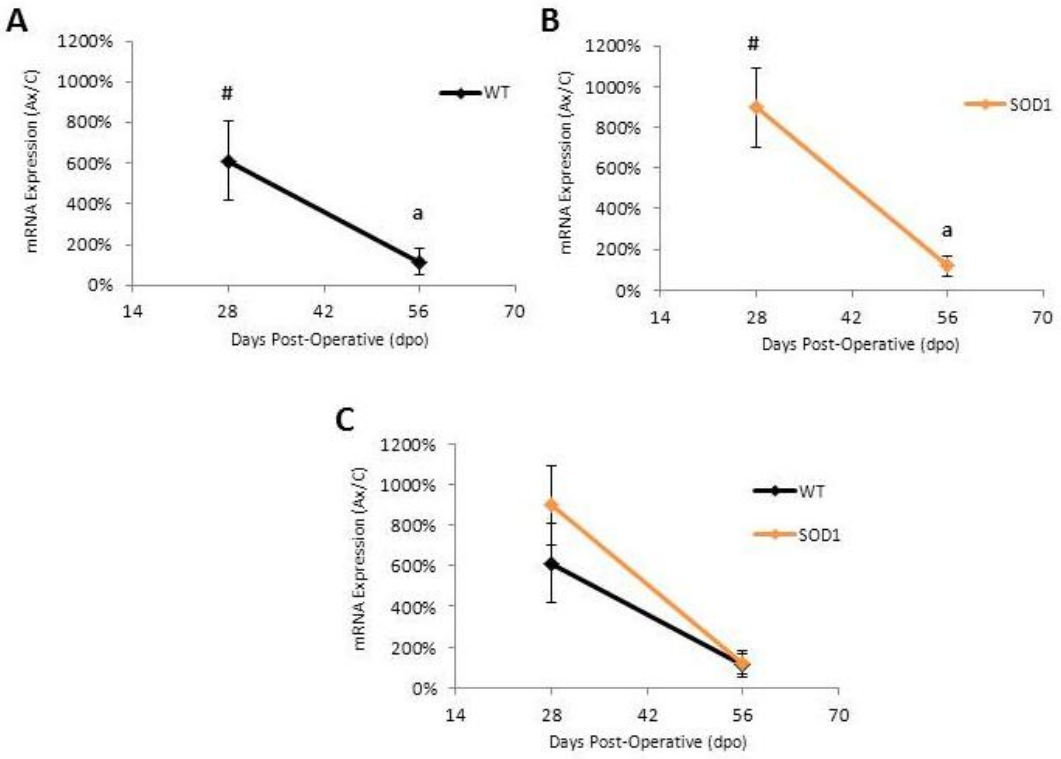

Figure 41. Percent change of **GAP-43** mRNA expression ± SEM in **WT** and **SOD1 axotomized** facial nuclei at 28 and 56 dpo relative to control. **A**, WT. **B**, SOD1. **C**, WT vs. SOD1. **#** represents a significant difference relative to the control; **a** represents a significant difference relative to the previous time-point at $p \leq 0.05$.

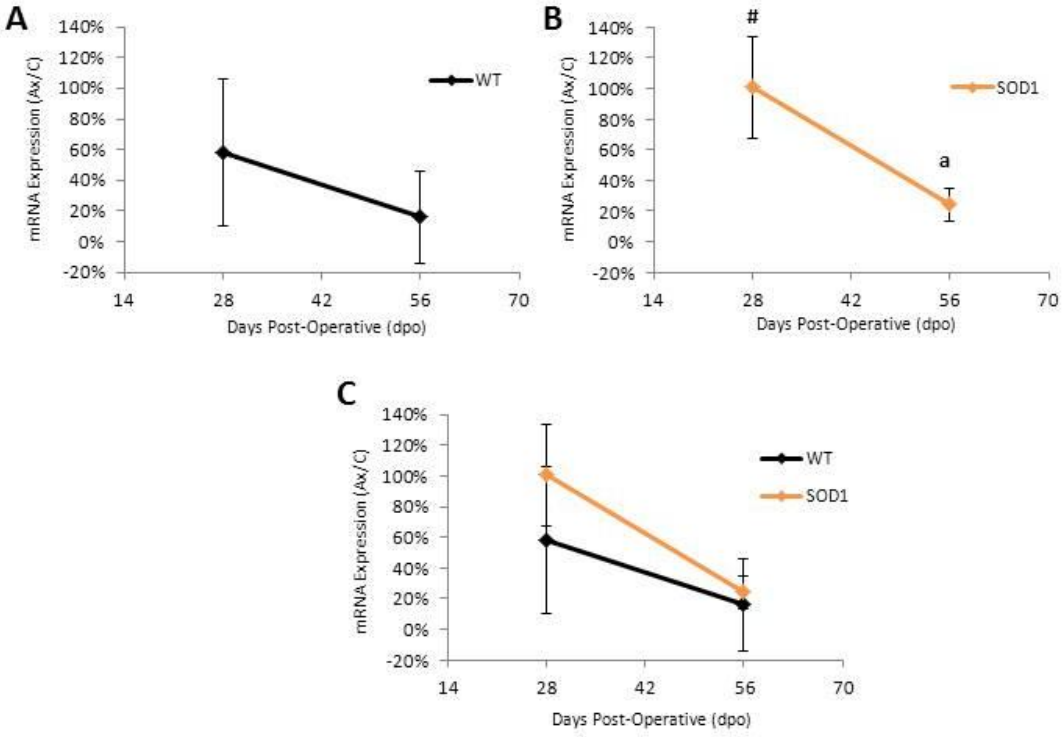

Figure 42. Percent change of **βII-Tubulin** mRNA expression ± SEM in **WT** and **SOD1 axotomized** facial nuclei at 28 and 56 dpo relative to control. **A**, WT. **B**, SOD1. **C**, WT vs. SOD1. **#** represents a significant difference relative to the control; **a** represents a significant difference relative to the previous time-point at $p \leq 0.05$.

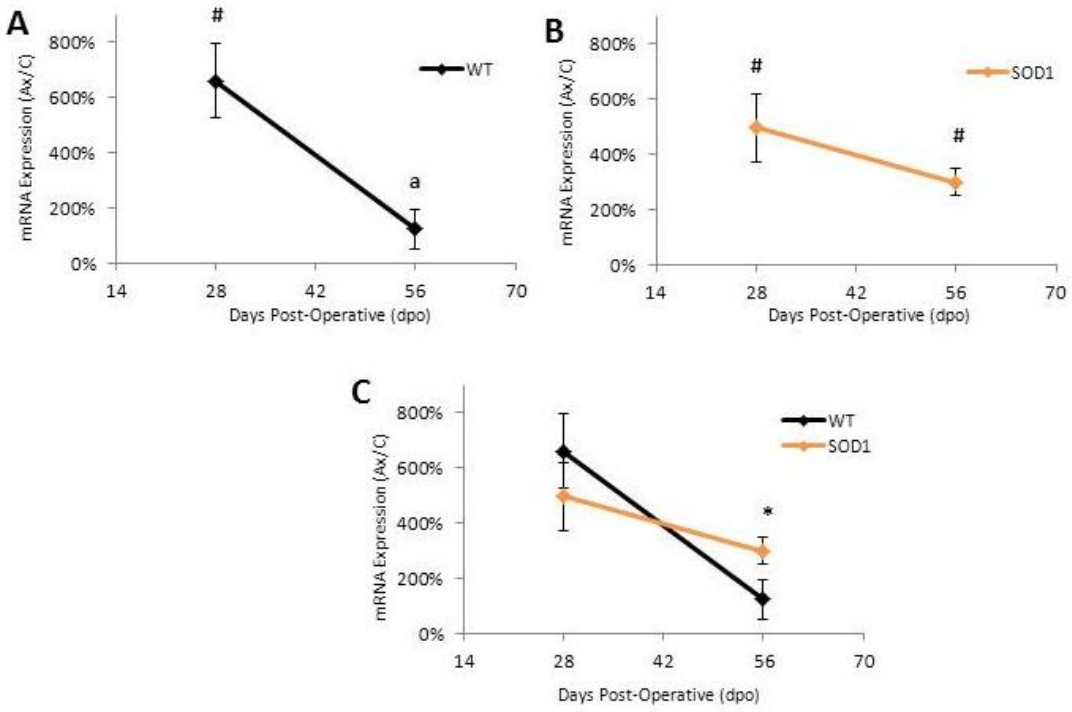

Figure 43. Percent change of **GFAP** mRNA expression ± SEM in **WT** and **SOD1 axotomized** facial nuclei at 28 and 56 dpo relative to control. **A**, WT. **B**, SOD1. **C**, WT vs. SOD1. **#** represents a significant difference relative to the control; **a** represents a significant difference relative to the previous time-point; ***** represents a significant difference relative to WT at $p \leq 0.05$.

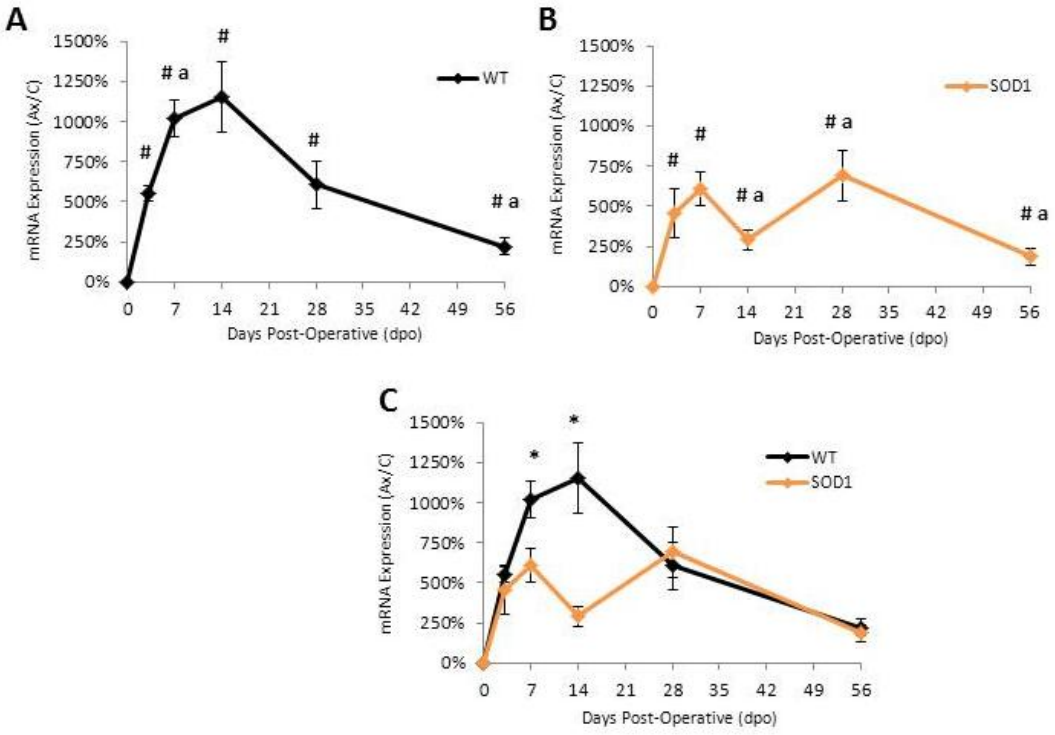

Figure 44. Percent change of **CD68** mRNA expression ± SEM in **WT** and **SOD1 axotomized** facial nuclei at 3, 7, 14, 28 and 56 dpo relative to control. **A**, WT. **B**, SOD1. **C**, WT vs. SOD1. **#** represents a significant difference relative to the control; **a** represents a significant difference relative to the previous time-point; ***** represents a significant difference relative to WT at $p \leq 0.05$.

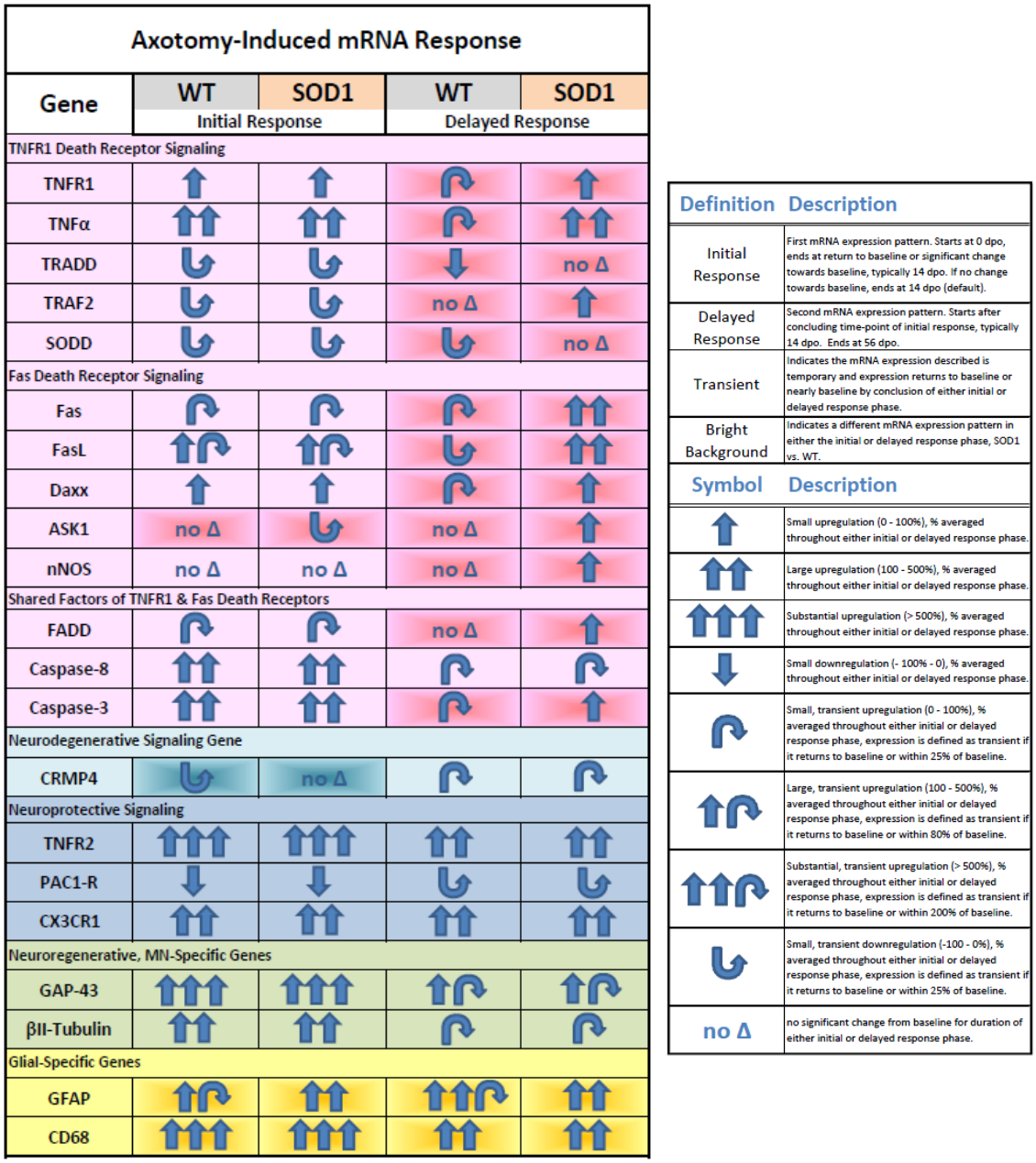

Table 4: Summary of axotomy-induced percent change mRNA expression responses % (Ax/C) in WT and SOD1 mice. Note that mRNA expression for the time-points of 3, 7, 14 and 28 dpo was previously determined by our laboratory and results from those genes (TNFα, Caspase-8, GAP-43, βII-Tubulin and GFAP) are summarized within this table (Mesnard et al., 2011).

E. Discussion

The experiments performed within this Chapter focused on MN survival and molecular expression following experimentally-induced neuronal target disconnection. It has been well-established that the initial pathological event in SOD1 disease progression is the loss of NMJ or target disconnection within the pre-symptomatic stage (Fischer et al., 2004; Dadon-Nachum et al., 2011). This denervation proceeds clinical symptoms and MN cell loss and therefore, resembles the "die-back" phenomenon.

Facial nerve axotomy within the SOD1 pre-symptomatic stage was assessed as an experimental model of the "die-back" that is evident in ALS. This Chapter details the responses to the experimentally-induced target disconnection within the SOD1 facial motor nucleus. The measured outcomes of these responses were FMN cell survival and mRNA expression of genes involved in neurodegeneration, neuroprotection and the glial response. The results obtained from the axotomized SOD1 facial motor nucleus were compared to WT, axotomized facial motor nucleus. The WT FMN percent survival as well as the mRNA expression levels and patterns of expression over time, provide a reference or a standard of what can be considered a "normal" response to target disconnection. The ability to compare the SOD1 target-disconnection response to the WT allows for identification of potential dysregulated mechanisms. Identification of potential neurodegenerative mechanisms is generally the first step in development of potential and prospective therapeutics and treatment interventions.

Subsequent Chapters focus on the theoretical, diseased-induced target disconnection of the facial motor nucleus. Responses within the disease-affected facial motor nucleus were analyzed utilizing the same measureable outcomes, FMN cell survival and mRNA expression of genes involved in neurodegeneration, neuroprotection and the glial response. Comparisons between FMN survival and gene expression within the SOD1 facial motor nucleus after axotomy and during disease progression suggest that facial nerve axotomy within the SOD1 pre-symptomatic stage resembles disease progression and strongly suggests disease progression is a result of a neuronal "die-back" phenomenon.

Susceptibility to Axotomy of the Immune-Dependent MN Subpopulation within the SOD1 Facial Motor Nucleus

After facial nerve axotomy, pre-symptomatic SOD1 mice display a dramatic reduction in FMN percent survival at 28 dpo compared to WT, which was previously reported by us (Mesnard et al., 2011). Additionally, WT FMN survival was only marginally decreased at 28 dpo but these levels were further reduced by 56 dpo, which is in agreement with our previous findings at 70 dpo (Serpe et al., 2000). The FMN survival experiment within this Chapter revealed that at the extended time-point of 56 dpo the level of FMN survival was maintained in the SOD1 mouse. This pattern of dramatic FMN loss at 28 dpo followed by maintenance of FMN survival with time after axotomy has been shown by our lab before using immunodeficient mouse models

(Serpe et al., 2000; Beahrs, 2009). These findings suggest a lack of neuroprotection of the immune-dependent MN population within the SOD1 facial motor nucleus. The lack of neuroprotection may be due to a deficit within the SOD1 peripheral immune system or lack of successful communication between the acquired immune system and facial motor nucleus. Investigation of the SOD1 peripheral immune system is ongoing and recent findings from our lab suggest that the immune-dependent MN population within the SOD1 facial motor nucleus is capable of being rescued to WT FMN survival levels after reconstitution with WT splenocytes (unpublished data).

Persistence of the Resilient MN Subpopulation within Axotomized SOD1 Facial Motor Nucleus at 56 dpo

Additionally these results show the SOD1 facial motor nucleus, similar to the WT and immunodeficient models, may include a second, subpopulation of MN in the facial motor nucleus which consists of the 40-50% of cells that are a resilient population and survive for long periods of time, regardless of immune-status or target reconnection (Jones et al., 2005). This resilient population of MN appears to be evident within the SOD1 and ALS literature (Felice, 1997; Dadon-Nachum et al., 2011).

mRNA Expression Time Course of 21 Genes within the WT and SOD1 Axotomized Facial Motor Nucleus

The axotomy-induced mRNA expression data in WT and SOD1 mice is summarized in **Table 4** and reveals several important conclusions.

Biphasic mRNA Expression Following Axotomy

The majority of genes assessed within the facial motor nucleus reveal a biphasic pattern of mRNA expression throughout the extended time course in response to facial nerve axotomy. Among the 21 genes assessed, some variation exists. In addition, the intersecting time-point between the 2 phases can be somewhat arbitrary, depending on the specific gene. However, in general the expression patterns of WT and SOD1 suggest the presence of an initial and a delayed molecular response to axotomy.

The distinct, initial phase typically includes the time-points of 3, 7, and 14 dpo and conclusion of this phase is marked by a return to baseline, i.e. a transient up/down-regulation, or a significant change towards baseline expression. In the WT the delayed phase is typically unchanged, following transient expressions that occur within the initial phase, or includes a return to baseline by the last time-point (56 dpo). Several genes, such as TNFR1 do not reveal a biphasic pattern, but for comparison purposes the most common intersecting time-point that usually distinguishes the two phases (14 dpo) was chosen. While TNFR1 expression is recorded within **Table 4** in both the initial and delayed response sections, the continued upregulation is still evident and reflected by the symbols within the table.

WT mRNA Expression Levels and Patterns

The only genes that remain upregulated in the WT and have therefore, not returned to baseline by 56 dpo are those related to the microglial response, CD68 and

the two neuroprotective receptors, localized to microglia, CX3CR1 and TNFR2. These findings suggest a continued response or sustained reactivity of microglia in the axotomized WT facial motor nucleus at 56 dpo.

Within the WT facial motor nucleus, all death receptor signaling genes for TNFR1 and Fas have returned to baseline by 56 dpo. The literature suggests that MN cell death after facial nerve axotomy most likely involves the TNFR1 death pathway (Mesnard et al., 2010; Mesnard, 2009; Raivich et al., 2002). The upregulation of TNFR1 genes within both the initial and delayed response phases supports this theory. Conversely, within the literature there is no indication that facial nerve axotomy results in Fas-induced MN cell death, yet upregulation of Fas genes occurs after axotomy in the WT. It has been recently determined that Fas-induced MN cell death requires activation of 2 pathways downstream of Fas (refer to Chapter II Section K.e.iii) and while these results show increased mRNA for factors involved in the more typical downstream pathway, shared by TNFR1 (FADD/Caspase-8/Caspase-3), several factors required in the MN-specific Fas pathway (ASK1/nNOS) are not upregulated at all following axotomy in WT. For Fas-induced MN cell death, both pathways downstream of Fas must be activated and blocking either pathway is protective. Potentially, the absence of increased expression of ASK1 and nNOS is evidence of regulation within the MN-specific Fas pathway and prevention of Fas-induced MN death in the WT after axotomy. However, it must be mentioned that these results are only suggestive and changes in mRNA expression levels

does not necessarily translate to protein concentration or activation states of those proteins. Further examination of protein concentrations, localization, and phosphorylation states will need to be examined to make more definitive conclusions.

Similar Response of mRNA Expression During the Initial-Response Phase Between WT and SOD1 Mice

In comparison to the WT, SOD1 mRNA expression within the initial-response phase following axotomy is overwhelmingly similar. Some similarities of expression between WT and SOD1 were anticipated; however the sheer number of genes that were expressed in a similar manner within the initial phase was surprising. Current theory, supported by the results of our previous studies as well as those conducted by other investigators, suggests that MN in the SOD1 mouse and in the ALS patient are capable of responding to injury or target disconnection in a regenerative manner. These mRNA expression results within the initial-response to axotomy support this theory.

SOD1 mRNA Expression is Dysregulated within the Delayed-Response Phase Compared to WT

Although most genes assessed displayed equivalent expression levels and patterns between WT and SOD1 during the initial-response to axotomy, mRNA expression throughout the delayed-response was vastly different in the SOD1 facial nucleus compared to WT. It was apparent that in the SOD1 many of the genes analyzed failed to return to baseline by 56 dpo and appeared to show either maintenance of the

upregulation or a continual increase in upregulation. These findings led to the conclusion that certain genes are dysregulated in the SOD1 axotomized facial nucleus compared to the WT.

Genes involved in the TNFR1 and Fas death receptor signaling pathways are all dysregulated in the SOD1 axotomized facial motor nucleus compared to WT. Every gene specific to the Fas pathway (Fas, FasL, Daxx, ASK1, nNOS) at 56 dpo are upregulated compared to WT and/or have not returned to baseline. Additionally FADD, Capsase-3, shared by TNFR1 and Fas signaling are also dysregulated compared to WT. Among genes involved in TNFR1 death pathway, TNFR1, TNFα, and TRAF2 are dysregulated in the SOD1 and this is evident by their increased upregulation and failure to return to baseline by 56 dpo. Other genes such as TRADD, SODD, and CRMP4 show a dysregulation in the SOD1 by an absence downregulation that is evident in the WT. This downregulation may be important in regulation of the signaling and inhibition of further neurodegeneration however these ideas are speculative.

Glial cell response to axotomy initially appeared similar however it too is dysregulated following neuronal target disconnection in the SOD1 compared to WT. In SOD1 both genes, GFAP and CD68 do not reach the level mRNA expression seen in the WT response to axotomy. In addition, the upregulation of GFAP expression, while suppressed in the SOD1 compared to the WT is maintained at 56 dpo in the SOD1 facial nucleus and does not return to baseline as was seen in the WT facial nucleus. The

suppression of glial-specific genes in the SOD1 axotomized facial nucleus suggest that microglia and astrocytes do respond to neuronal target disconnection, however their response is significantly less robust than that seen in the WT. Therefore the glial response is dysregulated within the SOD1 facial nucleus (Mesnard et. al., 2011).

While the majority of genes appeared dysregulated in the SOD1 several were regulated or expressed in a similar pattern and to an equivalent degree. These regulated genes included Caspase-8, the neuroprotective signaling genes (TNFR2, PAC1-R and CX3CR1) and the neuroregenerative genes (GAP-43 and βII-Tubulin). These results support what has been previously mentioned, that SOD1 MN are capable of regeneration and attempt to survive after peripheral nerve injury or target disconnection. It is unclear why Caspase-8 is only death receptor-associated signaling gene that appears regulated in the SOD1 compared to WT. This result may be better understood if protein levels for the activated form of the Caspase-8 were assessed.

It should be mentioned that while the experiments within this dissertation focus FMN survival, many of these genes are ubiquitously expressed and the use of relative mRNA expression of the facial nucleus does not provide any information indicative as to which cell type is expressing the mRNA.

Subsequent Chapters focus on the theoretical, diseased-induced target disconnection of the facial motor nucleus. Responses within the disease-affected facial motor nucleus were analyzed utilizing the same measureable outcomes, FMN cell

survival and mRNA expression of genes involved in neurodegeneration, neuroprotection and the glial response. Comparisons between FMN survival and gene expression within the SOD1 facial motor nucleus after axotomy and during disease progression suggest that facial nerve axotomy within the SOD1 pre-symptomatic stage resembles disease progression and strongly suggests disease progression is a result of a neuronal “die-back” phenomenon.

CHAPTER V

DISEASE-INDUCED MOLECULAR EXPRESSION IN SYMPTOMATIC SOD1 FACIAL MOTOR NUCLEUS

A. Abstract

ALS is a neurodegenerative disease resulting in MN cell death. The SOD1 transgenic mouse model of ALS has similar disease pathology as observed clinically. Disease onset is initiated during the pre-symptomatic stage where MN axons withdraw from target muscles, i.e., an axonal die-back process. The process of axonal die-back results in a cellular response resembling peripheral nerve chronic transection axotomy. The well-established facial nerve axotomy model is used to investigate the properties of MN survival and regeneration. We have shown that pre-symptomatic SOD1 FMN are significantly more susceptible to axotomy-induced cell death compared to WT. In addition, we identified that the MN-specific gene expression response in pre-symptomatic SOD1 facial nucleus after axotomy was similar to the WT response. However, a dysregulated neuropil gene expression response was observed in the pre-symptomatic SOD1 facial nucleus after axotomy, which was significantly distinct from the WT response. Specifically, pre-symptomatic SOD1 MN in the facial nucleus are surrounded by a pro-inflammatory microenvironment constitutively expressing TNFα.

Recently, we examined the response of death receptor signaling gene expression after axotomy in WT and pre-symptomatic SOD1 mice. The results demonstrate that axotomy, itself, induces a characteristic molecular response in WT and SOD1 facial nuclei, involving the upregulation of death receptors and downstream apoptotic signaling molecules. Therefore, we propose that SOD1 MN susceptibility to cell death is due to a dysregulated interaction between the existing pro-inflammatory microenvironment and the MN molecular response to axonal injury. The current study investigated the molecular response to disease progression at the level of the facial nucleus in symptomatic SOD1 mice, and compared this molecular response to pre-symptomatic SOD1 axotomy-induced response. The results indicate that the molecular response to disease within the control, facial motor nucleus of symptomatic SOD1 mice, resembles the axotomy-induced molecular response in pre-symptomatic mice.

B. Introduction

Chapter V investigates the molecular response to SOD1 disease progression within the facial motor nucleus. This molecular response is compared to the axotomy-induced molecular response determined in Chapter IV. For specifics regarding the molecular response to axotomy in the pre-symptomatic SOD1 facial nucleus, refer to Chapter IV.

The SOD1 mouse appears to develop normally, well into adulthood. The first symptoms develop at approximately 90 doa and consist of a slight tremor of the hind-

limbs. This tremor becomes more pronounced, including both hind-limbs and sometimes the forelimbs. Proximal muscle weakness and atrophy begin to develop by 120 doa as evident by shortness of stride. SOD1 mice reach end-stage disease by 136 doa, marked by severe paralysis. The mice are unable to lift their pelvis, generally do not respond to tapping on the cage, and are unable to groom themselves. MN cell death accompanies the progression of symptoms. At symptomatic stage, 90 days, the decrease in the number of somatic MN in C7 and L3 segments reaches significance compared to aged-matched controls. The MN death continues into end-stage disease where the MN loss reaches 50% in the ventral horn of spinal cord. Previous studies within the brainstem showed MN in the hypoglossal motor nucleus revealed a trend for MN loss, however significance was not reached by end-stage disease (Chiu et al., 1995).

However, the initial pathological event that is thought to initiate the disease is denervation of muscle endplates. Early within the pre-symptomatic stage loss of NMJ becomes significant within the hind-limb musculature. This is followed by evidence of distal axonopathy. Concurrent electrophysiological assessments reveal abnormalities which validate the histological findings (Fischer et al., 2004; Durand et al., 2006; Mancuso et al., 2011). Decreases in muscle mass and muscle fiber diameter are likely a result of the loss of functional motor units (Marcuzzo et al., 2011). Compensatory axonal sprouting is evident following the initial target disconnection and while some successful reinnervation occurs, NMJ loss continues and it is evident that with time compensatory

sprouting is inadequate (Schaefer et al., 2005; Hegedus et al., 2007). The loss of motor units continues with age and is paralleled by reductions in whole muscle force (Hegedus et al., 2007). By the time the SOD1 mouse reaches the symptomatic stage, significant loss of MN within the ventral horn and behavioral assessments reveal functional motor impairments (Zang et al., 2005; Chiu et al., 1995; Fischer et al., 2004; Durand et al., 2006).

Due to the increased susceptibility of SOD1 FMN to axotomy as well as the dysregulated molecular response after axotomy (see Chapter IV), we propose the increased susceptibility of SOD1 FMN cell death is not due to an aberrant MN response to injury, but the presence of a pro-inflammatory microenvironment within the pre-symptomatic stage and a dysregulation of the neuropil after injury that results in the increased MN cell death. Our current working model of peripheral immune-mediated neuroprotection suggests that the glial cells play important roles in this communication between the acquired immune system and the injured neuron. Potentially, the dysregulated glial cells may not be functioning in a manner conducive to mediating the signals from the periphery to the CNS and within the CNS to the MN.

Aim #2 of this dissertation was to determine whether molecular response to axotomy within the pre-symptomatic SOD1 facial motor nucleus resemble the disease-induced molecular response within the facial motor nucleus. The working hypothesis for this aim was that the molecular response following facial nerve axotomy in pre-

symptomatic SOD1 mice resembles the molecular response of disease progression and subsequent MN degeneration within the symptomatic SOD1 facial motor nucleus. It has been well established in the SOD1 mouse model that neuronal target disconnection precedes MN cell death in the spinal cord and brainstem during disease progression. The experiments in Aim2 examined the effects of disease on FMN survival and mRNA expression of glial-specific genes and genes involved in neuroprotective and neurodegenerative signaling systems within the neurodegenerating, disease-affected facial motor nucleus.

C. Materials and Methods

Animals

Mice were obtained and housed as previously described in Chapter III Section A, refer to experimental designs illustrated in **Figures 45** and **47** of this Chapter.

Tissue Preparation

Refer to Chapter III Sections C and D as well as **Figures 45** and **47** of this Chapter for details.

FMN Survival Counts

The experimental design for the FMN survival experiment is illustrated in **Figure 45**. Refer to Chapter III Section E for further details.

Laser Microdissection

Details are described in Chapter III Section F and the experimental design illustrated in **Figure 47** of this Chapter.

RNA Isolation and Real-Time RT-PCR

Relative mRNA expression was analyzed for 70, 84, and 112 doa time-points for all of the following genes: CX3CR1, TNFR1, TNFR2, FasL, Caspase-3, PAC1-R, CRMP4, ASK1, Daxx, FADD, TRAF2, TRADD, SODD, and nNOS. Because of significant differences between early time-points, Fas was analyzed at one additional time-point (63 doa) and CD68 was analyzed for two additional time-points (59 and 63 doa). The genes TNFα, Caspase-8, GFAP, GAP-43, and βII-Tubulin were previously analyzed by our laboratory for the time-points up to 84 doa and no changes relative to age or disease progress where found. For this dissertation the time course was extended to 112 doa, therefore the time-point of 84 doa was replicated to confirm consistency purposes and the 112 doa time-point was additionally assessed. However, the gene Caspase-8 does not include the fourth data point of WT 112 doa. Due to failure of amplification during the real-time PCR run and insufficient volume of remaining WT 112 doa samples, the time-point could not be included in the analysis. For specific details refer to Chapter III Section G and the experimental design illustrated in **Figure 47** of this Chapter.

Statistical Analysis

Details of statistical analysis for average FMN per section and relative facial motor nucleus mRNA expression can be located in Chapter III Section J.

D. Results

By 112 doa, Symptomatic SOD1 Mice Display Significant MN Loss in the Facial Motor Nucleus

Average FMN numbers per section was assessed for WT and SOD1 mice at 84 and 112 doa in control, uninjured facial motor nuclei. No differences between FMN numbers per section were seen between WT 84 (100 ± 9; **Figure 21A**) and 112 (93 ± 10; **Figure 21C**) or SOD1 84 doa (97 ± 8; **Figure 21E**) and these findings are consistent with previous, published data from our laboratory (Serpe et al., 2000; Mesnard et al., 2011). However, by 112 doa, symptomatic SOD1 facial motor nuclei reveal a significant loss of FMN (59 ± 5; **Figures 21G** and **46**). Therefore by 112 doa, disease-induced MN loss of approximately 40% of FMN has occurred in the symptomatic SOD1 facial motor nucleus.

Increased Expression of Disease-Induced mRNA in Symptomatic SOD1 Facial Motor Nucleus.

Specific details of all 21 genes analyzed can be found in **Table 2**. Results from Chapter IV, axotomy-induced molecular responses of pre-symptomatic SOD1 mice are summarized with in **Table 5**, as well as results from this Chapter, disease-induced molecular responses. Comparisons were made between the two.

TNFR1: The relative mRNA expression for WT facial motor nuclei are as follows; 70 (0.0139 ± 0.0005), 84 (0.0126 ± 0.0029) and 112 (0.0111 ± 0.0015) doa. The relative mRNA expression for SOD1 facial motor nuclei are as follows; 70 (0.0125 ± 0.0022), 84 (0.0088 ± 0.0023) and 112 (0.0217 ± 0.0040) doa (**Figure 48**). SOD1 mRNA expression was significantly higher compared to WT at 112 doa. Increased variability within the SOD1 facial nucleus at 84 doa, is likely the reason it is significant to WT 70 doa.

TNFα: TNFα was not detectable within the WT 112 doa facial motor nucleus (**Figure 25**). The relative mRNA expression for SOD1 facial motor nuclei are as follows; 70 (3.1E-04 ± 2.9E-04), 84 (2.9E-05 ± 2.9E-06) and 112 (4.2E-05 ± 1.5E-05) doa (**Figure 49**).

Fas: The relative mRNA expression for WT facial motor nuclei are as follows; 63 (2.9E-04 ± 2.3E-05), 70 (3.3E-04 ± 7.8E-05), 84 (3.7E-04 ± 1.2E-04) and 112 (3.1E-04 ± 6.4E-05) doa. The relative mRNA expression for SOD1 facial motor nuclei are as follows; 63 (4.4E-04 ± 1.4E-04), 70 (6.3E-04 ± 4.8E-05), 84 (5.7E-04 ± 2.0E-04) and 112 (8.1E-04 ± 1.8E-04) doa (**Figure 50**). Significant differences were apparent between aged-matched SOD1 and WT at 70 and 112 doa. The additional time-point of 63 doa was added to determine a likely time course of a Fas-induced molecular response to disease. The additional time-point supports the conclusion that Fas-induced molecular response to disease occurs by 70 doa, there is a significant increase in mRNA expression between

SOD1 63 and 70 doa. SOD1 expression at 70 doa is also significantly higher than WT 63 doa. A pattern of expression was revealed that is discussed in Section E of this Chapter.

FasL: The relative mRNA expression for WT facial motor nuclei are as follows; 70 (7.9E-06 ± 6.0E-06), 84 (7.1E-06 ± 3.1E-06) and 112 (9.5E-06 ± 6.6E-06) doa. The relative mRNA expression for SOD1 facial motor nuclei are as follows; 70 (1.1E-05 ± 2.7E-06), 84 (8.8E-06 ± 4.7E-06) and 112 (1.5E-05 ± 4.8E-06) doa (**Figure 51**). No differences in mRNA expression were detected. High variability was seen.

TRADD: The relative mRNA expression for WT facial motor nuclei are as follows; 70 (0.0034 ± 0.0005), 84 (0.0029 ± 0.0004) and 112 (0.0036 ± 0.0006) doa. The relative mRNA expression for SOD1 facial motor nuclei are as follows; 70 (0.0040 ± 0.0004), 84 (0.0026 ± 0.0007) and 112 (0.0041 ± 0.0008) doa (**Figure 52**). No differences in mRNA expression were detected.

FADD: The relative mRNA expression for WT facial motor nuclei are as follows; 70 (8.1E-04 ± 1.8E-04), 84 (4.3E-04 ± 2.7E-04) and 112 (7.2E-04 ± 4.5E-05) doa. The relative mRNA expression for SOD1 facial motor nuclei are as follows; 70 (8.3E-04 ± 1.0E-04), 84 (4.9E-04 ± 1.1E-04) and 112 (7.6E-04 ± 6.2E-05) doa (**Figure 53**). While no difference between WT and FADD was seen at 112 doa, a significant increase was seen in the SOD1 control facial nucleus from 84 to 112 doa. Although, high variability within the 84 doa time-point for both WT and SOD1 mice was shown. Additional n's should be added to these groups.

Daxx: The relative mRNA expression for WT facial motor nuclei are as follows; 70 (0.0050 ± 0.0004), 84 (0.0033 ± 0.0012) and 112 (0.0038 ± 0.0007) doa. The relative mRNA expression for SOD1 facial motor nuclei are as follows; 70 (0.0044 ± 0.0002), 84 (0.0040 ± 0.0002) and 112 (0.0046 ± 0.0006) doa (**Figure 54**). No differences in mRNA expression were detected.

ASK1: The relative mRNA expression for WT facial motor nuclei are as follows; 70 (0.0026 ± 0.0003), 84 (0.0018 ± 0.0008) and 112 (0.0034 ± 0.0005) doa. The relative mRNA expression for SOD1 facial motor nuclei are as follows; 70 (0.0028 ± 0.0004), 84 (0.0030 ± 0.0004) and 112 (0.0050 ± 0.0004) doa (**Figure 55**). The SOD1 diseased, control facial nucleus revealed a dramatic increase in ASK1 mRNA at 112 doa which was statistically higher than WT and SOD1 at 70, 84, and 112 doa.

nNOS: The relative mRNA expression for WT facial motor nuclei are as follows; 70 (2.0E-04 ± 5.6E-05), 84 (2.3E-04 ± 1.0E-04) and 112 (1.7E-04 ± 3.4E-05) doa. The relative mRNA expression for SOD1 facial motor nuclei are as follows; 70 (1.8E-04 ± 4.6E-05), 84 (2.3E-04 ± 6.7E-05) and 112 (1.3E-04 ± 3.2E-05) doa (**Figure 56**). nNOS mRNA expression revealed high variability and no statistical differences.

Caspase-3: The relative mRNA expression for WT facial motor nuclei are as follows; 70 (0.0020 ± 0.0005), 84 (0.0018 ± 0.0001) and 112 (0.0019 ± 0.0004) doa. The relative mRNA expression for SOD1 facial motor nuclei are as follows; 70 (0.0020 ± 0.0003), 84 (0.0019 ± 0.0004) and 112 (0.0033 ± 0.0005) doa (**Figure 57**). Caspase-3

expression in the SOD1 control facial nucleus was significantly higher than SOD1 at 84 doa and WT at both 84 and 112 doa.

Caspase-8: The relative mRNA expression for WT facial motor nuclei are as follows; 84 (3.3E-05 ± 5.8E-06) doa. The relative mRNA expression for SOD1 facial motor nuclei are as follows; 84 (5.0E-05 ± 1.7E-05) and 112 (1.2E-04 ± 3.1E-05) doa (**Figure 58**). Previously our lab assessed Caspase-8 mRNA within WT and SOD1 control facial nuclei at 70 and 84 doa and found no differences. Additionally, loss of the samples during the PCR run and insufficient remaining sample is the explanation for the lack of WT 112 doa expression data. However, Capase-8 mRNA expression within the SOD1 control nucleus is significantly higher than WT and SOD1 at 84 doa.

TRAF2: The relative mRNA expression for WT facial motor nuclei are as follows; 70 (0.0039 ± 0.0003), 84 (0.0038 ± 0.0008) and 112 (0.0036 ± 0.0003) doa. The relative mRNA expression for SOD1 facial motor nuclei are as follows; 70 (0.0042 ± 0.0004), 84 (0.0041 ± 0.0005) and 112 (0.0044 ± 0.0004) doa (**Figure 59**). No differences in mRNA expression were detected.

SODD: The relative mRNA expression for WT facial motor nuclei are as follows; 70 (0.0089 ± 0.0004), 84 (0.0111 ± 0.0011) and 112 (0.0107 ± 0.0016) doa. The relative mRNA expression for SOD1 facial motor nuclei are as follows; 70 (0.0109 ± 0.0011), 84 (0.0070 ± 0.0013) and 112 (0.0137 ± 0.0017) doa (**Figure 60**). SOD1 mRNA expression at 112 doa was not significantly different that WT at 112 doa, but it was higher compared

to WT at 70 doa. Interestingly, SOD1 mRNA expression of SODD was decreased at 84 doa, compared to WT. A pattern of expression was revealed that is discussed in Section E of this Chapter.

TNFR2: The relative mRNA expression for WT facial motor nuclei are as follows; 70 (4.8E-04 ± 6.8E-05), 84 (5.1E-04 ± 1.1E-04) and 112 (4.1E-04 ± 8.3E-05) doa. The relative mRNA expression for SOD1 facial motor nuclei are as follows; 70 (3.9E-04 ± 8.2E-05), 84 (4.8E-04 ± 5.5E-05) and 112 (7.5E-04 ± 3.4E-04) doa (**Figure 61**). While no statistical differences were seen, mean mRNA levels were increased in SOD1 control facial nucleus at 112 doa. High variability was also seen at that time-point.

PAC1-R: The relative mRNA expression for WT facial motor nuclei are as follows; 70 (0.0413 ± 0.0110), 84 (0.0483 ± 0.0087) and 112 (0.0449 ± 0.118) doa. The relative mRNA expression for SOD1 facial motor nuclei are as follows; 70 (0.0050 ± 0.0040), 84 (0.0353 ± 0.0020) and 112 (0.0382 ± 0.0037) doa (**Figure 62**). No differences in mRNA expression were detected.

CX3CR1: The relative mRNA expression for WT facial motor nuclei are as follows; 70 (0.0074 ± 0.0030), 84 (0.0063 ± 0.0010) and 112 (0.0071 ± 0.0013) doa. The relative mRNA expression for SOD1 facial motor nuclei are as follows; 70 (0.0057 ± 0.0015), 84 (0.0091 ± 0.0011) and 112 (0.0196 ± 0.0040) doa (**Figure 63**). The SOD1 diseased, control facial nucleus revealed a dramatic increase in CX3CR1 mRNA at 112 doa which was statistically higher than WT and SOD1 at 70, 84, and 112 doa.

CRMP4: The relative mRNA expression for WT facial motor nuclei are as follows; 70 (0.0664 ± 0.0059), 84 (0.0814 ± 0.0136) and 112 (0.1377 ± 0.0859) doa. The relative mRNA expression for SOD1 facial motor nuclei are as follows; 70 (0.0903 ± 0.0068), 84 (0.0640 ± 0.0139) and 112 (0.1208 ± 0.0256) doa (**Figure 64**). CRMP4 expression was highly variable at 112 doa, particularly within the WT facial nucleus. The mean for CRMP4 mRNA expression is higher than WT and SOD1 at 70 and 84 doa, however significance was only seen compared to WT at 70 doa. Later time-points will need to be assessed for CRMP4 expression.

GAP-43: The relative mRNA expression for WT facial motor nuclei are as follows; 84 (0.0111 ± 0.0026) and 112 (0.0069 ± 0.0009) doa. The relative mRNA expression for SOD1 facial motor nuclei are as follows; 84 (0.0136 ± 0.0023) and 112 (0.0154 ± 0.0021) doa (**Figure 65**). Previously our lab assessed GAP-43 mRNA within WT and SOD1 control facial nuclei at 70 and 84 doa and found no differences. Significantly higher SOD1 mRNA expression for GAP-43 was seen at 112 doa compared to WT.

βII-Tubulin: The relative mRNA expression for WT facial motor nuclei are as follows; 84 (0.1411 ± 0.0302) and 112 (0.0879 ± 0.0144) doa. The relative mRNA expression for SOD1 facial motor nuclei are as follows; 84 (0.1224 ± 0.0256) and 112 (0.1023 ± 0.0128) doa (**Figure 66**). Previously our lab assessed βII-Tubulin mRNA within WT and SOD1 control facial nuclei at 70 and 84 doa and found no differences. No differences in mRNA expression were detected.

GFAP: The relative mRNA expression for WT facial motor nuclei are as follows; 84 (0.0266 ± 0.0064) and 112 (0.0130 ± 0.0035) doa. The relative mRNA expression for SOD1 facial motor nuclei are as follows; 84 (0.1254 ± 0.0124) and 112 (0.1690 ± 0.0606) doa (**Figure 67**). Previously our lab assessed GFAP mRNA within WT and SOD1 control facial nuclei at 70 and 84 doa and found no differences. However, GFAP expression was significantly higher than WT at both 84 and 112 doa. This inconsistency is likely due to variation in SOD1 molecular responses to disease. Different rates of SOD1 disease progression are investigated in Chapter VI.

CD68: The relative mRNA expression for WT facial motor nuclei are as follows; 59 (0.0010 ± 0.0001), 63 (0.0012 ± 0.0002), 70 (0.0017 ± 0.0003), 84 (0.0018 ± 0.0004) and 112 (0.0012 ± 0.0000) doa. The relative mRNA expression for SOD1 facial motor nuclei are as follows; 59 (0.0025 ± 0.0012), 63 (0.0051 ± 0.0015), 70 (0.0083 ± 0.0009), 84 (0.0119 ± 0.0016) and 112 (0.0172 ± 0.0053) doa (**Figure 68**). Great differences in mRNA expression within the SOD1 control, facial motor nucleus was seen within the SOD1 for 63, 70, 84, and 112 doa. This dramatic increasing expression over time indicates a pattern that is discussed in Section E of this Chapter.

Figure 45. Experimental Design: FMN survival, average FMN per section of control facial motor nucleus in WT, pre-symptomatic and symptomatic SOD1 mice

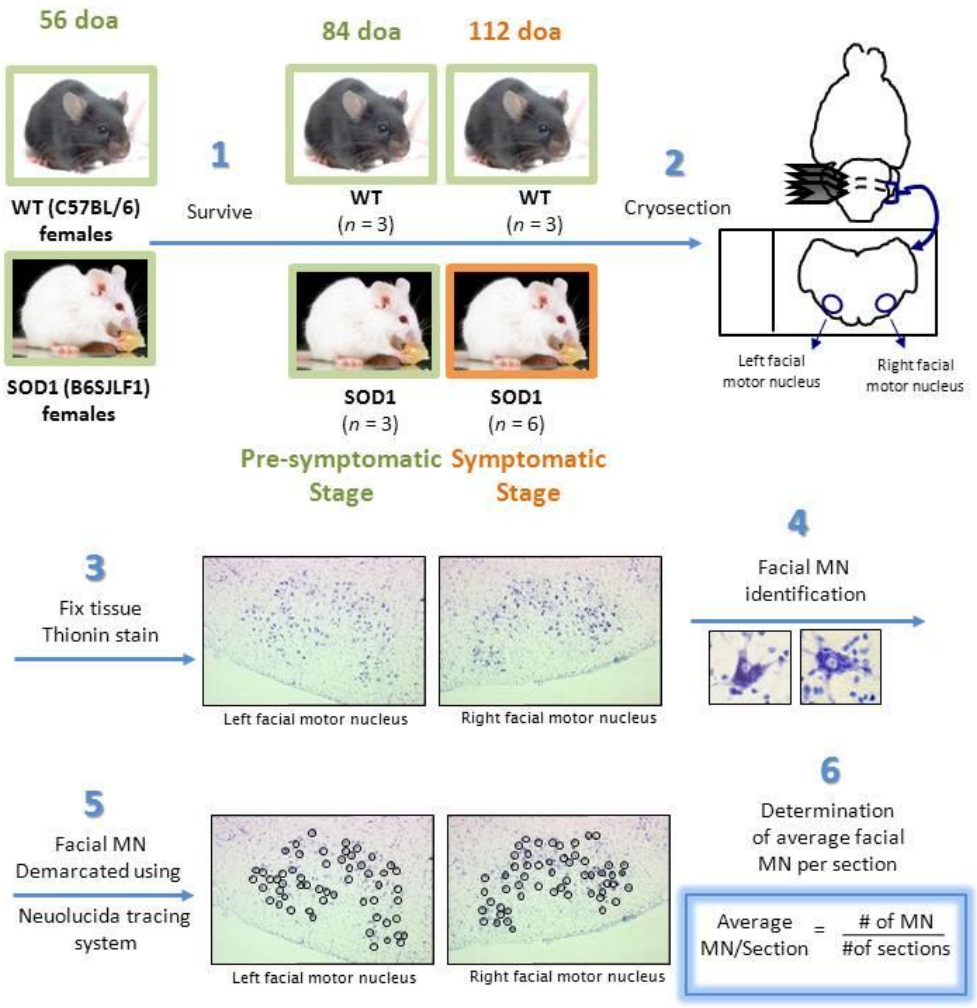

1. WT and SOD1 mice were euthanized at 84 and 112 doa.
2. Brains were removed and cryosectioned through the facial motor nucleus at 25 µm.
3. Sections were fixed with 4% PFA and stained with thionin.
4. FMN identified by morphology and a defined nucleus and nucleolus.
5. FMN within the facial motor nuclei were demarcated under light microscopy using the Neurolucida Tracing System and total number of MN per section were recorded.
6. The average FMN per section was calculated by dividing the total number of MN counted by the number of tissue sections counted.

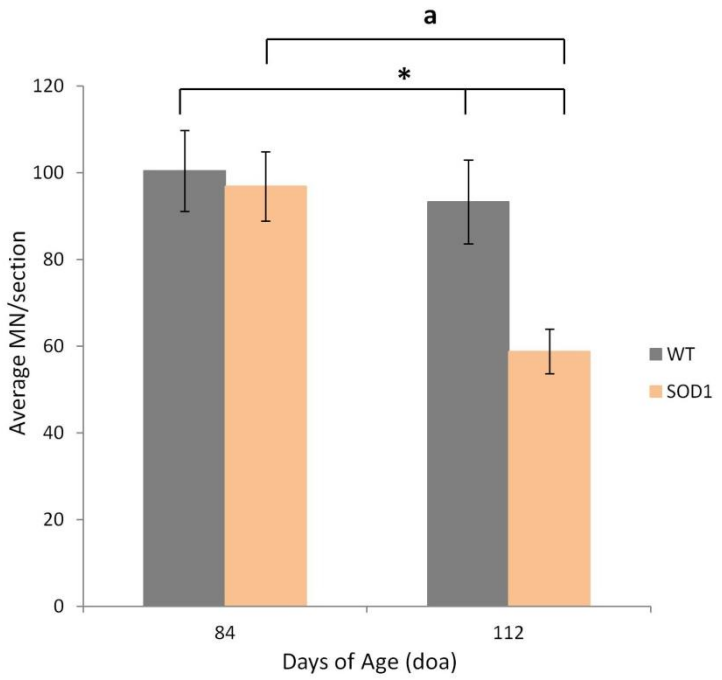

Figure 46. Average FMN per section ± SEM in **WT** and **SOD1** uninjured, **control** facial motor nuclei at 84 and 112 doa. **a** represents a significant difference relative to another time-point within the same strain of mouse; ***** represents a significant difference relative to WT at $p \leq 0.05$.

Figure 47. Experimental Design: LMD of WT and SOD1 uninjured, control facial motor nuclei, real time RT-PCR and analysis of mRNA expression

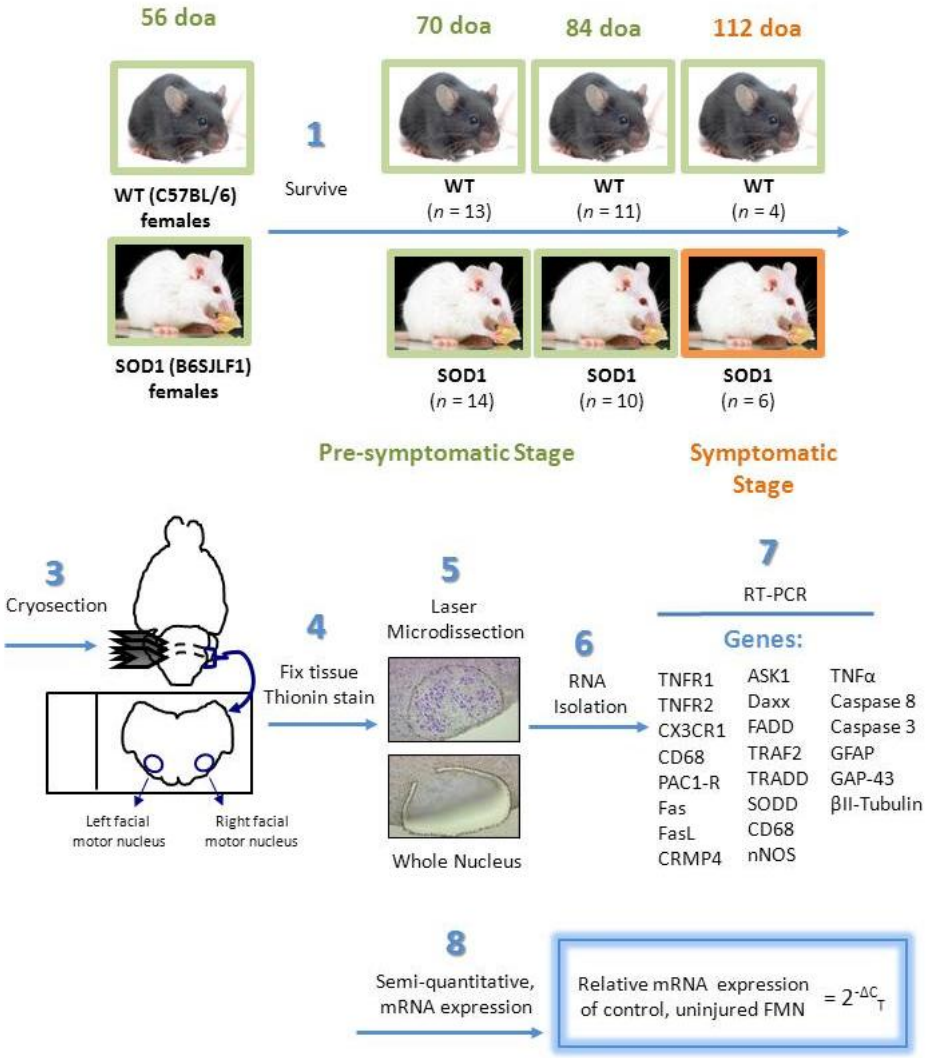

1. WT and SOD1 were euthanized at 70, 84 and 112 doa.
2. Brains were removed and cryosectioned through the facial motor nucleus at 25 µm.
3. Sections were fixed with 100% ETOH and stained with thionin.
4. Left, uninjured facial motor nuclei were collected by laser microdissected for each mouse.
5. RNA was isolated from facial motor nucleus samples.
6. Real-time, RT-PCR was performed for specific genes to profile the relative mRNA expression in the SOD1 compared to the WT.
7. The semi-quantitative, relative mRNA expression, normalized to GAPDH in the facial motor nucleus was calculated using the $2^{-\Delta C}{}_T$ method.

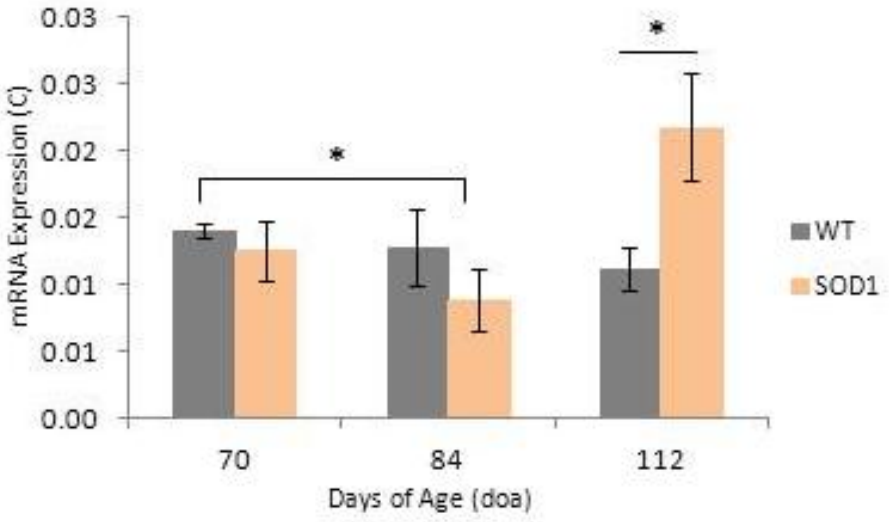

Figure 48. Relative mRNA expression ± SEM of **TNFR1**, normalized to GAPDH, in **WT** and **SOD1** uninjured, **control** facial motor nuclei at 70, 84 and 112 doa. ***** represents a significant difference relative to WT at $p \leq 0.05$.

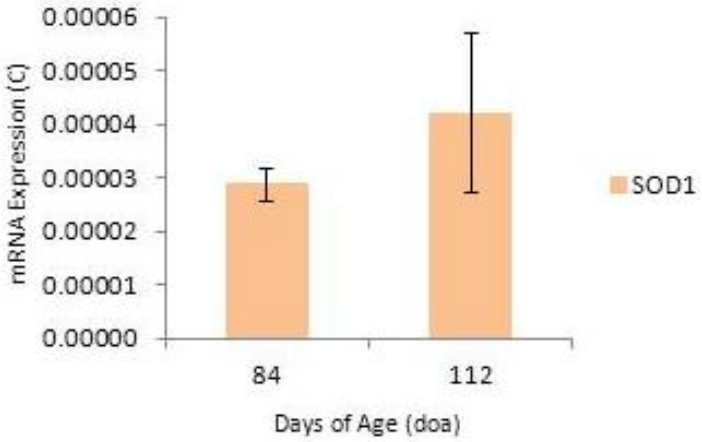

Figure 49. Relative mRNA expression ± SEM of **TNFα**, normalized to GAPDH, in **SOD1** uninjured, **control** facial motor nuclei at 84 and 112 doa.

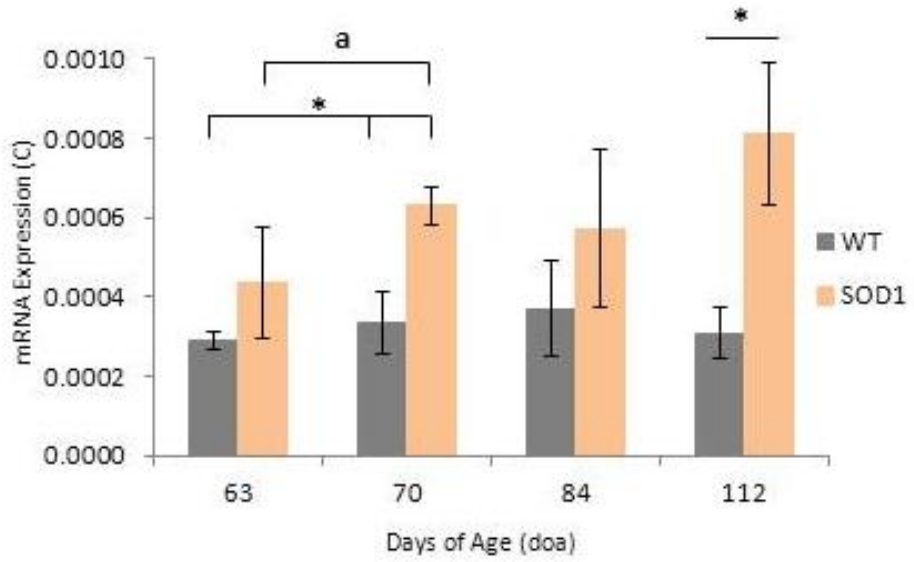

Figure 50. Relative mRNA expression ± SEM of **Fas**, normalized to GAPDH, in **WT** and **SOD1** uninjured, **control** facial motor nuclei at 63, 70, 84 and 112 doa. **a** represents a significant difference relative to another time-point within the same strain of mouse; ***** represents a significant difference relative to WT at $p \leq 0.05$.

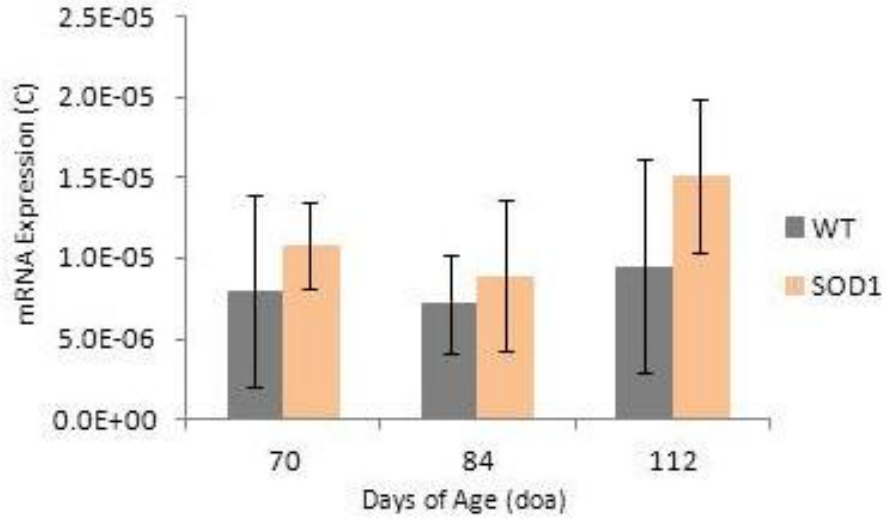

Figure 51. Relative mRNA expression ± SEM of **FasL**, normalized to GAPDH, in **WT** and **SOD1** uninjured, **control** facial motor nuclei at 70, 84 and 112 doa.

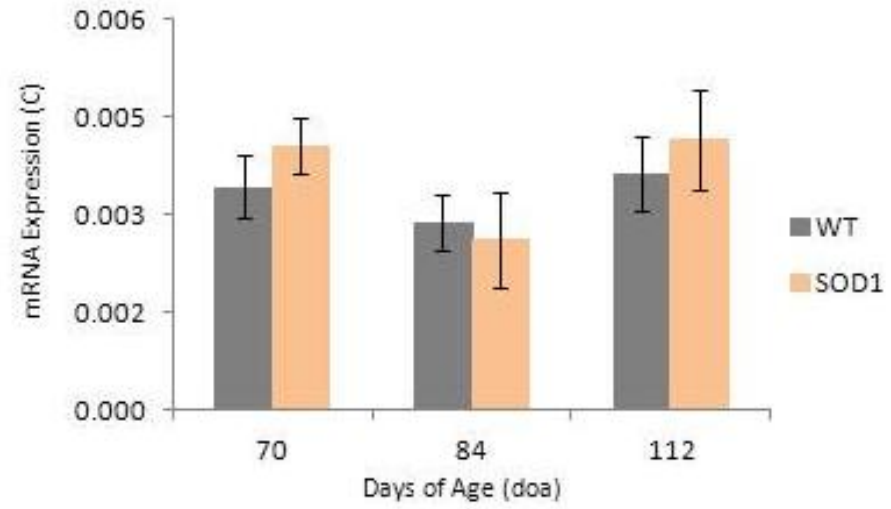

Figure 52. Relative mRNA expression ± SEM of **TRADD**, normalized to GAPDH, in **WT** and **SOD1** uninjured, **control** facial motor nuclei at 70, 84 and 112 doa.

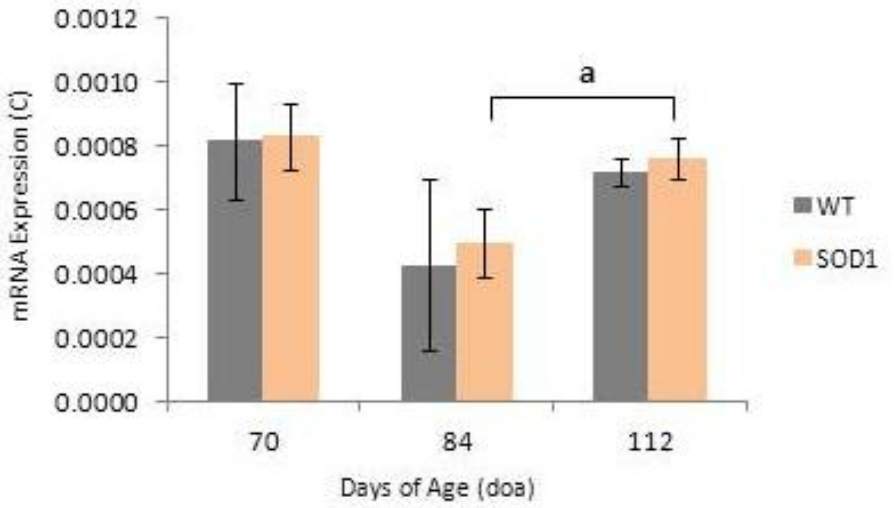

Figure 53. Relative mRNA expression ± SEM of **FADD**, normalized to GAPDH, in **WT** and **SOD1** uninjured, **control** facial motor nuclei at 70, 84 and 112 doa. **a** represents a significant difference relative to another time-point within the same strain of mouse at $p \leq 0.05$.

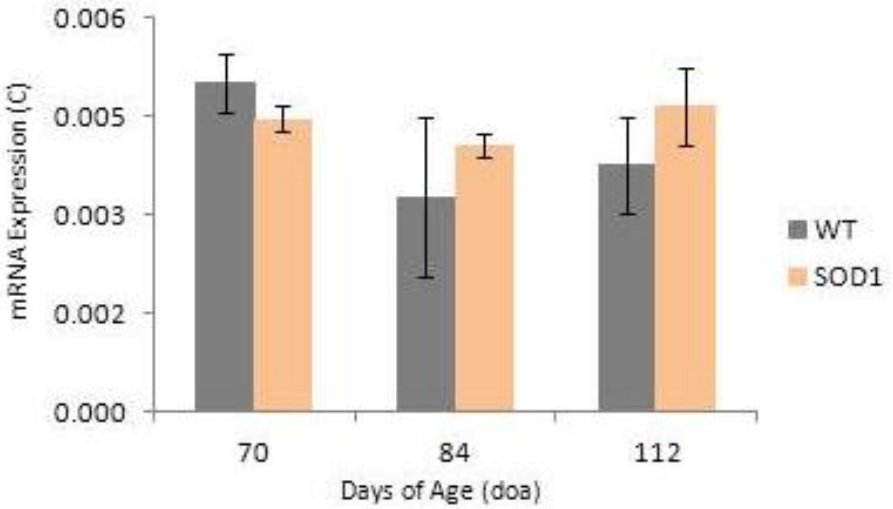

Figure 54. Relative mRNA expression ± SEM of **Daxx**, normalized to GAPDH, in **WT** and **SOD1** uninjured, **control** facial motor nuclei at 70, 84 and 112 doa.

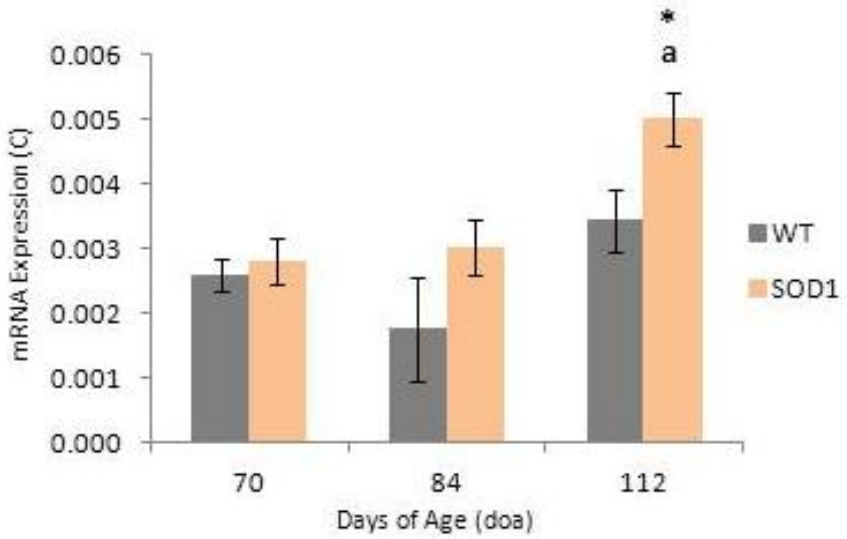

Figure 55. Relative mRNA expression ± SEM of **ASK1**, normalized to GAPDH, in **WT** and **SOD1** uninjured, **control** facial motor nuclei at 70, 84 and 112 doa. **a** represents a significant difference relative to another time-point within the same strain of mouse; ***** represents a significant difference relative to WT at $p \leq 0.05$.

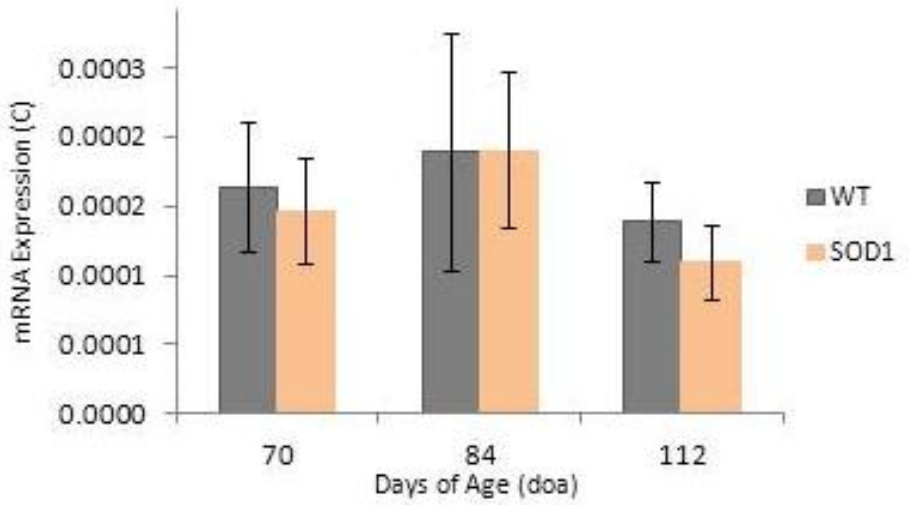

Figure 56. Relative mRNA expression ± SEM of **nNOS**, normalized to GAPDH, in **WT** and **SOD1** uninjured, **control** facial motor nuclei at 70, 84 and 112 doa.

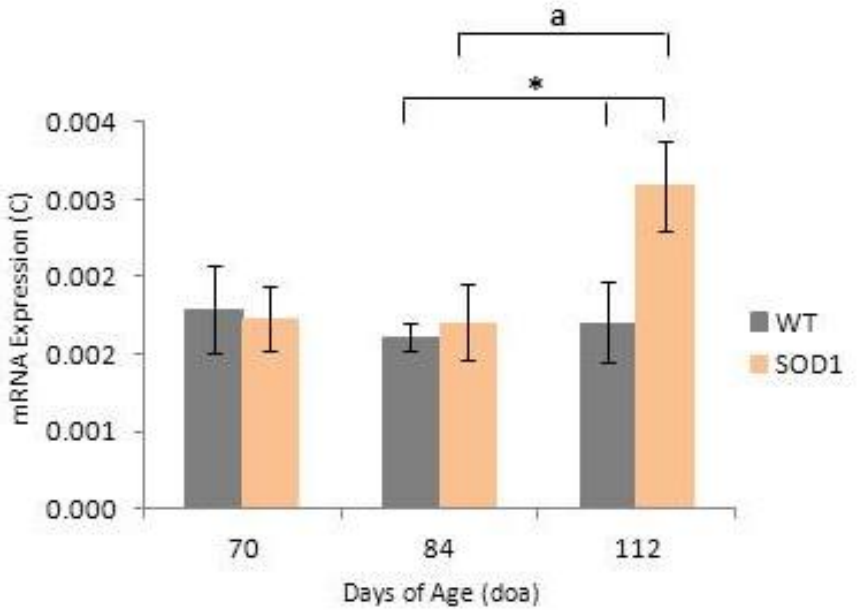

Figure 57. Relative mRNA expression ± SEM of **Caspase-3**, normalized to GAPDH, in **WT** and **SOD1** uninjured, **control** facial motor nuclei at 70, 84 and 112 doa. **a** represents a significant difference relative to another time-point within the same strain of mouse; ***** represents a significant difference relative to WT at $p \leq 0.05$.

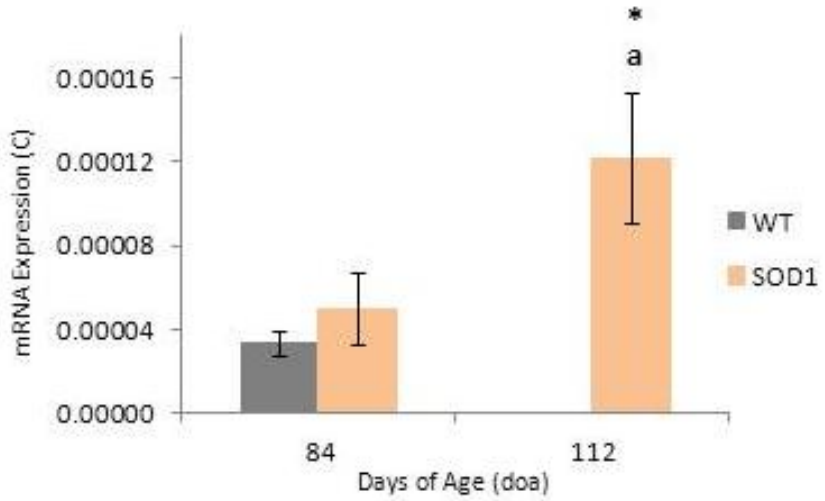

Figure 58. Relative mRNA expression ± SEM of **Caspase-8**, normalized to GAPDH, in **SOD1** uninjured, **control** facial motor nuclei at 84 and 112 doa **WT control** facial motor nucleus at 84 doa only. **a** represents a significant difference relative to another time-point within the same strain of mouse; ***** represents a significant difference relative to WT at $p \leq 0.05$.

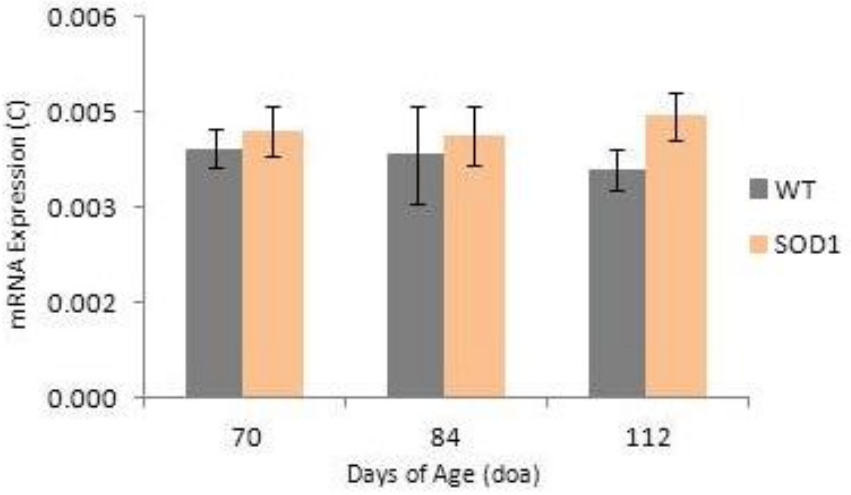

Figure 59. Relative mRNA expression ± SEM of **TRAF2**, normalized to GAPDH, in **WT** and **SOD1** uninjured, **control** facial motor nuclei at 70, 84 and 112 doa.

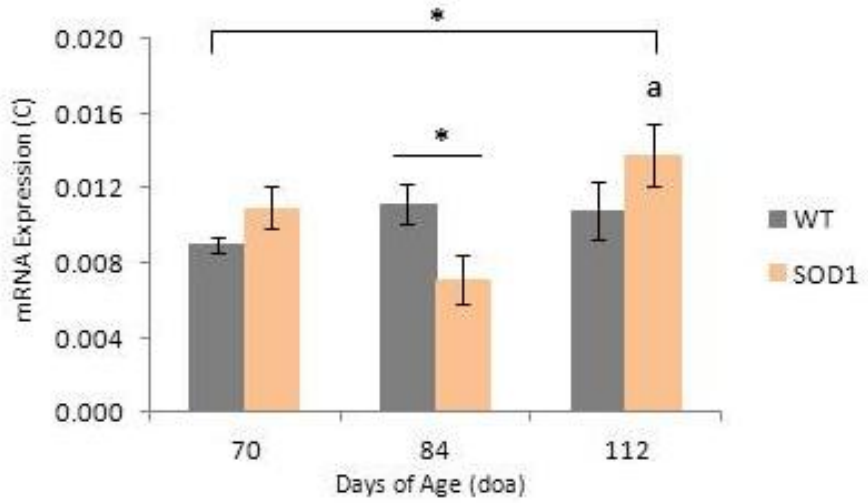

Figure 60. Relative mRNA expression ± SEM of **SODD**, normalized to GAPDH, in **WT** and **SOD1** uninjured, **control** facial motor nuclei at 70, 84 and 112 doa. **a** represents a significant difference relative to another time-point within the same strain of mouse; ***** represents a significant difference relative to WT at $p \leq 0.05$.

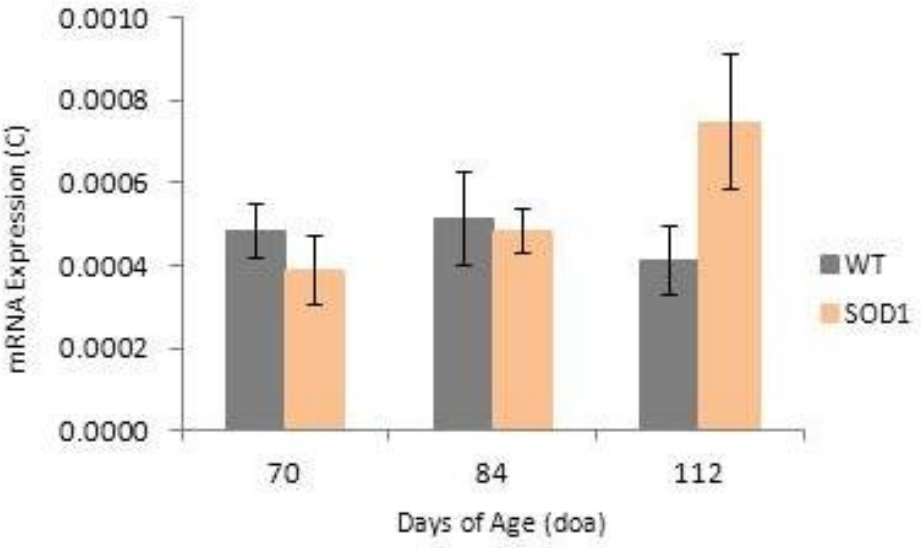

Figure 61. Relative mRNA expression ± SEM of **TNFR2**, normalized to GAPDH, in **WT** and **SOD1** uninjured, **control** facial motor nuclei at 70, 84 and 112 doa.

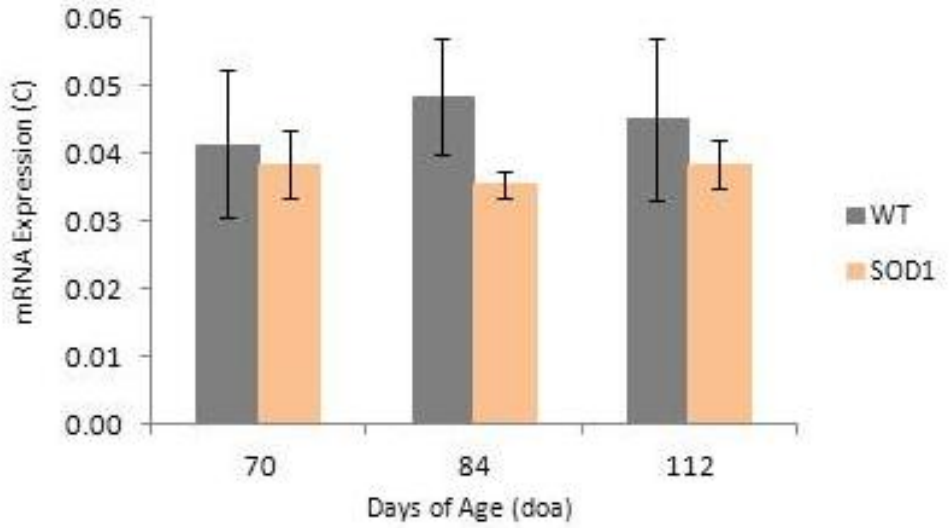

Figure 62. Relative mRNA expression ± SEM of **PAC1-R**, normalized to GAPDH, in **WT** and **SOD1** uninjured, **control** facial motor nuclei at 70, 84 and 112 doa.

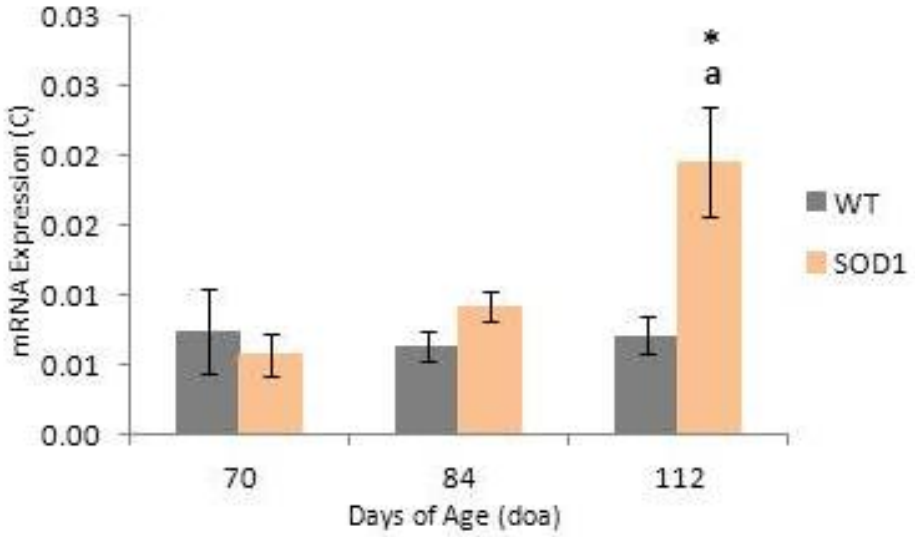

Figure 63. Relative mRNA expression ± SEM of **CX3CR1**, normalized to GAPDH, in **WT** and **SOD1** uninjured, **control** facial motor nuclei at 70, 84 and 112 doa. **a** represents a significant difference relative to another time-point within the same strain of mouse; ***** represents a significant difference relative to WT at $p \leq 0.05$.

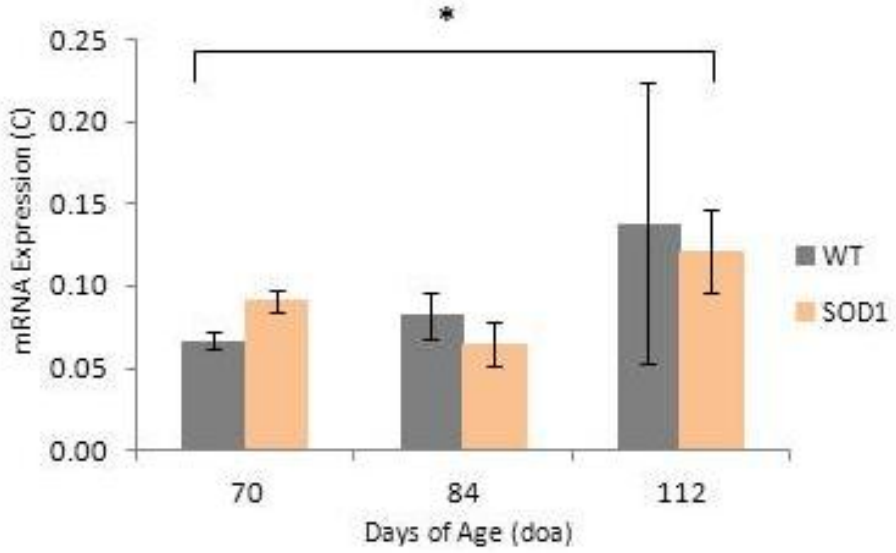

Figure 64. Relative mRNA expression ± SEM of **CRMP4**, normalized to GAPDH, in **WT** and **SOD1** uninjured, **control** facial motor nuclei at 70, 84 and 112 doa. **a** represents a significant difference relative to another time-point within the same strain of mouse; ***** represents a significant difference relative to WT at $p \leq 0.05$.

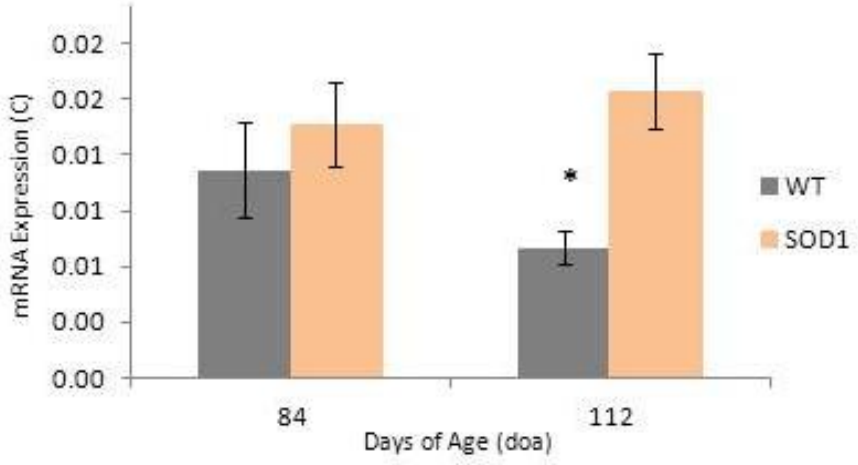

Figure 65. Relative mRNA expression ± SEM of **GAP-43**, normalized to GAPDH, in **WT** and **SOD1** uninjured, **control** facial motor nuclei at 84 and 112 doa. **a** represents a significant difference relative to another time-point within the same strain of mouse; ***** represents a significant difference relative to WT at $p \leq 0.05$.

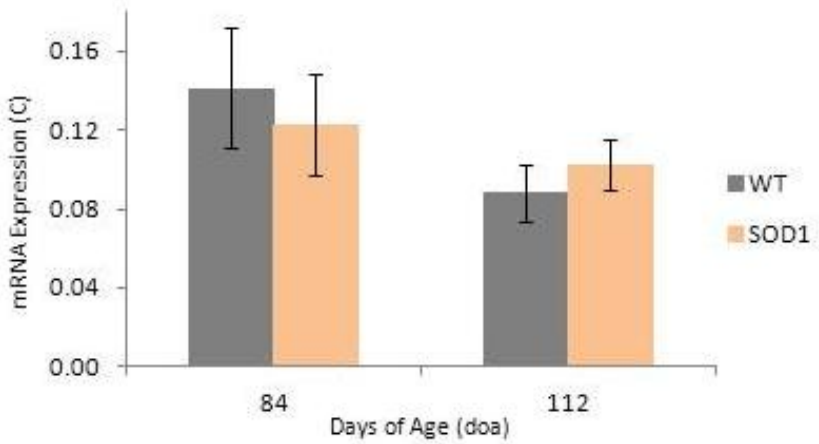

Figure 66. Relative mRNA expression ± SEM of **βII-Tubulin**, normalized to GAPDH, in **WT** and **SOD1** uninjured, **control** facial motor nuclei at 84 and 112 doa.

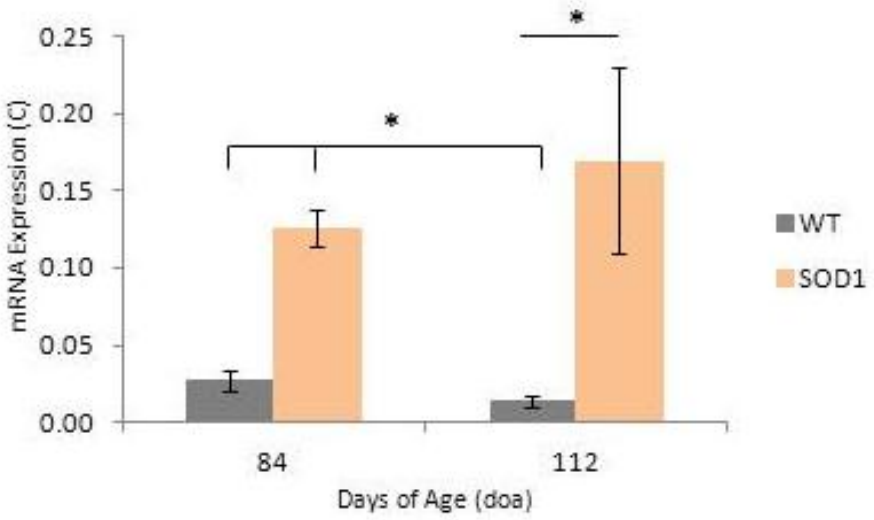

Figure 67. Relative mRNA expression ± SEM of **GFAP**, normalized to GAPDH, in **WT** and **SOD1** uninjured, **control** facial motor nuclei at 84 and 112 doa. ***** represents a significant difference relative to WT at $p \leq 0.05$.

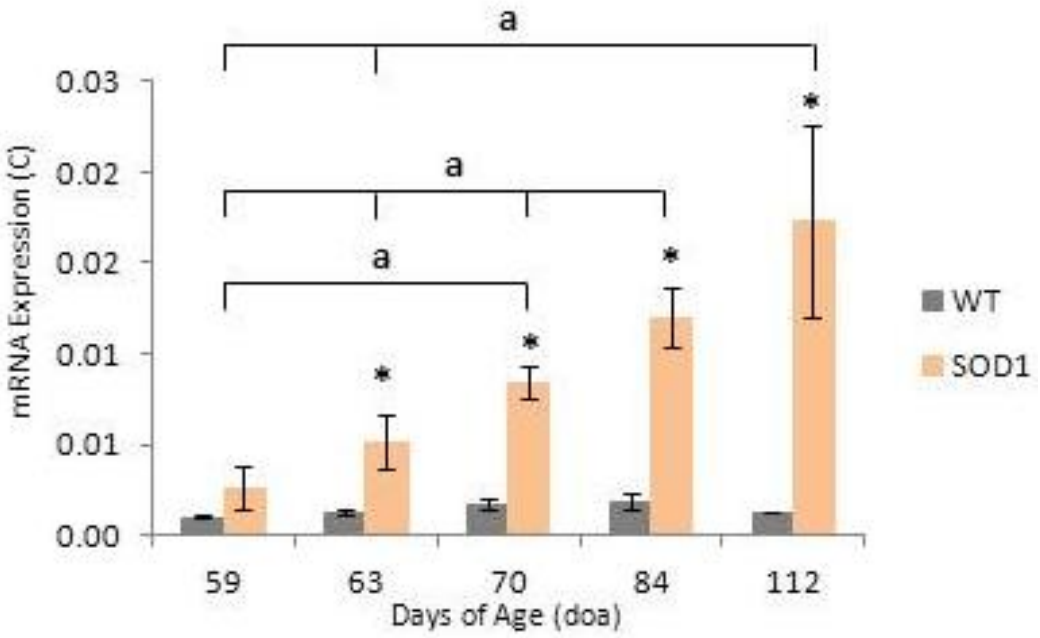

Figure 68. Relative mRNA expression ± SEM of **CD68**, normalized to GAPDH, in **WT** and **SOD1** uninjured, **control** facial motor nuclei at 59, 63, 70, 84 and 112 doa. **a** represents a significant difference relative to another time-point within the same strain of mouse; ***** represents a significant difference relative to WT at $p \leq 0.05$.

Disease vs. Axotomy mRNA Response in SOD1 mice				
Gene	Axotomy-Induced		Disease-Induced	Similar Response
	Initial	Delayed		
TNFR1 Death Receptor Signaling				
TNFR1	↑	↑	↑	Yes
TNFα	↑	↑↑	↑	Yes
TRADD	↳	no Δ	no Δ	Yes
TRAF2	↳	↑	no Δ	No
SODD	↳	no Δ	↳, no Δ	Yes
Fas Death Receptor Signaling				
Fas	↷	↑	↷, ↑	Yes
FasL	↑↷	↑	no Δ	No
Daxx	↑	↑	no Δ	No
ASK1	↳	↑	↑	Yes
nNOS	no Δ	↑	no Δ	Yes
Shared Factors of TNFR1 & Fas Death Receptors				
FADD	↷	↑	↑	Yes
Caspase-8	↑↑	↷	↑	Yes
Caspase-3	↑↑	↑	↑	Yes
Neurodegenerative Signaling Gene				
CRMP4	no Δ	↷	↑	Yes
Neuroprotective Signaling				
TNFR2	↑↑↑	↑↑	no Δ	No
PAC1-R	↓	↳	no Δ	No
CX3CR1	↑↑↑	↑↑	↑	Yes
Neuroregenerative, MN-Specific Genes				
GAP-43	↑↑↑	↑↷	↑	Yes
βII-Tubulin	↑↑	↷	no Δ	No
Glial-Specific Genes				
GFAP	↑↑	↑↑	↑	Yes
CD68	↑↑	↑	↑↑	Yes

Table 5: Comparison of disease-induced mRNA expression in the facial motor nucleus to axotomy-induced mRNA expression in pre-symptomatic SOD1 mice. Axotomy-Induced columns: SOD1 mRNA expression during the initial and delayed response to axotomy (refer to Chapter IV). Disease-Induced column: relative mRNA expression level in SOD1 diseased, control facial motor nucleus compared to aged-matched WT or younger, pre-symptomatic SOD1 mice. A comma (,) separates disease-induced mRNA expression differences at multiple time-points.

E. Discussion

In order to show that facial nerve axotomy in the pre-symptomatic SOD1 mouse can be used as a model for the target disconnection that initiates SOD1 disease progression, two requirements must be fulfilled. 1) diseased-induced FMN cell loss must occur and 2) the mRNA expression in the diseased facial motor nucleus must resemble that seen after SOD1 facial nerve axotomy.

Significant Disease-Induced FMN Loss Occurs within the SOD1 Facial Motor Nucleus by 112 doa

The SOD1 facial motor nucleus to susceptible MN cell loss, however this loss has only been documented within end stage (Haenggeli and Kato, 2002; Niessen et al., 2006). Additionally, neurodegeneration within the facial motor nucleus of ALS patients has also been documented (DePaul et al., 1988). Results from the FMN survival experiment within this Chapter reveal that the average number of MN within the SOD1 facial motor nucleus at 112 doa are significantly less than aged-matched WT or WT and SOD1 at 84 doa. This FMN loss is a result of the disease process.

We hypothesizes that the FMN undergoing degeneration at 112 doa are most likely those within the immune-dependent population and once FMN numbers reach 40-50%, a plateau will be reached and these remaining MN will be considered the resilient population. However this is a future direction and the identity of the FMN

population undergoing neurodegeneration at 112 doa is unclear within the context of the current experiments.

It has been well-established that the initial pathological event in SOD1 disease progression is the loss of NMJ or target disconnection within the pre-symptomatic stage (Fischer et al., 2004; Dadon-Nachum et al., 2011). This denervation proceeds clinical symptoms and MN cell loss and therefore, resembles the “die-back” phenomenon. Therefore, conformation that at 112 doa, the control, uninjured facial motor nucleus is undergoing MN cell death due to disease progression allows for the investigation of mRNA expression in response to the “theoretical” target-disconnection that we hypothesizes is occurring.

Experiments within Chapter IV examined the molecular response for genes known to be involved in neurodegeneration, neuroprotection and the glial response. These genes were assessed within the pre-symptomatic SOD1 facial motor nucleus after axotomy through an extended time course and those results have been re-summarized in **Table 5**. Experiments performed within this Chapter investigated the molecular expression within the SOD1 control facial nucleus, affected by disease, and was compared to relative mRNA expression levels in aged-matched WT control facial nuclei. Additionally, relative mRNA expression was compared between SOD1 and WT facial nuclei at earlier ages for control purposes and to confirm the age at which SOD1 disease-induced mRNA expression occurs.

Considerations about Target Disconnection when Comparing Axotomy-Induced and Disease-Induced mRNA Expression

When comparing mRNA expression levels within the diseased, SOD1 facial nucleus to mRNA expression levels of SOD1 axotomized facial nucleus, several aspects need to be kept in mind during analysis and interpretation of the results. The target disconnection produced by a transection axotomy severs all axons within the peripheral nerve and is therefore, greatly exaggerated and standardized in comparison to the target disconnection that occurs during SOD1 disease progression. The target disconnection during disease progression could be considered hundreds or thousands of individual transection axotomies per nucleus over an undetermined period of time. Thus, the time course of the mRNA expression response within the facial motor nucleus would not be expected to be the same during disease progression as it would after axotomy. This doesn't suggest that the pattern of mRNA expression will not be present, but suggests that the pattern of mRNA expression per cell will be occurring at different times. Therefore, in order to achieve a significant difference in the mRNA expression level for a particular gene within the entire SOD1 nucleus, enough cells, MN or glia, will need to be affected by target disconnection for the mRNA difference to reach a threshold. It is expected that some MN will be target disconnected while others will not and results from Chapter IV suggest some the target disconnected MN may be within different phases of molecular expression depending on their individual time course.

However, the results of the FMN survival experiment demonstrates that a significant amount of neurodegeneration has occurred and regardless of the ratio of target disconnected MN vs. target connected MN, many MN and glia will be well within the experimental time course used in Chapter IV.

Disease-Induced mRNA Expression Resembles Axotomy-Induced mRNA Expression at 112 doa

It is overwhelmingly clear that the mRNA expression within the SOD1 diseased facial motor nucleus at 112 doa resembles the mRNA expression seen after axotomy (initial or delayed response phase) in the SOD1 facial motor nucleus, refer to **Table 6**. The following genes have reached an expression level similar to that seen during the delayed-response to axotomy: TNFR1, TNFα, TRADD, Fas, ASK1, Caspase-3, Caspase-8, PAC1-R, CX3CR1, GAP-43, GFAP and CD68. In addition, there are gene expression differences that suggest they are equivalent to or within that of the initial-response to SOD1 axotomy: Fas, SODD, nNOS, CRMP4 and CD68.

Several genes (TRAF2, FasL, FADD) do not reflect a significant change in relative mRNA expression levels. However, it is possible that the degree of target disconnection at 112 doa could place the mRNA expression somewhere between the initial and delayed response phase and therefore at this time-point may reflect a transient baseline expression. The following genes have no change in expression level and compared to the axotomy-induced mRNA expression should be upregulated throughout the initial

and delayed phase, Daxx, TNFR2, and βII-Tubulin. It is not clear why the mRNA expression level has not reached a threshold of significance. TNFR2 mRNA expression shows a trend for higher mRNA levels, but at 112 doa, the level is not significant. This may be reflective of differences between the two types of target disconnection injuries.

Disease-Induced mRNA Expression Resembles Axotomy-Induced mRNA Expression at Multiple Time-Points

Of particular interest are the results of genes Fas, SODD, CD68 and GFAP. Through analysis at earlier time-points/ages it was revealed that significant differences in relative mRNA expression are apparent earlier than 112 doa. GFAP expression is significantly higher in SOD1 control, diseased facial nucleus at 84 and 112 doa. Suggesting the astrocyte reaction to target disconnection and subsequent upregulation of GFAP mRNA has occurred as early as 84 doa. GFAP was previously assessed in our laboratory at earlier time-points and no differences were seen between SOD1 control mRNA expression and aged-matched WT, therefore GFAP was only assessed at 84 and 112 doa for this dissertation (Mesnard et al., 2011).

Fas showed higher mRNA expression levels within the SOD1 112 doa nucleus as well as 70 doa. Therefore, mRNA expression levels were analyzed from WT and SOD1 facial nuclei at earlier time-points. In comparison to age-matched WT control facial motor nuclei, the SOD1 displays no difference in mRNA expression at 63 doa, an upregulation at 70 doa, which appears to be transient and back to baseline (WT level) at

84 doa followed by a return in significant Fas mRNA upregulation at 112 doa. Interestingly, this pattern reflects that seen during both the initial and the delayed-response to axotomy.

Regarding CD68, no differences between WT control facial nuclei and SOD1 was seen at 59 doa, but subsequent, significant increases in CD68 upregulation can be seen in 63, 70, 84 and 112 doa SOD1 mice, which is also replicative of the initial and delayed-response to axotomy. These results suggest that microglia have already begun to respond to the disease by 63 doa.

While the gene SODD was not found to reveal significant differences between expression within the SOD1 112 doa control nucleus compared to WT, a significantly lower mRNA expression was seen within the SOD1 control nucleus at 84 doa compared to the aged-matched WT. This transient downregulation at 84 doa and return to baseline (WT level) at 112 doa in SOD1 diseased nucleus is again, similar to both the initial and delayed-response to axotomy.

Adding additional time-points to the to assess mRNA changes within the SOD1 diseased, control facial nucleus before and after 112 doa is underway. Additionally, an experiment will be performed to quantify denervated neuromuscular junctions within the auricular and vibrissae muscles to confirm target disconnection of FMN.

Conclusions

These findings lend support to the use of facial nerve axotomy as a model for the target disconnection that occurs during disease progression and strongly suggest that if a time course were performed throughout disease progression, similar patterns will likely become apparent and add strength to the model. These conclusions suggest that the constitutive expression of TNFα mRNA seen as early as 59 doa, previously shown by our laboratory, may not be evidence of a pro-inflammatory microenvironment present prior to disease onset, but may be the early response of the SOD1 facial motor nucleus to initial target disconnection. TNFα mRNA expression may be highly responsive to target disconnection and therefore one of the most sensitive mRNA expression marker we have analyzed to date to reveal initial target disconnection. The fact that the mRNA is induced in WT supports this idea as well as preliminary data from SOD1 uninjured control facial motor nucleus at 42 doa, which contained no measureable TNFα mRNA expression (data not shown). Therefore, it is entirely possible that sometime after 42 doa and before 59 doa, a small population of FMN undergo initial target disconnection and therefore an induction of TNFα mRNA. This is followed by a microglial response as evidenced by the upregulation of CD68 at 63 doa and a transient upregulation of Fas mRNA occurring by 70 doa, indicative of the initial-response to target disconnection. Downregulation of the gene SODD occurs as early as 84 doa as well as the presence of reactive astrocyte, evident by the upregulation of GFAP. After a significant amount of

time passes (28 days) and significant MN cell loss has occurred, Fas mRNA upregulation has returned (the delayed-response), TNFR1, Caspase-3, Caspase-8, CX3CR1, and GAP-43 mRNA expression levels are up and these genes are most-likely somewhere within their time course response to axotomy, since no clear distinction exists between the two phases. Due to the considerable amount of time between 84 and 112 doa it is not clear if the initial, transient downregulation of TRADD, ASK1, and PAC1-R has already occurred (initial-response) and the expression levels are within the delayed-response phase (baseline for TRADD/PAC1-R and upregulated for ASK1). If the initial, transient upregulation of FasL and FADD as well as the initial, transient downregulation of TRAF2 has occurred prior to 112 doa, it is possible that the upregulation within the delayed-response phase is mounting or has not yet occurred for FasL, FADD, and TRAF2. The two genes that do not show an initial-response to axotomy but reveal upregulation within the delayed-response phase are CRMP4 and nNOS. Analysis of later time-points, greater than or after 112 doa, may reveal the presence of the delayed-response phase and increased mRNA expression.

Results presented in Chapter IV and V concludes that facial nerve axotomy in the pre-symptomatic SOD1 mouse can be used as a model for disease that occurs in the SOD1 mouse.

CHAPTER VI

TWO RATES OF DISEASE PROGRESSION IN SYMPTOMATIC SOD1 MICE

A. Abstract

ALS is a disease targeting MN. In the SOD1 mouse model of ALS, an axonal die-back process is initiated during the pre-symptomatic stage where MN axons withdraw from target muscle. We have used facial nerve axotomy, which resembles the axonal die-back response, in pre-symptomatic SOD1 mice to investigate aspects of the disease. Apoptotic and pro-inflammatory gene expression is upregulated in pre-symptomatic SOD1 axotomized facial nuclei in addition to significant SOD1 MN death. Disease progression in symptomatic SOD1 facial nuclei resembles the molecular response initiated by axotomy. MN survival levels in symptomatic SOD1 and axotomized, pre-symptomatic SOD1 facial nuclei are similar. Therefore, facial nerve axotomy produces a disease onset-like response. The current study used behavioral testing to assess motor function, and revealed two groups of SOD1 mice with differing rates of symptomatic disease progression. The slow progression group had significantly less motor impairments compared to the fast progression group, but no difference in symptom onset was seen. Fast progression group showed higher mRNA levels for genes related to axonal injury. Symptomatic severity in SOD1 mice correlates to the cellular and

molecular responses to axonal injury. Therefore, research using treatments to slow disease or extend survival needs to assess different symptomatic progression groups.

B. Introduction

Development of this behavioral assessment protocol has important future implications. Delaying or slowing disease progression could be measured by behavioral assessment as an increase in age of symptom onset or a slower rate of disease progression in terms of the slope of the increased motor scores. Additionally, a decrease in the age of symptom onset or an increase in the slope of the increasing motor scores would signify a more severe disease pathology or a faster disease progression rate.

While variability in symptoms, markers of disease progression, and survival is observed within the literature, only one other laboratory has described the presence of two different disease progression rates within the $SOD1^{G93A}$ mouse model and their discovery of these two groups is hardly discussed within the abstract of the publication. The existence of two different disease progression groups were revealed when their pre-determined endpoint criteria (hind-limb ataxia and inability to forage due to paralysis) resulted in half of the SOD1 mice being euthanized a week later than the previous group. After significantly higher MN per section counted in the retrodorsal lateral nucleus (RDLN) of the older, slow disease progression group, they concluded that they had identified two groups of SOD1 mice with different rates of disease progression; both symptom progression and MN cell death, with respect to the RDLN. They termed

these two groups the fast disease progression group (FPG) and the slow disease progression group (SPG; Rinke, 1976).

Aim #3 of this dissertation was to confirm that a group of symptomatic SOD1 mice displaying a faster rate of symptom progression also demonstrate a faster rate of disease progression within the facial motor nucleus. The working hypothesis for this aim was that the variability seen among motor scores during behavioral assessment is a result of two different rates of symptom progression which correlates with evidence of increased disease progression rate within the SOD1 facial motor nucleus. Dramatic differences among severity of symptoms were apparent during behavioral assessment of motor function following symptom onset. The experiments analyzed FMN survival levels as well as differences in expression of genes involved in target disconnection between the two symptomatic groups.

C. Materials and Methods

Animals and Surgical Procedures

Mice were obtained and housed as previously described in Chapter III Section A and all mice received a right facial nerve axotomy described in Chapter III Section B. Also refer to experimental designs illustrated in **Figures 69, 71** and **74** of this Chapter.

Behavioral Assessment

Starting at 79 doa, SOD1 mice were assessed for motor function three times per week using seven behavioral tests. After euthanasia at 112 doa, the SOD1 mice were

divided into two groups based on averaged motor score throughout the symptomatic stage, the FPG (Fast) and the SPG (Slow). Refer to Chapter III Section I and behavioral testing experimental design, **Figure 69**, of this Chapter.

Tissue Preparation

Refer to Chapter III Sections C and D and experimental designs illustrated in **Figures 69, 71** and **74** of this Chapter for further details.

FMN Survival

The average percent of FMN survival for the whole facial nucleus was calculated for SPG and FPG by dividing the number of total MN in the axotomized facial motor nucleus by the number of FMN in the 84 doa uninjured WT, control facial motor nucleus then multiplying by 100. Average number of FMN in the 84 doa facial nucleus was previously determined and is used to calculate axotomy-induced FMN loss in symptomatic SOD1 mice. Refer to Chapter V Section D and **Figure 46** for details regarding the average control FMN numbers of 84 doa SOD1 mice. The average FMN per section for the whole facial nucleus was calculated for each time-point and reflects disease-induced FMN cell loss. For specific details on FMN counts, refer to Chapter III Section E and the experimental design in **Figure 71** of this Chapter.

Laser Microdissection

LMD was performed on axotomized and contralateral control facial motor nuclei at of SPG and FPG mice at 56 dpo (112 doa). Details are described in Chapter III Section F and the experimental design in **Figure 74** of this Chapter.

RNA Isolation and Real-Time RT-PCR

Percent change of mRNA expression in the axotomized facial motor nucleus was assessed between SPG and FPG at 56 dpo. Additionally the relative mRNA expression within the contralateral, disease-affected facial motor nuclei between SPG and FPG at 112 doa as well as the relative mRNA expression within the axotomized facial motor nucleus. The genes investigated were as follows: CX3CR1, TNFR1, TNFR2, Fas, FasL, Caspase-3, PAC1-R, CRMP4, ASK1, Daxx, FADD, TRAF2, TRADD, SODD, CD68, nNOS, TNFα, Caspase-8, GFAP, GAP-43, and βII-Tubulin. Refer to **Figure 74** for details on the experimental design or Chapter III Section G for more details.

Statistical Analysis

Refer to Chapter III Section J.

D. Results

Symptom Onset Occurs at 100 doa

Seven different behavioral tests were used to determine age of symptom onset. Test scores from the seven tests were combined to yield the motor score for the time-point and the motor scores were compared to determine at what is the increase in

motor score significant for the entire group of SOD1 mice. Average motor scores ± SEM per time-point are as follows, 79 (0.13 ± 0.037), 81 (0 ± 0), 84 (0.13 ± 0.025), 86 (0.07 ± 0.018), 88 (0.13 ± 0.025), 91 (0.07 ± 0.018), 93 (0 ± 0), 95 (0.27 ± 0.057), 98 (0.80 ± 0.112), 100 (2.47 ± 0.164), 102 (3.47 ± 0.114), 105 (4.80 ± 0.098), 107 (6.53 ± 0.222), 109 (9.67 ± 0.319) and 112 (12.73 ± 0.446) doa (**Figure 70A**). Significance between motor scores of 98 and 100 doa determined that based on the behavioral tests used, symptom onset occurs by 100 doa. In addition, significant difference between 102 and 105, 107 and 109, as well as 109 and 112 doa was also seen (**Figure 70A**).

Behavioral Assessment Reveals Significant Differences in Rates of Motor Symptom Progression Among Symptomatic SOD1 mice

Behavioral testing revealed two different groups of SOD1 mice which displayed different rates of symptom progression. In order separate these two groups for further analysis the average motor score per mouse during the symptomatic stage (100 to 112 doa) was calculated. A median split was performed to separate the two groups into the SPG (slow) and FPG (fast). Average motor scores throughout the symptomatic stage for mice designated as part of the SPG were as follows: 6.2, 6, 3.2, 4.6, 5.6, 5.8, and 4.6. Average motor scores throughout the symptomatic stage for mice designated as part of the FPG were as follows: 7.6, 6.8, 9, 9.4, 10.4, 12.4, 8, 12. Once separate, the rate of symptom progression was calculated for each group using the average motor score per

group, per time-point and displayed graphically (**Figure 70B**). The slope of the FPG is 2.9714 while the slope of the SPG was calculated to be 0.9918.

No Difference in FMN Survival Within the Facial Motor Nucleus Between SPG and FPG

The two symptomatic SOD1 groups, SGP and FPG displayed dramatic differences in rate of symptom progression during behavioral assessments for motor function. In order to investigate whether this difference was specific to motor symptom progression or overall increased rate of disease progression FMN survival was assessed between the FPG and SPG.

Comparison of percent FMN survival following axotomy was compared at 56 dpo in SPG (45 ± 8%; **Figure 72B**) and FPG (38 ± 2%; **Figure 72D**). No significant differences were revealed (**Figure 73A**). Average FMN per section was also assessed for differences in disease progression within the facial motor nucleus at 112 doa in SPG (63 ± 11; **Figure 72A**) and FPG (55 ± 5; **Figure 72C**). No significant differences were seen between average MN per section in the facial motor nucleus (**Figure 73B**). High variability coupled with low sample number (*n* = 3, per group) may have played a role in the results. Future analysis increasing the *n* per group may clarify whether FMN survival differences exist between the SPG and FPG.

No Differences in Axotomy-Induced Relative mRNA Expression Between FPG and SPG Within Only the Axotomized Facial Motor Nucleus

Relative mRNA expression for **TNFR1** in axotomized, facial motor nuclei was determined for symptomatic SOD1 groups. No significant difference between SPG (0.0223 ± 0.0002) mRNA expression and FPG (0.0351 ± 0.0100) within the facial motor nuclei at 112 doa (**Figure 75C**). The high variability seen within the FPG group may explain the lack of significance. Increasing the number of mice is a future direction.

Relative mRNA expression for **TNFα** in axotomized, facial motor nuclei was determined for symptomatic SOD1 groups. No significant difference between SPG (1.0E-04 ± 7.3E-05) mRNA expression and FPG (2.5E-04± 1.0E-04) within the facial motor nuclei at 112 doa (**Figure 76C**).

Relative mRNA expression for **Fas** in axotomized, facial motor nuclei was determined for symptomatic SOD1 groups. No significant difference between SPG (1.3E-03 ± 3.3E-04) mRNA expression and FPG (4.0E-03 ± 4.5E-03) within the facial motor nuclei at 112 doa (**Figure 77C**). As with TNFR1, high variability with the FPG may explain the lack of significance. Future direction is to increase number of mice per group.

Relative mRNA expression for **FasL** in axotomized, facial motor nuclei was determined for symptomatic SOD1 groups. No significant difference was observed between SPG (3.5E-05 ± 1.9E-05) mRNA expression and FPG (2.4E-05 ± 7.0E-06) within the facial motor nuclei at 112 do. (**Figure 78C**).

Relative mRNA expression for **TRADD** in axotomized, facial motor nuclei was determined for symptomatic SOD1 groups. No significant difference between SPG (0.0041 ± 0.0011) mRNA expression and FPG (0.0044 ± 0.0014) within the facial motor nuclei at 112 doa (**Figure 79C**).

Relative mRNA expression for **FADD** in axotomized, facial motor nuclei was determined for symptomatic SOD1 groups. No significant difference between SPG (1.1E-03 ± 1.5E-04) mRNA expression and FPG (1.4E-03 ± 2.8E-04) within the facial motor nuclei at 112 doa (**Figure 80C**).

Relative mRNA expression for **Daxx** in axotomized, facial motor nuclei was determined for symptomatic SOD1 groups. No significant difference between SPG (0.0059 ± 0.0002) mRNA expression and FPG (0.0071 ± 0.0008) within the facial motor nuclei at 112 doa (**Figure 81C**).

Relative mRNA expression for **ASK1** in axotomized, facial motor nuclei was determined for symptomatic SOD1 groups. No significant difference was seen between SPG (0.0077 ± 0.0009) mRNA expression and FPG (0.0076 ± 0.0008) within the facial motor nuclei at 112 doa (**Figure 82C**).

Relative mRNA expression for **nNOS** in axotomized, facial motor nuclei was determined for symptomatic SOD1 groups. FPG mRNA levels (3.9E-04 ± 9.1E-05) were significantly higher than SPG (1.4E-04 ± 2.6E-05) mRNA expression within the facial motor nuclei at 112 doa (**Figure 83C**).

Relative mRNA expression for **Capsase-3** in axotomized, facial motor nuclei was determined for symptomatic SOD1 groups. No significant difference between SPG (0.0047 ± 0.0008) mRNA expression and FPG (0.0089 ± 0.0037) within the facial motor nuclei at 112 doa (**Figure 84C**). High variability was seen within the FPG.

Relative mRNA expression for **Caspase-8** in axotomized, facial motor nuclei was determined for symptomatic SOD1 groups. No significant difference between SPG (1.0E-04 ± 1.6E-05) mRNA expression and FPG (1.5E-04 ± 7.1E-06) within the facial motor nuclei at 112 doa (**Figure 85C**). There is a trend for higher expression within the FPG, however variability within the SPG may account for the lack of a significant difference.

Relative mRNA expression for **TRAF2** in axotomized, facial motor nuclei was determined for symptomatic SOD1 groups. No significant difference between SPG (0.0064 ± 0.0006) mRNA expression and FPG (0.0068 ± 0.0013) within the facial motor nuclei at 112 doa (**Figure 86C**).

Relative mRNA expression for **SODD** in axotomized, facial motor nuclei was determined for symptomatic SOD1 groups. No significant difference between SPG (0.0121 ± 0.0053) mRNA expression and FPG (0.0087 ± 0.0019) within the facial motor nuclei at 112 doa (**Figure 87C**).

Relative mRNA expression for **TNFR2** in axotomized, facial motor nuclei was determined for symptomatic SOD1 groups. No significant difference between SPG (1.3E-

03 ± 2.0E-04) mRNA expression and FPG (2.2E-03± 6.3E-04) within the facial motor nuclei at 112 doa (**Figure 88C**). High variability seen again within the FPG.

Relative mRNA expression for **PAC1-R** in axotomized, facial motor nuclei was determined for symptomatic SOD1 groups. No significant difference between SPG (0.0409 ± 0.0047) mRNA expression and FPG (0.0459 ± 0.0093) within the facial motor nuclei at 112 doa (**Figure 89C**).

Relative mRNA expression for **CX3CR1** in axotomized, facial motor nuclei was determined for symptomatic SOD1 groups. No significant difference between SPG (0.0255 ± 0.0036) mRNA expression and FPG (0.0447 ± 0.0123) within the facial motor nuclei at 112 doa (**Figure 90C**). Data suggests that reducing variability within the FPG may lead to significantly higher expression within the FPG.

Relative mRNA expression for **CRMP4** in axotomized, facial motor nuclei was determined for symptomatic SOD1 groups. No significant difference between SPG (0.1090 ± 0.0236) mRNA expression and FPG (0.0917 ± 0.0090) within the facial motor nuclei at 112 doa (**Figure 91C**).

Relative mRNA expression for **GAP-43** in axotomized, facial motor nuclei was determined for symptomatic SOD1 groups. No significant difference between SPG (0.0295 ± 0.0082) mRNA expression and FPG (0.0307 ± 0.0069) within the facial motor nuclei at 112 doa (**Figure 92C**).

Relative mRNA expression for **βII-Tubulin** axotomized, facial motor nuclei was determined for symptomatic SOD1 groups. No significant difference between SPG (0.1029 ± 0.0142) mRNA expression and FPG (0.1120 ± 0.0135) within the facial motor nuclei at 112 doa (**Figure 93C**).

Relative mRNA expression for **GFAP** in axotomized, facial motor nuclei was determined for symptomatic SOD1 groups. No significant difference between SPG (0.3099 ± 0.0402) mRNA expression and FPG (0.9146 ± 0.4147) within the facial motor nuclei at 112 doa (**Figure 94C**). Although there is no significant difference between the two groups, high variability within the FPG may be the cause. Average mRNA expression is much higher in the FPG. This strongly suggests increasing the number of mice per group will clarify these findings.

Relative mRNA expression for **CD68** in axotomized, facial motor nuclei was determined for symptomatic SOD1 groups. No significant difference between SPG (0.0266 ± 0.0053) mRNA expression and FPG (0.0455 ± 0.0177) within the facial motor nuclei at 112 doa (**Figure 95C**). Again there is a trend for increased expression in the FPG, however, high variability is seen within that group.

No Difference in Percent Change mRNA Expression Between the FPG and SPG Facial Motor Nucleus (Ax/C)

TNFR1 percent change in mRNA expression (Ax/C) was in facial motor nuclei for symptomatic SOD1 groups. No significant difference in percent mRNA expression in

axotomized facial motor nucleus compared to control nucleus for SPG (63 ± 5%) or FPG (53 ± 15%) at 56 dpo (**Figure 75A**).

TNFα percent change in mRNA expression (Ax/C) was in facial motor nuclei for symptomatic SOD1 groups. No significant difference in percent mRNA expression in axotomized facial motor nucleus compared to control nucleus for SPG (436 ± 146%) or FPG (261 ± 108%) at 56 dpo (**Figure 76A**). High variability within both groups makes it difficult to even assess for potential trends.

Fas percent change in mRNA expression (Ax/C) was in facial motor nuclei for symptomatic SOD1 groups. No significant difference in percent mRNA expression in axotomized facial motor nucleus compared to control nucleus for SPG (145 ± 35%) or FPG (257 ± 100%) at 56 dpo (**Figure 77A**). High variability is seen within the FPG, but average percent change is much higher.

FasL percent change in mRNA expression (Ax/C) was in facial motor nuclei for symptomatic SOD1 groups. No significant difference in percent mRNA expression in axotomized facial motor nucleus compared to control nucleus for SPG (106 ± 30%) or FPG (98 ± 14%) at 56 dpo (**Figure 78A**).

TRADD percent change in mRNA expression (Ax/C) was in facial motor nuclei for symptomatic SOD1 groups. No significant difference in percent mRNA expression in axotomized facial motor nucleus compared to control nucleus for SPG (26 ± 22%) or FPG (-21 ± 5%) at 56 dpo (**Figure 79A**). The percent change mRNA for FPG reveals an

interesting reduced expression in the FPG axotomized nucleus compared to its control. Increasing number of mice per group may reveal interesting patterns such as this.

FADD percent change in mRNA expression (Ax/C) was in facial motor nuclei for symptomatic SOD1 groups. No significant difference in percent mRNA expression in axotomized facial motor nucleus compared to control nucleus for SPG (69 ± 36%) or FPG (76 ± 49) at 56 dpo (**Figure 80A**). Results are extremely variable for both groups.

Daxx percent change in mRNA expression (Ax/C) was in facial motor nuclei for symptomatic SOD1 groups. No significant difference in percent mRNA expression in axotomized facial motor nucleus compared to control nucleus for SPG (64 ± 25%) or FPG (33 ± 32%) at 56 dpo (**Figure 81A**). Again, results are extremely variable for both groups.

ASK1 percent change in mRNA expression (Ax/C) was in facial motor nuclei for symptomatic SOD1 groups. No significant difference in percent mRNA expression in axotomized facial motor nucleus compared to control nucleus for SPG (66 ± 44%) or FPG (52 ± 23%) at 56 dpo (**Figure 82A**). Results are extremely variable for both groups. Demonstrates the need for increased number of mice per group.

nNOS percent change in mRNA expression (Ax/C) was in facial motor nuclei for symptomatic SOD1 groups. No significant difference in percent mRNA expression in axotomized facial motor nucleus compared to control nucleus for SPG (103 ± 31%) or FPG (105 ± 38%) at 56 dpo (**Figure 83A**).

Caspase-3 percent change in mRNA expression (Ax/C) was in facial motor nuclei for symptomatic SOD1 groups. No significant difference in percent mRNA expression in axotomized facial motor nucleus compared to control nucleus for SPG (76 ± 78%) or FPG (147 ± 71%) at 56 dpo (**Figure 84A**). Results are extremely variable for both groups, however mean is higher in FPG.

Caspase-8 percent change in mRNA expression (Ax/C) was in facial motor nuclei for symptomatic SOD1 groups. No significant difference in percent mRNA expression in axotomized facial motor nucleus compared to control nucleus for SPG (34 ± 22%) or FPG (-23 ± 9%) at 56 dpo (**Figure 85A**). Caspase-8 displays an interesting decreased percent change expression in the FPG compared to the SPG that was seen previously with TRADD expression. However, statistical significance must be reached to verify that these differences in expression patterns exist between the groups.

TRAF2 percent change in mRNA expression (Ax/C) was in facial motor nuclei for symptomatic SOD1 groups. No significant difference in percent mRNA expression in axotomized facial motor nucleus compared to control nucleus for SPG (70 ± 29%) or FPG (39 ± 33%) at 56 dpo (**Figure 86A**). TRAF2 percent change mRNA expression is highly variable in both groups.

SODD percent change in mRNA expression (Ax/C) was in facial motor nuclei for symptomatic SOD1 groups. No significant difference in percent mRNA expression in

axotomized facial motor nucleus compared to control nucleus for SPG (-4 ± 28%) or FPG (-38 ± 25%) at 56 dpo (**Figure 87A**).

TNFR2 percent change in mRNA expression (Ax/C) was in facial motor nuclei for symptomatic SOD1 groups. No significant difference in percent mRNA expression in axotomized facial motor nucleus compared to control nucleus for SPG (132 ± 21%) or FPG (143 ± 26%) at 56 dpo (**Figure 88A**).

PAC1-R percent change in mRNA expression (Ax/C) was in facial motor nuclei for symptomatic SOD1 groups. No significant difference in percent mRNA expression in axotomized facial motor nucleus compared to control nucleus for SPG (13 ± 20%) or FPG (17 ± 4%) at 56 dpo (**Figure 89A**). It is not clear why PAC1-R percent change in mRNA is so variable within the SPG. No other genes have shown this type of variability within the SPG.

CX3CR1 percent change in mRNA expression (Ax/C) was in facial motor nuclei for symptomatic SOD1 groups. No significant difference in percent mRNA expression in axotomized facial motor nucleus compared to control nucleus for SPG (104 ± 33%) or FPG (68 ± 14%) at 56 dpo (**Figure 90A**).

CRMP4 percent change in mRNA expression (Ax/C) was in facial motor nuclei for symptomatic SOD1 groups. No significant difference in percent mRNA expression in axotomized facial motor nucleus compared to control nucleus for SPG (22 ± 34%) or FPG (-37 ± 30%) at 56 dpo (**Figure 91A**). Another trend for decreased percent change in

mRNA within the FPG, previously seen with the death receptor adapter protein TRADD, and Caspase-8. Increased CRMP4 expression considered to be neurodegenerative, especially in SOD1 MN. Future direction is to increase group sizes.

GAP-43 percent change in mRNA expression (Ax/C) was in facial motor nuclei for symptomatic SOD1 groups. No significant difference in percent mRNA expression in axotomized facial motor nucleus compared to control nucleus for SPG (155 ± 101%) or FPG (80 ± 40%) at 56 dpo (**Figure 92A**). High variability shown within the SPG, similar to the high variability seen in PAC1-R percent change in expression.

βII-Tubulin percent change in mRNA expression (Ax/C) was in facial motor nuclei for symptomatic SOD1 groups. No significant difference in percent mRNA expression in axotomized facial motor nucleus compared to control nucleus for SPG (21 ± 7%) or FPG (28 ± 26%) at 56 dpo (**Figure 93A**). Extremely high variability exists within the FPG.

GFAP percent change in mRNA expression (Ax/C) was in facial motor nuclei for symptomatic SOD1 groups. No significant difference in percent mRNA expression in axotomized facial motor nucleus compared to control nucleus for SPG (378 ± 56%) or FPG (218 ± 55%) at 56 dpo (**Figure 94A**). There appears to be a definite trend for higher percent change mRNA expression within the SPG however these results were not significant.

CD68 percent change in mRNA expression (Ax/C) was in facial motor nuclei for symptomatic SOD1 groups. No significant difference in percent mRNA expression in

axotomized facial motor nucleus compared to control nucleus for SPG (263 ± 79%) or FPG (106 ± 8%) at 56 dpo (**Figure 95A**). Interestingly, as seen with GFAP there appears to be a definite trend for increase percent change GFAP expression within the SPG, this was also seen with CD68. Future directions will increase group numbers to reduce variability.

FPG Displays Increased Relative mRNA Expression Levels Within Disease-Affected, Control Facial Motor Nucleus Compared to the SPG

Relative mRNA expression for **TNFR1** in disease-affected, control facial motor nuclei was determined for symptomatic SOD1 groups. No significant difference between SPG (0.0166 ± 0.0034) mRNA expression and FPG (0.0268 ± 0.0071) within the facial motor nuclei at 112 doa (**Figure 75B**). Increased average TNFRI mRNA in the FPG control nucleus, however there is high variability.

Relative mRNA expression for **TNFα** in disease-affected, control facial motor nuclei was determined for symptomatic SOD1 groups. A significant difference between SPG (1.7E-05 ± 8.2E-06) mRNA expression and FPG (6.8E-05± 1.9E-05) was found within the facial motor nuclei at 112 doa (**Figure 76B**). TNFα mRNA expression levels are greatly increased within the FPG compared to the slow progression group.

Relative mRNA expression for **Fas** in disease-affected, control facial motor nuclei was determined for symptomatic SOD1 groups. A significant difference between SPG

(5.2E-04 ± 6.1E-05) mRNA expression and FPG (1.1E-03 ± 2.6E-04) was seen within the facial motor nuclei at 112 doa (**Figure 77B**).

Relative mRNA expression for **FasL** in disease-affected, control facial motor nuclei was determined for symptomatic SOD1 groups. No significant difference between SPG (1.8E-05 ± 1.1E-05) mRNA expression and FPG (1.2E-05 ± 3.5E-06) within the facial motor nuclei at 112 doa (**Figure 78B**). FasL displayed high variability among both groups.

Relative mRNA expression for **TRADD** in disease-affected, control facial motor nuclei was determined for symptomatic SOD1 groups. No significant difference between SPG (0.0032 ± 0.0005) mRNA expression and FPG (0.0055 ± 0.0014) within the facial motor nuclei at 112 doa (**Figure 79B**). However, the FPG has a higher mean, but is also highly variable.

Relative mRNA expression for **FADD** in disease-affected, control facial motor nuclei was determined for symptomatic SOD1 groups. No significant difference between SPG (6.9E-04 ± 8.3E-05) mRNA expression and FPG (8.3E-04 ± 9.6E-05) within the facial motor nuclei at 112 doa (**Figure 80B**).

Relative mRNA expression for **Daxx** in disease-affected, control facial motor nuclei was determined for symptomatic SOD1 groups. No significant difference between SPG (0.0037 ± 0.0007) mRNA expression and FPG (0.0056 ± 0.0007) within the facial motor nuclei at 112 doa (**Figure 81B**). Daxx mRNA expression is similar to that seen with another adapter protein TRADD, a higher mean in the FPG, but high variability as well.

Relative mRNA expression for **ASK1** in disease-affected, control facial motor nuclei was determined for symptomatic SOD1 groups. No significant difference between SPG (0.0049 ± 0.0009) mRNA expression and FPG (0.0051 ± 0.0006) within the facial motor nuclei at 112 doa (**Figure 82B**).

Relative mRNA expression for **nNOS** in disease-affected, control facial motor nuclei was determined for symptomatic SOD1 groups. A significant difference between SPG (7.1E-05 ± 1.7E-06) mRNA expression and FPG (1.9E-04 ± 3.0E-05) was seen within the facial motor nuclei at 112 doa (**Figure 83B**). This significant increase is likely due to the unusually low variability in the SPG.

Relative mRNA expression for **Capsase-3** in disease-affected, control facial motor nuclei was determined for symptomatic SOD1 groups. No significant difference between SPG (0.0031 ± 0.0008) mRNA expression and FPG (0.0036 ± 0.0008) within the facial motor nuclei at 112 doa (**Figure 84B**).

Relative mRNA expression for **Caspase-8** in disease-affected, control facial motor nuclei was determined for symptomatic SOD1 groups. A significant difference between SPG (7.6E-05 ± 1.1E-06) mRNA expression and FPG (1.9E-04 ± 1.4E-05) was found within the facial motor nuclei at 112 doa (**Figure 85B**). Like nNOS an unusually low variability within the SPG may have resulted in this significant difference. Larger groups are needed to reduce variability so more consistent expression levels can be analyzed.

Relative mRNA expression for **TRAF2** in disease-affected, control facial motor nuclei was determined for symptomatic SOD1 groups. No significant difference between SPG (0.0039 ± 0.0006) mRNA expression and FPG (0.0050 ± 0.0003) within the facial motor nuclei at 112 doa (**Figure 86B**).

Relative mRNA expression for **SODD** in disease-affected, control facial motor nuclei was determined for symptomatic SOD1 groups. No significant difference between SPG (0.0122 ± 0.0026) mRNA expression and FPG (0.0160 ± 0.0014) within the facial motor nuclei at 112 doa (**Figure 87B**).

Relative mRNA expression for **TNFR2** in disease-affected, control facial motor nuclei was determined for symptomatic SOD1 groups. No significant difference between SPG (5.6E-04 ± 4.9E-05) mRNA expression and FPG (9.3E-04± 3.4E-04) within the facial motor nuclei at 112 doa (**Figure 88B**). High variability was seen in the FPG.

Relative mRNA expression for **PAC1-R** in disease-affected, control facial motor nuclei was determined for symptomatic SOD1 groups. No significant difference between SPG (0.0371 ± 0.0046) mRNA expression and FPG (0.0394 ± 0.0078) within the facial motor nuclei at 112 doa (**Figure 89B**).

Relative mRNA expression for **CX3CR1** in disease-affected, control facial motor nuclei was determined for symptomatic SOD1 groups. A significant difference between SPG (0.0129 ± 0.0026) mRNA expression and FPG (0.0262 ± 0.0051) was seen within the

facial motor nuclei at 112 doa (**Figure 90B**). FPG revealed increased mRNA expression within the diseased, control nucleus compared to the SPG.

Relative mRNA expression for **CRMP4** in disease-affected, control facial motor nuclei was determined for symptomatic SOD1 groups. No significant difference between SPG (0.0947 ± 0.0202) mRNA expression and FPG (0.1598 ± 0.0611) within the facial motor nuclei at 112 doa (**Figure 91B**). CRMP4 reveals high variability within the FPG.

Relative mRNA expression for **GAP-43** in disease-affected, control facial motor nuclei was determined for symptomatic SOD1 groups. A significant difference between SPG (0.0134 ± 0.0039) mRNA expression and FPG (0.0174 ± 0.0024) was seen within the facial motor nuclei at 112 doa (**Figure 92B**).

Relative mRNA expression for **βII-Tubulin** disease-affected, control facial motor nuclei was determined for symptomatic SOD1 groups. No significant difference between SPG (0.1152 ± 0.0271) mRNA expression and FPG (0.0894 ± 0.0064) within the facial motor nuclei at 112 doa (**Figure 93B**).

Relative mRNA expression for **GFAP** in disease-affected, control facial motor nuclei was determined for symptomatic SOD1 groups. No significant difference between SPG (0.0648 ± 0.0027) mRNA expression and FPG (0.2733 ± 0.0817) within the facial motor nuclei at 112 doa (**Figure 94B**). The FPG revealed higher mRNA expression for GFAP, suggesting an increased astrocyte reaction compared to that within the SPG facial motor nucleus.

Relative mRNA expression for **CD68** in disease-affected, control facial motor nuclei was determined for symptomatic SOD1 groups. Similar to the previous glial-specific gene, GFAP, CD68 reveals a significant difference between SPG (0.0079 ± 0.0023) mRNA expression and FPG (0.0265 ± 0.0065) within the facial motor nuclei at 112 doa (**Figure 95B**). This also suggests an increased glial response, a microglial response within the diseased facial motor nucleus compared to that within the SPG facial nucleus.

Figure 69. Experimental Design: Behavioral testing of symptomatic SOD1 mice

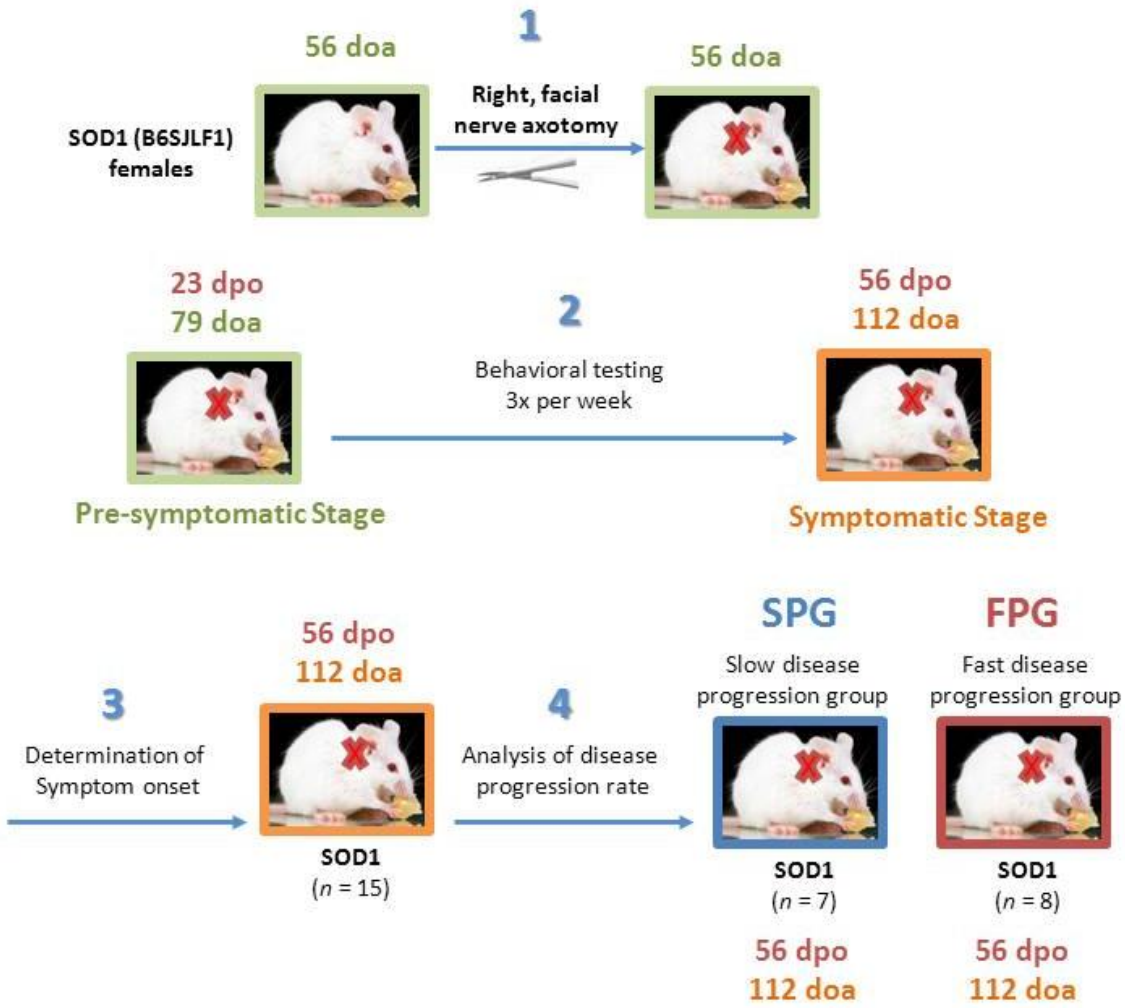

1. Pre-symptomatic SOD1 mice received a right facial nerve axotomy at 56 doa.
2. Starting at 79 doa mice underwent behavioral testing for assessment of motor function until euthanasia at 112 doa, 56 days post-operative (dpo).
3. Symptom onset was determined by statistical comparisons between averaged motor scores per time-point among the SOD1 mice.
4. Once symptomatic onset was determined, average motor score throughout the symptomatic stage was determined for each mouse and a median split was performed to separate the SOD1 mice into the following two symptomatic groups: the SPG (slow) and the FPG (fast).

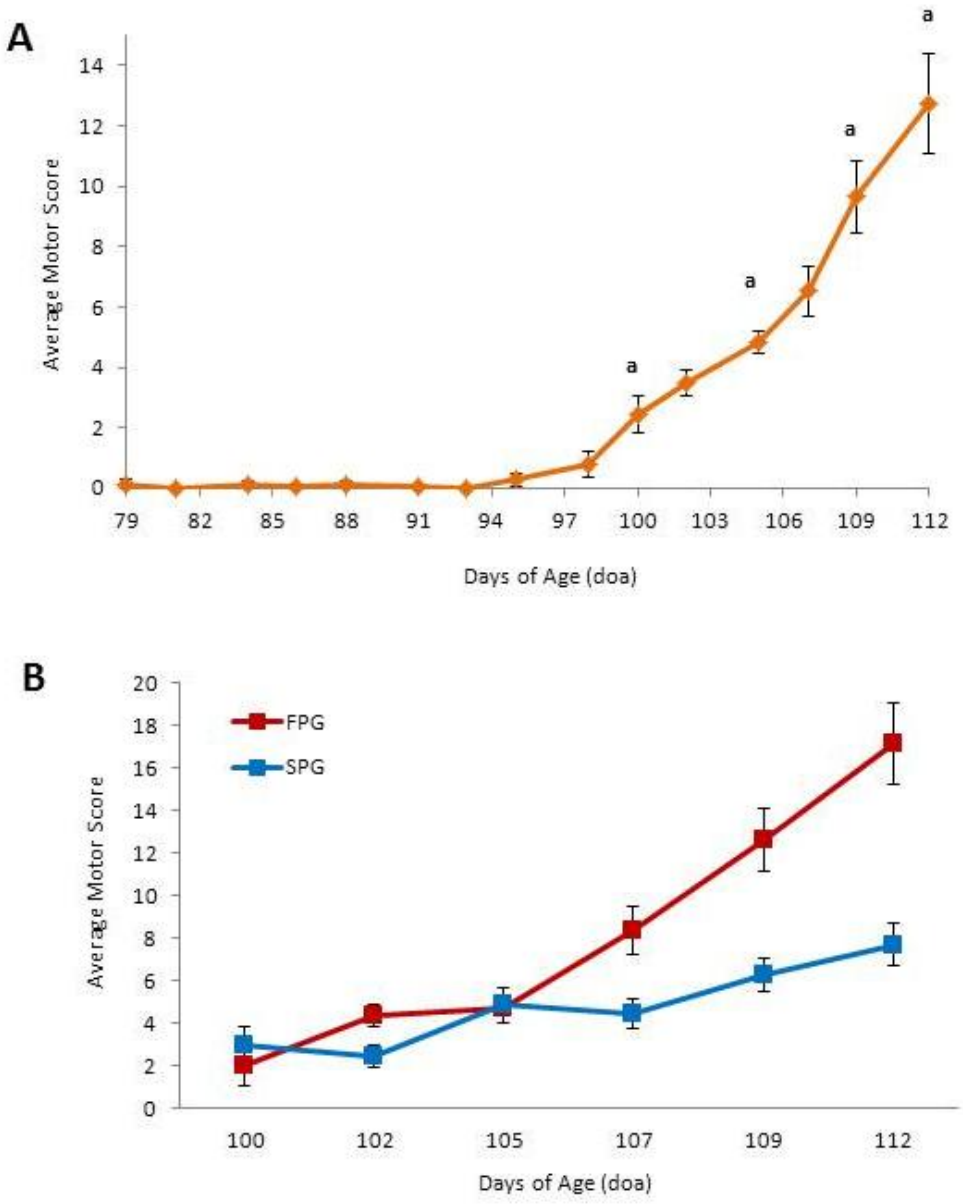

Figure 70. Behavioral testing for motor function during disease progression in SOD1 mice. **A,** Average motor scores of SOD1 mice across time. **a**, represents a significant difference in average motor score between the time-point and the previous, $p \leq 0.05$. **B**, rate of symptom progression between two symptomatic SOD1 groups, based on motor scores throughout the symptomatic stage.

Figure 71. Experimental Design: FMN Survival, average FMN per section of control facial motor nucleus and percent FMN survival after axotomy in symptomatic SOD1 groups (SPG & FPG)

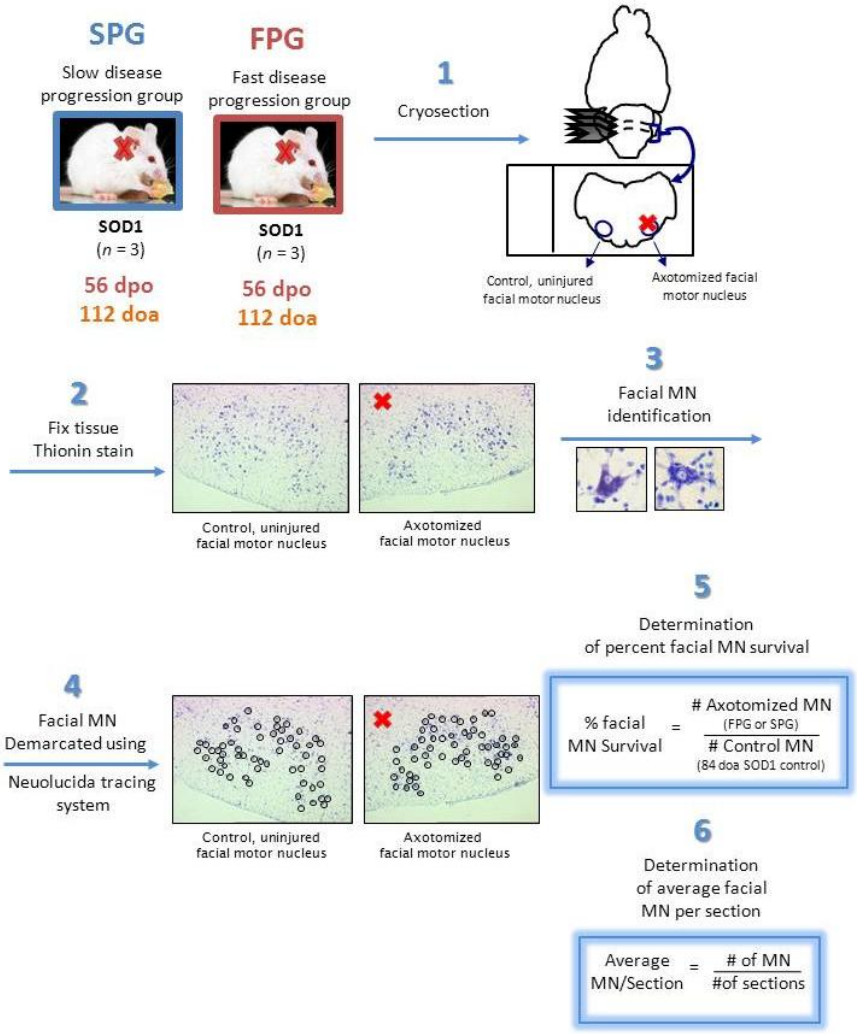

1. Mice, which previously received a facial nerve axotomy, were assigned to two groups; FPG and SPG (see **Figure 69**). Brains were removed and cryosectioned through the facial motor nucleus at 25 µm.
2. Sections were fixed with 4% PFA and stained with thionin.
3. FMN were identified by morphology and a defined nucleus and nucleolus.
4. FMN were demarcated under light microscopy using the Neurolucida Tracing System and total number of MN per section were recorded for both control (left) and axotomized (right) facial motor nuclei.
5. The average percent FMN survival was calculated by taking the total number of MN counted in the axotomized nucleus and dividing by the total number of MN in the 28 dpo (84 doa) control nucleus (previously determined, see Chapter VI) then multiplying by 100.
6. The average percent of FMN survival was calculated by taking the total number of MN counted and dividing by the total number of sections counted.

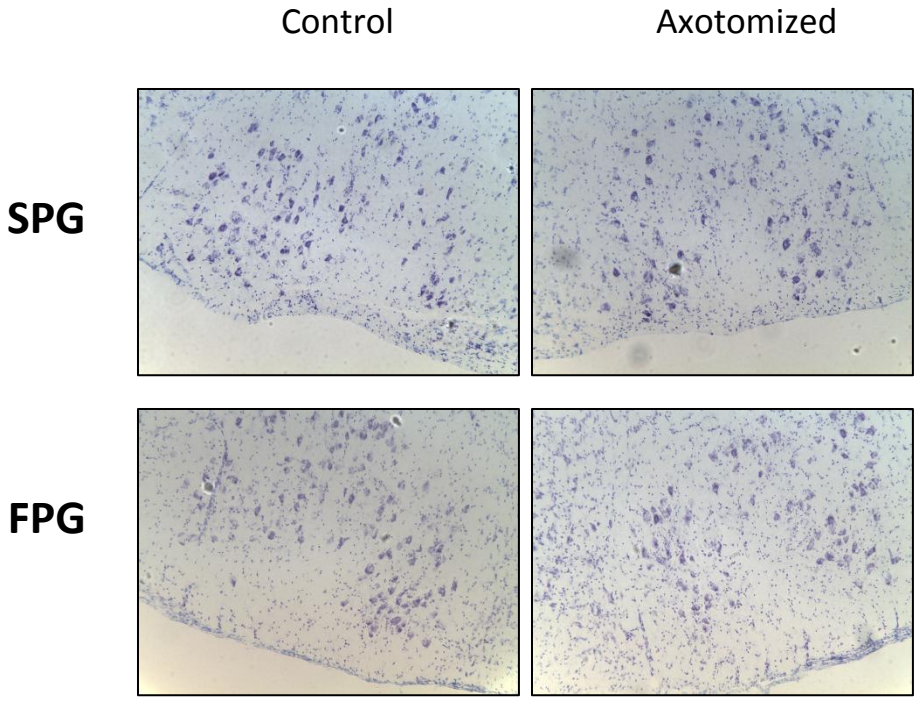

Figure 72. Representative photomicrographs of thionin-stained axotomized and control facial motor nuclei from symptomatic SOD1 groups (SPG and FPG) at 56 dpo (112 doa). Original magnification 20x.

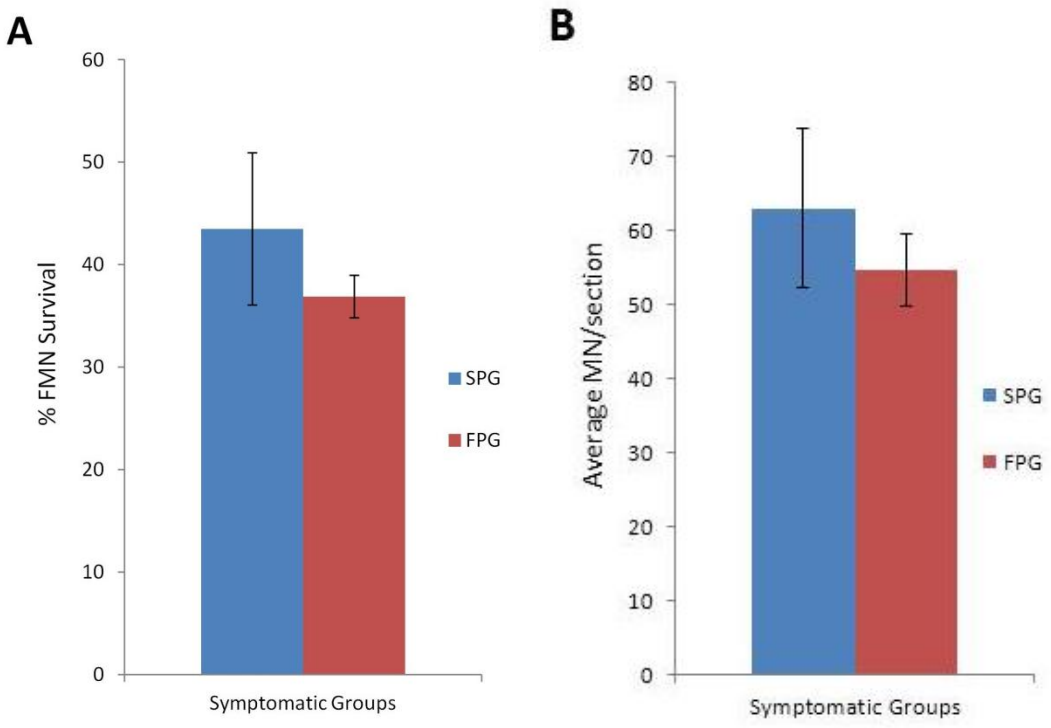

Figure 73. FMN survival ± SEM in symptomatic SOD1 groups (SPG and FPG) facial motor nuclei at 56 dpo (112 doa). **A**, Percent FMN survival in axotomized facial motor nucleus. **B**, Average MN per section in symptomatic SOD1 groups (SPG and FPG).

Figure 74. Experimental Design: LMD of SPG and FPG facial motor nuclei and real time RT-PCR analysis of mRNA expression

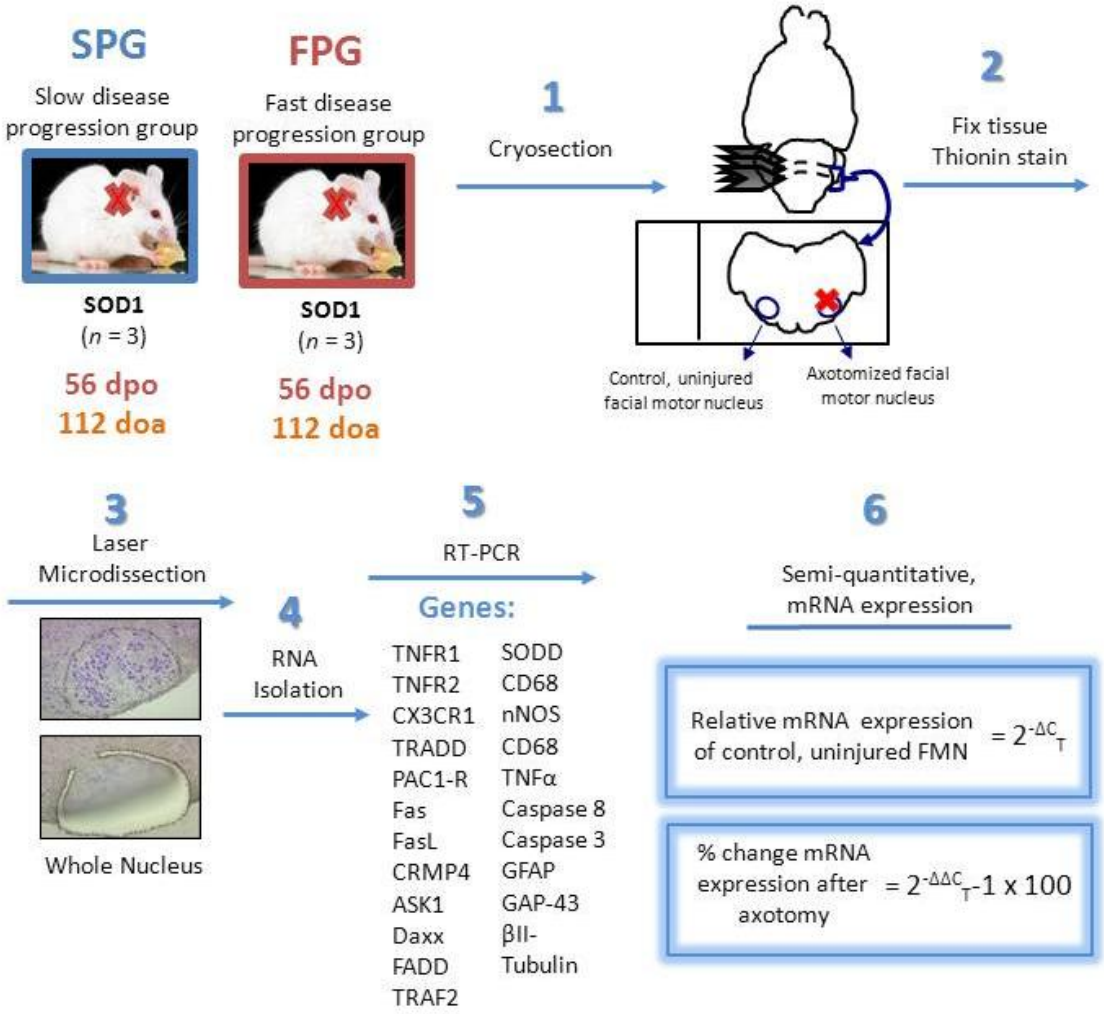

1. Mice, previously received a facial nerve axotomy and were assigned into two groups, FPG and SPG (see **Figure 69**). Brains were removed and cryosectioned through the facial motor nucleus at 25 µm.
2. Sections were fixed with 100% ETOH and stained with thionin.
3. Control and axotomized nuclei were separately collected by laser microdissected for each mouse.
4. RNA was isolated from control and axotomized facial motor nucleus samples.
5. Real-time, RT-PCR was performed for specific genes to profile mRNA expression in the facial motor nuclei of FPG compared to the SPG.
6. The semi-quantitative, relative mRNA expression, normalized to GAPDH in the facial motor nucleus was calculated using the $2^{-\Delta C}{}_T$ method. As well as the percent change of mRNA expression of the axotomized nucleus relative to the control nucleus was calculated using the $2^{-\Delta\Delta C}{}_T$ method

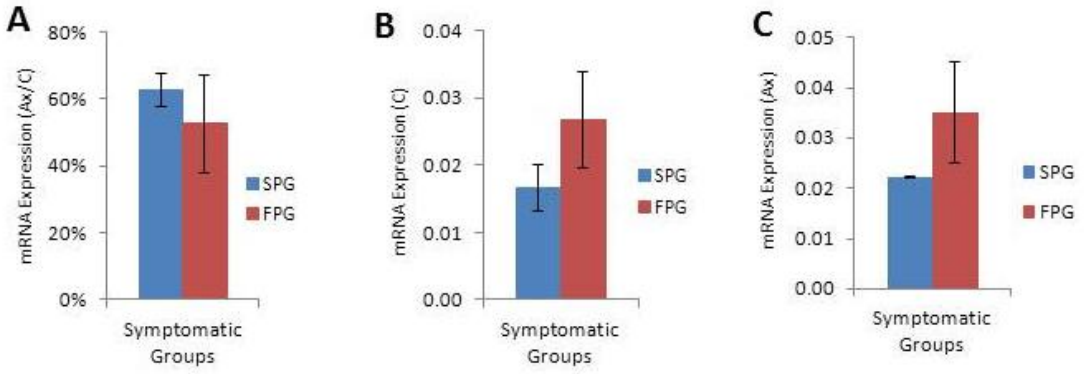

Figure 75. Relative mRNA expression of **TNFR1** in facial motor nucleus of symptomatic SOD1 groups (SPG and FPG) at 112 doa. **A**, Percent change of mRNA expression in SPG and FPG axotomized facial nuclei relative to control. **B**, Relative mRNA expression in SPG and FPG **control** facial motor nuclei. **C**, Relative mRNA expression in SPG and FPG **axotomized** facial motor nuclei.

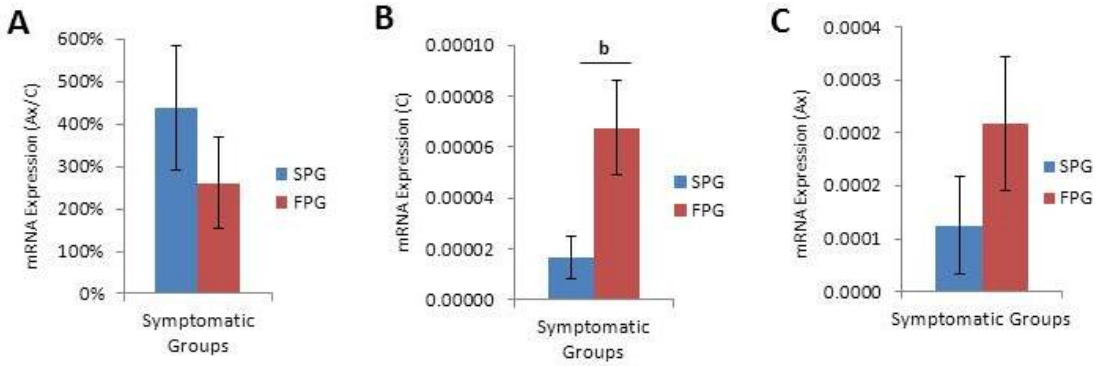

Figure 76. Relative mRNA expression of **TNFα** in facial motor nucleus of symptomatic SOD1 groups (SPG and FPG) at 112 doa. **A**, Percent change of mRNA expression in SPG and FPG axotomized facial nuclei relative to control. **B**, Relative mRNA expression in SPG and FPG **control** facial motor nuclei. **C**, Relative mRNA expression in SPG and FPG **axotomized** facial motor nuclei. **b** represents a significant difference in FPG mRNA relative to SPG at $p \leq 0.05$.

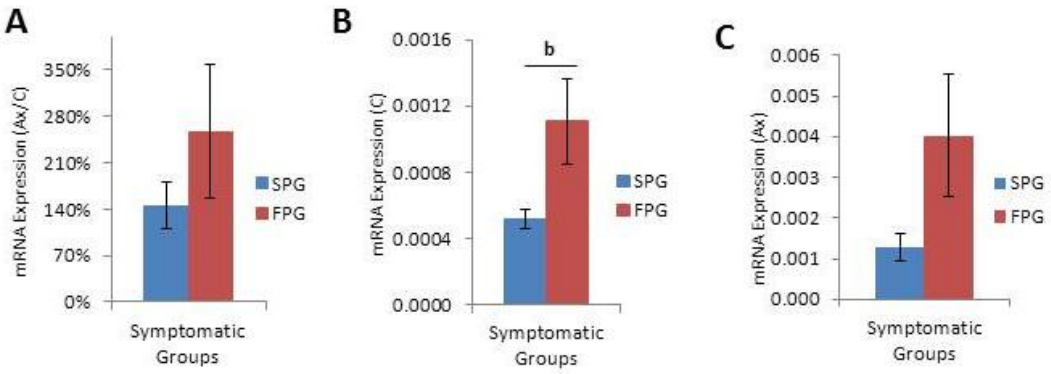

Figure 77. Relative mRNA expression of **Fas** in facial motor nucleus of symptomatic SOD1 groups (SPG and FPG) at 112 doa. **A**, Percent change of mRNA expression in SPG and FPG axotomized facial nuclei relative to control. **B**, Relative mRNA expression in SPG and FPG **control** facial motor nuclei. **C**, Relative mRNA expression in SPG and FPG **axotomized** facial motor nuclei. **b** represents a significant difference in FPG mRNA relative to SPG at $p \leq 0.05$.

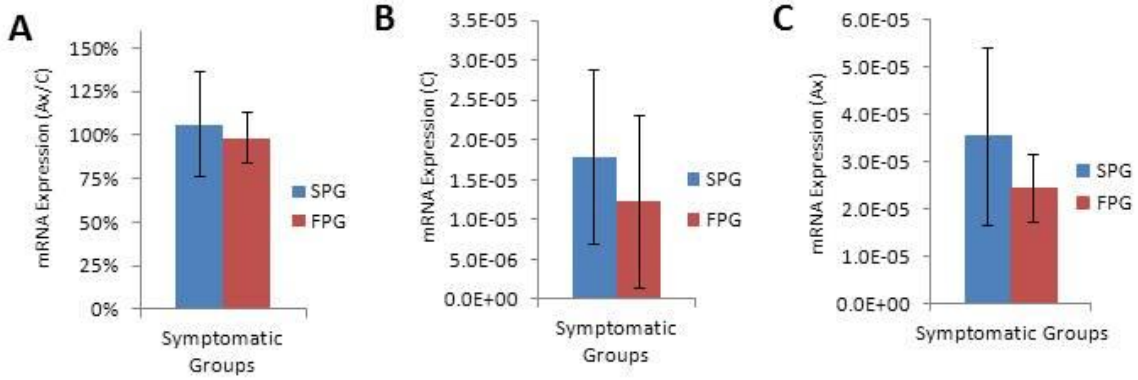

Figure 78. Relative mRNA expression of **FasL** in facial motor nucleus of symptomatic SOD1 groups (SPG and FPG) at 112 doa. **A**, Percent change of mRNA expression in SPG and FPG axotomized facial nuclei relative to control. **B**, Relative mRNA expression in SPG and FPG **control** facial motor nuclei. **C**, Relative mRNA expression in SPG and FPG **axotomized** facial motor nuclei.

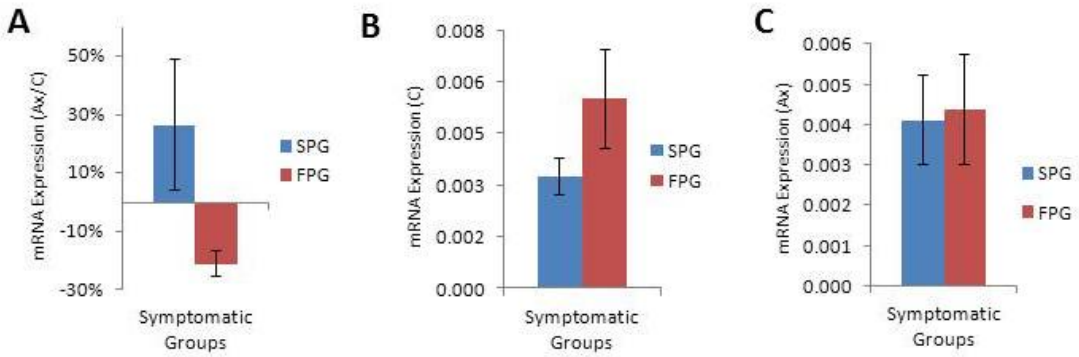

Figure 79. Relative mRNA expression of **TRADD** in facial motor nucleus of symptomatic SOD1 groups (SPG and FPG) at 112 doa. **A**, Percent change of mRNA expression in SPG and FPG axotomized facial nuclei relative to control. **B**, Relative mRNA expression in SPG and FPG **control** facial motor nuclei. **C**, Relative mRNA expression in SPG and FPG **axotomized** facial motor nuclei.

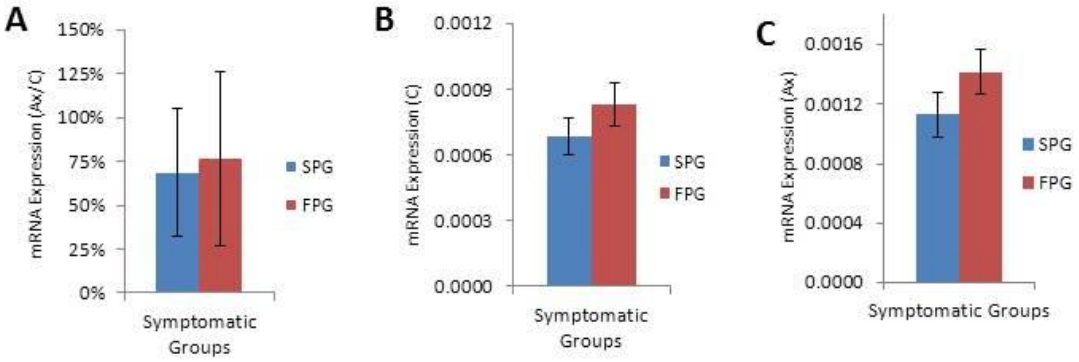

Figure 80. Relative mRNA expression of **FADD** in facial motor nucleus of symptomatic SOD1 groups (SPG and FPG) at 112 doa. **A**, Percent change of mRNA expression in SPG and FPG axotomized facial nuclei relative to control. **B**, Relative mRNA expression in SPG and FPG **control** facial motor nuclei. **C**, Relative mRNA expression in SPG and FPG **axotomized** facial motor nuclei.

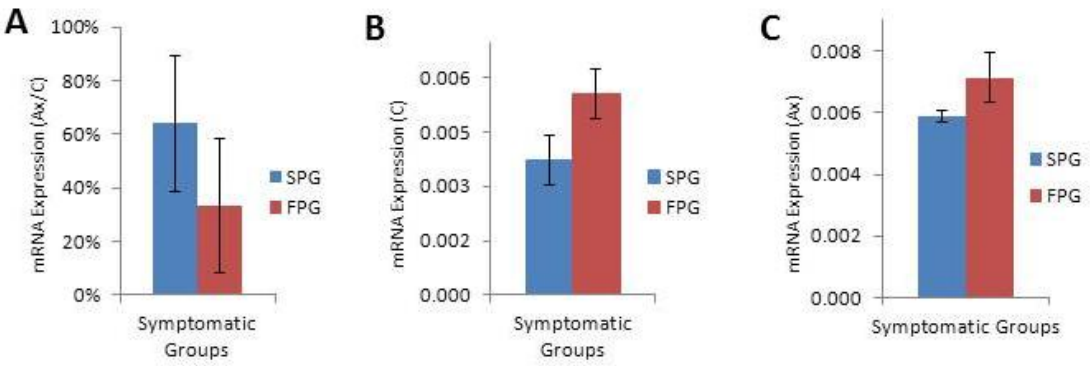

Figure 81. Relative mRNA expression of **Daxx** in facial motor nucleus of symptomatic SOD1 groups (SPG and FPG) at 112 doa. **A**, Percent change of mRNA expression in SPG and FPG axotomized facial nuclei relative to control. **B**, Relative mRNA expression in SPG and FPG **control** facial motor nuclei. **C**, Relative mRNA expression in SPG and FPG **axotomized** facial motor nuclei.

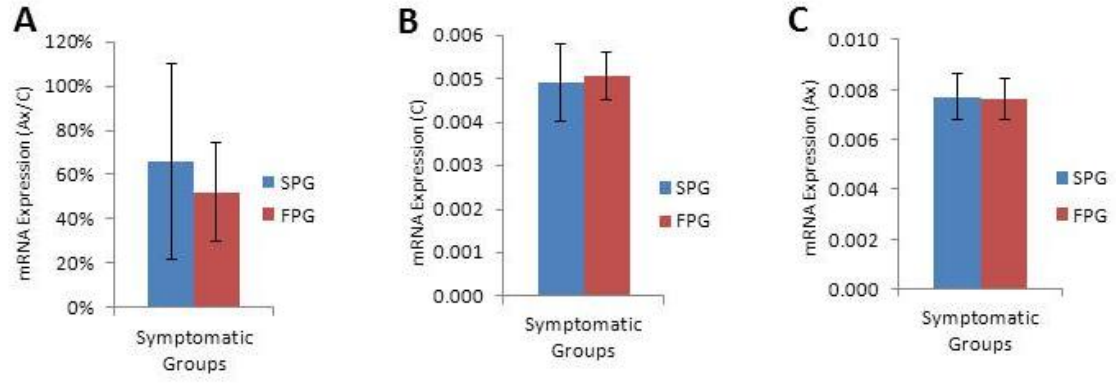

Figure 82. Relative mRNA expression of **ASK1** in facial motor nucleus of symptomatic SOD1 groups (SPG and FPG) at 112 doa. **A**, Percent change of mRNA expression in SPG and FPG axotomized facial nuclei relative to control. **B**, Relative mRNA expression in SPG and FPG **control** facial motor nuclei. **C**, Relative mRNA expression in SPG and FPG **axotomized** facial motor nuclei.

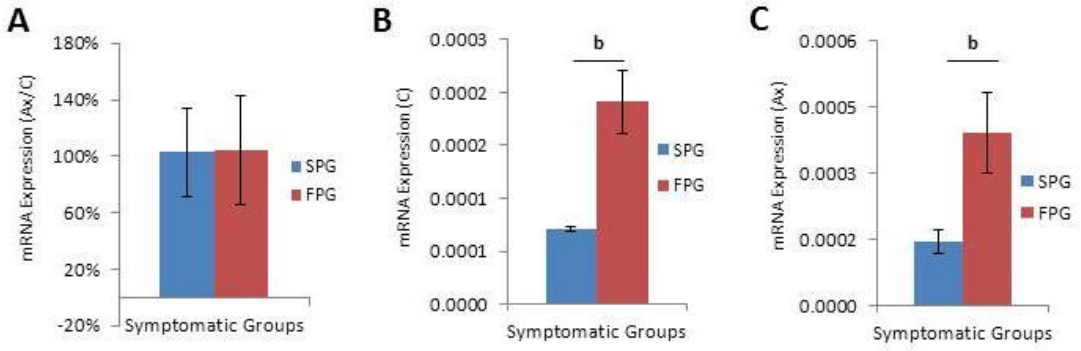

Figure 83. Relative mRNA expression of **nNOS** in facial motor nucleus of symptomatic SOD1 groups (SPG and FPG) at 112 doa. **A**, Percent change of mRNA expression in SPG and FPG axotomized facial nuclei relative to control. **B**, Relative mRNA expression in SPG and FPG **control** facial motor nuclei. **C**, Relative mRNA expression in SPG and FPG **axotomized** facial motor nuclei. **b** represents a significant difference in FPG mRNA relative to SPG at $p \leq 0.05$.

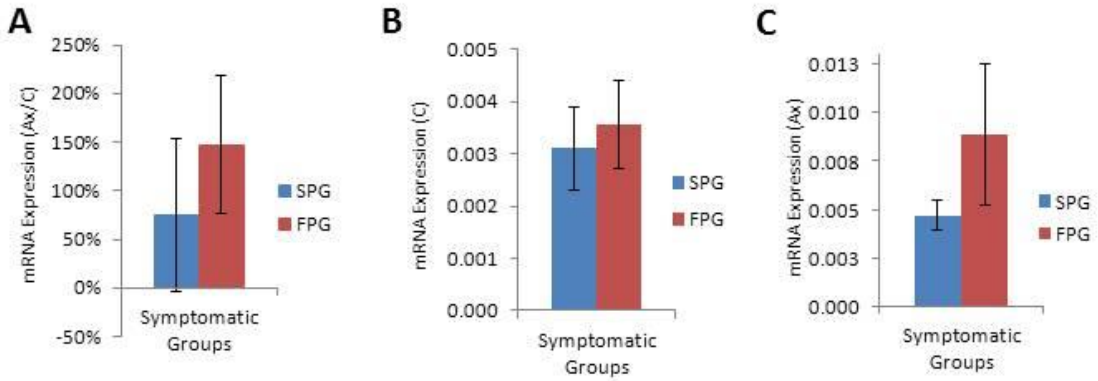

Figure 84. Relative mRNA expression of **Caspase-3** in facial motor nucleus of symptomatic SOD1 groups (SPG and FPG) at 112 doa. **A**, Percent change of mRNA expression in SPG and FPG axotomized facial nuclei relative to control. **B**, Relative mRNA expression in SPG and FPG **control** facial motor nuclei. **C**, Relative mRNA expression in SPG and FPG **axotomized** facial motor nuclei.

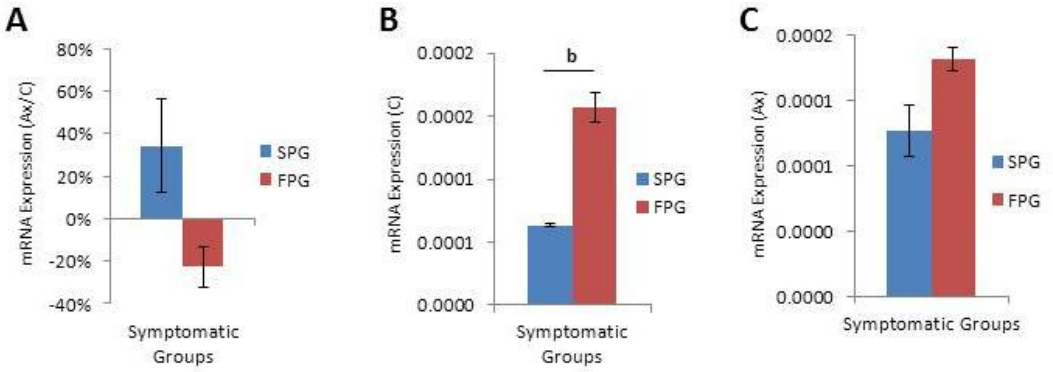

Figure 85. Relative mRNA expression of **Caspase-8** in facial motor nucleus of symptomatic SOD1 groups (SPG and FPG) at 112 doa. **A**, Percent change of mRNA expression in SPG and FPG axotomized facial nuclei relative to control. **B**, Relative mRNA expression in SPG and FPG **control** facial motor nuclei. **C**, Relative mRNA expression in SPG and FPG **axotomized** facial motor nuclei. **b** represents a significant difference in FPG mRNA relative to SPG at $p \leq 0.05$.

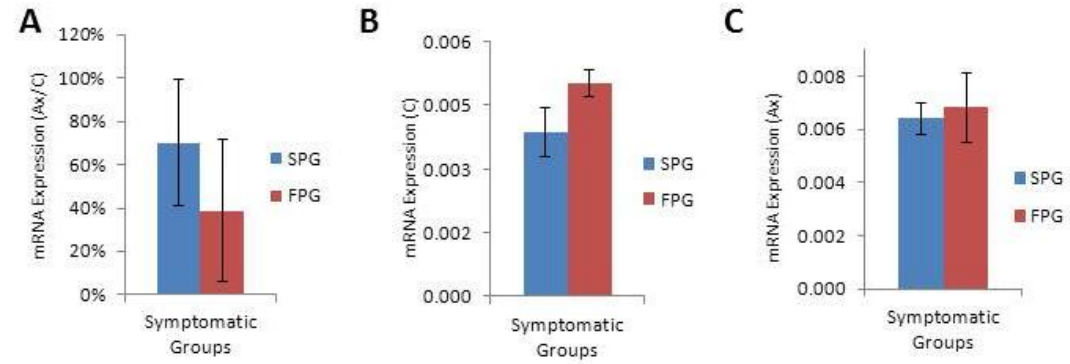

Figure 86. Relative mRNA expression of **TRAF2** in facial motor nucleus of symptomatic SOD1 groups (SPG and FPG) at 112 doa. **A**, Percent change of mRNA expression in SPG and FPG axotomized facial nuclei relative to control. **B**, Relative mRNA expression in SPG and FPG **control** facial motor nuclei. **C**, Relative mRNA expression in SPG and FPG **axotomized** facial motor nuclei.

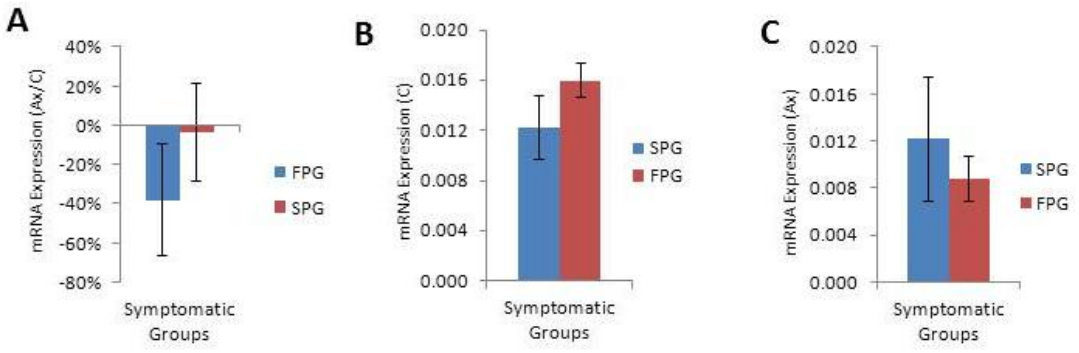

Figure 87. Relative mRNA expression of **SODD** in facial motor nucleus of symptomatic SOD1 groups (SPG and FPG) at 112 doa. **A**, Percent change of mRNA expression in SPG and FPG axotomized facial nuclei relative to control. **B**, Relative mRNA expression in SPG and FPG **control** facial motor nuclei. **C**, Relative mRNA expression in SPG and FPG **axotomized** facial motor nuclei.

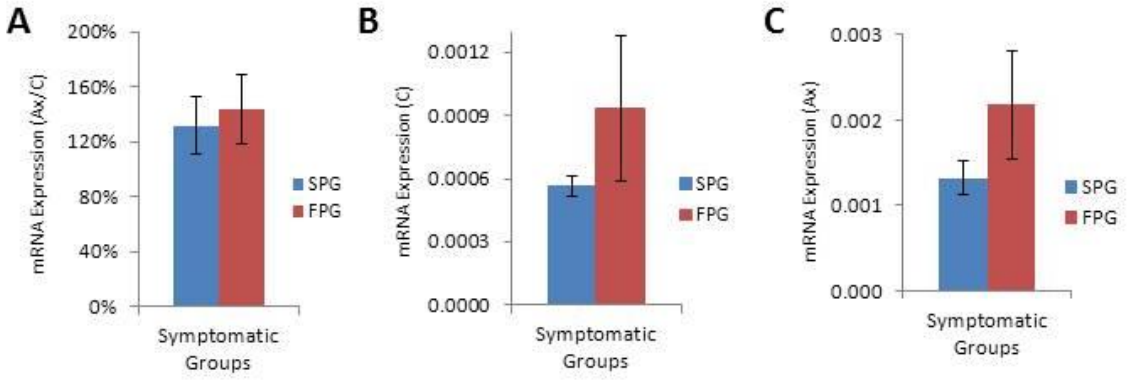

Figure 88. Relative mRNA expression of **TNFR2** in facial motor nucleus of symptomatic SOD1 groups (SPG and FPG) at 112 doa. **A**, Percent change of mRNA expression in SPG and FPG axotomized facial nuclei relative to control. **B**, Relative mRNA expression in SPG and FPG **control** facial motor nuclei. **C**, Relative mRNA expression in SPG and FPG **axotomized** facial motor nuclei.

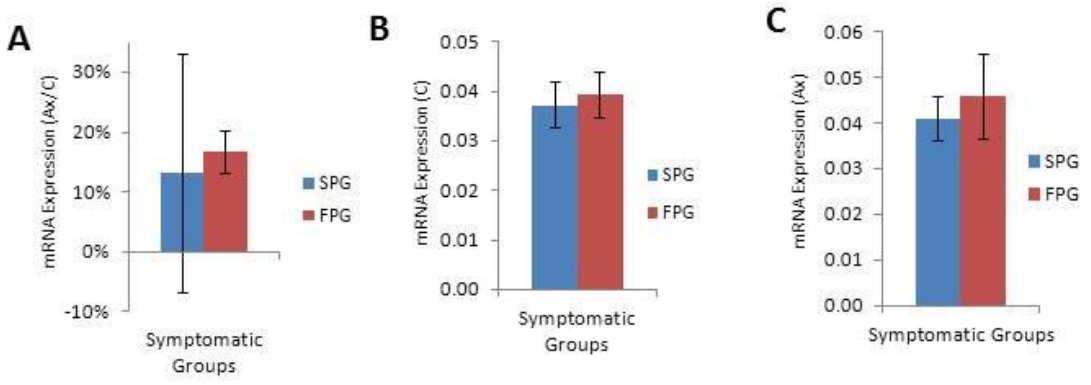

Figure 89. Relative mRNA expression of **PAC1-R** in facial motor nucleus of symptomatic SOD1 groups (SPG and FPG) at 112 doa. **A**, Percent change of mRNA expression in SPG and FPG axotomized facial nuclei relative to control. **B**, Relative mRNA expression in SPG and FPG **control** facial motor nuclei. **C**, Relative mRNA expression in SPG and FPG **axotomized** facial motor nuclei.

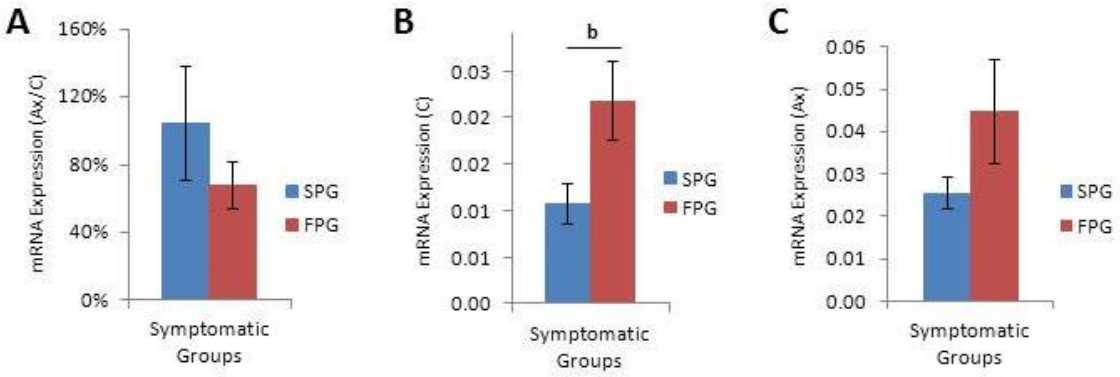

Figure 90. Relative mRNA expression of **CX3CR1** in facial motor nucleus of symptomatic SOD1 groups (SPG and FPG) at 112 doa. **A**, Percent change of mRNA expression in SPG and FPG axotomized facial nuclei relative to control. **B**, Relative mRNA expression in SPG and FPG **control** facial motor nuclei. **C**, Relative mRNA expression in SPG and FPG **axotomized** facial motor nuclei. **b** represents a significant difference in FPG mRNA relative to SPG at $p \leq 0.05$.

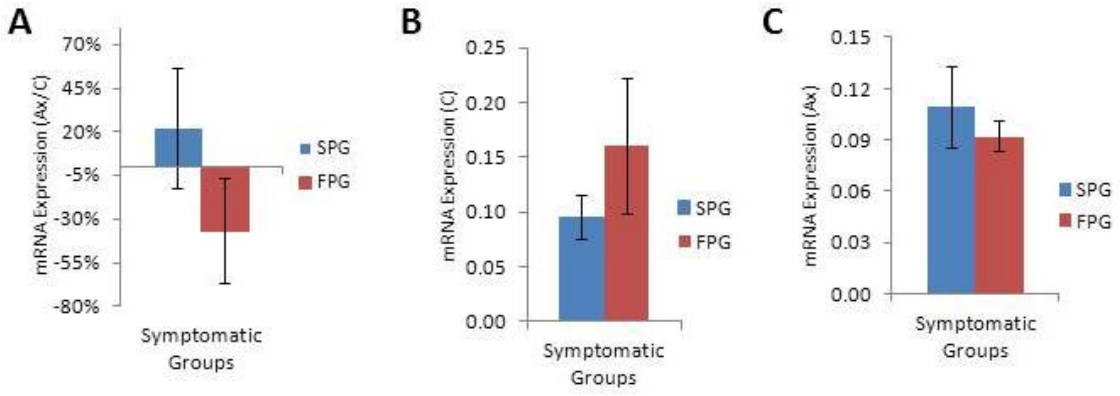

Figure 91. Relative mRNA expression of **CRMP4** in facial motor nucleus of symptomatic SOD1 groups (SPG and FPG) at 112 doa. **A**, Percent change of mRNA expression in SPG and FPG axotomized facial nuclei relative to control. **B**, Relative mRNA expression in SPG and FPG **control** facial motor nuclei. **C**, Relative mRNA expression in SPG and FPG **axotomized** facial motor nuclei.

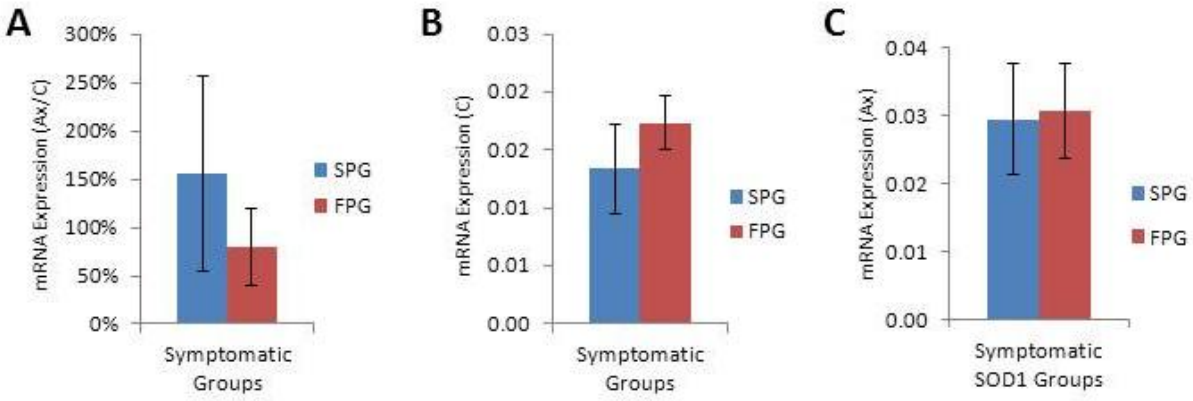

Figure 92. Relative mRNA expression of **GAP-43** in facial motor nucleus of symptomatic SOD1 groups (SPG and FPG) at 112 doa. **A**, Percent change of mRNA expression in SPG and FPG axotomized facial nuclei relative to control. **B**, Relative mRNA expression in SPG and FPG **control** facial motor nuclei. **C**, Relative mRNA expression in SPG and FPG **axotomized** facial motor nuclei.

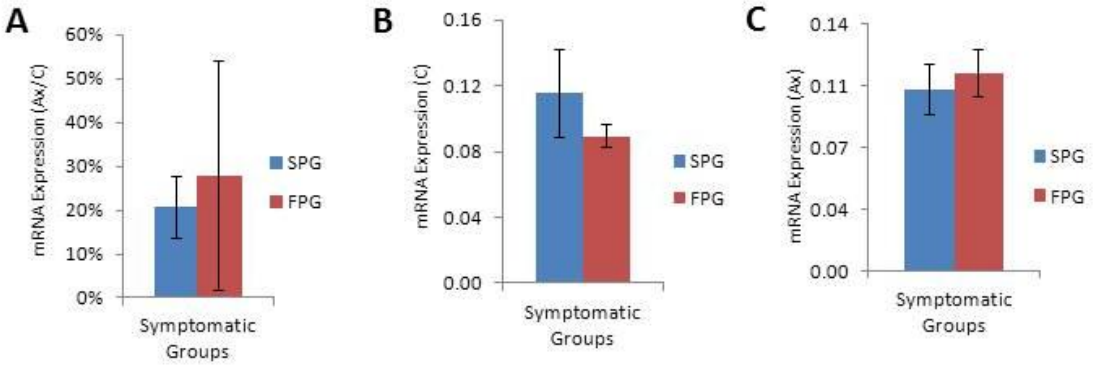

Figure 93. Relative mRNA expression of **βII-Tubulin** in facial motor nucleus of symptomatic SOD1 groups (SPG and FPG) at 112 doa. **A**, Percent change of mRNA expression in SPG and FPG axotomized facial nuclei relative to control. **B**, Relative mRNA expression in SPG and FPG **control** facial motor nuclei. **C**, Relative mRNA expression in SPG and FPG **axotomized** facial motor nuclei.

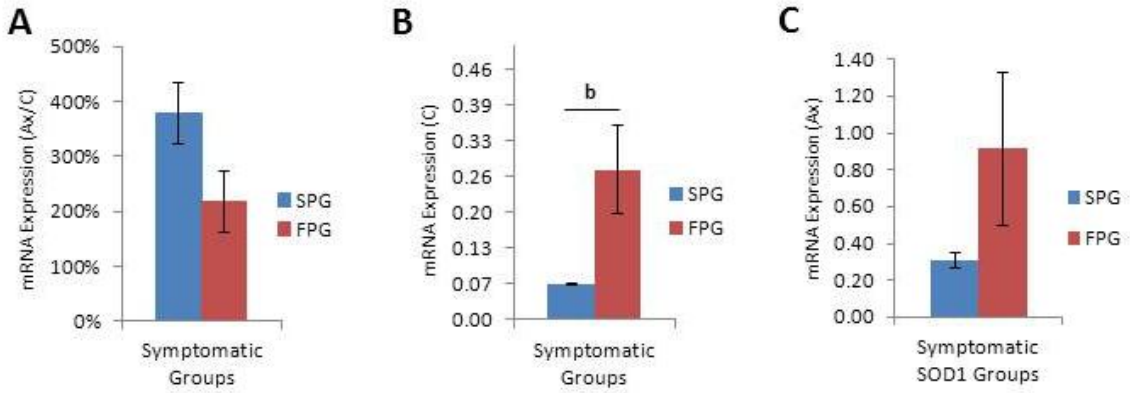

Figure 94. Relative mRNA expression of **GFAP** in facial motor nucleus of symptomatic SOD1 groups (SPG and FPG) at 112 doa. **A**, Percent change of mRNA expression in SPG and FPG axotomized facial nuclei relative to control. **B**, Relative mRNA expression in SPG and FPG **control** facial motor nuclei. **C**, Relative mRNA expression in SPG and FPG **axotomized** facial motor nuclei. **b** represents a significant difference in FPG mRNA relative to SPG at $p \leq 0.05$.

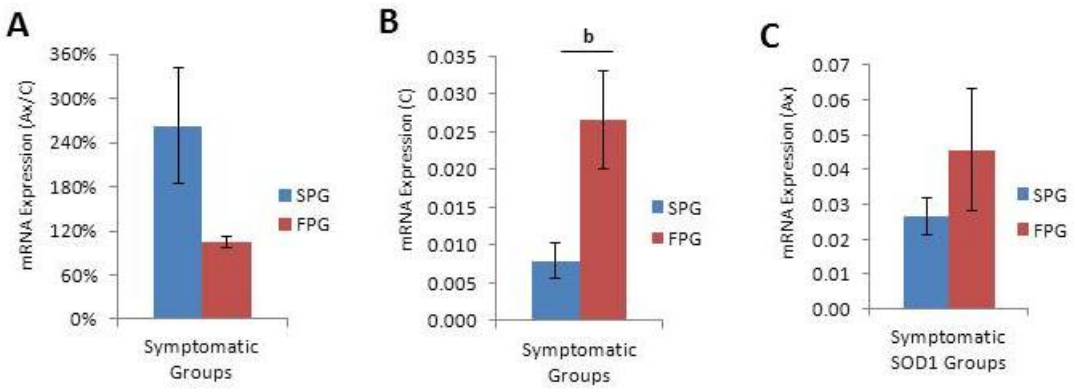

Figure 95. Relative mRNA expression of **CD68** in facial motor nucleus of symptomatic SOD1 groups (SPG and FPG) at 112 doa. **A**, Percent change of mRNA expression in SPG and FPG axotomized facial nuclei relative to control. **B**, Relative mRNA expression in SPG and FPG **control** facial motor nuclei. **C**, Relative mRNA expression in SPG and FPG **axotomized** facial motor nuclei. **b** represents a significant difference in FPG mRNA relative to SPG at $p \leq 0.05$.

Effects of Symptom Progression Rate on mRNA Responses (FPG vs. SPG)			
Gene	**Axotomy-Induced (Ax vs. Ax)**	**Disease-Induced (C vs. C)**	**Axotomy/Disease-Induced (Ax/C vs. Ax/C)**
TNFR1 Death Receptor Signaling			
TNFR1	no Δ	no Δ	no Δ
TNFα	no Δ	↑	no Δ
TRADD	no Δ	no Δ	no Δ
TRAF2	no Δ	no Δ	no Δ
SODD	no Δ	no Δ	no Δ
Fas Death Receptor Signaling			
Fas	no Δ	↑	no Δ
FasL	no Δ	no Δ	no Δ
Daxx	no Δ	no Δ	no Δ
ASK1	no Δ	no Δ	no Δ
nNOS	↑	↑	no Δ
Shared Factors of TNFR1 & Fas Death Receptors			
FADD	no Δ	no Δ	no Δ
Caspase-8	no Δ	no Δ	no Δ
Caspase-3	no Δ	↑	no Δ
Neurodegenerative Signaling Gene			
CRMP4	no Δ	no Δ	no Δ
Neuroprotective Signaling			
TNFR2	no Δ	no Δ	no Δ
PAC1-R	no Δ	no Δ	no Δ
CX3CR1	no Δ	↑	no Δ
Neuroregenerative, MN-Specific Genes			
GAP-43	no Δ	no Δ	no Δ
βII-Tubulin	no Δ	no Δ	no Δ
Glial-Specific Genes			
GFAP	no Δ	↑	no Δ
CD68	no Δ	↑	no Δ

Table 6: Summary of facial motor nuclei mRNA expression levels between symptomatic SOD1 groups, 112 doa. Axotomy-Induced column (Ax vs. Ax): relative mRNA expression level of axotomized, facial motor nucleus of FPG vs. SPG. Disease-Induced column (C vs. C): relative mRNA expression level of control, diseased facial motor nucleus of FPG vs. SPG. Axotomy/ Disease-Induced column (Ax/C vs. Ax/C): % change mRNA expression (Ax/C) FPG vs. SPG. ↑ indicates significantly higher mRNA expression in the FPG vs. SPG.

E. Discussion

Variability among SOD1 symptom progression and survival is evident when comparing the findings of multiple studies within the same SOD1 mouse model (Scott et al., 2008). Differences in reports of symptom onset can be attributed to the type of behavioral assessments used to measure changes in motor function and subsequently, symptom onset. It was important to use behavioral testing to determine symptom onset and symptom progression among the SOD1 mice used in Chapter IV and V. Additionally, development of a behavioral assessment protocol for use by our laboratory is essential for future research on the SOD1 mouse and will prove invaluable when potential therapeutic interventions or treatments are administered and changes in symptom onset and symptom progression are measureable outcomes of success.

Symptom Onset Occurs at 100 doa

Seven behavioral tests were to assess motor function in SOD1 mice starting at 79 doa and ending at the day of euthanasia, 112 doa. The seven combined test scores yielded the motor score which was used to determine symptom onset among the entire group of SOD1 mice. A significant increase in motor score or an increase in the severity of motor function led to the conclusion that symptom onset occurred at 100 doa, according to the behavioral assessment protocol used.

Results of this study revealed that throughout the symptomatic stage a subpopulation of SOD1 mice exhibited a far more rapid disease progression, relative to the severity of motor function or increased motor scores.

Two, SOD1 Symptomatic Groups with Different Symptom Progression Rates

After statistically separating the symptomatic SOD1 mice, it was apparent that there were two groups undergoing symptom progression at different rates within the relatively short period of time these symptomatic mice were behaviorally assessed. The faster symptom progressing group revealed a rate that was 3 times that of the slower progressing group. While variability in symptoms, markers of disease progression, and survival is readily observed within the literature, only one laboratory has described the presence of two different disease progression rates within the $SOD1^{G93A}$ mouse model. They termed these two groups the fast disease progression group (FPG) and the slow disease progression group (SPG) and concluded that they had identified two groups of SOD1 mice with different rates of disease progression, based on differences in symptom severity and MN cell loss (Rinke, 1976).

Therefore in addition to differences in symptom progression rates these two groups provided an excellent opportunity to use the facial motor nucleus to measure differences in disease progression (FMN survival and mRNA expression). Due to the fact that these two groups of symptomatic SOD1 mice were originally one experimental group, the result was an n=3 for each symptomatic group, for both the FMN survival experiments and the mRNA expression experiments. Therefore the FMN survival and

mRNA results are considered preliminary data and the experiments will be repeated with larger groups in the future.

No Differences in FMN Survival

No significant differences were seen between percent FMN survival after axotomy or between the average number of MN per section within the control, diseased facial motor nucleus of FPG compared to SPG. While there appears to be a trend for increased MN loss in the FPG, no difference is statistically apparent.

Increased, Disease-Induced mRNA Expression Within the FPG Compared to SPG, But Not Axotomy-Induced

Three different comparisons were made regarding mRNA expression levels between the FPG and SPG and are detailed in **Table 6**. First, relative mRNA expression levels within the control, diseased facial motor nucleus of the FPG were compared to the SPG. The FPG revealed significantly higher mRNA expression for the following genes: TNFα, Fas, nNOS, Caspase-8, CX3CR1, GFAP, and CD68. Comparisons between the other genes revealed no significant differences between the two groups and relative mRNA expression due to disease progression. While all 21 genes were differentially regulated by axotomy in the SOD1 facial nucleus (see Chapter IV, **Table 4**), it is important to keep in mind that at 112 doa, not all 21 genes were significantly different in comparison to WT (refer to Chapter V, **Table 5**). Within the SOD1 disease-induced mRNA expression at 112 doa, the majority of genes were considered of equivalent expression to “some” time-point relative to the degree of disease-induced target disconnection. This

conclusion was reached in part because of the ability to examine mRNA expression within earlier time-points. These observations indicated transient patterns that would be considered unchanged or upregulated depending on the time-point chosen for the comparison. Therefore, when taking into consideration only the time-point of 112 doa and only accepting significantly increased or decreased mRNA expression, Chapter V reveals 11 genes significantly different at 112 doa compared to WT.

Since the experiments in this Chapter, unlike those within Chapter V, provide no additional time-points, any difference in mRNA expression between FPG vs. SPG is considered substantial. Therefore, the seven upregulated genes in the FPG are due to disease-induced mRNA expression and among the seven genes, four are considered to be sensitive markers for target disconnection (TNFα, Fas, GFAP, and CD68). In addition, upregulation of nNOS suggests an increased rate of disease progression. Expression of nNOS after SOD1 facial nerve axotomy is not upregulated until the delayed-response phase. In addition, this upregulation was not seen at 70, 84, or 112 doa within the SOD1 control, facial motor nucleus and it was suggested that the upregulation of nNOS had not yet occurred. It seems that the increase in nNOS within the FPG supports the previous suggestion that nNOS expression had not yet, upregulated its expression.

Together, these mRNA expression results suggests one of two hypotheses, 1) that the FPG is undergoing disease progression at a more accelerated rate compared to the SPG, although the disease began at the same time in both groups, or 2) the FPG was subjected to an earlier disease onset and therefore initial target disconnection began

occurring earlier than the SPG, so while the two groups are the same age, they are not at the same time-point within the course of the disease.

Two additional comparisons were made between the FPG and SPG, the relative mRNA expression level within the axotomized, facial motor nucleus and the percent change mRNA expression in the axotomized nucleus compared to the internal, control facial nucleus. Originally comparisons between the percent change mRNA expression after axotomy was not going to be analyzed due to the prediction that detecting axotomy-induced changes would be compromised or not detectable because of differences of expression levels within the control nucleus. However, for that very reason the percent change mRNA was included to provide additional insight on those comparisons when control mRNA levels may not be equivalent. The results show no differences between the two groups. Six genes expressed significantly higher mRNA levels within the control nucleus but not the axotomized. These findings suggest that percent change mRNA expression (Ax/C) is relatively insensitive to differences within the control facial nucleus.

Regarding the relative mRNA expression within the axotomized FPG compared to the SPG, only one gene is expressed at a higher level. This suggests that while disease-induced mRNA expression divides the two groups, axotomy-induced mRNA expression does not. This lends support to the conclusion that the FPG was subjected to an earlier disease onset and the initial target disconnection began occurring earlier than the SPG. Therefore, while the two groups are the same age, they are not at the same time-point

within the disease. Performing a facial nerve axotomy at 56 doa standardized the time of disease onset within the axotomized facial motor nucleus and the axotomy-induced mRNA expression was similar between the two groups. In support of this, one study performed a sciatic nerve crush at 42 doa in SOD1 mice, and showed an acceleration in disease progression such that at 90 doa the injured mice showed deficits in muscle force, contractile characteristics, and MN survival that are only seen in uninjured, end-stage mice 130 doa (Sharp et al., 2005). Therefore, there is overwhelming support that target disconnection, experimentally-induced or disease-induced, initiates disease progression.

In conclusion, different rates of disease progression within symptomatic SOD1 mouse is likely due to time of disease onset, i.e. the initial target disconnection, and resulting in the appearance of accelerated disease progression.

CHAPTER VII

MOLECULAR EXPRESSION OF SINGALING SYSTEMS IN REGENERATIVE AND DEGENERATIVE SUBNUCLEI FOLLOWING FACIAL NERVE ACOTOMY

A. Abstract

Facial nerve axotomy in the WT and SOD1 mice results in significant FMN loss, and to a far greater extent in the SOD1 facial motor nucleus. The distribution of loss over the six facial motor subnuclei is uneven. While the VM subnucleus retains nearly 100% MN survival (28 dpo), the VL subnucleus displays the most FMN loss of all, retaining only 70% survival. This interesting finding led us to profile the molecular response to axotomy to determine whether differential gene expression in response to axotomy was a potential mechanism in the VL, increased FMN death. Surprisingly, the "degenerative" VL subnucleus responded similarly as the "regenerative" VM subnucleus. The VL upregulated MN-specific regenerative genes to an even greater extent, compared to WT for some time-points (Mesnard et. al., 2010). Similar findings were reported in the SOD1 VM and VL (Mesnard, 2009). The experiments performed within the Chapter were aimed at identifying possible increased expression of death receptor signaling genes within the VL subnucleus that could lead to greater understanding of the molecular mechanisms that mediate the "degenerative"

phenotype. Results show an increase in death receptor gene expression within the VL subnucleus compared to the VM.

B. Introduction

Facial nerve axotomy has been used extensively to investigate MN survival and peripheral nerve regeneration. An additional level of analysis can be reached by studying axotomies effects among the subnuclei. The distribution of FMN survival across the six subnuclei allows us to investigate functional or topographical responses to nerve injury. Previous studies revealed an uneven distribution of FMN survival at 28 dpo, with the VL showing the lowest percent survival at 70% and the VM subnuclei maintaining the highest level of FMN survival at almost 100% (Canh et al., 2006). Additionally in the RAG-2 KO, this same variance in numbers of surviving MN was seen, although percentage FMN survival was much lower. This distribution was also maintained after FMN rescue by reconstituting the RAG-2 KO mouse prior to facial nerve axotomy. This identification of differing populations of MN within the facial nucleus is important and provides two populations with intrinsic differences and/or surrounding environments that can be further studied. Additionally, SOD1 FMN distribution is uneven and closely resembles survival levels seen in the RAG-2 KO (Canh et al., 2006; Mesnard, 2009).

The technique of LMD was utilized to accurately dissect the VM and VL subnuclei and analyzed for mRNA expression following axotomy. WT comparisons between the regenerative VM, maintaining almost 100% FMN survival after axotomy, and the degenerative VL, displaying the greatest cell loss among the six subnuclei at 70% FMN

survival, were performed using the same experimental design. It was determined that regardless of neuronal fate after injury, both subnuclear populations responded with a similar survival/regenerative profile of mRNA expression. In addition differences within mRNA expression specific to the neuropil were evident (Mesnard et al., 2010). Additionally, comparison was made between the pre-symptomatic SOD1 VM and VL subnuclei after axotomy. Similar results from this study support the previous findings (Mesnard, 2009). In summary, we propose that MN fate is ultimately controlled or regulated by cells within the neuropil, We hypothesize that this lack of regulation by the neuropil may also result in the MN degeneration that occurs during disease progression.

Aim #4 of this dissertation was to analyze the axotomy-induced molecular expression of neuroprotective and neurodestructive signaling systems within the regenerative and degenerative subnuclei of the facial motor nucleus. The working hypothesis for this aim was that the regenerative, VM subnucleus of the facial motor nucleus will display attenuated molecular expression of genes related to neurodegenerative signaling systems compared to the degenerative, VL subnucleus in both WT and SOD1 mice following axotomy. The experiments investigated differences between axotomy-induced mRNA expression within the WT VM and VL subnuclei, and separately, within the SOD1 VM and VL subnuclei. The purpose of these experiments was to provide additional information regarding axotomy-induced molecular responses of genes involved in neuroprotective and neurodestructive signaling systems among facial nuclei populations with inherent degenerative and regenerative characteristics.

C. Materials and Methods

Animals and Surgical Procedures

Mice were obtained and housed as previously described in Chapter III Section A. All mice received a right facial nerve transection axotomy described In Chapter III Section B. Also refer to experimental design illustrated in **Figure 96** of this Chapter.

Tissue Preparation

Refer to Chapter III Sections C and D as well as **Figure 96** of this Chapter for details.

Laser Microdissection

Details are described in Chapter III Section F and the experimental design illustrated in **Figure 96** of this Chapter.

RNA Isolation and Real-Time RT-PCR

Percent change of mRNA expression was assessed in WT VM and VL at 3, 7, 14, 28 and 56 dpo. Additionally, percent change of mRNA expression was analyzed in SOD1 VM and VL at 3, 7, 14 and 28 dpo. The SOD1 VM and VL subnuclei time course does not include a 56 dpo time-point because significant FMN cell loss due to axotomy and disease (control facial motor nucleus) resulted in extremely low levels of mRNA yield following RNA extraction. For this reason, there was not sufficient total RNA for successful reverse transcription. Therefore, WT VM and VL time courses contain an additional time-point which was incorporated in the analysis. The 56 dpo time-point was included because for many of the mRNA expression profiles, this last time-point

provides sufficient time to witness a return to baseline and additionally it is a comparison to data obtained from the WT and SOD1 whole, facial motor nucleus, which also contain a time course out to 56 dpo.

Both WT and SOD1 VM and VL subnuclei were investigated for mRNA expression of the following genes: CX3CR1, TNFR1, TNFR2, Fas, Caspase-3, PAC1-R, CRMP4, CD68, ASK1, Daxx, FADD, TRAF2, TRADD, SODD, and nNOS. Genes, Caspase-8, GFAP, GAP-43, and βII-Tubulin were previously analyzed by our laboratory for the time-points: 3, 7, 14, and 28 dpo. For this dissertation the time course was extended to 56 dpo, in WT VM and VL only, and therefore the time-point of WT 28 dpo (VM and VL) was replicated for conformation and comparison as well as 56 dpo. The gene CD68 does not include the WT, VM or VL 3 dpo data point. Due to failure of amplification during the real-time PCR run and insufficient volume of remaining WT VM and VL 3 dpo samples, the time-point could not be included in the analysis.

For specific details refer to Chapter III Section G and the experimental design illustrated in **Figure 96** of this Chapter.

Statistical Analysis

Details of statistical analysis for FMN percent survival following axotomy and axotomy-induced percent change mRNA expression can be located in Chapter III Section J.

D. Results

Comparisons of Percent Change of mRNA expression in WT VM Relative to WT VL Subnuclei, and Comparisons Between SOD1 mRNA Expression in VM and VL Subnuclei

Comparisons were made between WT VM vs. VL and SOD1 VM vs. VL, at the time-points of 0 – 28 dpo. High variability and lower expression level changes particular to the genes analyzed did not reveal any additional benefit to the analysis between SOD1 and WT subnuclei. Therefore, analysis was limited to VM vs. VL of either WT or SOD1. See **Table 7** for information regarding more specific information about statistical differences between the subnuclei. Additionally, the time-point of 56 dpo was analyzed in WT only. See **Table 8** for WT, 56 dpo, VM vs. VL comparisons.

TNFR1 mRNA expression in the **WT** VM subnucleus was upregulated following facial nerve axotomy relative to the control at 3 (41 ± 7%), 7 (73 ± 13%), 14 (47 ± 24%), 28 (29 ± 15%), and 56 (41 ± 11%) dpo (**Figure 97A**). In the WT VL subnucleus mRNA expression for TNFR1 was upregulated relative to the control at 3 (109 ± 19%), 7 (103 ± 18%), 14 (156 ± 32%), 28 (114 ± 41%), and 56 (46 ± 35%) dpo (**Figure 97B**).

TNFR1 mRNA expression in the **SOD1** VM subnucleus was upregulated after facial nerve axotomy at 3 (66 ± 33%), 7 (57 ± 28%), 14 (101 ± 22%) and 28 (52 ± 28%) dpo (**Figure 98A**). In the SOD1 VL subnucleus mRNA expression for TNFR1 was upregulated relative to the control at 3 (53 ± 14%), 7 (137 ± 37%), 14 (108 ± 37%) and 28 (58 ± 52%) dpo (**Figure 98B**).

Fas mRNA expression in the **WT** VM subnucleus was upregulated following facial nerve axotomy relative to the control at 3 (25 ± 5%), 7 (5 ± 7%), 14 (-6 ± 11%), 28 (-7 ± 9%), and 56 (12 ± 40%) dpo (**Figure 99A**). In the WT VL subnucleus mRNA expression for Fas was upregulated relative to the control at 3 (79 ± 16%), 7 (1 ± 3%), 14 (24 ± 8%), 28 (27 ± 6%), and 56 (-1 ± 12%) dpo (**Figure 99B**).

Fas mRNA expression in the **SOD1** VM subnucleus was upregulated after facial nerve axotomy at 3 (53 ± 9%), 7 (64 ± 6%), 14 (75 ± 19%) and 28 (154 ± 9%) dpo (**figure 100A**). In the SOD1 VL subnucleus mRNA expression for Fas was upregulated relative to the control at 3 (98 ± 9%), 7 (78 ± 7%), 14 (135 ± 47%) and 28 (162 ± 27%) dpo (**figure 100B**).

TRADD mRNA expression in the **WT** VM subnucleus was downregulated following facial nerve axotomy relative to the control at 3 (-21 ± 5%), 7 (-26 ± 8%), 14 (-17 ± 11%), 28 (-10 ± 12%), and 56 (-20 ± 7%) dpo (**Figure 101A**). In the WT VL subnucleus mRNA expression for TRADD was downregulated relative to the control at 3 (-30 ± 6%), 7 (-27 ± 8%), 14 (-32 ± 8%), 28 (3 ± 16%), and 56 (13 ± 17%) dpo (**Figure 101B**).

TRADD mRNA expression in the **SOD1** VM subnucleus was downregulated after facial nerve axotomy at 3 (-2 ± 17%), 7 (-32 ± 14%), 14 (-17 ± 4%) and 28 (6 ± 16%) dpo (**Figure 102A**). In the SOD1 VL subnucleus mRNA expression for TRADD was downregulated relative to the control at 3 (-19 ± 4%), 7 (-32 ± 16%), 14 (-3 ± 18%) and 28 (-3 ± 10%) dpo (**Figure 102B**).

FADD mRNA expression in the **WT** VM subnucleus was upregulated following facial nerve axotomy relative to the control at 3 (37 ± 22%), 7 (-11 ± 19%), 14 (30 ± 20%), 28 (13 ± 10%), and 56 (-10 ± 5%) dpo (**Figure 103A**). In the WT VL subnucleus mRNA expression for FADD was upregulated relative to the control at 3 (44 ± 26%), 7 (26 ± 19%), 14 (17 ± 8%), 28 (-3 ± 16%), and 56 (19 ± 15%) dpo (**Figure 103B**).

FADD mRNA expression in the **SOD1** VM subnucleus was upregulated after facial nerve axotomy at 3 (58 ± 13%), 7 (34 ± 18%), 14 (21 ± 30%) and 28 (52 ± 26%) dpo (**Figure 104A**). In the SOD1 VL subnucleus mRNA expression for FADD was upregulated relative to the control at 3 (15 ± 14%), 7 (19 ± 17%), 14 (8 ± 21%) and 28 (77 ± 25%) dpo (**Figure 104B**).

Daxx mRNA expression in the **WT** VM subnucleus was upregulated following facial nerve axotomy relative to the control at 3 (15 ± 12%), 7 (44 ± 15%), 14 (2 ± 13%), 28 (9 ± 14%), and 56 (-15 ± 17%) dpo (**Figure 105A**). In the WT VL subnucleus mRNA expression for Daxx was upregulated relative to the control at 3 (52 ± 25%), 7 (51 ± 24%), 14 (56 ± 11%), 28 (6 ± 21%), and 56 (6 ± 32%) dpo (**Figure 105B**).

Daxx mRNA expression in the **SOD1** VM subnucleus was upregulated after facial nerve axotomy at 3 (27 ± 21%), 7 (19 ± 15%), 14 (12 ± 3%) and 28 (-12 ± 19%) dpo (**Figure 106A**). In the SOD1 VL subnucleus mRNA expression for Daxx was upregulated relative to the control at 3 (-4 ± 15%), 7 (26 ± 15%), 14 (6 ± 12%) and 28 (-1 ± 26%) dpo (**Figure 106B**).

ASK1 mRNA expression in the **WT** VM subnucleus was not significantly different from baseline following facial nerve axotomy 3 (31 ± 17%), 7 (24 ± 15%), 14 (19 ± 17%), 28 (6 ± 11%), and 56 (-10 ± 8%) dpo (**Figure 107A**). In the WT VL subnucleus mRNA expression for ASK1 not significantly different from baseline following facial nerve axotomy l at 3 (33 ± 22%), 7 (-20 ± 15%), 14 (-4 ± 4%), 28 (-4 ± 9%), and 56 (7 ± 6%) dpo (**Figure 107B**).

ASK1 mRNA expression in the **SOD1** VM subnucleus was not significantly different from baseline following facial nerve axotomy at 3 (5 ± 10%), 7 (5 ± 7%), 14 (12 ± 10%) and 28 (-8 ± 21%) dpo (**Figure 108A**). In the SOD1 VL subnucleus mRNA expression for ASK1 was not significantly different from baseline following facial nerve axotomy at 3 (-6 ± 7%), 7 (-15 ± 9%), 14 (-21 ± 11%) and 28 (52 ± 31%) dpo (**Figure 108B**).

nNOS mRNA expression in the **WT** VM subnucleus was not significantly different from baseline following facial nerve axotomy at 3 (-2 ± 20%), 7 (-11 ± 32%), 14 (23 ± 30%), 28 (-15 ± 29%), and 56 (11 ± 28%) dpo (**Figure 109A**). In the WT VL subnucleus mRNA expression for nNOS was upregulated relative to the control at 3 (-24 ± 17%), 7 (10 ± 33%), 14 (3 ± 29%), 28 (63 ± 27%), and 56 (41 ± 10%) dpo (**Figure 109B**).

nNOS mRNA expression in the **SOD1** VM subnucleus was not significantly different from baseline following facial nerve axotomy at 3 (32 ± 53%), 7 (6 ± 43%), 14 (7 ± 29%) and 28 (38 ± 35%) dpo (**Figure 110A**). In the SOD1 VL subnucleus mRNA

expression for nNOS was upregulated relative to the control at 3 (1 ± 69%), 7 (77 ± 47%), 14 (29 ± 18%) and 28 (128 ± 24%) dpo (**Figure 110B**).

Caspase-3 mRNA expression in the **WT** VM subnucleus was upregulated following facial nerve axotomy relative to the control at 3 (163 ± 50%), 7 (319 ± 55%), 14 (465 ± 94%), 28 (91 ± 35%), and 56 (17 ± 36%) dpo (**Figure 111A**). In the WT VL subnucleus mRNA expression for Caspase-3 was upregulated relative to the control at 3 288 ± 85%), 7 (693 ± 177%), 14 (670 ± 91%), 28 (146 ± 60%), and 56 (42 ± 12%) dpo (**Figure 111B**).

Caspase-3 mRNA expression in the SOD1 VM subnucleus was upregulated after facial nerve axotomy at 3 (228 ± 46%), 7 (466 ± 172%), 14 (410 ± 66%) and 28 (92 ± 24%) dpo (**Figure 112A**). In the SOD1 VL subnucleus mRNA expression for Caspase-3 was upregulated relative to the control at 3 (291 ± 97%), 7 (395± 133%), 14 (428 ± 55%) and 28 (274± 92%) dpo (**Figure 112B**).

Caspase-8 mRNA expression was previously analyzed up to 28 dpo for WT and SOD1 VM and VL subnuclei, therefore in the WT the 28 dpo time-point was repeated and the additional time-point of 56 dpo was analyzed to determine whether mRNA expression returned to control levels in VM and VL. VM subnucleus was significantly increased following axotomy relative to the WT control at 28 dpo (70 ± 26%) and returns to baseline mRNA expression levels by 56 dpo (11 ± 23%; **Figure 113A**). In the WT VL subnucleus mRNA expression for Caspase-8 was significantly increased following

axotomy relative to the WT control at 28 dpo (112 ± 26%) and returns to baseline mRNA expression levels by 56 dpo (38 ± 32%; **Figure 113B**).

Caspase-8 mRNA expression in the SOD1 VM and VL subnucleus was previously assessed by our laboratory through 28 dpo. The SOD1 VM and VL subnucleus at 56 dpo did not yield total RNA levels conducive to reverse transcription. Therefore the SOD1 time course was not extended to 56 dpo and Caspase-8 mRNA expression in the SOD1 was not performed.

TRAF2 mRNA expression in the **WT** VM subnucleus was downregulated following facial nerve axotomy relative to the control at 3 (-16 ± 14%), 7 (-20 ± 6%), 14 (-15 ± 6%), 28 (-11 ± 6%), and 56 (-16 ± 10%) dpo (**Figure 114A**). In the WT VL subnucleus mRNA expression for TRAF2 was no downregulated relative to baseline at 3 (-4 ± 15%), 7 (-25 ± 8%), 14 (-4 ± 17%), 28 (-1 ± 16%), and 56 (16 ± 8%) dpo (**Figure 114B**).

TRAF2 mRNA expression in the **SOD1** VM subnucleus was downregulated after facial nerve axotomy at 3 (-25 ± 13%), 7 (-36 ± 8%), 14 (-17 ± 9%) and 28 (8 ± 12%) dpo (**Figure 115A**). In the SOD1 VL subnucleus mRNA expression for TRAF2 was no different than baseline at 3 (-17 ± 10%), 7 (-26 ± 13%), 14 (-12 ± 14%) and 28 (16 ± 22%) dpo (**Figure 115B**).

SODD mRNA expression in the **WT** VM subnucleus was downregulated following facial nerve axotomy relative to the control at 3 (-30 ± 5%), 7 (-28 ± 3%), 14 (-27 ± 5%), 28 (-16 ± 6%), and 56 (-14 ± 7%) dpo (**Figure 116A**). In the WT VL subnucleus mRNA

expression for SODD was downregulated relative to the control at 3 (-2 ± 10%), 7 (-28 ± 7%), 14 (-28 ± 7%), 28 (-9 ± 10%), and 56 (7 ± 7%) dpo (**Figure 116B**).

SODD mRNA expression in the **SOD1** VM subnucleus was downregulated after facial nerve axotomy at 3 (-27 ± 7%), 7 (-26 ± 13%), 14 (-35 ± 2%) and 28 (-15 ± 9%) dpo (**Figure 117A**). In the SOD1 VL subnucleus mRNA expression for SODD was downregulated relative to the control at 3 (-22 ± 7%), 7 (-20 ± 10%), 14 (-27 ±10%) and 28 (-1 ± 15%) dpo (**Figure 117B**).

TNFR2 mRNA expression in the **WT** VM subnucleus was upregulated following facial nerve axotomy relative to the control at 3 (933 ± 257%), 7 (1127 ± 296%), 14 (1305 ± 456%), 28 (560 ± 67%), and 56 (279 ± 196%) dpo (**Figure 118A**). In the WT VL subnucleus mRNA expression for TNFR2 was upregulated relative to the control at 3 (1369 ± 203%), 7 (1888 ± 497%), 14 (1406 ± 467%), 28 (1126 ± 118%), and 56 (286 ± 125%) dpo (**Figure 118B**).

TNFR2 mRNA expression in the **SOD1** VM subnucleus was upregulated after facial nerve axotomy at 3 (448 ± 103%), 7 (1005 ± 216%), 14 (1036 ± 296%) and 28 (874 ± 599%) dpo (**Figure 119A**). In the SOD1 VL subnucleus mRNA expression for TNFR2 was upregulated relative to the control at 3 (1848 ± 463%), 7 (2191 ± 753%), 14 (1690 ± 716%) and 28 (915 ± 624%) dpo (**Figure 119B**).

PAC1-R mRNA expression in the **WT** VM subnucleus was downregulated following facial nerve axotomy relative to the control at 3 (-64 ± 5%), 7 (-65 ± 6%), 14 (-61 ± 5%), 28 (-18 ± 12%), and 56 (-19 ± 2%) dpo (**Figure 120A**). In the WT VL subnucleus

mRNA expression for PAC1-R was downregulated relative to the control at 3 (-52 ± 3%), 7 (-63 ± 3%), 14 (-27 ± 13%), 28 (17 ± 8%), and 56 (9 ± 9%) dpo (**Figure 120B**).

PAC1-R mRNA expression in the **SOD1** VM subnucleus was downregulated after facial nerve axotomy at 3 (-61 ± 3%), 7 (-59 ± 5%), 14 (-46 ± 9%) and 28 (-4 ± 8%) dpo (**Figure 121A**). In the SOD1 VL subnucleus mRNA expression for PAC1-R was downregulated relative to the control at 3 (-52 ± 7%), 7 (-53 ± 8%), 14 (-26 ± 9%) and 28 (44 ± 13%) dpo (**Figure 121B**).

CX3CR1 mRNA expression in the **WT** VM subnucleus was upregulated following facial nerve axotomy relative to the control at 3 (330 ± 42%), 7 (503 ± 67%), 14 (283 ± 68%), 28 (176 ± 54%), and 56 (33 ± 6%) dpo (**Figure 122A**). In the WT VL subnucleus mRNA expression for CX3CR1 was upregulated relative to the control at 3 (992± 161%), 7 (934± 168%), 14 (975 ± 130%), 28 (342 ± 85%), and 56 (198 ± 50%) dpo (**Figure 122B**).

CX3CR1 mRNA expression in the **SOD1** VM subnucleus was upregulated after facial nerve axotomy at 3 (239 ± 76%), 7 (315 ± 62%), 14 (367 ± 37%) and 28 (259 ± 102%) dpo (**Figure 123A**). In the SOD1 VL subnucleus mRNA expression for CX3CR1 was upregulated relative to the control at 3 (572 ± 91%), 7 (967 ± 128%), 14 (577 ± 122%) and 28 (719 ± 138%) dpo (**Figure 123B**).

CRMP4 mRNA expression in the **WT** VM subnucleus was upregulated following facial nerve axotomy relative to the control at 3 (15 ± 12%), 7 (40 ± 17%), 14 (49 ± 20%), 28 (47 ± 7%), and 56 (-6 ± 10%) dpo (**Figure 124A**). In the WT VL subnucleus mRNA

expression for CRMP4 was upregulated relative to the control at 3 (-16 ± 3%), 7 (22 ± 11%), 14 (69 ± 20%), 28 (20 ± 12%), and 56 (22 ± 11%) dpo (**Figure 124B**).

CRMP4 mRNA expression in the **SOD1** VM subnucleus was upregulated after facial nerve axotomy at 3 (10 ± 6%), 7 (41 ± 18%), 14 (47 ± 15%) and 28 (48 ± 8%) dpo (**Figure 125A**). In the SOD1 VL subnucleus mRNA expression for CRMP4 was upregulated relative to the control at 3 (-10 ± 6%), 7 (44 ± 29%), 14 (60 ± 24%) and 28 (9 ± 14%) dpo (**Figure 125B**).

GAP-43 mRNA expression was previously analyzed up to 28 dpo for WT and SOD1 VM and VL subnuclei, therefore in the **WT** the 28 dpo time-point was repeated and the additional time-point of 56 dpo was analyzed to determine whether mRNA expression returned to control levels in VM and VL. VM subnucleus was significantly increased following axotomy relative to the WT control at 28 dpo (425 ± 106%) and returns to baseline mRNA expression levels by 56 dpo (49 ± 21%; **Figure 126A**). In the WT VL subnucleus mRNA expression for GAP-43 was significantly increased following axotomy relative to the WT control at 28 dpo (661 ± 60%) and remains significantly increased at 56 dpo (254 ± 34%; **Figure 126B**).

GAP-43 mRNA expression in the **SOD1** VM and VL subnucleus was previously assessed by our laboratory through 28 dpo. The SOD1 VM and VL subnucleus at 56 dpo did not yield total RNA levels conducive to reverse transcription. Therefore the SOD1 time course was not extended to 56 dpo and GAP-43 mRNA expression in the SOD1 was not performed.

βII-Tubulin mRNA expression was previously analyzed up to 28 dpo for WT and SOD1 VM and VL subnuclei, therefore in the **WT** the 28 dpo time-point was repeated and the additional time-point of 56 dpo was analyzed to determine whether mRNA expression returned to control levels in VM and VL. VM subnucleus was significantly increased following axotomy relative to the WT control at 28 dpo (65 ± 12%) and returns to baseline mRNA expression levels by 56 dpo (19 ± 11%; **Figure 127A**). In the WT VL subnucleus mRNA expression for βII-Tubulin was significantly increased following axotomy relative to the WT control at 28 dpo (102 ± 18%) and remains upregulated at 56 dpo (16 ± 6%; **Figure 127B**).

βII-Tubulin mRNA expression in the **SOD1** VM and VL subnucleus was previously assessed by our laboratory through 28 dpo. The SOD1 VM and VL subnucleus at 56 dpo did not yield total RNA levels conducive to reverse transcription. Therefore the SOD1 time course was not extended to 56 dpo and βII-Tubulin mRNA expression in the SOD1 was not performed.

GFAP mRNA expression was previously analyzed up to 28 dpo for WT and SOD1 VM and VL subnuclei, therefore in the **WT** the 28 dpo time-point was repeated and the additional time-point of 56 dpo was analyzed to determine whether mRNA expression returned to control levels in VM and VL. VM subnucleus was significantly increased following axotomy relative to the WT control at 28 dpo (586 ± 403%) and returns to baseline mRNA expression levels by 56 dpo (285 ± 259%; **Figure 128A**). In the WT VL subnucleus mRNA expression for GFAP was significantly increased following axotomy

relative to the WT control at 28 dpo (947 ± 409%) and remains upregulated at 56 dpo (583 ± 176%; **Figure 128B**).

GFAP mRNA expression in the **SOD1** VM and VL subnucleus was previously assessed by our laboratory through 28 dpo. The SOD1 VM and VL subnucleus at 56 dpo did not yield total RNA levels conducive to reverse transcription. Therefore the SOD1 time course was not extended to 56 dpo and GFAP mRNA expression in the SOD1 was not performed.

CD68 mRNA expression in the **WT** VM subnucleus was upregulated following facial nerve axotomy relative to the control at 7 (799 ± 243%), 14 (479 ± 172%), 28 (274 ± 53%), and 56 (123 ± 69%) dpo (**Figure 129A**). Due to failure of amplification during the real-time PCR run and insufficient volume of remaining WT 3 dpo VM and VL samples, the time-point could not be included in the analysis. In the WT VL subnucleus mRNA expression for CD68 was upregulated relative to the control at 7 (1200 ± 367%), 14 (970 ± 363%), 28 (719 ± 179%), and 56 (379 ± 192%) dpo (**Figure 129B**).

CD68 mRNA expression in the **SOD1** VM subnucleus was upregulated after facial nerve axotomy at 3 (198 ± 170%), 7 (174 ± 17%), 14 (529 ± 152%) and 28 (479 ± 283%) dpo (**Figure 130A**). In the SOD1 VL subnucleus mRNA expression for CD68 was upregulated relative to the control at 3 (404 ± 42%), 7 (354 ± 99%), 14 (496 ± 176%) and 28 (677 ± 207%) dpo (**Figure 130B**).

Figure 96. Experimental Design: LMD of WT and SOD1 facial subnuclei (VM & VL), real time RT-PCR and analysis of mRNA Expression.

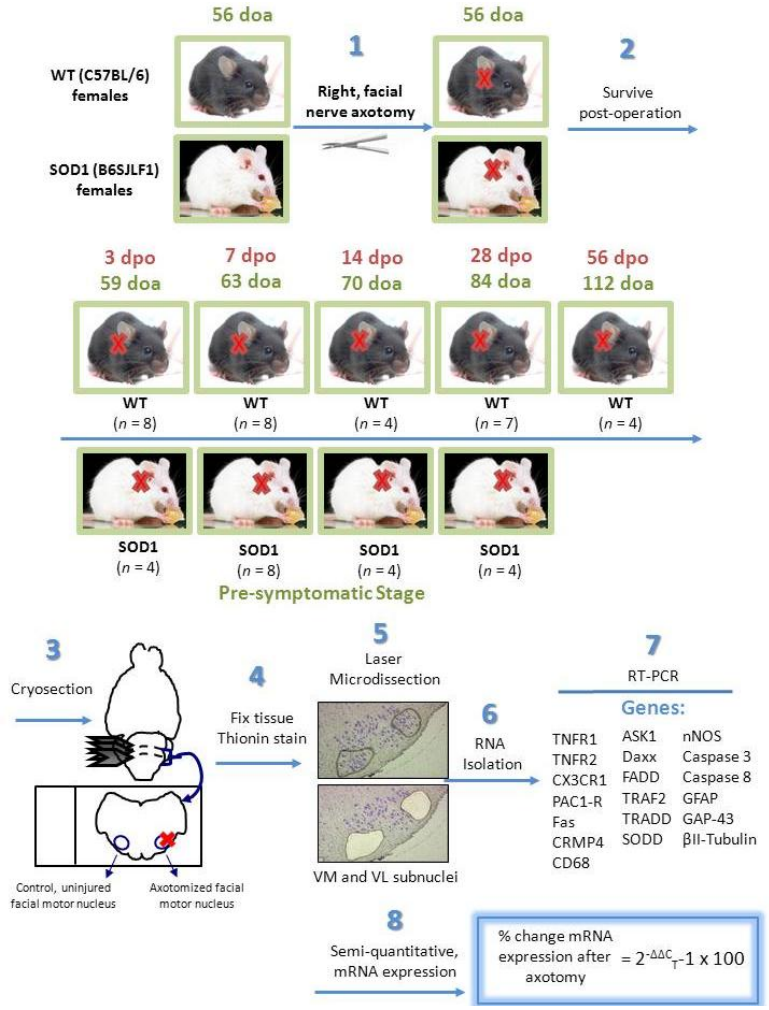

1. WT and SOD1 mice received a right facial nerve axotomy at 56 doa.
2. Mice were euthanized at 3, 7, 14, 28 and 56 dpo.
3. Brains were removed and cryosectioned through the facial motor nucleus at 25 µm.
4. Sections were fixed with 100% ETOH and stained with thionin.
5. Control and axotomized VM and VL subnuclei were separately collected by laser microdissected for each mouse.
6. RNA was isolated from control and axotomized VM and VL subnuclei samples.
7. Real-time, RT-PCR was performed for specific genes to profile the axotomy-induced molecular response.
8. The semi-quantitative, percent change of mRNA expression of the axotomized subnucleus relative to the uninjured, control subnucleus was calculated using the $2^{-\Delta\Delta C}{}_T$ method.

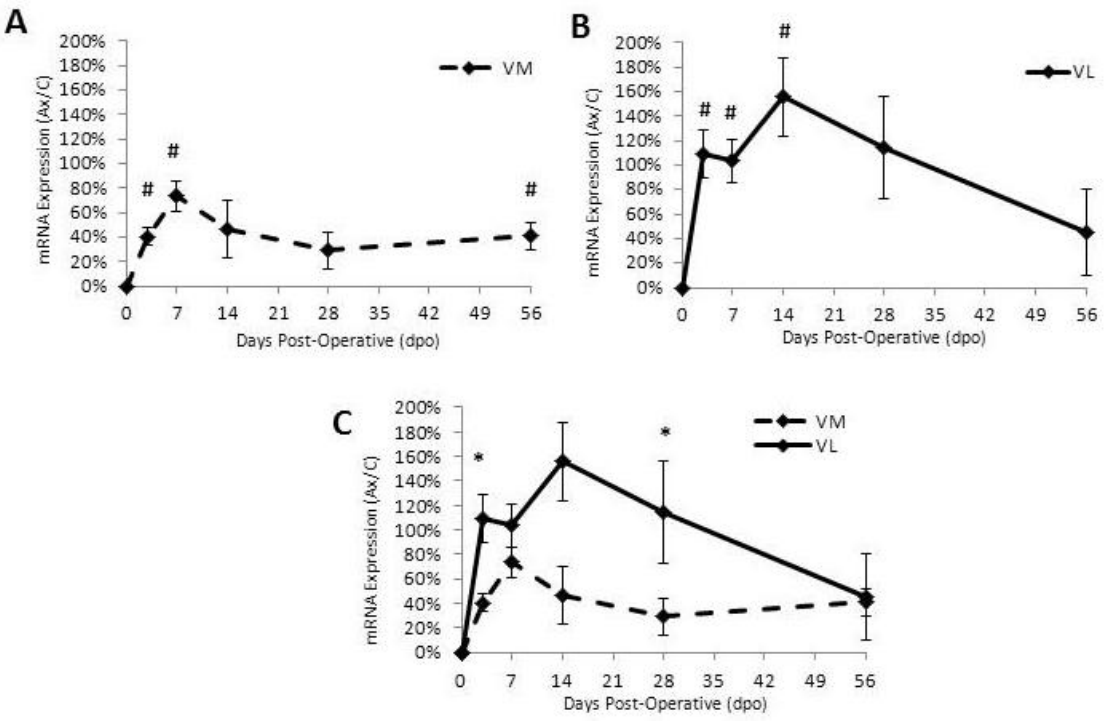

Figure 97. Percent change of **TNFR1** mRNA expression ± SEM in **WT** VM and VL axotomized facial motor nucleus subnuclei at 3, 7, 14, 28 and 56 dpo relative to control. **A**, VM. **B**, VL. **C**, VM vs. VL. **#** represents a significant difference relative to the control; ***** represents a significant difference relative to VM at $p \leq 0.05$.

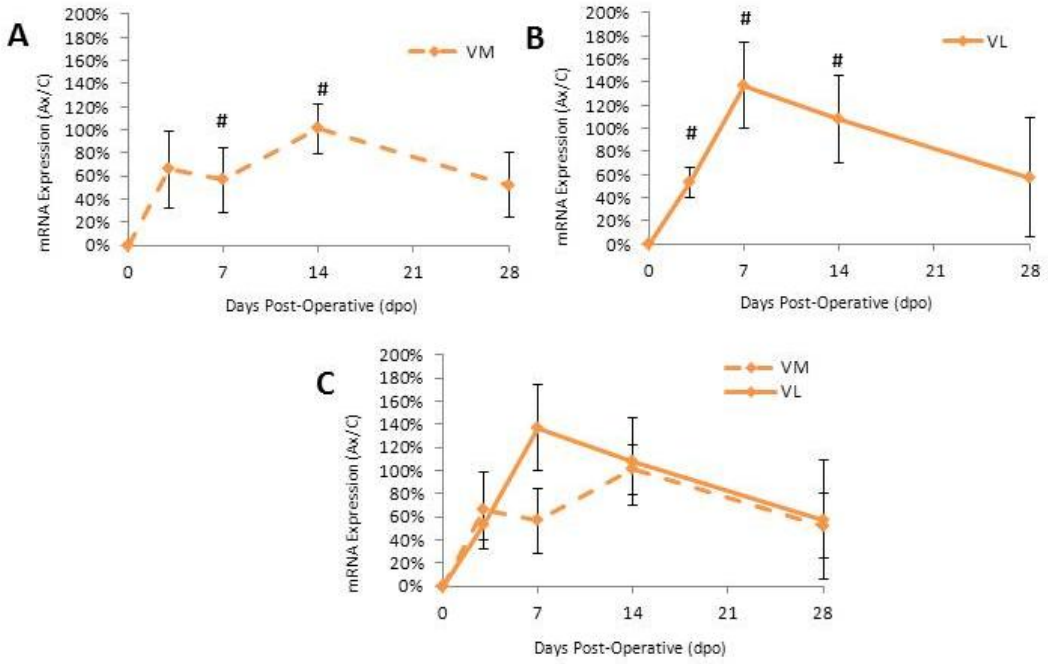

Figure 98. Percent change of **TNFR1** mRNA expression ± SEM in **SOD1** VM and VL axotomized facial motor nucleus subnuclei at 3, 7, 14 and 28 dpo relative to control. **A**, VM. **B**, VL. **C**, VM vs. VL. **#** represents a significant difference relative to the control at $p \leq 0.05$.

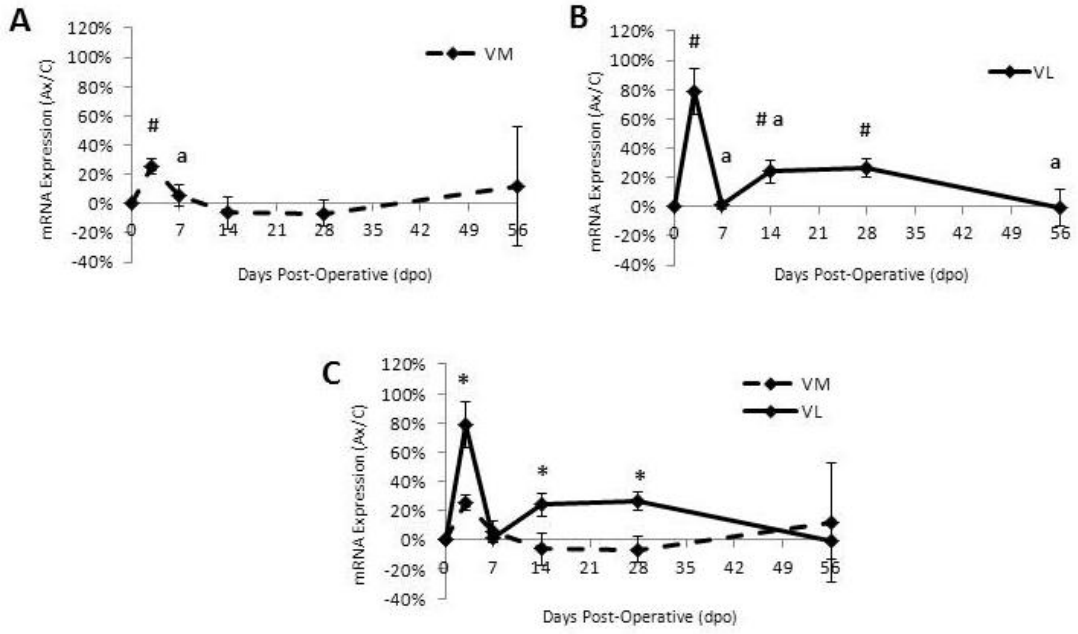

Figure 99. Percent change of **Fas** mRNA expression ± SEM in **WT** VM and VL axotomized facial motor nucleus subnuclei at 3, 7, 14, 28 and 56 dpo relative to control. **A**, VM. **B**, VL. **C**, VM vs. VL. **#** represents a significant difference relative to the control; **a** represents a significant difference relative to the previous time-point; ***** represents a significant difference relative to VM at $p \leq 0.05$.

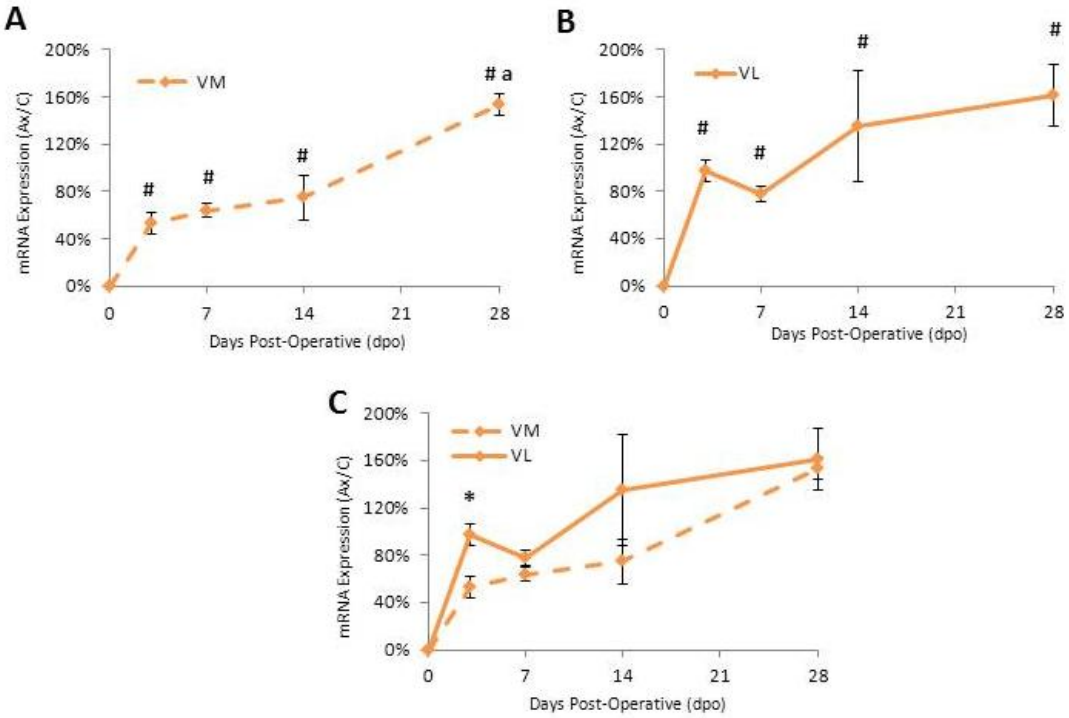

Figure 100. Percent change of **Fas** mRNA expression ± SEM in **SOD1** VM and VL axotomized facial motor nucleus subnuclei at 3, 7, 14 and 28 dpo relative to control. **A**, VM. **B**, VL. **C**, VM vs. VL. **#** represents a significant difference relative to the control; **a** represents a significant difference relative to the previous time-point; ***** represents a significant difference relative to VM at $p \leq 0.05$.

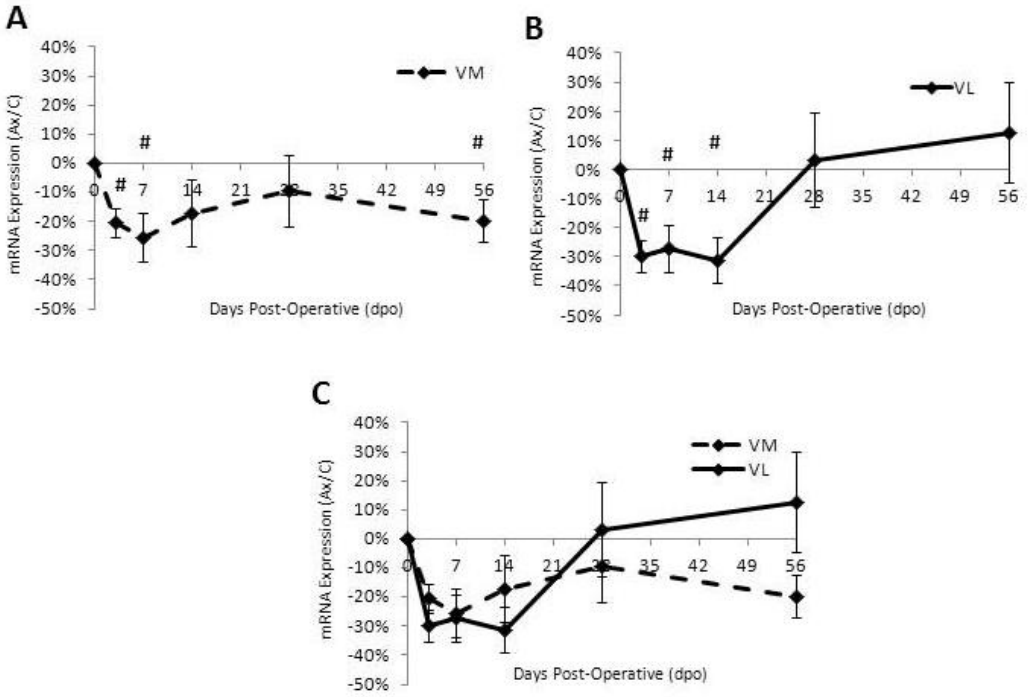

Figure 101. Percent change of **TRADD** mRNA expression ± SEM in **WT** VM and VL axotomized facial motor nucleus subnuclei at 3, 7, 14, 28 and 56 dpo relative to control. **A**, VM. **B**, VL. **C**, VM vs. VL. **#** represents a significant difference relative to the control; **a** represents a significant difference relative to the previous time-point at $p \leq 0.05$.

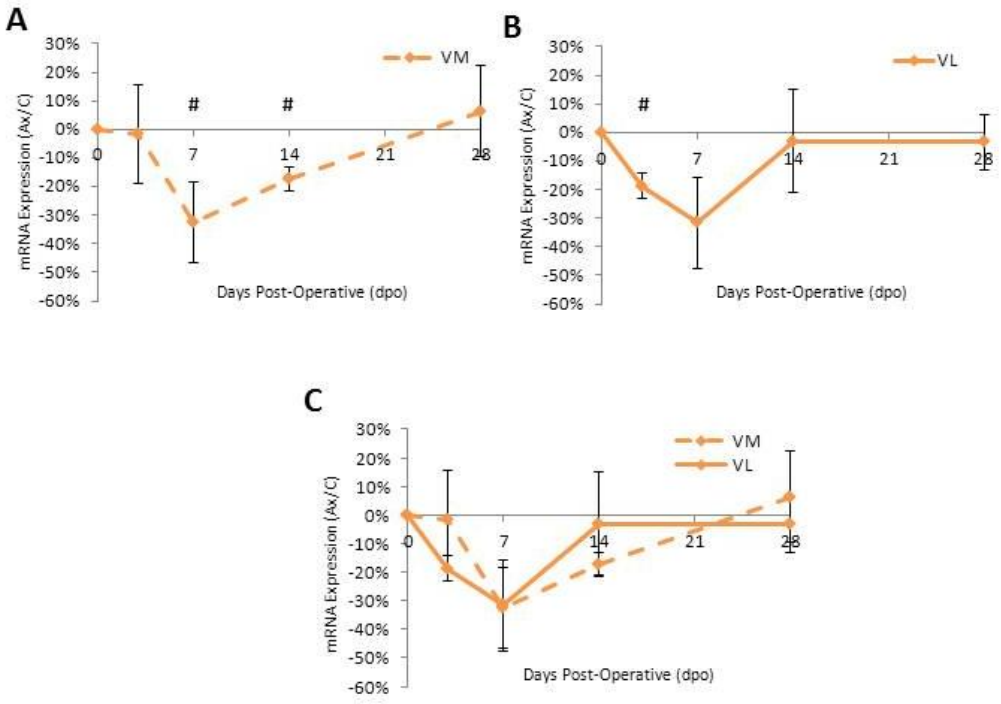

Figure 102. Percent change of **TRADD** mRNA expression ± SEM in **SOD1** VM and VL axotomized facial motor nucleus subnuclei at 3, 7, 14 and 28 dpo relative to control. **A**, VM. **B**, VL. **C**, VM vs. VL. **#** represents a significant difference relative to the control at $p \leq 0.05$.

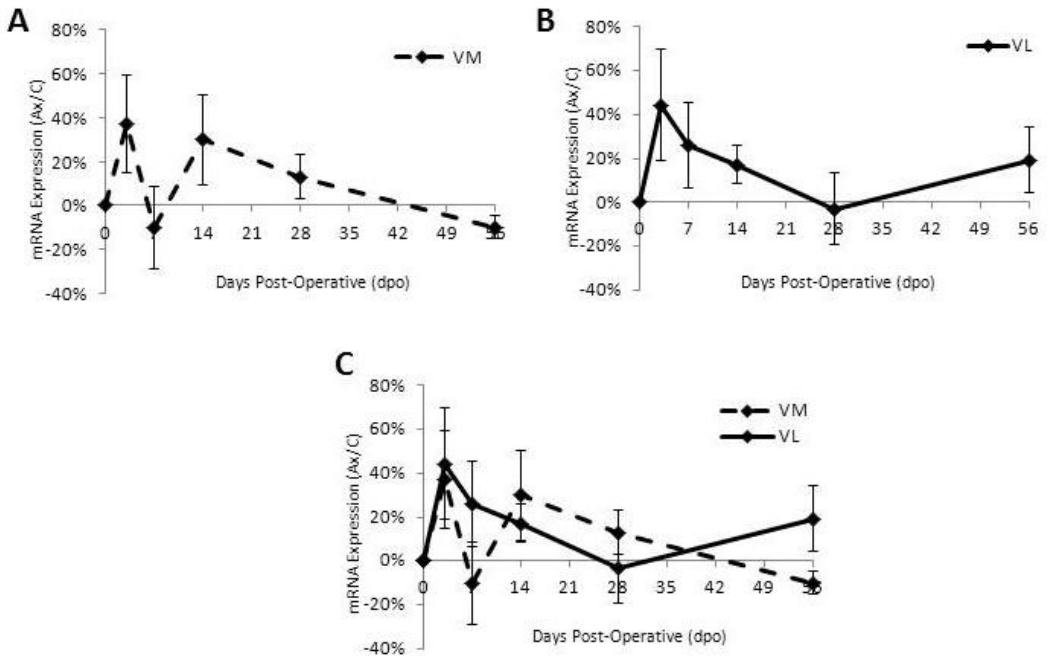

Figure 103. Percent change of **FADD** mRNA expression ± SEM in **WT** VM and VL axotomized facial motor nucleus subnuclei at 3, 7, 14, 28 and 56 dpo relative to control. **A**, VM. **B**, VL. **C**, VM vs. VL.

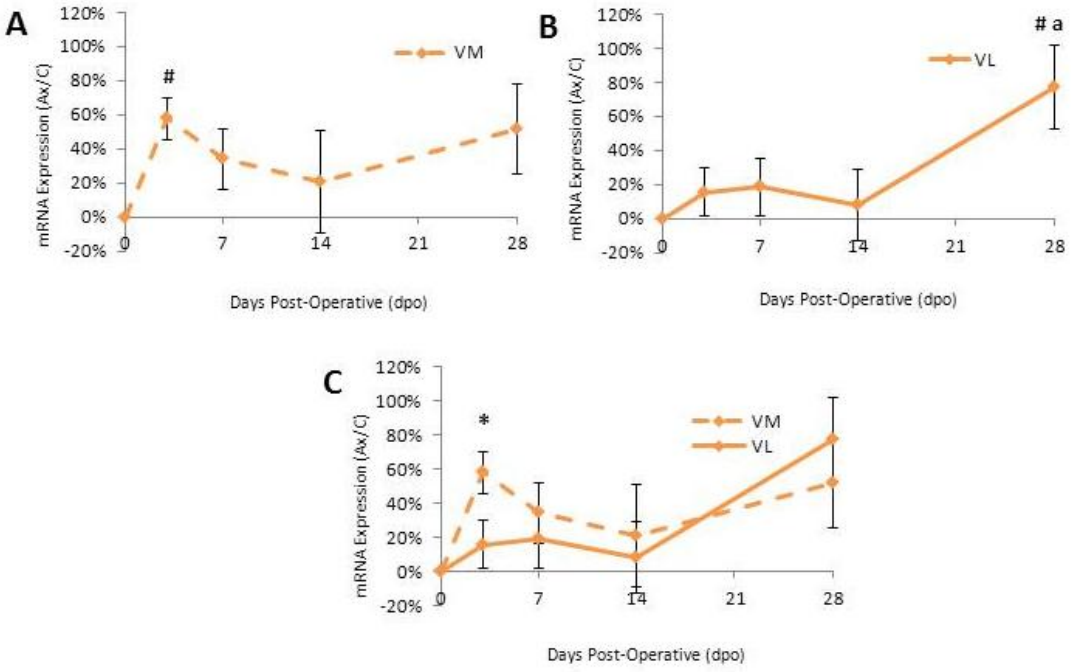

Figure 104. Percent change of **FADD** mRNA expression ± SEM in **SOD1** VM and VL axotomized facial motor nucleus subnuclei at 3, 7, 14 and 28 dpo relative to control. **A**, VM. **B**, VL. **C**, VM vs. VL. **#** represents a significant difference relative to the control; **a** represents a significant difference relative to the previous time-point; ***** represents a significant difference relative to VL at $p \leq 0.05$.

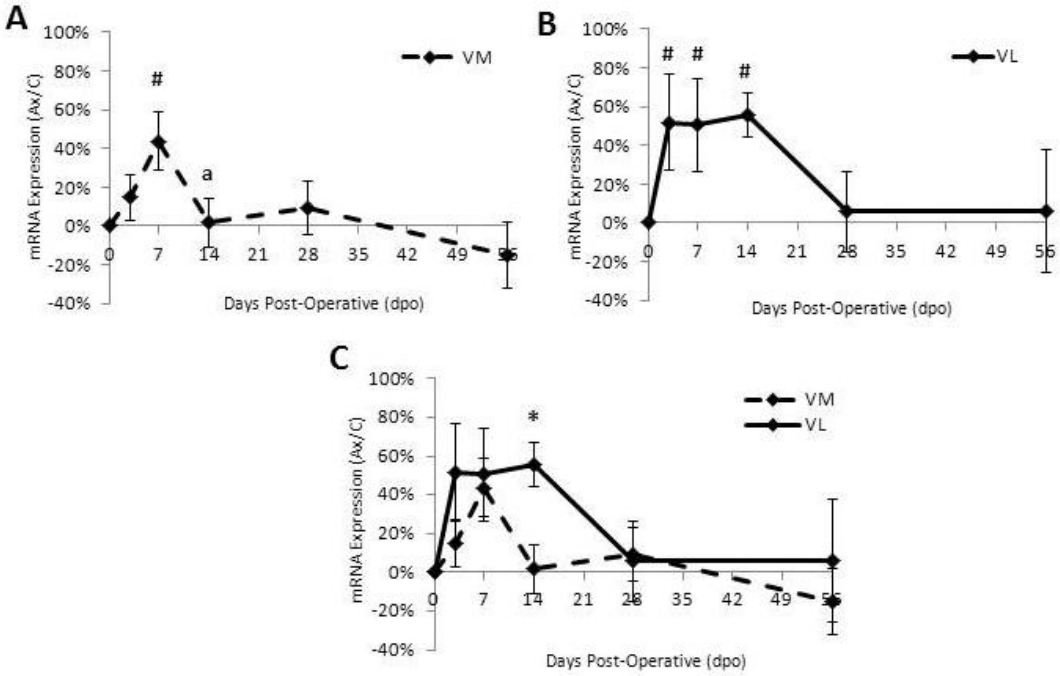

Figure 105. Percent change of **Daxx** mRNA expression ± SEM in **WT** VM and VL axotomized facial motor nucleus subnuclei at 3, 7, 14, 28 and 56 dpo relative to control. **A**, VM. **B**, VL. **C**, VM vs. VL. **#** represents a significant difference relative to the control; **a** represents a significant difference relative to the previous time-point; ***** represents a significant difference relative to VM at $p \leq 0.05$.

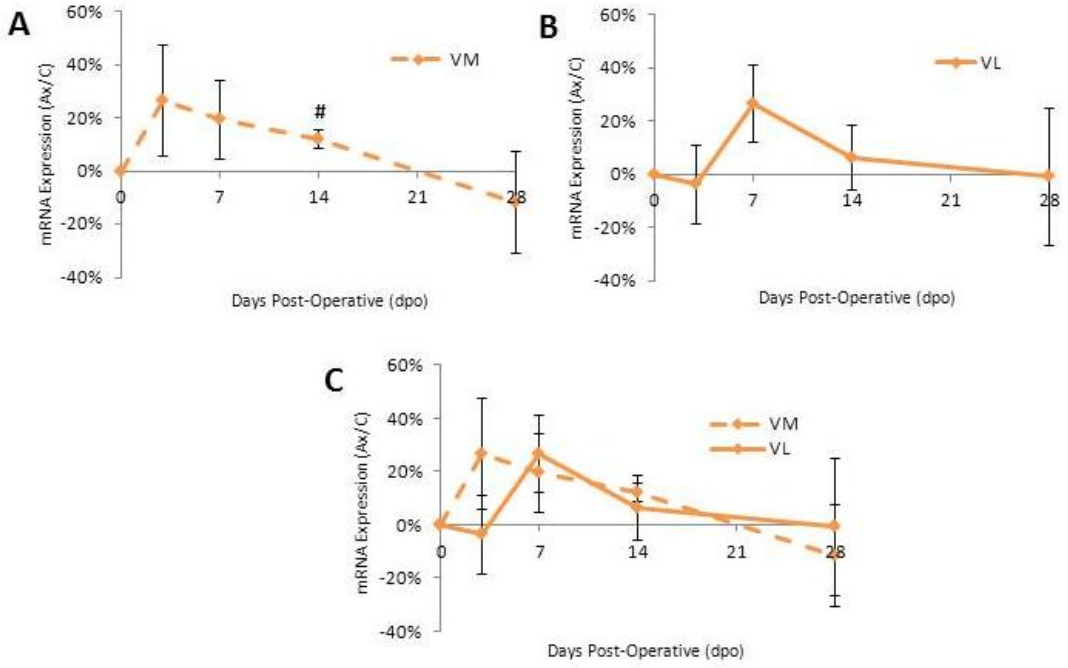

Figure 106. Percent change of **Daxx** mRNA expression ± SEM in **SOD1** VM and VL axotomized facial motor nucleus subnuclei at 3, 7, 14 and 28 dpo relative to control. **A**, VM. **B**, VL. **C**, VM vs. VL. **#** represents a significant difference relative to the control at $p \leq 0.05$.

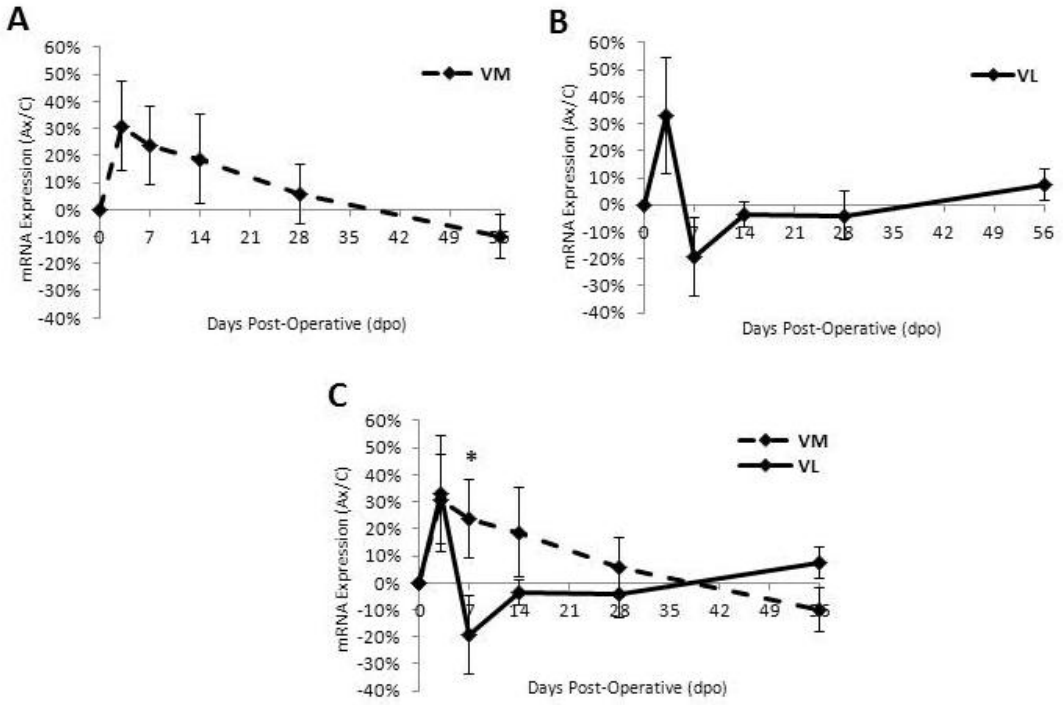

Figure 107. Percent change of **ASK1** mRNA expression ± SEM in **WT** VM and VL axotomized facial motor nucleus subnuclei at 3, 7, 14, 28 and 56 dpo relative to control. **A**, VM. **B**, VL. **C**, VM vs. VL. ***** represents a significant difference relative to VM at $p \leq 0.05$.

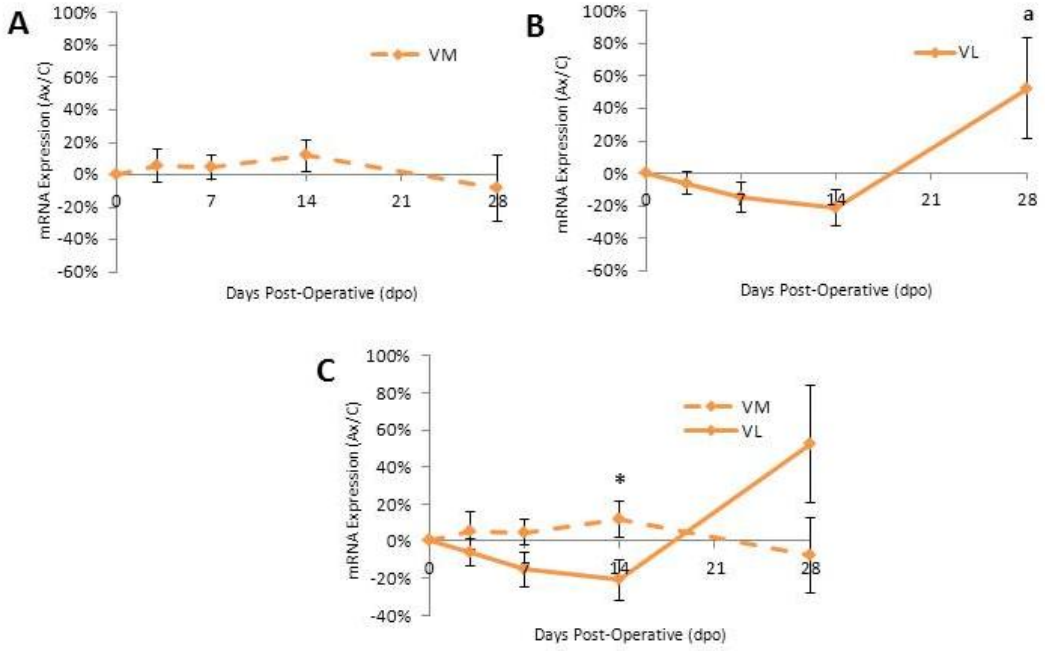

Figure 108. Percent change of **ASK1** mRNA expression ± SEM in **SOD1** VM and VL axotomized facial motor nucleus subnuclei at 3, 7, 14 and 28 dpo relative to control. **A**, VM. **B**, VL. **C**, VM vs. VL. **a** represents a significant difference relative to the previous time-point; ***** represents a significant difference relative to VL at $p \leq 0.05$.

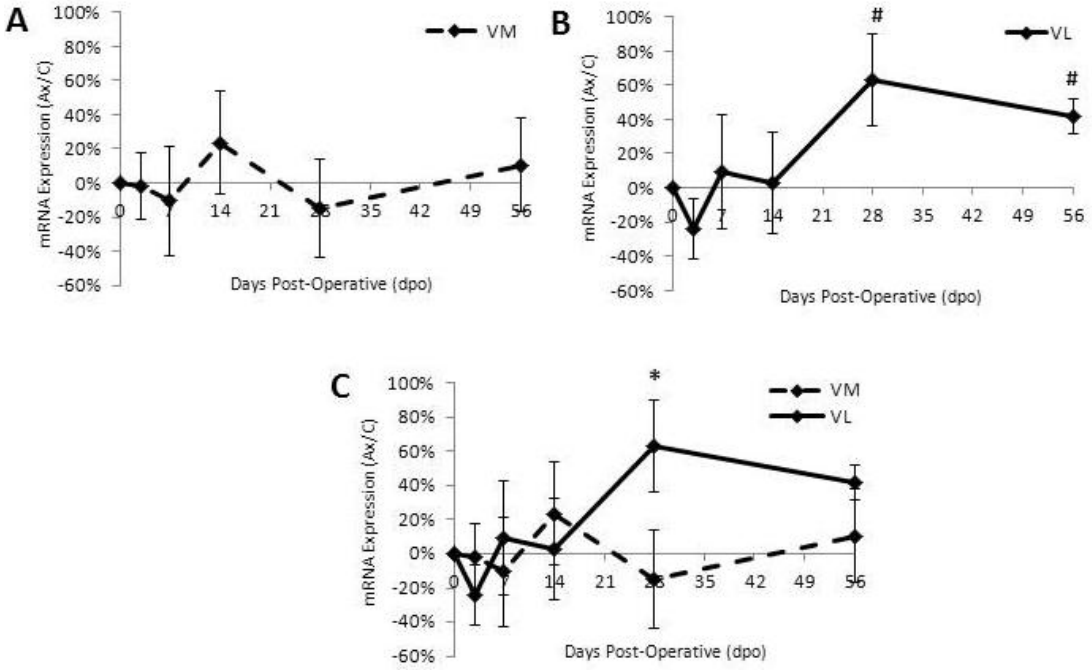

Figure 109. Percent change of **nNOS** mRNA expression ± SEM in **WT** VM and VL axotomized facial motor nucleus subnuclei at 3, 7, 14, 28 and 56 dpo relative to control. **A**, VM. **B**, VL. **C**, VM vs. VL. **#** represents a significant difference relative to the control; ***** represents a significant difference relative to VM at $p \leq 0.05$.

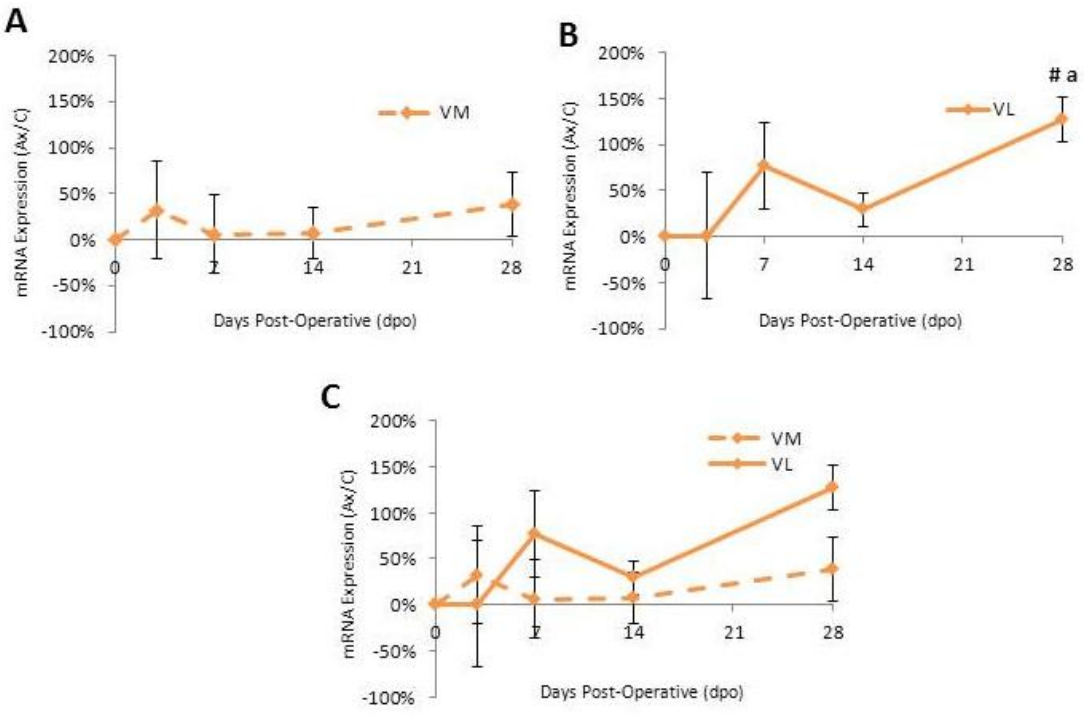

Figure 110. Percent change of **nNOS** mRNA expression ± SEM in **SOD1** VM and VL axotomized facial motor nucleus subnuclei at 3, 7, 14 and 28 dpo relative to control. **A**, VM. **B**, VL. **C**, VM vs. VL. **#** represents a significant difference relative to the control; **a** represents a significant difference relative to the previous time-point at $p \leq 0.05$.

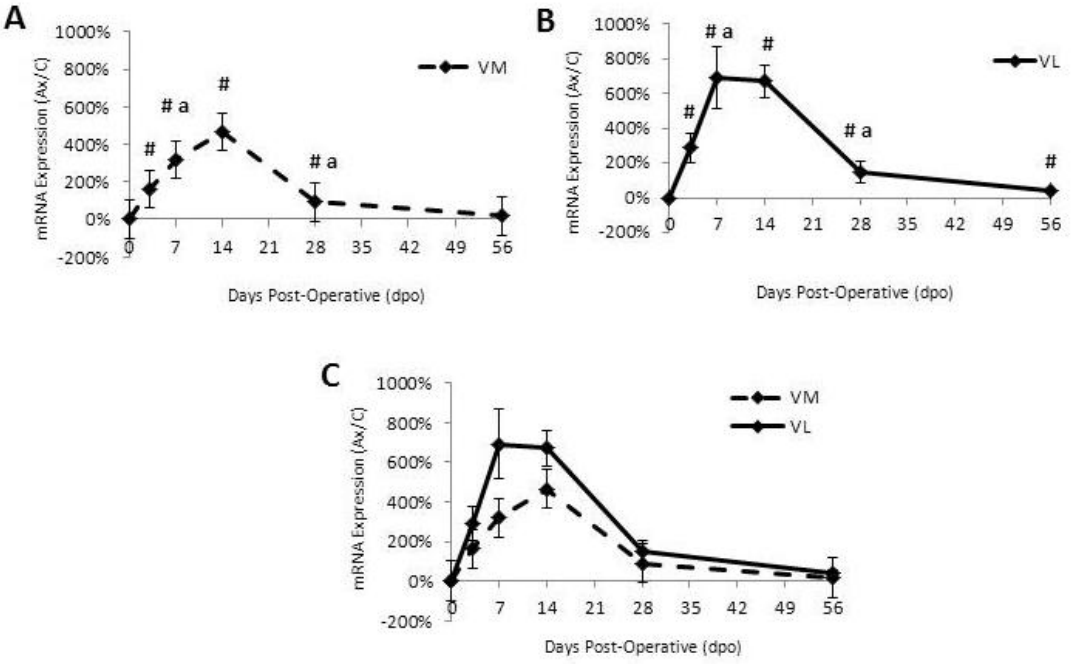

Figure 111. Percent change of **Caspase-3** mRNA expression ± SEM in **WT** VM and VL axotomized facial motor nucleus subnuclei at 3, 7, 14, 28 and 56 dpo relative to control. **A**, VM. **B**, VL. **C**, VM vs. VL. **#** represents a significant difference relative to the control; **a** represents a significant difference relative to the previous time-point at $p \leq 0.05$.

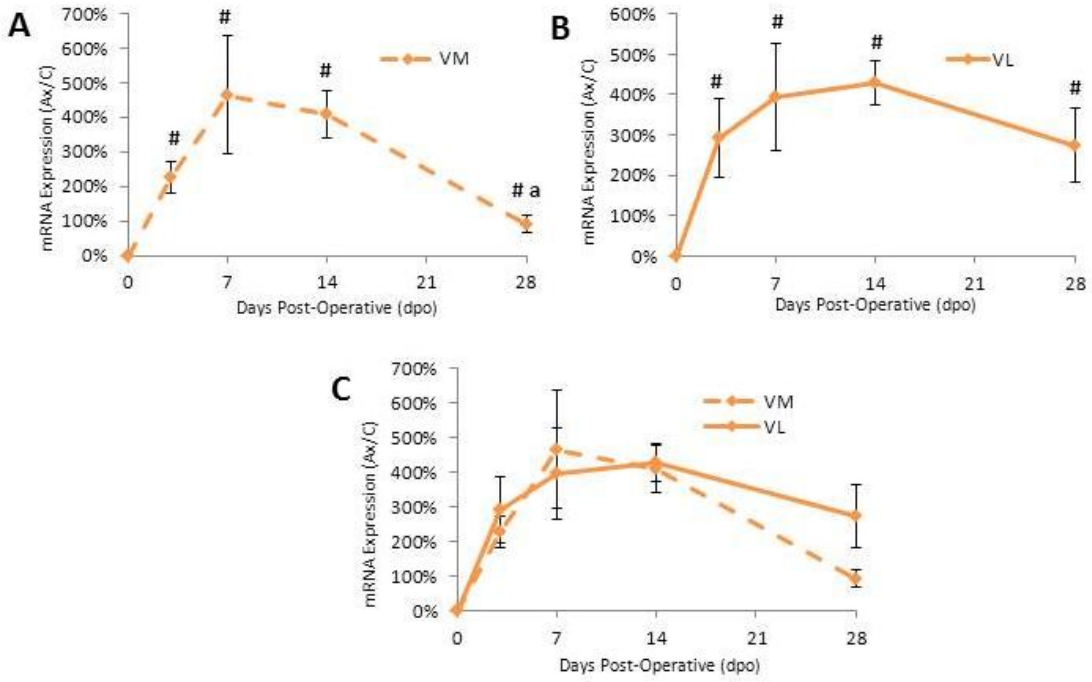

Figure 112. Percent change of **Caspase-3** mRNA expression ± SEM in **SOD1** VM and VL axotomized facial motor nucleus subnuclei at 3, 7, 14 and 28 dpo relative to control. **A**, VM. **B**, VL. **C**, VM vs. VL. **#** represents a significant difference relative to the control; **a** represents a significant difference relative to the previous time-point at $p \leq 0.05$.

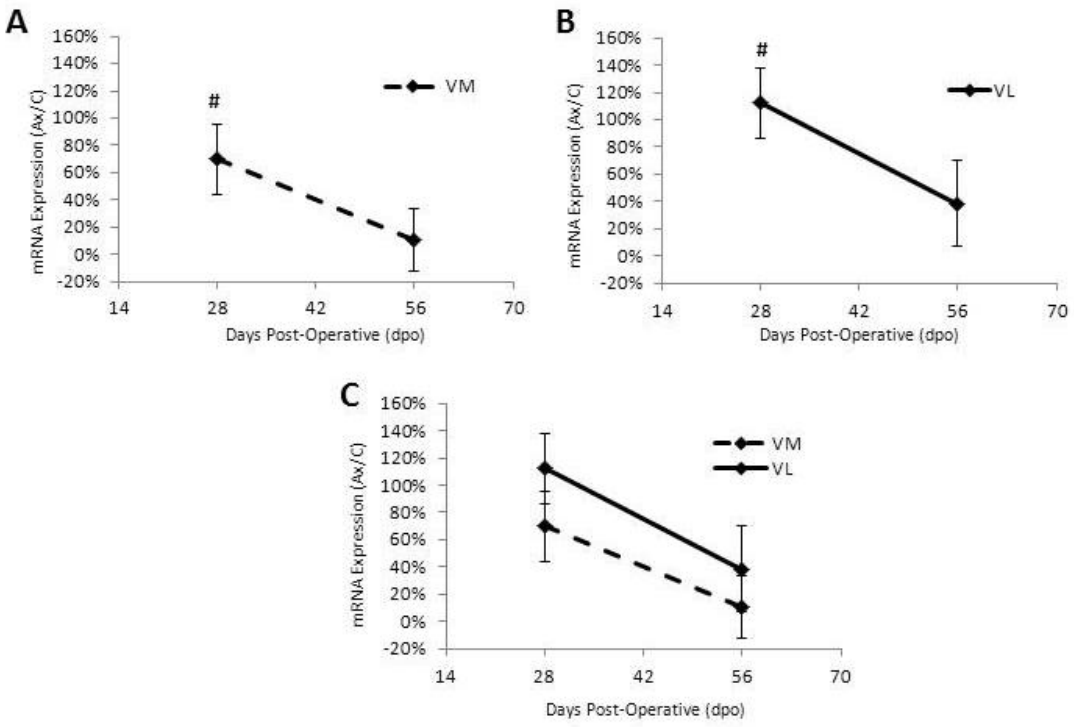

Figure 113. Percent change of **Caspase-8** mRNA expression ± SEM in **WT** VM and VL axotomized facial motor nucleus subnuclei at 28 and 56 dpo relative to control. **A**, VM. **B**, VL. **C**, VM vs. VL. **#** represents a significant difference relative to the control at $p \leq 0.05$.

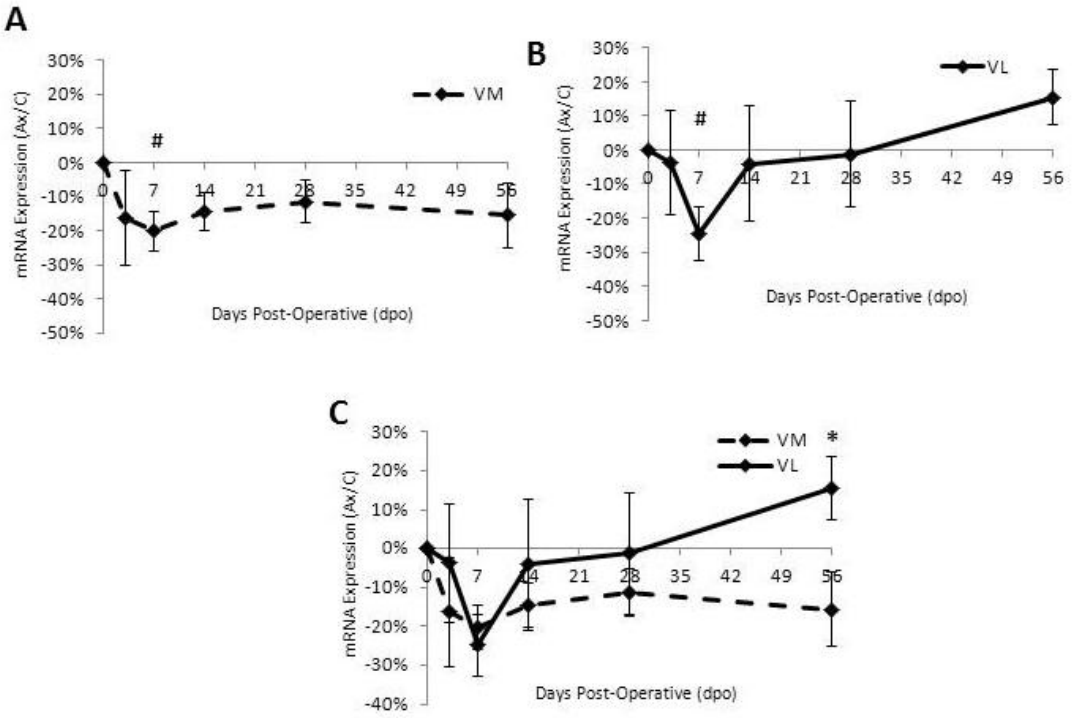

Figure 114. Percent change of **TRAF2** mRNA expression ± SEM in **WT** VM and VL axotomized facial motor nucleus subnuclei at 3, 7, 14, 28 and 56 dpo relative to control. **A**, VM. **B**, VL. **C**, VM vs. VL. **#** represents a significant difference relative to the control; ***** represents a significant difference relative to VM at $p \leq 0.05$.

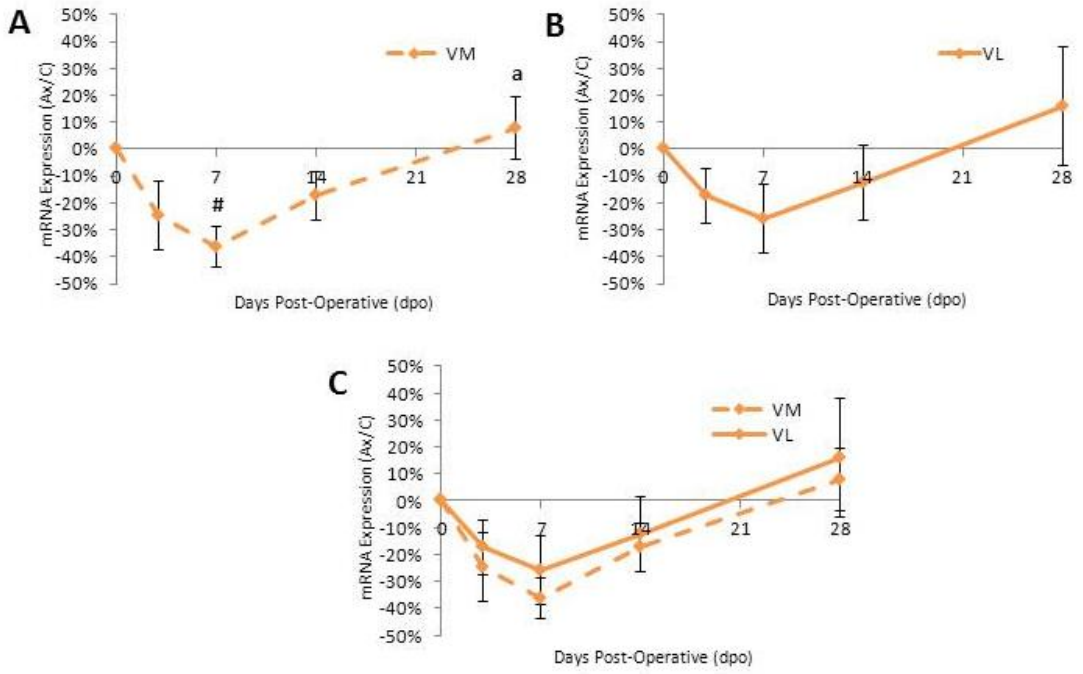

Figure 115. Percent change of **TRAF2** mRNA expression ± SEM in **SOD1** VM and VL axotomized facial motor nucleus subnuclei at 3, 7, 14 and 28 dpo relative to control. **A**, VM. **B**, VL. **C**, VM vs. VL. **#** represents a significant difference relative to the control at $p \leq 0.05$.

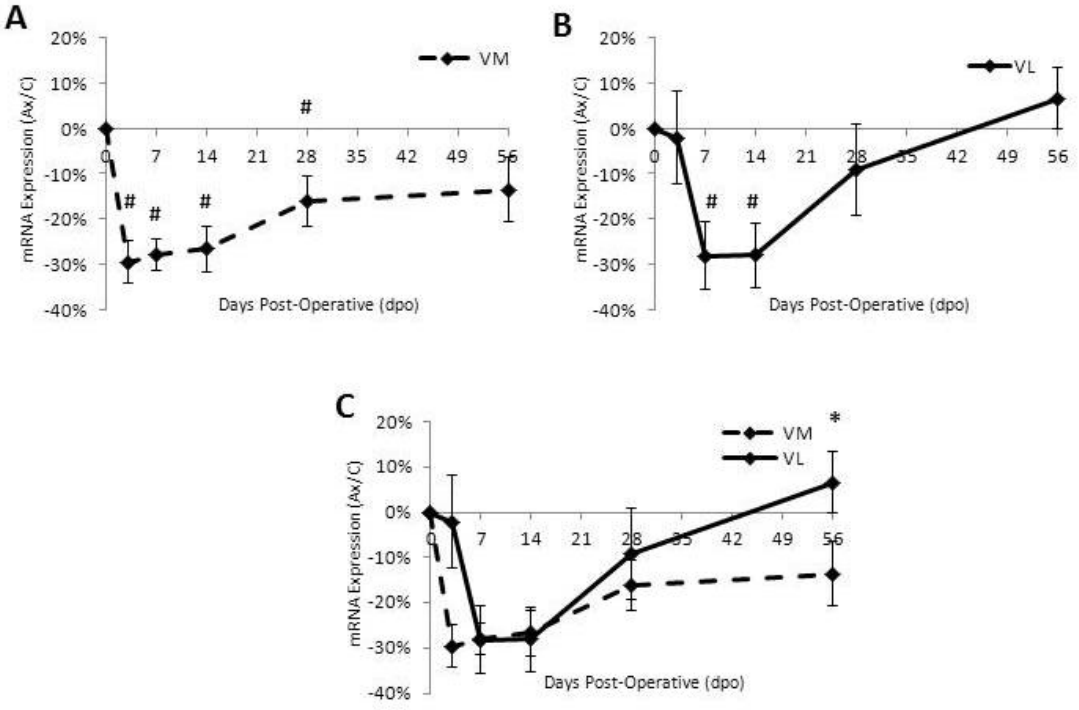

Figure 116. Percent change of **SODD** mRNA expression ± SEM in **WT** VM and VL axotomized facial motor nucleus subnuclei at 3, 7, 14, 28 and 56 dpo relative to control. **A**, VM. **B**, VL. **C**, VM vs. VL. **#** represents a significant difference relative to the control; ***** represents a significant difference relative to VM at $p \leq 0.05$.

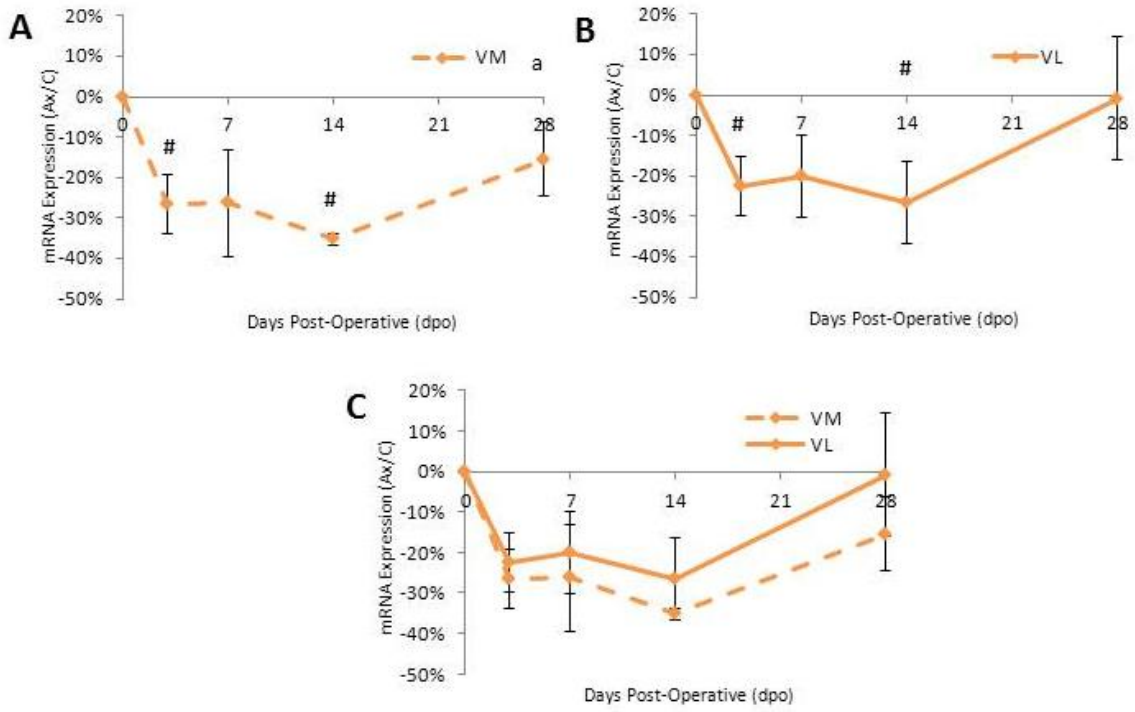

Figure 117. Percent change of **SODD** mRNA expression ± SEM in **SOD1** VM and VL axotomized facial motor nucleus subnuclei at 3, 7, 14 and 28 dpo relative to control. **A**, VM. **B**, VL. **C**, VM vs. VL. **#** represents a significant difference relative to the control; **a** represents a significant difference relative to the previous time-point at $p \leq 0.05$.

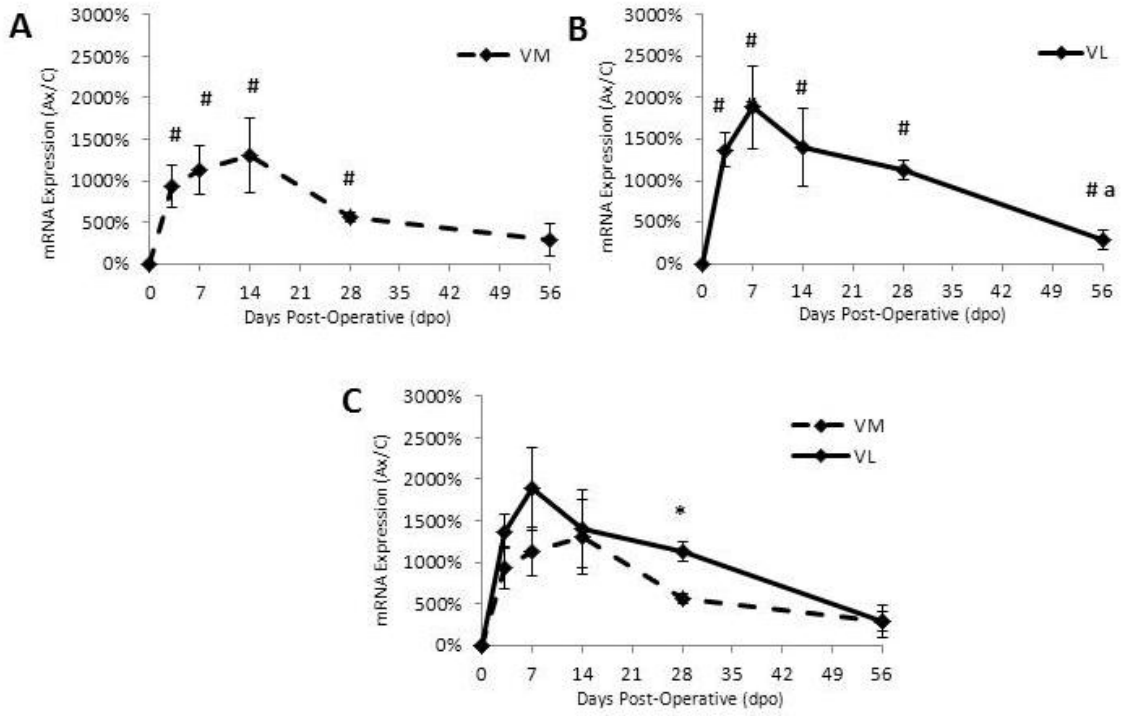

Figure 118. Percent change of **TNFR2** mRNA expression ± SEM in **WT** VM and VL axotomized facial motor nucleus subnuclei at 3, 7, 14, 28 and 56 dpo relative to control. **A**, VM. **B**, VL. **C**, VM vs. VL. **#** represents a significant difference relative to the control; **a** represents a significant difference relative to the previous time-point; ***** represents a significant difference relative to VM at $p \leq 0.05$.

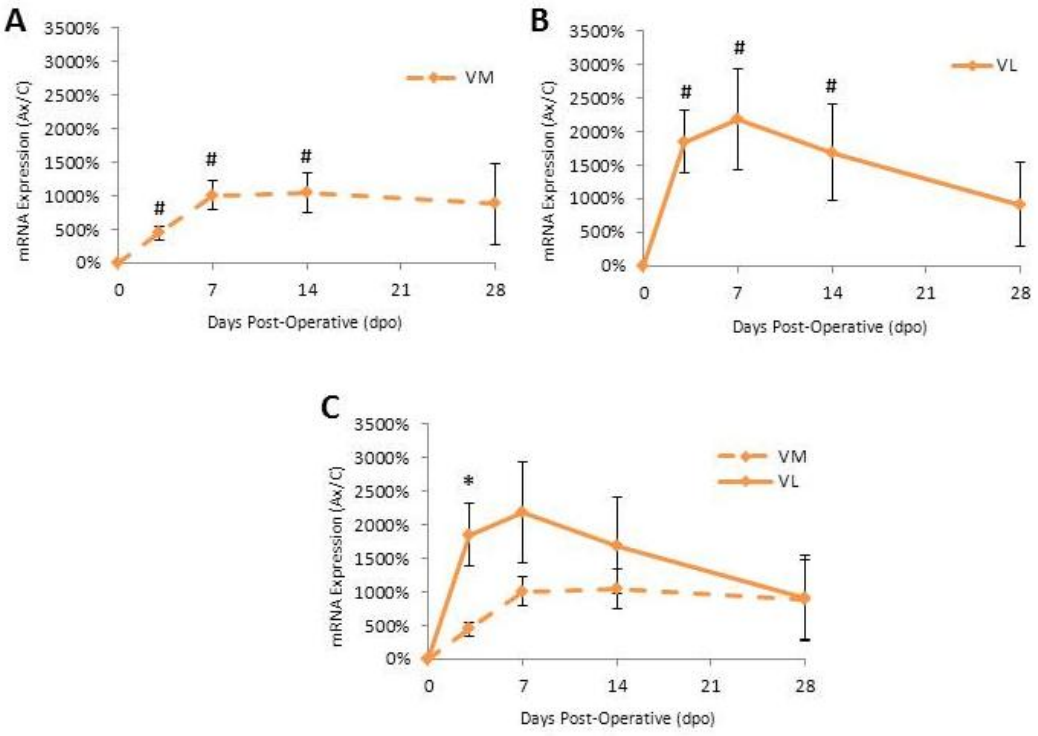

Figure 119. Percent change of **TNFR2** mRNA expression ± SEM in **SOD1** VM and VL axotomized facial motor nucleus subnuclei at 3, 7, 14 and 28 dpo relative to control. **A**, VM. **B**, VL. **C**, VM vs. VL. **#** represents a significant difference relative to the control; ***** represents a significant difference relative to VM at $p \leq 0.05$.

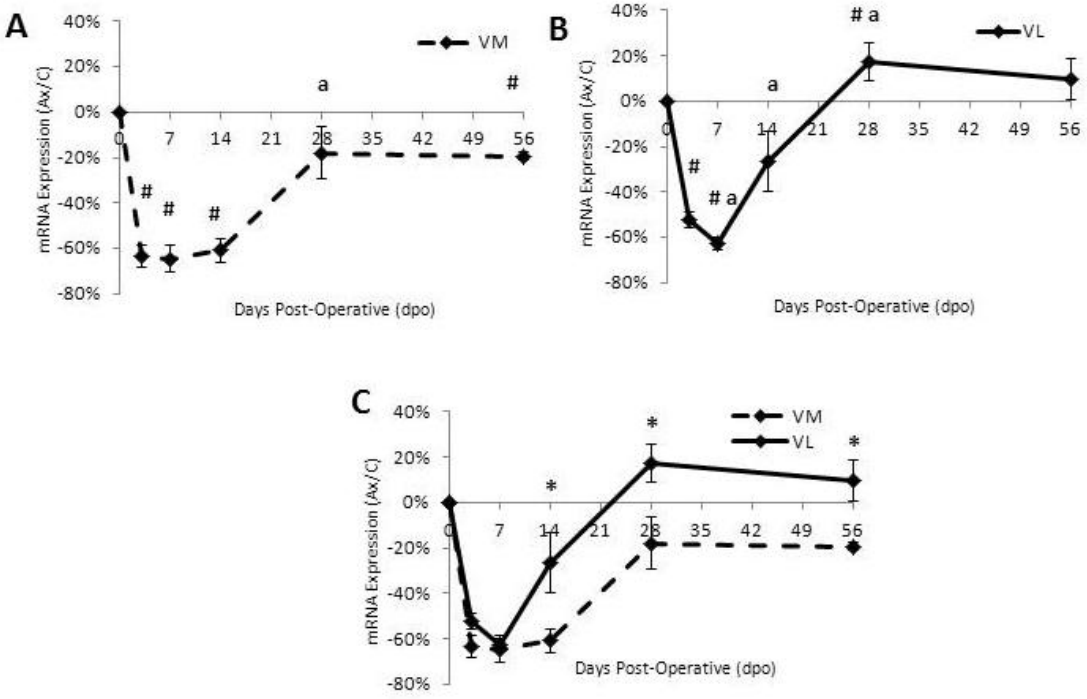

Figure 120. Percent change of **PAC1-R** mRNA expression ± SEM in **WT** VM and VL axotomized facial motor nucleus subnuclei at 3, 7, 14, 28 and 56 dpo relative to control. **A**, VM. **B**, VL. **C**, VM vs. VL. **#** represents a significant difference relative to the control; **a** represents a significant difference relative to the previous time-point; ***** represents a significant difference relative to VM at $p \leq 0.05$.

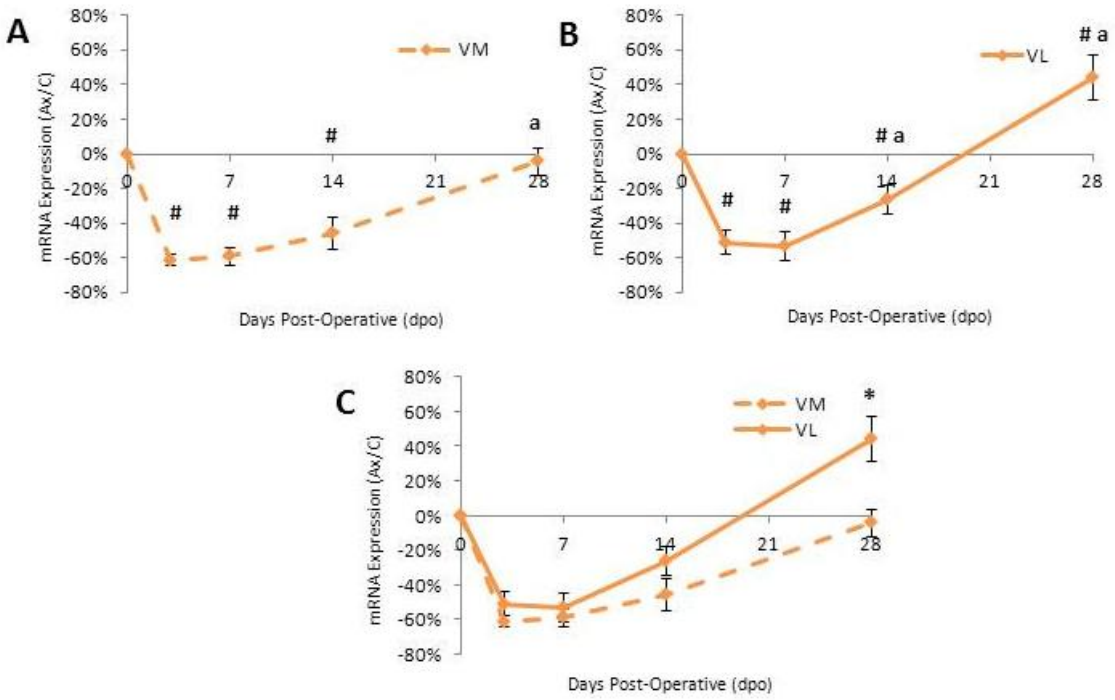

Figure 121. Percent change of **PAC1-R** mRNA expression ± SEM in **SOD1** VM and VL axotomized facial motor nucleus subnuclei at 3, 7, 14 and 28 dpo relative to control. **A**, VM. **B**, VL. **C**, VM vs. VL. **#** represents a significant difference relative to the control; **a** represents a significant difference relative to the previous time-point; ***** represents a significant difference relative to VM at $p \leq 0.05$.

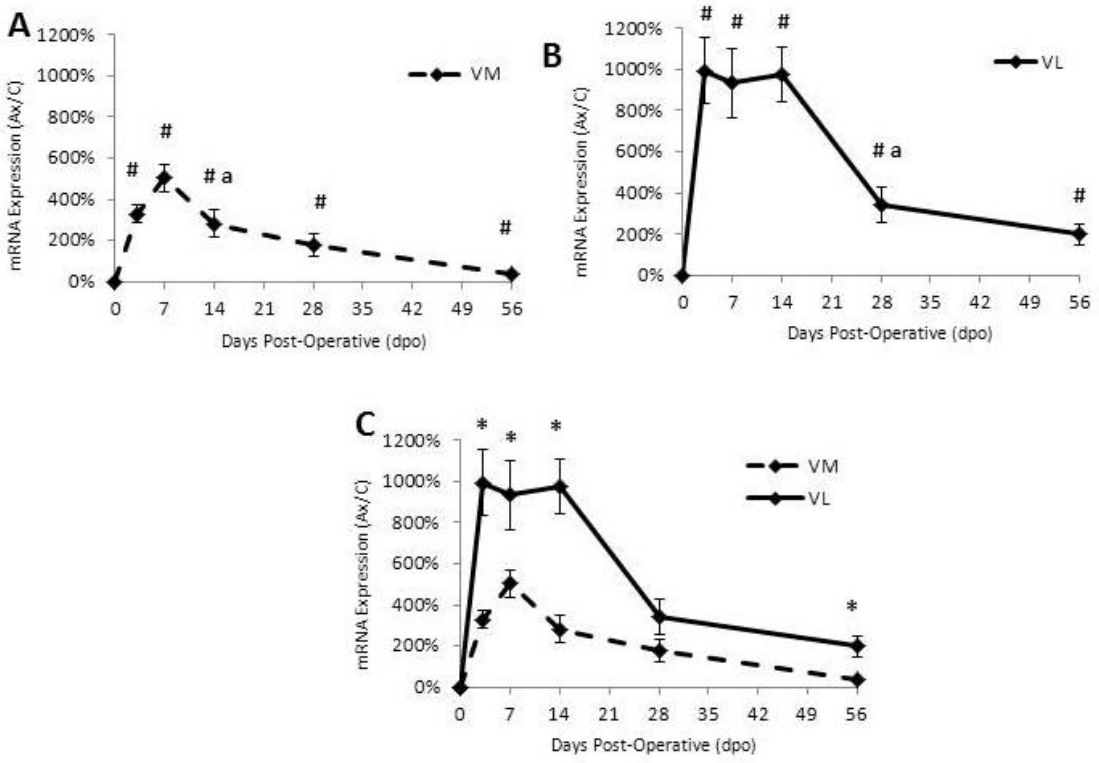

Figure 122. Percent change of **CX3CR1** mRNA expression ± SEM in **WT** VM and VL axotomized facial motor nucleus subnuclei at 3, 7, 14, 28 and 56 dpo relative to control. **A**, VM. **B**, VL. **C**, VM vs. VL. **#** represents a significant difference relative to the control; **a** represents a significant difference relative to the previous time-point; ***** represents a significant difference relative to VM at $p \leq 0.05$.

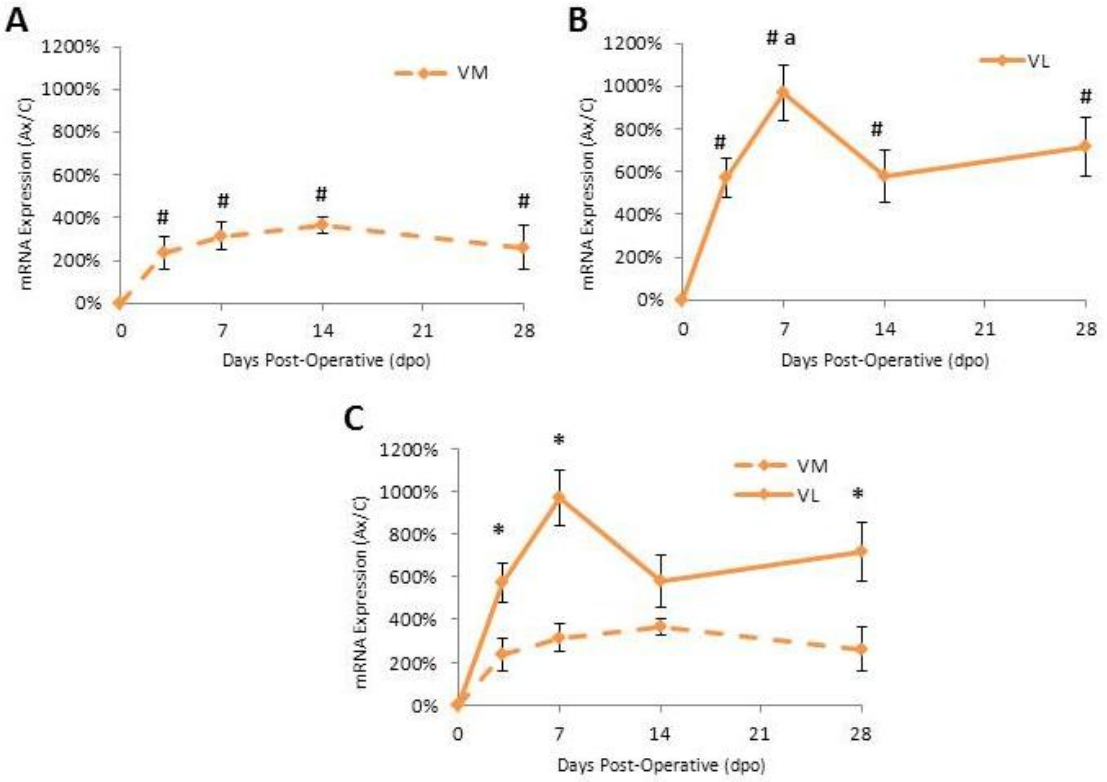

Figure 123. Percent change of **CX3CR1** mRNA expression ± SEM in **SOD1** VM and VL axotomized facial motor nucleus subnuclei at 3, 7, 14 and 28 dpo relative to control. **A**, VM. **B**, VL. **C**, VM vs. VL. **#** represents a significant difference relative to the control; **a** represents a significant difference relative to the previous time-point; ***** represents a significant difference relative to VM at $p \leq 0.05$.

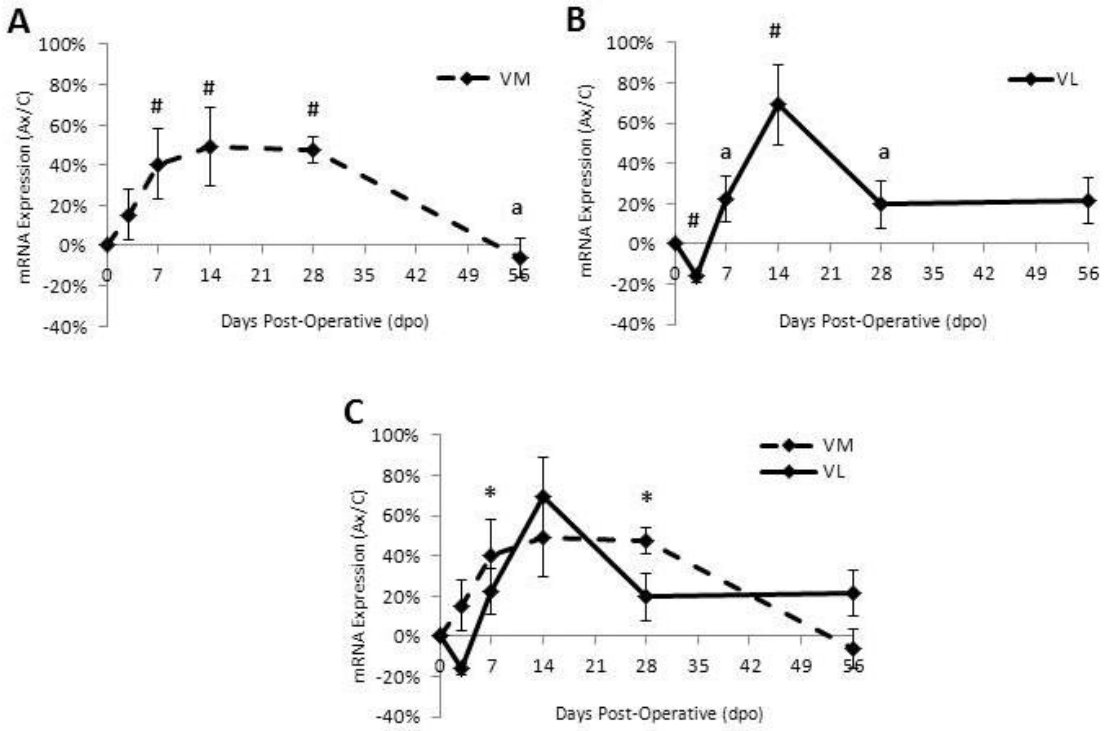

Figure 124. Percent change of **CRMP4** mRNA expression ± SEM in **WT** VM and VL axotomized facial motor nucleus subnuclei at 3, 7, 14, 28 and 56 dpo relative to control. **A**, VM. **B**, VL. **C**, VM vs. VL. **#** represents a significant difference relative to the control; **a** represents a significant difference relative to the previous time-point; ***** represents a significant difference relative to VM at $p \leq 0.05$.

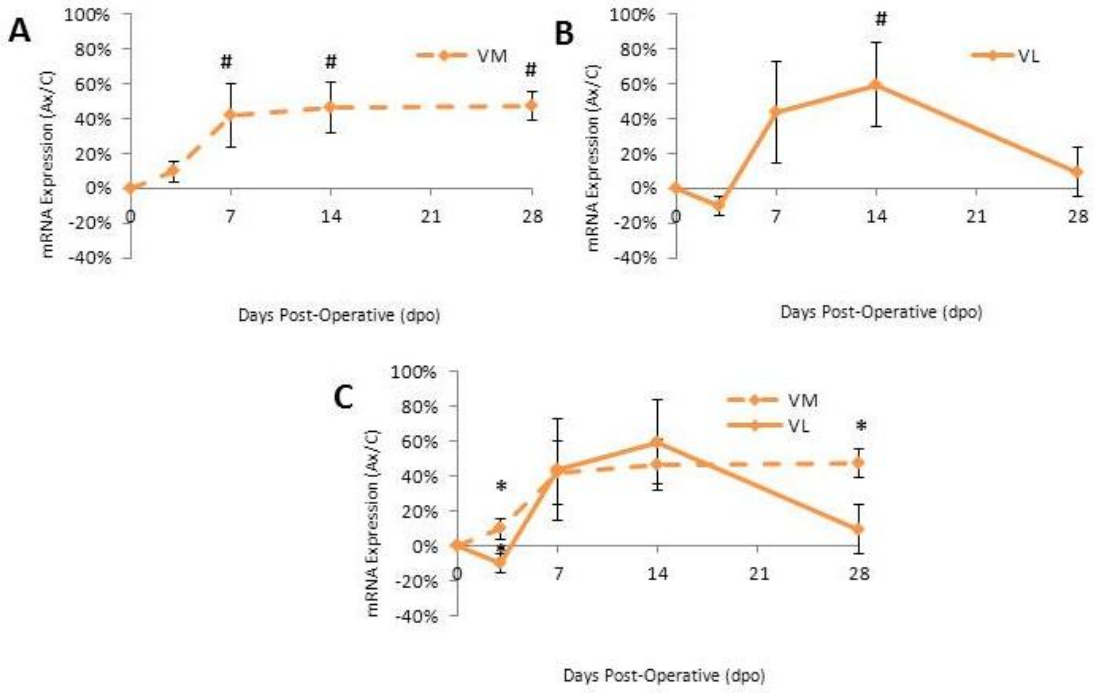

Figure 125. Percent change of **CRMP4** mRNA expression ± SEM in **SOD1** VM and VL axotomized facial motor nucleus subnuclei at 3, 7, 14 and 28 dpo relative to control. **A**, VM. **B**, VL. **C**, VM vs. VL. **#** represents a significant difference relative to the control; ***** represents a significant difference relative to VL at $p \leq 0.05$.

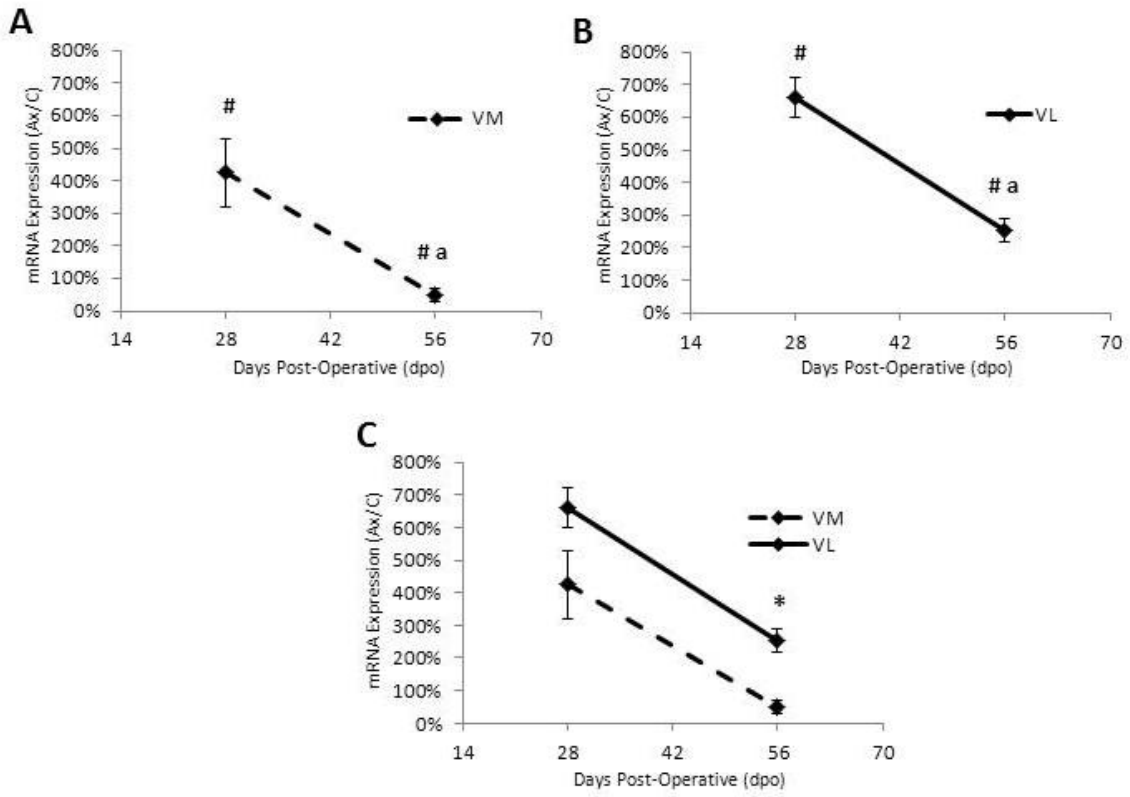

Figure 126. Percent change of **GAP-43** mRNA expression ± SEM in **WT** VM and VL axotomized facial motor nucleus subnuclei at 28 and 56 dpo relative to control. **A**, VM. **B**, VL. **C**, VM vs. VL. **#** represents a significant difference relative to the control; **a** represents a significant difference relative to the previous time-point; ***** represents a significant difference relative to VM at $p \leq 0.05$.

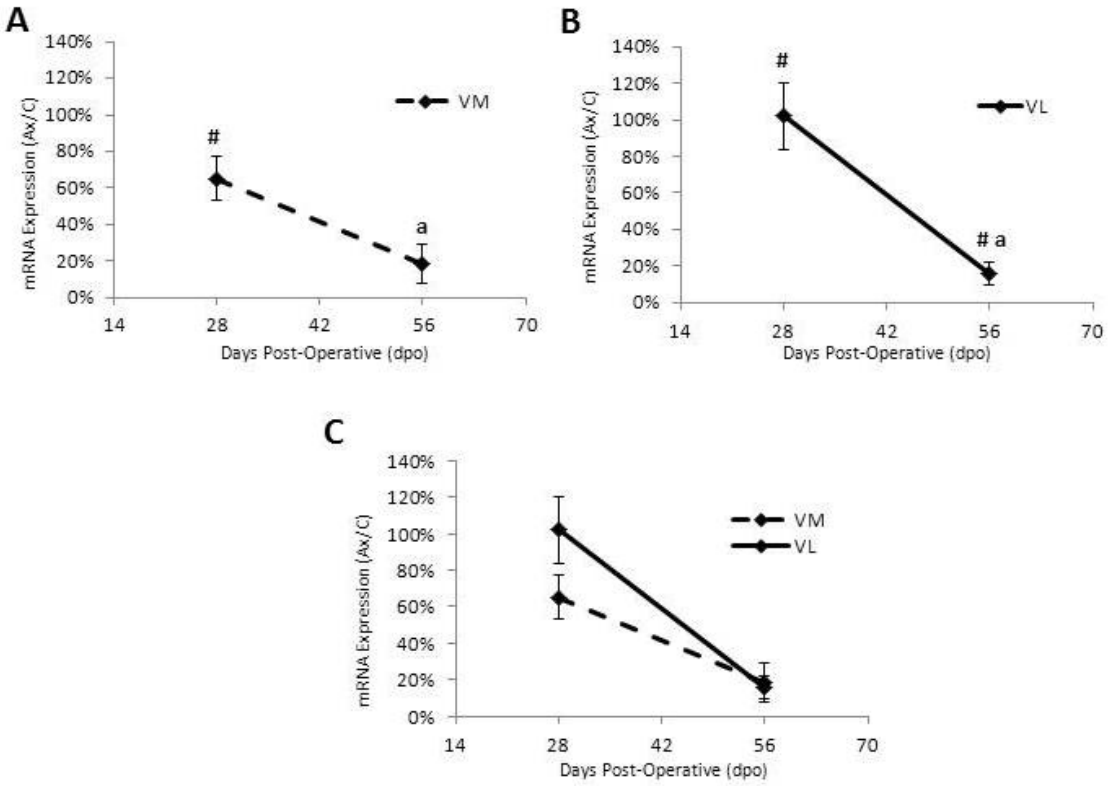

Figure 127. Percent change of **βII-Tubulin** mRNA expression ± SEM in **WT** VM and VL axotomized facial motor nucleus subnuclei at 28 and 56 dpo relative to control. **A**, VM. **B**, VL. **C**, VM vs. VL. **#** represents a significant difference relative to the control; **a** represents a significant difference relative to the previous time-point at $p \leq 0.05$.

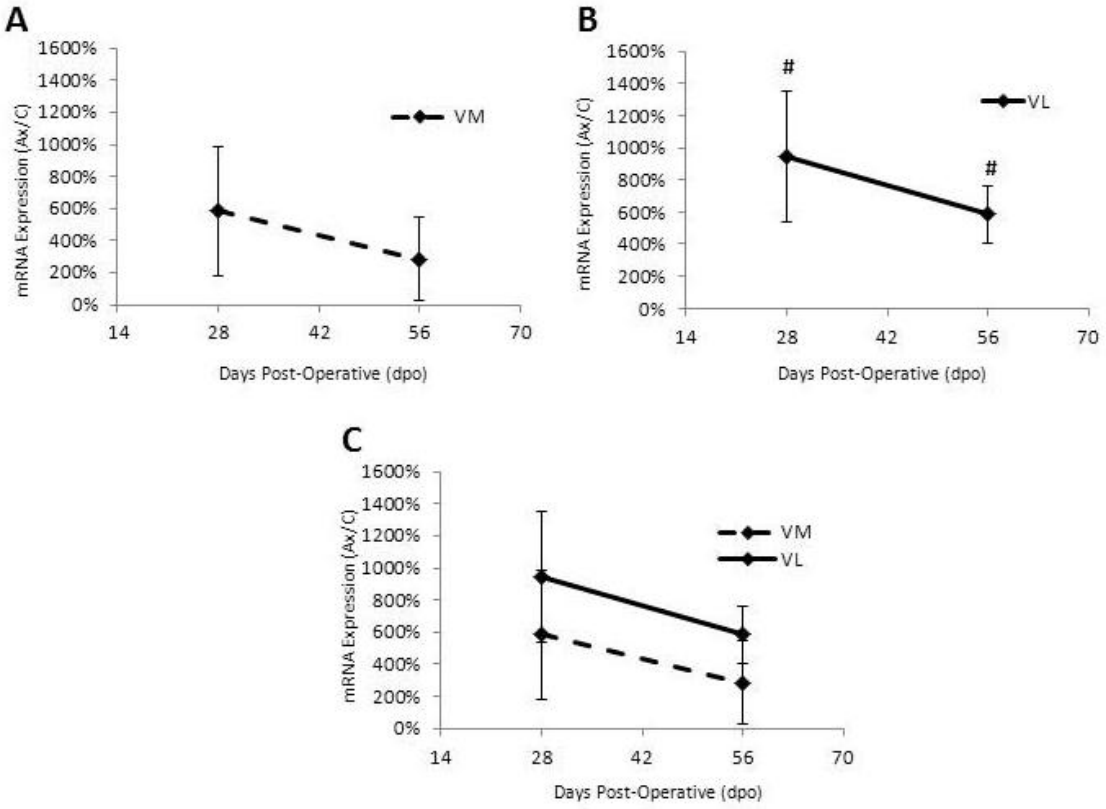

Figure 128. Percent change of **GFAP** mRNA expression ± SEM in **WT** VM and VL axotomized facial motor nucleus subnuclei at 28 and 56 dpo relative to control. **A**, VM. **B**, VL. **C**, VM vs. VL. **#** represents a significant difference relative to the control at $p \leq 0.05$.

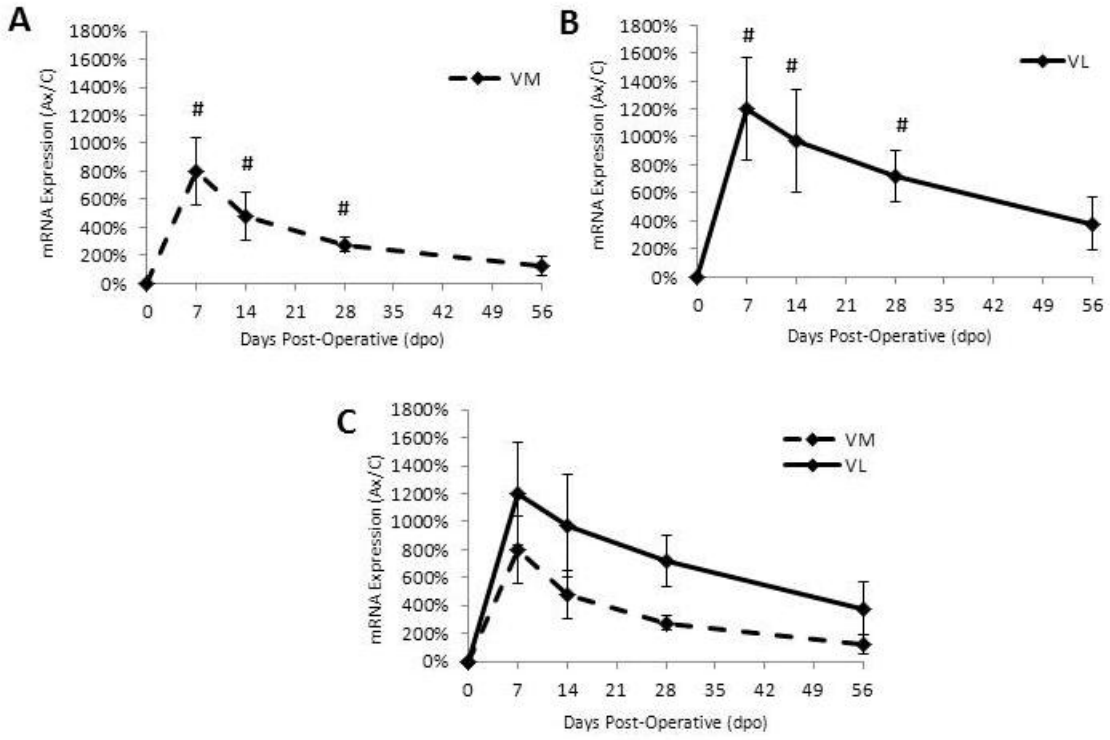

Figure 129. Percent change of **CD68** mRNA expression ± SEM in **WT** VM and VL axotomized facial motor nucleus subnuclei at 7, 14, 28 and 56 dpo relative to control. **A**, VM. **B**, VL. **C**, VM vs. VL. **#** represents a significant difference relative to the control at $p \leq 0.05$.

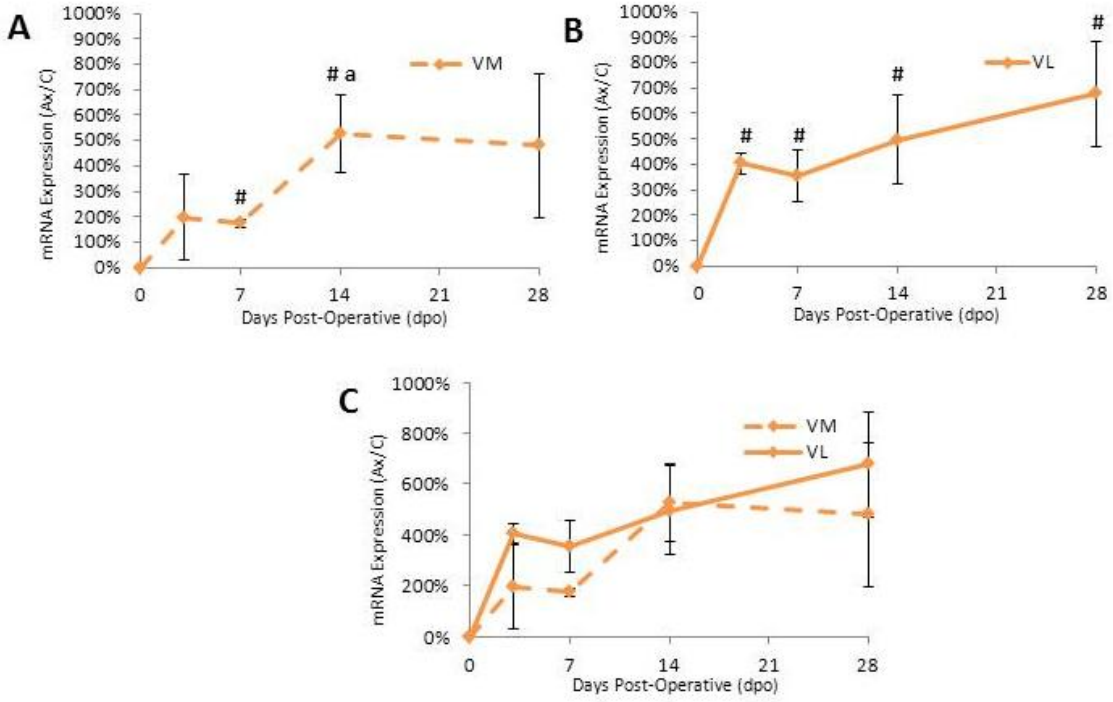

Figure 130. Percent change of **CD68** mRNA expression ± SEM in **SOD1** VM and VL axotomized facial motor nucleus subnuclei at 3, 7, 14 and 28 dpo relative to control. **A**, VM. **B**, VL. **C**, VM vs. VL. **#** represents a significant difference relative to the control; **a** represents a significant difference relative to the previous time-point at $p \leq 0.05$.

Axotomy-Induced mRNA Expression Regenerative FMN Subnuclei (VM) vs. Degenerative FMN Subnuclei (VL)		
Gene	**WT VM vs. VL (0 - 28 dpo)**	**SOD1 VM vs. VL (0 - 28 dpo)**
TNFR1 Death Receptor Signaling		
TNFR1	↑↑ VL	no Δ
TRADD	no Δ	↑ VM
TRAF2	↑ VL	no Δ
SODD	no Δ	no Δ
Fas Death Receptor Signaling		
Fas	↑↑↑ VL	↑ VL
Daxx	↑ VL	no Δ
ASK1	↑ VM	↑ VM
nNOS	↑ VL	no Δ
Shared Factors of TNFR1 & Fas Death Receptors		
FADD	no Δ	no Δ
Caspase-3	no Δ	no Δ
Neurodegenerative Signaling Gene		
CRMP4	↑↑ VM	↑↑ VM
Neuroprotective Signaling		
TNFR2	↑ VL	↑ VL
PAC1-R	↑↑ VL	↑ VL
CX3CR1	↑↑↑↑ VL	↑↑↑ VL
Neuroregenerative, MN-Specific Genes		
Glial-Specific Genes		
CD68	no Δ	no Δ

Table 7: Percent change mRNA expression (Ax/C) after axotomy, comparisons between WT VM and VL and SOD1 VM and VL. Time-points used were 3, 7, 14, 28 dpo, WT and SOD1. ↑ represents significant increased expression at one time-point, comparison of VM vs. VL, multiple arrows indicated significant increased expression at additional time-points. No Δ indicated no difference in expression between the subnuclei.

WT Axotomy-Induced mRNA Expression at 56 dpo Regenerative FMN Subnuclei (VM) vs. Degenerative FMN Subnuclei (VL)			
Gene	mRNA Expression (compare to baseline)		Increased Expression VM vs. VL
	VM	VL	
TNFR1 Death Receptor Signaling			
TNFR1	Upregulated	Baseline	no Δ
TRADD	Downregulated	Baseline	no Δ
TRAF2	Baseline	Upregulated	↑ VL
SODD	Baseline	Baseline	↑ VL
Fas Death Receptor Signaling			
Fas	Baseline	Baseline	no Δ
Daxx	Baseline	Baseline	no Δ
ASK1	Baseline	Baseline	no Δ
nNOS	Baseline	Upregulated	no Δ
Shared Factors of TNFR1 & Fas Death Receptors			
FADD	Baseline	Baseline	no Δ
Caspase-8	Baseline	Baseline	no Δ
Caspase-3	Baseline	Upregulated	no Δ
Neurodegenerative Signaling Gene			
CRMP4	Baseline	Baseline	no Δ
Neuroprotective Signaling			
TNFR2	Baseline	Upregulated	no Δ
PAC1-R	Downregulated	Baseline	↑ VL
CX3CR1	Upregulated	Upregulated	↑ VL
Neuroregenerative, MN-Specific Genes			
GAP-43	Upregulated	Upregulated	↑ VL
βII-Tubulin	Baseline	Upregulated	no Δ
Glial-Specific Genes			
GFAP	Baseline	Upregulated	no Δ
CD68	Baseline	Baseline	no Δ

Table 8: WT VM and VL subnuclei expression mRNA at 56 dpo. Summary of the mRNA expression in each subnuclei (VM or VL) relative to baseline and comparisons between VM and VL mRNA expression. ↑ indicates a significant increase in mRNA expression in the VL relative to the VM.

E. Discussion

The distribution of FMN survival across the six subnuclei has proven to be a valuable model to study the mechanisms underlying axotomy-induced MN loss. We initially proposed that the VM "regenerative" subnucleus would present with a degenerative response to axotomy that would coincide with the increased MN loss. However, we were surprised to find that the WT VL subnucleus responded with a regenerative profile and actually revealed increased expression of MN-regenerative genes compared to the VM. We hypothesize that this increase in regenerative gene expression is a compensatory mechanism for the increased MN death. Neuropil genes, such as TNFα and Caspase-8, were slightly increased at certain time-points (Mesnard et al., 2010).

"*Degenerative" VL Subnucleus Reveals an Increased Axotomy-Induced Molecular Response Compared to VM*

Over the time course of 28 dpo, WT VL reveals increased mRNA expression throughout many of the genes analyzed as opposed to WT VM (**Table 7**). Increased mRNA expression for death receptor genes suggests they may play a role in the enhanced MN-loss within the VL subnucleus following axotomy. In support of our previous findings of increased regenerative-associated genes, the neuroprotective signaling receptor genes were also upregulated to a greater degree than in VM. Further

investigation will have to be performed in order to determine if the increase expression in death receptor genes plays a role in the enhanced FMN cell death.

In comparison, the SOD1 VL does not appear to differ from its VM neighbor to such an extent. There are significant differences within the neuroprotective genes, this also supports previous findings from our lab that found a similar regenerative response in the SOD1 VL as seen in the SOD1 VM (**Table 7**; Mesnard, 2009). It appears from this data and previous work that the differences between the VM and VL subnuclei are not as pronounced as compared to the WT. Additionally, comparisons between WT VM vs. SOD1 VM, as well as WT VL vs. SOD1 VL were also analyzed (data not shown) but was similar to the differences seen between WT vs. SOD1 whole nucleus. Therefore, investigation of molecular phenotypes after axotomy is more beneficial when performed within the WT VM and VL.

Axotomy-Induced Response Persists in WT Degenerative (VL) Subnuclei

To add to previous data, the time course for WT was extended out to 56 dpo, refer to **Table 8**. This was performed to determine if specific axotomy-induced gene expression returns to baseline and whether the degenerative VL displays any increases in death receptor mRNA see during the delayed-response to axotomy in SOD1 whole facial motor nucleus. Degenerative VL subnucleus still differentially expresses some genes induced by axotomy, compared to baseline. Surprisingly, the majority of the genes are MN regenerative genes and the neuroprotective receptors. VM and VL results are often highly variable, most likely due to the small sample size during LMD resulting

in less total RNA for real time, RT-PCR. Increasing the number of samples would likely improve variability and that is a future direction. Nevertheless, differences within mRNA expression between the VM and VL subnuclei were also compared and revealed some differences that were not apparent with the original analysis. Overall, the VL subnuclei with enhanced MN cell loss at 28 dpo, reveals a persisting axotomy response that involves mostly neuroprotective and neuroregenerative genes.

Future use of the VM and VL axotomy model will be performed in WT to detect maximal differences between the two and additionally, this date presented here and throughout the dissertation that molecular responses during the delayed-phase are often more pronounced. Therefore time courses after axotomy should be extended to at least 56 dpo.

CHAPTER VIII

CONCLUSIONS, SUMMARY AND FUTURE DIRECTIONS

A. Background

ALS is the most common adult MN degenerative disease with a mean survival of only three – five years after onset. Only a small portion of cases are inherited resulting in 90% of cases that seem to occur randomly. Initial symptoms of the disease often go unnoticed which delays diagnosis. Once motor symptoms have become apparent the disease is already entering final stages of progression and severe MN degeneration has already occurred. Current treatments are virtually nonexistent, only extending the lives of patients for a maximum of four months.

Research suggests that ALS is a multifactorial disease, arising through a combination of several mechanisms as well as a multisystemic disease affecting several cell types. Recent advances in understanding molecular mechanisms underlying the disease can be attributed to development of the SOD1 mouse model that overexpresses the human mutant SOD1 gene found in a portion of fALS cases. Disease progression within the SOD1 mouse resembles the clinical and pathological hallmarks that are observed in ALS patients. Use of the SOD1 model, experimentally, has revealed that the selective vulnerability of MN is likely due to some combination of mechanisms such as

mitochondrial dysfunction, oxidative damage, cytoskeletal abnormalities, protein misfolding, deficits in axonal transport, excitotocixity, inadequate growth factor signaling and inflammation (Shaw and Eggett, 2000; Cozzolino et al., 2008; Shaw, 2005; Bilsland et al., 2010; Sahawneh et al., 2010). The majority of these mechanisms appear to be involved during disease progression. However, the initial pathological event that is thought to initiate the disease is denervation of muscle endplates. Early within the pre-symptomatic stage loss of NMJ becomes significant within the hind-limb musculature. This is followed by evidence of distal axonopathy. Concurrent electrophysiological assessments reveal abnormalities which validate the histological findings (Fischer et al., 2004; Durand et al., 2006; Mancuso et al., 2011). Decreases in muscle mass and muscle fiber diameter are likely a result of the loss of functional motor units (Marcuzzo et al., 2011). Compensatory axonal sprouting is evident following the initial target disconnection and while some successful reinnervation occurs, NMJ loss continues and it is evident that with time compensatory sprouting is inadequate (Schaefer et al., 2005; Hegedus et al., 2007). The loss of motor units continues with age and is paralleled by reductions in whole muscle force (Hegedus et al., 2007). By the time the SOD1 mouse reaches the symptomatic stage, significant loss of MN within the ventral horn and behavioral assessments reveal functional motor impairments (Zang et al., 2005; Chiu et al., 1995; Fischer et al., 2004; Durand et al., 2006).

B. Conclusions

The die-back theory of ALS suggests that physical loss of target leads to subsequent MN degeneration. Early in adulthood, SOD1 mice reveal no differences in quantity, morphology, or functional abilities of the MN-muscular system. However, an undetermined pathological event results in MN die-back. Our initial studies were geared towards assessing the SOD1 MN reaction to axonal injury. We performed facial nerve axotomy within the pre-symptomatic stage, at an age where no indications of the die-back process are present within the facial motor nucleus (Niessen et al., 2006; Haenggeli and Kato, 2002). Axotomy-induced FMN death was dramatic compared to WT at 28 dpo (Mesnard et al., 2011). This loss of approximately 50% of FMN resembles the FMN survival seen in immunodeficient models, *Scid* and RAG-2 KO. Reconstitution of the immunodeficient mice prior to injury rescues this subpopulation of FMN to WT survival levels (Serpe et al., 2000). This rescue of FMN is achieved by functional $CD4^+$ T cells which play an important role in the mechanisms of immune-mediated neuroprotection (Serpe et al., 2003). However, the survival of this immune-dependent subpopulation of FMN is transient in both WT and reconstituted immunodeficient mice, and without target reconnection the MN are lost. The remaining subpopulation is termed the resilient-subpopulation. This subpopulation, present in WT and immunodeficient mice, is resistance to axotomy-induced cell death irrespective of immune or target connection (Jones et al., 2005). We have shown that the resilient-subpopulation is still maintained 26 weeks after axotomy (Beahrs, 2009).

FMN survival studies within this dissertation extended the time course following axotomy and revealed the presence of a resilient-subpopulation in the SOD1 facial nucleus that make up 45% of FMN. Reports within the literature of MN numbers within the lumbar and cervical spinal cord at end-stage support this finding and interestingly describe remaining MN levels at approximately 50% (Chiu et al., 1995; Zang et al., 2005; Fischer et al., 2004; Mancuso et al., 2011). Additionally, continued presence of the resilient-subpopulation insinuates that the initial axotomy-induced decrease in FMN is due to complete loss of the immune-dependent population. We have shown that the vulnerability of the immune-dependent subpopulation after axotomy in immunodeficient mice is due to a lack of neuroprotection mediated by the acquired immune system (Serpe et al., 2003). To date, there is no agreement within the literature of peripheral immune deficits with in the pre-symptomatic SOD1 mouse (Barbeito et al., 2010). However, our laboratory has been studying immune-mediated neuroprotection for the last decade and understands the level of complexity of the signaling between the injured CNS and the peripheral immune system resulting in neuroprotection. Therefore, we propose lack of sufficient neuroprotection within the SOD1 mice leads to increased axotomy-induced FMN loss.

To further investigate the susceptibility of SOD1 MN, we analyzed mRNA expression following axotomy of WT and pre-symptomatic SOD1 mice. Surprisingly, both WT and SOD1 FMN displayed a pro-survival/regenerative response, despite the dramatic SOD1 FMN loss. However, several differences were revealed during

comparisons of neuropil-specific genes. Additionally, the SOD1 control, uninjured facial nucleus revealed constitutive expression of TNFα (Mesnard et al., 2011). This constitutive expression was not seen within the WT control and is indicative of the presence of a pro-inflammatory microenvironment within the early pre-symptomatic stage. Therefore, we propose the increased susceptibility of SOD1 FMN cell death is not due to an aberrant MN response to injury, but the presence of a pro-inflammatory microenvironment within the pre-symptomatic stage and a dysregulation of the neuropil after injury results in the MN cell death. Our current working model of peripheral immune-mediated neuroprotection suggests that the glial cells play important roles in this communication between the acquired immune system and the injured neuron. Dysregulated glial cells may not be functioning in a manner conducive to mediating the signals from the periphery to the CNS and between the CNS to the MN.

Determining the dysfunction or deficit that leads to this lack of neuroprotection may rescue the immune-dependent FMN subpopulation, however, future directions are aimed at uncovering underlying mechanisms of MN degeneration that occur during disease progression. Validation is required to show that mechanisms mediating MN death and glial dysregulation that occur after axotomy resemble those mechanisms involved in or present during disease progression.

Almost all SOD1 research takes place either *in vitro* or within the spinal cord during the symptomatic stage. While these studies have obvious strengths, they also have disadvantages. Benefits of using facial nerve axotomy as opposed to the target

disconnection during disease progression allows; 1) initiation of target within a motor nucleus before it is affected by disease, i.e. controlled environment, 2) axotomy transects all axons at once, standardizing the disconnection in contrast to disease-induced target disconnection that occurs over time. Standardization not only allows assessment of molecular responses over time but also detection of initial and/or transient expression which would likely go undetected without the standardization, and 3) allows for comparisons to be made to between the SOD1 response compared to the WT response. Initiating disease-induced target disconnection in the WT lumbar spinal cord is not a realistic possibility. Therefore, responses in the SOD1 to the target disconnection during disease have no control to make comparisons.

The strengths of the facial nerve axotomy model have allowed us to begin initial investigation of dysregulation within the glial response, to identify mechanisms mediating MN degeneration and to determine potential factors involved in immune-mediated neuroprotection. While axotomy is a target disconnection, it is experimentally-induced and is not identical to the target disconnection that occurs during disease progression. Therefore, in order to validate facial nerve axotomy in the pre-symptomatic SOD1 as resembling disease progression, comparisons must be limited to the responses of the facial motor nuclei.

Therefore, t**he central hypothesis of the research presented in this dissertation is that the molecular response to axotomy in the pre-symptomatic SOD1 is similar to the molecular response to disease.**

Evidence exists, within the literature that target disconnection during disease resembles axotomy. Within the early pre-symptomatic stage partially occupied NMJs display fragmented axon tips resembling fragmentation seen during Wallerian degeneration and are not the characteristic morphology of naturally occurring synapse elimination (Schaefer et al., 2005; Keller-Peck et al., 2001). Following disease-induced target disconnection, there is a loss of upper MN synapses on lumbar MN, evidence of synaptic stripping that occurs following axotomy (Zang et al., 2005). There are many other aspects of disease progression that resemble axotomy, but it is difficult to be certain it is not an affect of other aspects of the disease.

This dissertation analyzed the axotomy-induced molecular expression of genes involved in MN-regeneration, neuroprotective signaling, death receptor signaling, and the glial cell response in WT and SOD1 mice. The initial mRNA expression response of 21 genes revealed that WT and SOD1 respond similarly to axotomy for nearly all genes analyzed. This finding was unexpected since more than half of these genes are involved death receptor signaling systems (TNFR1, TNFα, TRADD, TRAF2, SODD, Fas, FasL, Daxx ASK1, nNOS FADD, Caspase-3 and Caspase-8). Upregulation of these systems in WT after axotomy has not been shown previously. While mRNA for both systems is initially upregulated, genes involved in the Fas pathway display transient expression and return to baseline relatively quickly, suggesting a possible regulatory mechanism is present. There is no indication within the literature that facial nerve axotomy results in Fas-induced MN cell death. Studies using TNFR KO suggests MN cell death after facial nerve

axotomy involves the TNFR1 death pathway (Mesnard et al., 2010; Mesnard, 2009; Raivich et al., 2002). The upregulation of TNFR1 genes remain elevated during the delayed-response to axotomy, a time consistent with axotomy-induced cell death in the WT, and supports findings within the literature. Although unlike Fas, TNFR1 genes remain elevated for longer, they eventually return to baseline.

Death receptor gene expression for TNFR1 in the axotomized SOD1 facial nucleus was similar to WT. Although, comparable Fas signaling gene expression was seen initially seen in WT and SOD1, only the SOD1 facial nucleus revealed an upregulation during the delayed-response to axotomy. This delayed upregulation in the SOD1 is accompanied by the distinct amount of MN loss that occurs following axotomy. The literature reports that during SOD1 disease progression MN degeneration occurs via Fas-induced cell death (Raoul et al., 2006; Raoul et al., 2002; Xiong and McNamara, 2002). These results suggest that in the pre-symptomatic SOD1 axotomized facial nucleus Fas signaling genes are dysregulated and are suspected to be involved in the increased axotomy-induced FMN loss.

Genes specific to the glial response (GFAP and CD68) displayed a similar mRNA expression pattern between WT and SOD1, however the levels appear to be suppressed and remain at this low level. Therefore, the SOD1 astrocytes and microglia respond differently to injured MN. Astrocytes and microglia play important, well-defined roles in response to MN injury. Microglial responses include proliferation of endogenous microglia, displacement of synaptic terminals from the injured MN and phagocytosis of

neuronal debris following FMN death (Blinzinger and Kreutzberg, 1968; Graeber et al., 1988; Kreutzberg, 1996; Rinaman et al., 1991). After MN injury astrocytes become reactive, undergo hypertrophy and ensheath regenerating MN with their processes after microglia have removed synapses (Graeber and Kreutzberg, 1988). Additionally, activated microglia and reactive astrocytes secrete a variety of neurotrophic factors, such as growth factors and neurotrophic cytokines (Nakajima and Kohsaka, 2004; Streit, 2002; Liberto et al., 2004). Trophic factors are important in MN survival and enhanced secretion after neuronal injury suggests they are vital to injured MN. In vitro trophic factor withdrawal induces apoptosis in MN which can be inhibited by blocking the Fas pathway (Estevez et al., 1998; Raoul et al., 2002; Raoul et al., 2006). Further investigation will be performed to determine what effects this reduced glial-specific gene expression in the SOD1 facial nucleus is having on glial cell's ability to mediate neuroprotection.

WT and pre-symptomatic SOD1 MN respond similarly to axotomy with respect to MN-specific regenerative genes (GFAP and βII-Tubulin; Mesnard et al., 2011). Additional neuroprotective genes (CX3CR1, PAC1-R, TNFR2) analyzed within this dissertation include receptor systems used by injured MN to signal and communicate between other MN and glial cells (Re and Przedborski, 2006; Reglodi et al., 2011). While PAC1-R mRNA is localized to the MN, CX3CR1 and TNFR2 are expressed on microglia (Harrison et al., 1998; Hundhausen et al., 2003; Vaudry et al., 2000,). Similar expression of these receptors in SOD1 and WT may provide insights during further investigation of the SOD1

microglia response. In general, these results are evidence of the ability for SOD1 injured MN and perhaps microglia to express a regenerative/pro-survival phenotype and not only by upregulating genes directly involved in axon regeneration, but those involved in signaling among other neurons and glial cells.

The analysis of gene expression after axotomy in WT and pre-symptomatic SOD1 mice has provided a greater understanding of the molecular responses to MN injury and has uncovered several responses that appear to be dysregulated within the SOD1 mouse. Further investigation may determine mechanisms important in the increased susceptibility of SOD1 MN to axotomy. However, the purpose of investigating MN cell in SOD1 mice is ultimately not to understand the MN degeneration that occurs after axotomy, but that which occurs after target disconnection during disease progression. In order to conclude that the molecular response to experimentally-induced target disconnection is similar to the molecular response to disease-induced target disconnection, mRNA expression analysis was performed on the control, uninjured facial nucleus within the symptomatic stage.

It was determined through MN cell counts that within the symptomatic stage (112 doa), disease-induced FMN loss (40%) has occurred. This is the first report of FMN survival levels during the symptomatic stage, although it has been documented that MN levels reach approximately 50% by end-stage (Haenggeli and Kato, 2002; Niessen et al., 2006). Using SOD1 disease-affected, control facial motor nuclei, the relative mRNA

expression levels of the 21 genes were compared to the expression levels in WT control facial nuclei.

Results indicate that disease progression within the facial motor nucleus induces a similar molecular expression pattern to that seen after facial nerve axotomy in pre-symptomatic SOD1. All 21 genes were differentially regulated by axotomy in both WT and SOD1 mice, if not within the initial-response phase then within the delayed phase. More than half of all genes revealed expression levels that were consistent with those seen after axotomy in the pre-symptomatic SOD1 and, in particular, the delayed-response. As for many of the remaining genes additional time-points need to be assessed. mRNA levels after axotomy reveal dynamic patterns of expression over time. Confirmation that all genes are regulated by disease and axotomy in the same manner requires additional time points to capture the mRNA during its peak expression. Additionally, earlier time points were assessed but, they were within the pre-symptomatic stage and were used mainly to confirm and establish baseline levels of expression. For several genes these early time-points revealed increased expression and these genes can be considered as early markers of target disconnection or disease. Among these early responders, Fas and CD68 showed differences in expression levels over several earlier time-points. Interestingly, the mRNA expression levels over time coincide with an identical pattern of expression seen throughout the axotomy-induced expression pattern over time.

C. Summary

The mRNA expression results from this dissertation are in agreement with our previous findings that revealed a “regenerative-SOD1 MN” and a “dysregulated neuropil”. This dissertation identified that like SOD1 astrocytes, microglia show abnormal responses to axonal injury. In addition, increased molecular expression of death receptor genes is a reaction to MN injury in WT as well as in the SOD1. However, in comparison to WT these genes are dysregulated in the SOD1 axotomized facial nucleus, particularly the expression of Fas-associated genes which occurs at a time consistent with enhanced FMN loss. Increased mRNA expression was also seen in the SOD1 disease-affected nucleus during the symptomatic stage. This response of genes analyzed in this dissertation is in agreement with reports of their differential expression in ALS patients and SOD1 mice. Most importantly, the increased mRNA expression seen in the SOD1 disease-affected nucleus during the symptomatic stage is consistent with the mRNA expression response after axotomy in pre-symptomatic SOD1 mice. It has been well-established that target disconnection precedes MN degeneration in SOD1 mice and likely occurs in the ALS patient. This further validates the use of facial nerve axotomy in pre-symptomatic mice as an experimentally-induced target disconnection that resembles die-back during SOD1 disease progression. The work presented within this dissertation concludes that the molecular response within the SOD1 facial nucleus is similar regardless of the method MN injury (axotomy/disease) and therefore, allows for axotomy to be used in the pre-symptomatic mouse as a model of disease progression.

D. Significance

This validation of facial nerve axotomy in the pre-symptomatic SOD1 mouse as a model for disease progression will likely have significant impact within the field of ALS research. The advantages of the facial nerve axotomy model have been exploited for many years in the field of peripheral nerve injury and those strengths of the facial nerve axotomy will prove invaluable for investigating molecular mechanisms of the disease and identification of checkpoints for therapeutic intervention. This model will also be beneficial during assessment of therapeutic compounds and treatments. Their effects on the molecular mechanisms and FMN survival can provide details on mechanism of actions and beneficial properties.

E. Future Directions

It is likely that the molecular response to disease is truly the response to target disconnection and subsequent die-back, but requires further investigation for validation. Future analysis of NMJ loss within muscles innervated by the facial nucleus, such as the auricular and nasolabial musculature, will be performed to confirm NMJ loss precedes FMN loss.

The use of facial nerve axotomy within pre-symptomatic mice has already proven to be a valuable tool in uncovering potential mechanisms involved in response to injury and MN survival in WT and in SOD1 mice. Several potential mechanisms were uncovered within this dissertation. Future studies will be designed to further understand the mechanisms of immune-mediated neuroprotection. While some of the

peripheral immune components and mechanisms have been identified using the RAG-2 KO, information regarding the CNS molecular response to injury has not. Previous findings and the results within this dissertation have identified several aspects of the molecular response to injury both in the WT and in the SOD1. Future studies will combine WT, RAG-2 KO, SOD1 and use facial nerve axotomy as well as LMD to assess molecular responses to injury. Reconstitutions to modify the peripheral immune system, and a variety of techniques will be used to profile the peripheral immune cell within the pre-symptomatic SOD1 (**Figure 131**). The molecular response to axotomy in WT, RAG-2 KO, reconstituted RAG-2 KO, and SOD1 mice will be compared and differences will help identify how neuroprotection is mediated from peripheral $CD4^+$ T cell to injured MN.

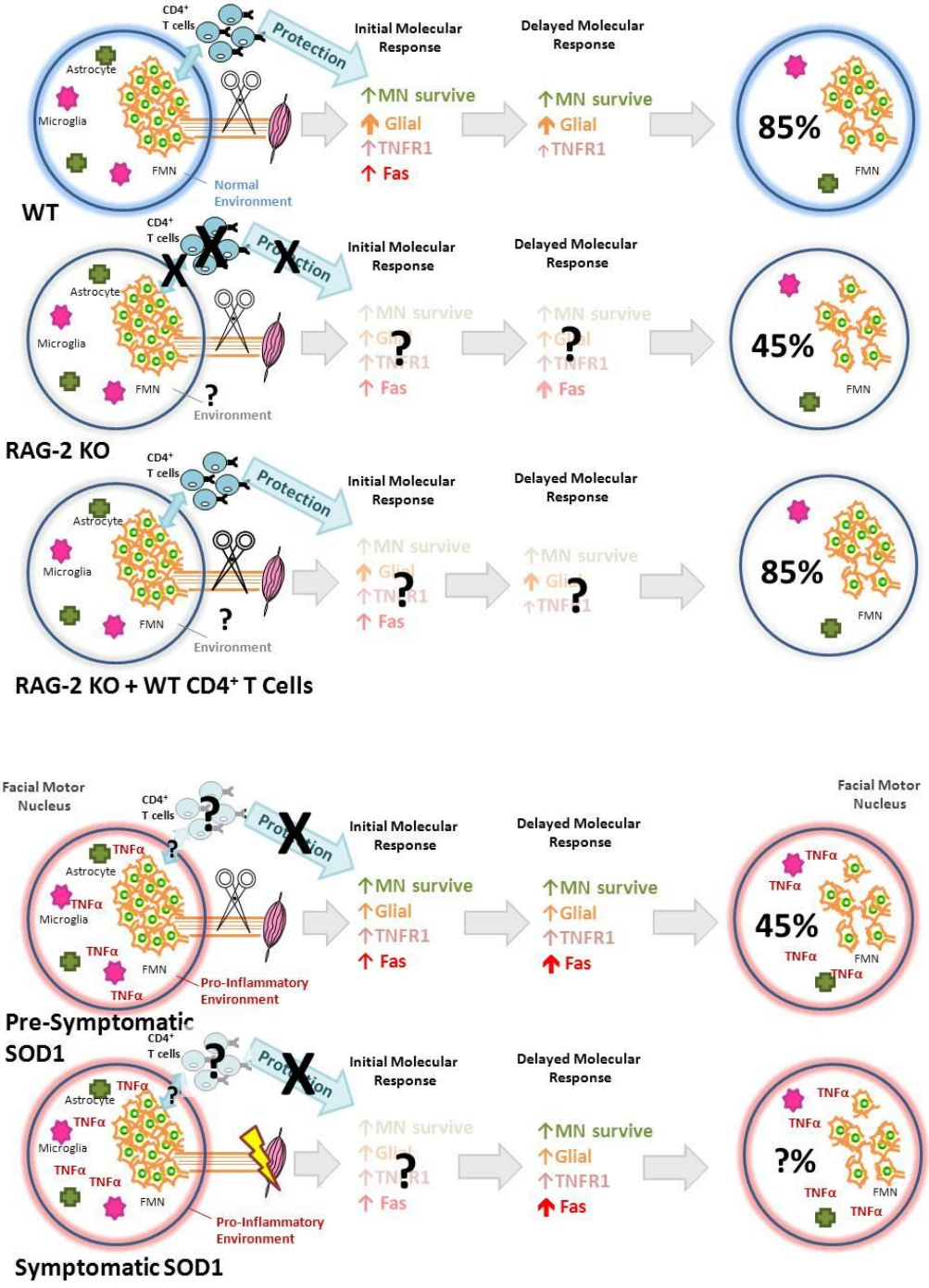

Figure 131: Future directions to identify molecular mechanisms in immune-mediated neuroprotection.

REFERENCE

Alabed, Y.Z., Pool, M., Ong Tone, S., and Fournier, A.E. (2007). Identification of CRMP4 as a convergent regulator of axon outgrowth inhibition. The Journal of neuroscience : the official journal of the Society for Neuroscience *27*, 1702-1711.

Ando, Y., Liang, Y., Ishigaki, S., Niwa, J., Jiang, Y., Kobayashi, Y., Yamamoto, M., Doyu, M., and Sobue, G. (2003). Caspase-1 and -3 mRNAs are differentially upregulated in motor neurons and glial cells in mutant SOD1 transgenic mouse spinal cord: a study using laser microdissection and real-time RT-PCR. Neurochemical research *28*, 839-846.

Armstrong, B.D., Abad, C., Chhith, S., Cheung-Lau, G., Hajji, O.E., Nobuta, H., and Waschek, J.A. (2008). Impaired nerve regeneration and enhanced neuroinflammatory response in mice lacking pituitary adenylyl cyclase activating peptide. Neuroscience *151*, 63-73.

Ashwell, K.W. (1982). The adult mouse facial nerve nucleus: morphology and musculotopic organization. Journal of anatomy *135*, 531-538.

Barbeito, A.G., Mesci, P., and Boillee, S. (2010). Motor neuron-immune interactions: the vicious circle of ALS. J Neural Transm *117*, 981-1000.

Beahrs, T., Tanzer, L., Sanders, V.M., and Jones, K.J. (2010). Functional recovery and facial motoneuron survival are influenced by immunodeficiency in crush-axotomized mice. Experimental neurology *221*, 225-230.

Beahrs, T.R. (2009). Facial Motorneuron Survival and Functional Recovery After Facial Nerve Axotomy: Effects of Time, Type of Injury, and Immunodeficiency. In Cell Biology, Neurobiology and Anatomy (Loyola University Chicago), p. 100.

Beer, R., Franz, G., Schopf, M., Reindl, M., Zelger, B., Schmutzhard, E., Poewe, W., and Kampfl, A. (2000). Expression of Fas and Fas ligand after experimental traumatic brain injury in the rat. J Cereb Blood Flow Metab *20*, 669-677.

Beers, D.R., Zhao, W., Liao, B., Kano, O., Wang, J., Huang, A., Appel, S.H., and Henkel, J.S. (2011). Neuroinflammation modulates distinct regional and temporal clinical responses in ALS mice. Brain, behavior, and immunity *25*, 1025-1035.

Beleza-Meireles, A., and Al-Chalabi, A. (2009). Genetic studies of amyotrophic lateral sclerosis: controversies and perspectives. Amyotrophic lateral sclerosis : official publication of the World Federation of Neurology Research Group on Motor Neuron Diseases *10*, 1-14.

Bilsland, L.G., Sahai, E., Kelly, G., Golding, M., Greensmith, L., and Schiavo, G. (2010). Deficits in axonal transport precede ALS symptoms in vivo. Proceedings of the National Academy of Sciences of the United States of America *107*, 20523-20528.

Blinzinger, K., and Kreutzberg, G. (1968). Displacement of synaptic terminals from regenerating motoneurons by microglial cells. Z Zellforsch Mikrosk Anat *85*, 145-157.

Boatright, K.M., and Salvesen, G.S. (2003). Mechanisms of caspase activation. Curr Opin Cell Biol *15*, 725-731.

Bohatschek, M., Kloss, C.U., Hristova, M., Pfeffer, K., and Raivich, G. (2004). Microglial major histocompatibility complex glycoprotein-1 in the axotomized facial motor nucleus: regulation and role of tumor necrosis factor receptors 1 and 2. The Journal of comparative neurology *470*, 382-399.

Borchelt, D.R., Guarnieri, M., Wong, P.C., Lee, M.K., Slunt, H.S., Xu, Z.S., Sisodia, S.S., Price, D.L., and Cleveland, D.W. (1995). Superoxide dismutase 1 subunits with mutations linked to familial amyotrophic lateral sclerosis do not affect wild-type subunit function. The Journal of biological chemistry *270*, 3234-3238.

Borchelt, D.R., Lee, M.K., Slunt, H.S., Guarnieri, M., Xu, Z.S., Wong, P.C., Brown, R.H., Jr., Price, D.L., Sisodia, S.S., and Cleveland, D.W. (1994). Superoxide dismutase 1 with mutations linked to familial amyotrophic lateral sclerosis possesses significant activity. Proceedings of the National Academy of Sciences of the United States of America *91*, 8292-8296.

Bruijn, L.I., Miller, T.M., and Cleveland, D.W. (2004). Unraveling the mechanisms involved in motor neuron degeneration in ALS. Annual review of neuroscience *27*, 723-749.

Brum, J.A. (1991). Electronic properties of quantum-dot superlattices. Physical review. B, Condensed matter *43*, 12082-12085.

Cammermeyer, J. (1963). Peripheral Chromatolysis after Transection of Mouse Facial Nerve. Acta neuropathologica *3*, 213-230.

Canh, M.Y., Serpe, C.J., Sanders, V., and Jones, K.J. (2006). CD4(+) T cell-mediated facial motoneuron survival after injury: Distribution pattern of cell death and rescue throughout the extent of the facial motor nucleus. Journal of neuroimmunology *181*, 93-99.

Cardona, A.E., Pioro, E.P., Sasse, M.E., Kostenko, V., Cardona, S.M., Dijkstra, I.M., Huang, D., Kidd, G., Dombrowski, S., Dutta, R.*, et al.* (2006). Control of microglial neurotoxicity by the fractalkine receptor. Nature neuroscience *9*, 917-924.

Cereda, C., Baiocchi, C., Bongioanni, P., Cova, E., Guareschi, S., Metelli, M.R., Rossi, B., Sbalsi, I., Cuccia, M.C., and Ceroni, M. (2008). TNF and sTNFR1/2 plasma levels in ALS patients. Journal of neuroimmunology *194*, 123-131.

Chapman, G.A., Moores, K., Harrison, D., Campbell, C.A., Stewart, B.R., and Strijbos, P.J. (2000). Fractalkine cleavage from neuronal membranes represents an acute event in the inflammatory response to excitotoxic brain damage. The Journal of neuroscience : the official journal of the Society for Neuroscience *20*, RC87.

Chen, L.C., Smith, A., Ben, Y., Zukic, B., Ignacio, S., Moore, D., and Lee, N. (2004). Temporal gene expression patterns in G93A/SOD1 mouse. Amyotrophic lateral sclerosis and other motor neuron disorders : official publication of the World Federation of Neurology, Research Group on Motor Neuron Diseases *5*, 164-171.

Chiu, A.Y., Zhai, P., Dal Canto, M.C., Peters, T.M., Kwon, Y.W., Prattis, S.M., and Gurney, M.E. (1995). Age-dependent penetrance of disease in a transgenic mouse model of familial amyotrophic lateral sclerosis. Molecular and cellular neurosciences *6*, 349-362.

Choi, C., and Benveniste, E.N. (2004). Fas ligand/Fas system in the brain: regulator of immune and apoptotic responses. Brain research. Brain research reviews *44*, 65-81.

Coggeshall, R.E. (1992). A consideration of neural counting methods. Trends in neurosciences *15*, 9-13.

Combs, D.J., and D'Alecy, L.G. (1987). Motor performance in rats exposed to severe forebrain ischemia: effect of fasting and 1,3-butanediol. Stroke; a journal of cerebral circulation *18*, 503-511.

Cozzolino, M., Ferri, A., and Carri, M.T. (2008). Amyotrophic lateral sclerosis: from current developments in the laboratory to clinical implications. Antioxidants & redox signaling *10*, 405-443.

Culpan, D., Cram, D., Chalmers, K., Cornish, A., Palmer, L., Palmer, J., Hughes, A., Passmore, P., Craig, D., Wilcock, G.K.*, et al.* (2009). TNFR-associated factor-2 (TRAF-2) in Alzheimer's disease. Neurobiology of aging *30*, 1052-1060.

Dadon-Nachum, M., Melamed, E., and Offen, D. (2011). The "dying-back" phenomenon of motor neurons in ALS. Journal of molecular neuroscience : MN *43*, 470-477.

Dal Canto, M.C., and Gurney, M.E. (1995). Neuropathological changes in two lines of mice carrying a transgene for mutant human Cu,Zn SOD, and in mice overexpressing wild type human SOD: a model of familial amyotrophic lateral sclerosis (FALS). Brain research *676*, 25-40.

DePaul, R., Abbs, J.H., Caligiuri, M., Gracco, V.L., and Brooks, B.R. (1988). Hypoglossal, trigeminal, and facial motoneuron involvement in amyotrophic lateral sclerosis. Neurology *38*, 281-283.

Dissing-Olesen, L., Ladeby, R., Nielsen, H.H., Toft-Hansen, H., Dalmau, I., and Finsen, B. (2007). Axonal lesion-induced microglial proliferation and microglial cluster formation in the mouse. Neuroscience *149*, 112-122.

Duplan, L., Bernard, N., Casseron, W., Dudley, K., Thouvenot, E., Honnorat, J., Rogemond, V., De Bovis, B., Aebischer, P., Marin, P.*, et al.* (2010). Collapsin response mediator protein 4a (CRMP4a) is upregulated in motoneurons of mutant SOD1 mice and can trigger motoneuron axonal degeneration and cell death. The Journal of neuroscience : the official journal of the Society for Neuroscience *30*, 785-796.

Durand, J., Amendola, J., Bories, C., and Lamotte d'Incamps, B. (2006). Early abnormalities in transgenic mouse models of amyotrophic lateral sclerosis. Journal of physiology, Paris *99*, 211-220.

Elliott, J.L. (2001). Cytokine upregulation in a murine model of familial amyotrophic lateral sclerosis. Brain research. Molecular brain research *95*, 172-178.

Estevez, A.G., Spear, N., Manuel, S.M., Barbeito, L., Radi, R., and Beckman, J.S. (1998). Role of endogenous nitric oxide and peroxynitrite formation in the survival and death of motor neurons in culture. Progress in brain research *118*, 269-280.

Facchinetti, F., Sasaki, M., Cutting, F.B., Zhai, P., MacDonald, J.E., Reif, D., Beal, M.F., Huang, P.L., Dawson, T.M., Gurney, M.E.*, et al.* (1999). Lack of involvement of neuronal nitric oxide synthase in the pathogenesis of a transgenic mouse model of familial amyotrophic lateral sclerosis. Neuroscience *90*, 1483-1492.

Fargo, K.N., Alexander, T.D., Tanzer, L., Poletti, A., and Jones, K.J. (2008). Androgen regulates neuritin mRNA levels in an in vivo model of steroid-enhanced peripheral nerve regeneration. Journal of neurotrauma *25*, 561-566.

Feeney, D.M., Gonzalez, A., and Law, W.A. (1982). Amphetamine, haloperidol, and experience interact to affect rate of recovery after motor cortex injury. Science *217*, 855-857.

Felice, K.J. (1997). A longitudinal study comparing thenar motor unit number estimates to other quantitative tests in patients with amyotrophic lateral sclerosis. Muscle & nerve *20*, 179-185.

Feng, H.L., Leng, Y., Ma, C.H., Zhang, J., Ren, M., and Chuang, D.M. (2008). Combined lithium and valproate treatment delays disease onset, reduces neurological deficits and prolongs survival in an amyotrophic lateral sclerosis mouse model. Neuroscience *155*, 567-572.

Fischer, L.R., Culver, D.G., Tennant, P., Davis, A.A., Wang, M., Castellano-Sanchez, A., Khan, J., Polak, M.A., and Glass, J.D. (2004). Amyotrophic lateral sclerosis is a distal axonopathy: evidence in mice and man. Experimental neurology *185*, 232-240.

Forman, H.J., and Fridovich, I. (1973). On the stability of bovine superoxide dismutase. The effects of metals. The Journal of biological chemistry *248*, 2645-2649.

Frey, D., Schneider, C., Xu, L., Borg, J., Spooren, W., and Caroni, P. (2000). Early and selective loss of neuromuscular synapse subtypes with low sprouting competence in motoneuron diseases. The Journal of neuroscience : the official journal of the Society for Neuroscience *20*, 2534-2542.

Fu, S.Y., and Gordon, T. (1997). The cellular and molecular basis of peripheral nerve regeneration. Molecular neurobiology *14*, 67-116.

George, A., Buehl, A., and Sommer, C. (2005). Tumor necrosis factor receptor 1 and 2 proteins are differentially regulated during Wallerian degeneration of mouse sciatic nerve. Experimental neurology *192*, 163-166.

Gordon, R.D., Simpson, E., and Samelson, L.E. (1975). In vitro cell-mediated immune responses to the male specific(H-Y) antigen in mice. The Journal of experimental medicine *142*, 1108-1120.

Graeber, M.B., and Kreutzberg, G.W. (1988). Delayed astrocyte reaction following facial nerve axotomy. Journal of neurocytology *17*, 209-220.

Graeber, M.B., Streit, W.J., Kiefer, R., Schoen, S.W., and Kreutzberg, G.W. (1990). New expression of myelomonocytic antigens by microglia and perivascular cells following lethal motor neuron injury. Journal of neuroimmunology *27*, 121-132.

Graeber, M.B., Tetzlaff, W., Streit, W.J., and Kreutzberg, G.W. (1988). Microglial cells but not astrocytes undergo mitosis following rat facial nerve axotomy. Neuroscience letters *85*, 317-321.

Grivennikov, S.I., Kuprash, D.V., Liu, Z.G., and Nedospasov, S.A. (2006). Intracellular signals and events activated by cytokines of the tumor necrosis factor superfamily: From simple paradigms to complex mechanisms. Int Rev Cytol *252*, 129-161.

Guntinas-Lichius, O., Neiss, W.F., Schulte, E., and Stennert, E. (1996). Quantitative image analysis of the chromatolysis in rat facial and hypoglossal motoneurons following axotomy with and without reinnervation. Cell and tissue research *286*, 537-541.

Gurney, M.E., Pu, H., Chiu, A.Y., Dal Canto, M.C., Polchow, C.Y., Alexander, D.D., Caliendo, J., Hentati, A., Kwon, Y.W., Deng, H.X*., et al.* (1994). Motor neuron degeneration in mice that express a human Cu,Zn superoxide dismutase mutation. Science *264*, 1772-1775.

Haase, G., Pettmann, B., Raoul, C., and Henderson, C.E. (2008). Signaling by death receptors in the nervous system. Curr Opin Neurobiol *18*, 284-291.

Haenggeli, C., and Kato, A.C. (2002). Differential vulnerability of cranial motoneurons in mouse models with motor neuron degeneration. Neuroscience letters *335*, 39-43.

Hailer, N.P., Grampp, A., and Nitsch, R. (1999). Proliferation of microglia and astrocytes in the dentate gyrus following entorhinal cortex lesion: a quantitative bromodeoxyuridine-labelling study. The European journal of neuroscience *11*, 3359-3364.

Harrison, J.K., Jiang, Y., Chen, S., Xia, Y., Maciejewski, D., McNamara, R.K., Streit, W.J., Salafranca, M.N., Adhikari, S., Thompson, D.A*., et al.* (1998). Role for neuronally derived fractalkine in mediating interactions between neurons and CX3CR1-expressing microglia. Proceedings of the National Academy of Sciences of the United States of America *95*, 10896-10901.

Hashiguchi, K., Wada, H., Yamada, O., Yawata, Y., Yoshida, K., Okimoto, J., Umeki, S., Niki, Y., and Soejima, R. (1992). [A case of chronic myelogenous leukemia with pulmonary aspergillosis diagnosed by the detection of circulating Aspergillus antigen]. Kansenshogaku zasshi. The Journal of the Japanese Association for Infectious Diseases *66*, 1592-1596.

Hegedus, J., Putman, C.T., and Gordon, T. (2007). Time course of preferential motor unit loss in the SOD1 G93A mouse model of amyotrophic lateral sclerosis. Neurobiology of disease *28*, 154-164.

Hensley, K., Fedynyshyn, J., Ferrell, S., Floyd, R.A., Gordon, B., Grammas, P., Hamdheydari, L., Mhatre, M., Mou, S., Pye, Q.N*., et al.* (2003). Message and protein-level elevation of tumor necrosis factor alpha (TNF alpha) and TNF alpha-modulating cytokines in spinal cords of the G93A-SOD1 mouse model for amyotrophic lateral sclerosis. Neurobiology of disease *14*, 74-80.

Hensley, K., Floyd, R.A., Gordon, B., Mou, S., Pye, Q.N., Stewart, C., West, M., and Williamson, K. (2002). Temporal patterns of cytokine and apoptosis-related gene expression in spinal cords of the G93A-SOD1 mouse model of amyotrophic lateral sclerosis. Journal of neurochemistry *82*, 365-374.

Hoffman, P.N., and Cleveland, D.W. (1988). Neurofilament and tubulin expression recapitulates the developmental program during axonal regeneration: induction of a specific beta-tubulin isotype. Proceedings of the National Academy of Sciences of the United States of America *85*, 4530-4533.

Holness, C.L., and Simmons, D.L. (1993). Molecular cloning of CD68, a human macrophage marker related to lysosomal glycoproteins. Blood *81*, 1607-1613.

Hu, J.H., Chernoff, K., Pelech, S., and Krieger, C. (2003). Protein kinase and protein phosphatase expression in the central nervous system of G93A mSOD over-expressing mice. J Neurochem *85*, 422-431.

Hundhausen, C., Misztela, D., Berkhout, T.A., Broadway, N., Saftig, P., Reiss, K., Hartmann, D., Fahrenholz, F., Postina, R., Matthews, V.*, et al.* (2003). The disintegrin-like metalloproteinase ADAM10 is involved in constitutive cleavage of CX3CL1 (fractalkine) and regulates CX3CL1-mediated cell-cell adhesion. Blood *102*, 1186-1195.

Ikeda, K., Aoki, M., Kawazoe, Y., Sakamoto, T., Hayashi, Y., Ishigaki, A., Nagai, M., Kamii, R., Kato, S., Itoyama, Y.*, et al.* (2005). Motoneuron degeneration after facial nerve avulsion is exacerbated in presymptomatic transgenic rats expressing human mutant Cu/Zn superoxide dismutase. Journal of neuroscience research *82*, 63-70.

Ikemoto, A., Hirano, A., and Akiguchi, I. (1999). Increased expression of growth-associated protein 43 on the surface of the anterior horn cells in amyotrophic lateral sclerosis. Acta neuropathologica *98*, 367-373.

Jones, K.J., and Oblinger, M.M. (1994). Androgenic regulation of tubulin gene expression in axotomized hamster facial motoneurons. The Journal of neuroscience : the official journal of the Society for Neuroscience *14*, 3620-3627.

Jones, K.J., Serpe, C.J., Byram, S.C., Deboy, C.A., and Sanders, V.M. (2005). Role of the immune system in the maintenance of mouse facial motoneuron viability after nerve injury. Brain, behavior, and immunity *19*, 12-19.

Jones, K.J., Storer, P.D., Drengler, S.M., and Oblinger, M.M. (1999). Differential regulation of cytoskeletal gene expression in hamster facial motoneurons: effects of axotomy and testosterone treatment. Journal of neuroscience research *57*, 817-823.

Jones, L.L., Banati, R.B., Graeber, M.B., Bonfanti, L., Raivich, G., and Kreutzberg, G.W. (1997). Population control of microglia: does apoptosis play a role? Journal of neurocytology *26*, 755-770.

Jonsson, P.A., Graffmo, K.S., Andersen, P.M., Brannstrom, T., Lindberg, M., Oliveberg, M., and Marklund, S.L. (2006). Disulphide-reduced superoxide dismutase-1 in CNS of transgenic amyotrophic lateral sclerosis models. Brain : a journal of neurology *129*, 451-464.

Kage, M., Ikemoto, A., Akiguchi, I., Kimura, J., Matsumoto, S., Kimura, H., and Tooyama, I. (1998). Primary structure of GAP-43 mRNA expressed in the spinal cord of ALS patients. Neuroreport *9*, 1403-1406.

Kamel, F., Umbach, D.M., Munsat, T.L., Shefner, J.M., and Sandler, D.P. (1999). Association of cigarette smoking with amyotrophic lateral sclerosis. Neuroepidemiology *18*, 194-202.

Kee, N.J., Preston, E., and Wojtowicz, J.M. (2001). Enhanced neurogenesis after transient global ischemia in the dentate gyrus of the rat. Experimental brain research. Experimentelle Hirnforschung. Experimentation cerebrale *136*, 313-320.

Keller-Peck, C.R., Walsh, M.K., Gan, W.B., Feng, G., Sanes, J.R., and Lichtman, J.W. (2001). Asynchronous synapse elimination in neonatal motor units: studies using GFP transgenic mice. Neuron *31*, 381-394.

Kou, S.Y., Chiu, A.Y., and Patterson, P.H. (1995). Differential regulation of motor neuron survival and choline acetyltransferase expression following axotomy. Journal of neurobiology *27*, 561-572.

Kraemer, M., Buerger, M., and Berlit, P. (2010). Diagnostic problems and delay of diagnosis in amyotrophic lateral sclerosis. Clinical neurology and neurosurgery *112*, 103-105.

Kreutzberg, G.W. (1996). Microglia: a sensor for pathological events in the CNS. Trends in neurosciences *19*, 312-318.

Kurobe, N., Suzuki, F., Okajima, K., and Kato, K. (1990). Sensitive enzyme immunoassay for human Cu/Zn superoxide dismutase. Clinica chimica acta; international journal of clinical chemistry *187*, 11-20.

Larsen, J.O., Hannibal, J., Knudsen, S.M., and Fahrenkrug, J. (1997). Expression of pituitary adenylate cyclase-activating polypeptide (PACAP) in the mesencephalic trigeminal nucleus of the rat after transsection of the masseteric nerve. Brain research. Molecular brain research *46*, 109-117.

Laskawi, R., and Wolff, J.R. (1996). Changes in glial fibrillary acidic protein immunoreactivity in the rat facial nucleus following various types of nerve lesions. Eur Arch Otorhinolaryngol *253*, 475-480.

Lemstra, A.W., Groen in't Woud, J.C., Hoozemans, J.J., van Haastert, E.S., Rozemuller, A.J., Eikelenboom, P., and van Gool, W.A. (2007). Microglia activation in sepsis: a case-control study. Journal of neuroinflammation *4*, 4.

Li, M., Ona, V.O., Guegan, C., Chen, M., Jackson-Lewis, V., Andrews, L.J., Olszewski, A.J., Stieg, P.E., Lee, J.P., Przedborski, S.*, et al.* (2000). Functional role of caspase-1 and caspase-3 in an ALS transgenic mouse model. Science *288*, 335-339.

Liberto, C.M., Albrecht, P.J., Herx, L.M., Yong, V.W., and Levison, S.W. (2004). Pro-regenerative properties of cytokine-activated astrocytes. Journal of neurochemistry *89*, 1092-1100.

Lieberman, A.R. (1971). The axon reaction: a review of the principal features of perikaryal responses to axon injury. International review of neurobiology *14*, 49-124.

Liu, P.C., Yang, Z.J., Qiu, M.H., Zhang, L.M., and Sun, F.Y. (2003). Induction of CRMP-4 in striatum of adult rat after transient brain ischemia. Acta pharmacologica Sinica *24*, 1205-1211.

Livak, K.J., and Schmittgen, T.D. (2001). Analysis of relative gene expression data using real-time quantitative PCR and the 2(-Delta Delta C(T)) Method. Methods *25*, 402-408.

Locatelli, F., Corti, S., Papadimitriou, D., Fortunato, F., Del Bo, R., Donadoni, C., Nizzardo, M., Nardini, M., Salani, S., Ghezzi, S.*, et al.* (2007). Fas small interfering RNA reduces motoneuron death in amyotrophic lateral sclerosis mice. Ann Neurol *62*, 81-92.

Maciejewski-Lenoir, D., Chen, S., Feng, L., Maki, R., and Bacon, K.B. (1999). Characterization of fractalkine in rat brain cells: migratory and activation signals for CX3CR-1-expressing microglia. J Immunol *163*, 1628-1635.

Malaspina, A., and de Belleroche, J. (2004). Spinal cord molecular profiling provides a better understanding of amyotrophic lateral sclerosis pathogenesis. Brain research. Brain research reviews *45*, 213-229.

Mancuso, R., Santos-Nogueira, E., Osta, R., and Navarro, X. (2011). Electrophysiological analysis of a murine model of motoneuron disease. Clinical neurophysiology : official journal of the International Federation of Clinical Neurophysiology *122*, 1660-1670.

Marcuzzo, S., Zucca, I., Mastropietro, A., de Rosbo, N.K., Cavalcante, P., Tartari, S., Bonanno, S., Preite, L., Mantegazza, R., and Bernasconi, P. (2011). Hind limb muscle atrophy precedes cerebral neuronal degeneration in G93A-SOD1 mouse model of amyotrophic lateral sclerosis: A longitudinal MRI study. Experimental neurology *231*, 30-37.

Mariotti, R., Cristino, L., Bressan, C., Boscolo, S., and Bentivoglio, M. (2002). Altered reaction of facial motoneurons to axonal damage in the presymptomatic phase of a murine model of familial amyotrophic lateral sclerosis. Neuroscience *115*, 331-335.

Martin, D., Thompson, M.A., and Nadler, J.V. (1993). The neuroprotective agent riluzole inhibits release of glutamate and aspartate from slices of hippocampal area CA1. European journal of pharmacology *250*, 473-476.

Martin, L.J. (2007). Transgenic mice with human mutant genes causing Parkinson's disease and amyotrophic lateral sclerosis provide common insight into mechanisms of motor neuron selective vulnerability to degeneration. Reviews in the neurosciences *18*, 115-136.

McCoy, M.K., and Tansey, M.G. (2008). TNF signaling inhibition in the CNS: implications for normal brain function and neurodegenerative disease. Journal of neuroinflammation *5*, 45.

McPhail, L.T., McBride, C.B., McGraw, J., Steeves, J.D., and Tetzlaff, W. (2004). Axotomy abolishes NeuN expression in facial but not rubrospinal neurons. Experimental neurology *185*, 182-190.

Mesnard, N.A. (2009). A Model for the Investigation of Regenerative or Degenerative Motorneurons and Neuropil: Relevance to Injury and ALS. In Neuroscience (Loyola University Chicago), p. 186.

Mesnard, N.A., Alexander, T.D., Sanders, V.M., and Jones, K.J. (2010). Use of laser microdissection in the investigation of facial motoneuron and neuropil molecular phenotypes after peripheral axotomy. Experimental neurology *225*, 94-103.

Mesnard, N.A., Sanders, V.M., and Jones, K.J. (2011). Differential gene expression in the axotomized facial motor nucleus of pre-symptomatic SOD1 mice. The Journal of comparative neurology.

Miyazaki, K., Nagai, M., Morimoto, N., Kurata, T., Takehisa, Y., Ikeda, Y., and Abe, K. (2009). Spinal anterior horn has the capacity to self-regenerate in amyotrophic lateral sclerosis model mice. Journal of neuroscience research *87*, 3639-3648.

Moller, K., Reimer, M., Hannibal, J., Fahrenkrug, J., Sundler, F., and Kanje, M. (1997). Pituitary adenylate cyclase-activating peptide (PACAP) and PACAP type 1 receptor expression in regenerating adult mouse and rat superior cervical ganglia in vitro. Brain research *775*, 156-165.

Moran, L.B., and Graeber, M.B. (2004). The facial nerve axotomy model. Brain research. Brain research reviews *44*, 154-178.

Moskowitz, P.F., and Oblinger, M.M. (1995). Transcriptional and post-transcriptional mechanisms regulating neurofilament and tubulin gene expression during normal development of the rat brain. Brain research. Molecular brain research *30*, 211-222.

Mulder, D.W., Kurland, L.T., Offord, K.P., and Beard, C.M. (1986). Familial adult motor neuron disease: amyotrophic lateral sclerosis. Neurology *36*, 511-517.

Mullen, R.J., Buck, C.R., and Smith, A.M. (1992). NeuN, a neuronal specific nuclear protein in vertebrates. Development *116*, 201-211.

Naganska, E., and Matyja, E. (2011). Amyotrophic lateral sclerosis - looking for pathogenesis and effective therapy. Folia neuropathologica / Association of Polish Neuropathologists and Medical Research Centre, Polish Academy of Sciences *49*, 1-13.

Nakajima, K., and Kohsaka, S. (2004). Microglia: neuroprotective and neurotrophic cells in the central nervous system. Current drug targets. Cardiovascular & haematological disorders *4*, 65-84.

Netter, F.H. (1987). The Netter Collection of Medical Illustrations - Nervous System Part II - Neurologic and Neuromuscular Disorders (W B Saunders Co).

Netter, F.H. (1991). Nervous System, Part 1: Anatomy and Physiology (Ciba Collection of Medical Illustrations, Volume 1) (Ciba-Geigy Corporation).

Niessen, H.G., Angenstein, F., Sander, K., Kunz, W.S., Teuchert, M., Ludolph, A.C., Heinze, H.J., Scheich, H., and Vielhaber, S. (2006). In vivo quantification of spinal and bulbar motor neuron degeneration in the G93A-SOD1 transgenic mouse model of ALS by T2 relaxation time and apparent diffusion coefficient. Experimental neurology *201*, 293-300.

Novo, E., and Parola, M. (2008). Redox mechanisms in hepatic chronic wound healing and fibrogenesis. Fibrogenesis Tissue Repair *1*, 5.

Okado-Matsumoto, A., and Fridovich, I. (2001). Subcellular distribution of superoxide dismutases (SOD) in rat liver: Cu,Zn-SOD in mitochondria. The Journal of biological chemistry *276*, 38388-38393.

Pardo, C.A., Xu, Z., Borchelt, D.R., Price, D.L., Sisodia, S.S., and Cleveland, D.W. (1995). Superoxide dismutase is an abundant component in cell bodies, dendrites, and axons of motor neurons and in a subset of other neurons. Proceedings of the National Academy of Sciences of the United States of America *92*, 954-958.

Parhad, I.M., Oishi, R., and Clark, A.W. (1992). GAP-43 gene expression is increased in anterior horn cells of amyotrophic lateral sclerosis. Annals of neurology *31*, 593-597.

Pelvig, D.P., Pakkenberg, H., Stark, A.K., and Pakkenberg, B. (2008). Neocortical glial cell numbers in human brains. Neurobiology of aging *29*, 1754-1762.

Powrie, F., and Mason, D. (1989). Subsets of rat CD4+ T cells express different variants of the leukocyte-common antigen: functions and developmental relationships of the subsets. Journal of autoimmunity *2 Suppl*, 25-32.

Raivich, G., Jones, L.L., Kloss, C.U., Werner, A., Neumann, H., and Kreutzberg, G.W. (1998). Immune surveillance in the injured nervous system: T-lymphocytes invade the axotomized mouse facial motor nucleus and aggregate around sites of neuronal degeneration. The Journal of neuroscience : the official journal of the Society for Neuroscience *18*, 5804-5816.

Raivich, G., Liu, Z.Q., Kloss, C.U., Labow, M., Bluethmann, H., and Bohatschek, M. (2002). Cytotoxic potential of proinflammatory cytokines: combined deletion of TNF receptors TNFR1 and TNFR2 prevents motoneuron cell death after facial axotomy in adult mouse. Experimental neurology *178*, 186-193.

Raoul, C., Buhler, E., Sadeghi, C., Jacquier, A., Aebischer, P., Pettmann, B., Henderson, C.E., and Haase, G. (2006). Chronic activation in presymptomatic amyotrophic lateral sclerosis (ALS) mice of a feedback loop involving Fas, Daxx, and FasL. Proceedings of the National Academy of Sciences of the United States of America *103*, 6007-6012.

Raoul, C., Estevez, A.G., Nishimune, H., Cleveland, D.W., deLapeyriere, O., Henderson, C.E., Haase, G., and Pettmann, B. (2002). Motoneuron death triggered by a specific pathway downstream of Fas. potentiation by ALS-linked SOD1 mutations. Neuron *35*, 1067-1083.

Re, D.B., and Przedborski, S. (2006). Fractalkine: moving from chemotaxis to neuroprotection. Nature neuroscience *9*, 859-861.

Reaume, A.G., Elliott, J.L., Hoffman, E.K., Kowall, N.W., Ferrante, R.J., Siwek, D.F., Wilcox, H.M., Flood, D.G., Beal, M.F., Brown, R.H., Jr.*, et al.* (1996). Motor neurons in Cu/Zn superoxide dismutase-deficient mice develop normally but exhibit enhanced cell death after axonal injury. Nature genetics *13*, 43-47.

Reglodi, D., Kiss, P., Lubics, A., and Tamas, A. (2011). Review on the protective effects of PACAP in models of neurodegenerative diseases in vitro and in vivo. Current pharmaceutical design *17*, 962-972.

Rinaman, L., Milligan, C.E., and Levitt, P. (1991). Persistence of fluoro-gold following degeneration of labeled motoneurons is due to phagocytosis by microglia and macrophages. Neuroscience *44*, 765-776.

Rinke, W.J. (1976). Three major systems reviewed and evaluated. Hospitals *50*, 73-78.

Rosen, D.R., Siddique, T., Patterson, D., Figlewicz, D.A., Sapp, P., Hentati, A., Donaldson, D., Goto, J., O'Regan, J.P., Deng, H.X.*, et al.* (1993). Mutations in Cu/Zn superoxide dismutase gene are associated with familial amyotrophic lateral sclerosis. Nature *362*, 59-62.

Rowland, L.P., and Shneider, N.A. (2001). Amyotrophic lateral sclerosis. The New England journal of medicine *344*, 1688-1700.

Sahawneh, M.A., Ricart, K.C., Roberts, B.R., Bomben, V.C., Basso, M., Ye, Y., Sahawneh, J., Franco, M.C., Beckman, J.S., and Estevez, A.G. (2010). Cu,Zn-superoxide dismutase increases toxicity of mutant and zinc-deficient superoxide dismutase by enhancing protein stability. The Journal of biological chemistry *285*, 33885-33897.

Schaefer, A.M., Sanes, J.R., and Lichtman, J.W. (2005). A compensatory subpopulation of motor neurons in a mouse model of amyotrophic lateral sclerosis. The Journal of comparative neurology *490*, 209-219.

Schneider, J.S., Burgess, C., Sleiter, N.C., DonCarlos, L.L., Lydon, J.P., O'Malley, B., and Levine, J.E. (2005). Enhanced sexual behaviors and androgen receptor immunoreactivity in the male progesterone receptor knockout mouse. Endocrinology *146*, 4340-4348.

Scott, S., Kranz, J.E., Cole, J., Lincecum, J.M., Thompson, K., Kelly, N., Bostrom, A., Theodoss, J., Al-Nakhala, B.M., Vieira, F.G*., et al.* (2008). Design, power, and interpretation of studies in the standard murine model of ALS. Amyotrophic lateral sclerosis : official publication of the World Federation of Neurology Research Group on Motor Neuron Diseases *9*, 4-15.

Serpe, C.J., Byram, S.C., Sanders, V.M., and Jones, K.J. (2005). Brain-derived neurotrophic factor supports facial motoneuron survival after facial nerve transection in immunodeficient mice. Brain, behavior, and immunity *19*, 173-180.

Serpe, C.J., Coers, S., Sanders, V.M., and Jones, K.J. (2003). CD4+ T, but not CD8+ or B, lymphocytes mediate facial motoneuron survival after facial nerve transection. Brain, behavior, and immunity *17*, 393-402.

Serpe, C.J., Kohm, A.P., Huppenbauer, C.B., Sanders, V.M., and Jones, K.J. (1999). Exacerbation of facial motoneuron loss after facial nerve transection in severe combined immunodeficient (scid) mice. The Journal of neuroscience : the official journal of the Society for Neuroscience *19*, RC7.

Serpe, C.J., Sanders, V.M., and Jones, K.J. (2000). Kinetics of facial motoneuron loss following facial nerve transection in severe combined immunodeficient mice. Journal of neuroscience research *62*, 273-278.

Sharma, N., Marzo, S.J., Jones, K.J., and Foecking, E.M. (2010). Electrical stimulation and testosterone differentially enhance expression of regeneration-associated genes. Experimental neurology *223*, 183-191.

Sharp, P.S., Dick, J.R., and Greensmith, L. (2005). The effect of peripheral nerve injury on disease progression in the SOD1(G93A) mouse model of amyotrophic lateral sclerosis. Neuroscience *130*, 897-910.

Shaw, P.J. (2005). Molecular and cellular pathways of neurodegeneration in motor neurone disease. Journal of neurology, neurosurgery, and psychiatry *76*, 1046-1057.

Shaw, P.J., and Eggett, C.J. (2000). Molecular factors underlying selective vulnerability of motor neurons to neurodegeneration in amyotrophic lateral sclerosis. Journal of neurology *247 Suppl 1*, I17-27.

Shin, J.H., Cho, S.I., Lim, H.R., Lee, J.K., Lee, Y.A., Noh, J.S., Joo, I.S., Kim, K.W., and Gwag, B.J. (2007). Concurrent administration of Neu2000 and lithium produces marked improvement of motor neuron survival, motor function, and mortality in a mouse model of amyotrophic lateral sclerosis. Mol Pharmacol *71*, 965-975.

Shinohara, H. (1999). The musculature of the mouse tail is characterized by metameric arrangements of bicipital muscles. Okajimas folia anatomica Japonica *76*, 157-169.

Somogyvari-Vigh, A., and Reglodi, D. (2004). Pituitary adenylate cyclase activating polypeptide: a potential neuroprotective peptide. Current pharmaceutical design *10*, 2861-2889.

Streit, W.J. (2002). Microglia as neuroprotective, immunocompetent cells of the CNS. Glia *40*, 133-139.

Sutedja, N.A., Veldink, J.H., Fischer, K., Kromhout, H., Wokke, J.H., Huisman, M.H., Heederik, D.J., and Van den Berg, L.H. (2007). Lifetime occupation, education, smoking, and risk of ALS. Neurology *69*, 1508-1514.

Tan, Z., Levid, J., and Schreiber, S.S. (2001). Increased expression of Fas (CD95/APO-1) in adult rat brain after kainate-induced seizures. Neuroreport *12*, 1979-1982.

Tetzlaff, W., Alexander, S.W., Miller, F.D., and Bisby, M.A. (1991). Response of facial and rubrospinal neurons to axotomy: changes in mRNA expression for cytoskeletal proteins and GAP-43. The Journal of neuroscience : the official journal of the Society for Neuroscience *11*, 2528-2544.

Tetzlaff, W., Bisby, M.A., and Kreutzberg, G.W. (1988a). Changes in cytoskeletal proteins in the rat facial nucleus following axotomy. The Journal of neuroscience : the official journal of the Society for Neuroscience *8*, 3181-3189.

Tetzlaff, W., Graeber, M.B., Bisby, M.A., and Kreutzberg, G.W. (1988b). Increased glial fibrillary acidic protein synthesis in astrocytes during retrograde reaction of the rat facial nucleus. Glia *1*, 90-95.

Torvik, A., and Skjorten, F. (1971). Electron microscopic observations on nerve cell regeneration and degeneration after axon lesions. I. Changes in the nerve cell cytoplasm. Acta neuropathologica *17*, 248-264.

Traynor, B.J., Alexander, M., Corr, B., Frost, E., and Hardiman, O. (2003). An outcome study of riluzole in amyotrophic lateral sclerosis--a population-based study in Ireland, 1996-2000. Journal of neurology *250*, 473-479.

Vanderluit, J.L., McPhail, L.T., Fernandes, K.J., McBride, C.B., Huguenot, C., Roy, S., Robertson, G.S., Nicholson, D.W., and Tetzlaff, W. (2000). Caspase-3 is activated following axotomy of neonatal facial motoneurons and caspase-3 gene deletion delays axotomy-induced cell death in rodents. The European journal of neuroscience *12*, 3469-3480.

Vaudry, D., Gonzalez, B.J., Basille, M., Yon, L., Fournier, A., and Vaudry, H. (2000). Pituitary adenylate cyclase-activating polypeptide and its receptors: from structure to functions. Pharmacological reviews *52*, 269-324.

Veglianese, P., Lo Coco, D., Bao Cutrona, M., Magnoni, R., Pennacchini, D., Pozzi, B., Gowing, G., Julien, J.P., Tortarolo, M., and Bendotti, C. (2006). Activation of the p38MAPK cascade is associated with upregulation of TNF alpha receptors in the spinal motor neurons of mouse models of familial ALS. Molecular and cellular neurosciences *31*, 218-231.

Wainwright, D.A., Mesnard, N.A., Xin, J., Sanders, V.M., and Jones, K.J. (2009). Effects of facial nerve axotomy on Th2-associated and Th1-associated chemokine mRNA expression in the facial motor nucleus of wild-type and presymptomatic SOD1 mice. Journal of neurodegeneration & regeneration *2*, 39-44.

Wang, L.H., and Strittmatter, S.M. (1996). A family of rat CRMP genes is differentially expressed in the nervous system. The Journal of neuroscience : the official journal of the Society for Neuroscience *16*, 6197-6207.

Waterston, R.H., Lindblad-Toh, K., Birney, E., Rogers, J., Abril, J.F., Agarwal, P., Agarwala, R., Ainscough, R., Alexandersson, M., An, P.*, et al.* (2002). Initial sequencing and comparative analysis of the mouse genome. Nature *420*, 520-562.

Whitehouse, L.W., Wong, L.T., Paul, C.J., Pakuts, A., and Solomonraj, G. (1985). Postabsorption antidotal effects of N-acetylcysteine on acetaminophen-induced hepatotoxicity in the mouse. Canadian journal of physiology and pharmacology *63*, 431-437.

Wijesekera, L.C., and Leigh, P.N. (2009). Amyotrophic lateral sclerosis. Orphanet journal of rare diseases *4*, 3.

Xin, J., Wainwright, D.A., Mesnard, N.A., Serpe, C.J., Sanders, V.M., and Jones, K.J. (2011). IL-10 within the CNS is necessary for CD4(+) T cells to mediate neuroprotection. Brain, behavior, and immunity *25*, 820-829.

Xiong, Z.Q., and McNamara, J.O. (2002). Fas(t) balls and Lou Gehrig disease. A clue to selective vulnerability of motor neurons? Neuron *35*, 1011-1013.

Yoshihara, T., Ishigaki, S., Yamamoto, M., Liang, Y., Niwa, J., Takeuchi, H., Doyu, M., and Sobue, G. (2002). Differential expression of inflammation- and apoptosis-related genes in spinal cords of a mutant SOD1 transgenic mouse model of familial amyotrophic lateral sclerosis. Journal of neurochemistry *80*, 158-167.

Zang, D.W., Lopes, E.C., and Cheema, S.S. (2005). Loss of synaptophysin-positive boutons on lumbar motor neurons innervating the medial gastrocnemius muscle of the SOD1G93A G1H transgenic mouse model of ALS. Journal of neuroscience research *79*, 694-699.

Zhang, Q., Shi, T.J., Ji, R.R., Zhang, Y.Z., Sundler, F., Hannibal, J., Fahrenkrug, J., and Hokfelt, T. (1995). Expression of pituitary adenylate cyclase-activating polypeptide in dorsal root ganglia following axotomy: time course and coexistence. Brain research *705*, 149-158.

Zhang, Y.Z., Hannibal, J., Zhao, Q., Moller, K., Danielsen, N., Fahrenkrug, J., and Sundler, F. (1996). Pituitary adenylate cyclase activating peptide expression in the rat dorsal root ganglia: up-regulation after peripheral nerve injury. Neuroscience *74*, 1099-1110.

Zhou, X., Rodriguez, W.I., Casillas, R.A., Ma, V., Tam, J., Hu, Z., Lelievre, V., Chao, A., and Waschek, J.A. (1999). Axotomy-induced changes in pituitary adenylate cyclase activating polypeptide (PACAP) and PACAP receptor gene expression in the adult rat facial motor nucleus. Journal of neuroscience research *57*, 953-961.

Zujovic, V., Luo, D., Baker, H.V., Lopez, M.C., Miller, K.R., Streit, W.J., and Harrison, J.K. (2005). The facial motor nucleus transcriptional program in response to peripheral nerve injury identifies Hn1 as a regeneration-associated gene. Journal of neuroscience research *82*, 581-591.

VITA

Melissa Haulcomb, previously Quaka, was born in Winfield, IL on February 13, 1982 to Thomas and Debra Quaka. She received a Bachelor of Science in Psychology from Michigan State University (East Lansing, MI) in May of 2004. During the course of her undergraduate studies she was a Research Paper Finalist in 2001 at the 6th Annual Conference for Student Scholars, for a psychology research project on "The Tendency of Pet Owners to Anthropomorphize Their Dogs". She carried out an additional research project in 2003, under the guidance of John Goudreau, D.O., Ph.D., where she studied "The Effect of MPTP on Dopamine Neuronal Systems in α-Synuclein Knockout Mice". Melissa was also employed as a research assistant for the Osteopathic Medicine Department at Michigan State University. Under direction of Dr. John I. Johnson, Ph.D., she worked on several projects involving comparative analysis of mammalian brain structures and computerized mapping.

During the years 2004 – 2006, Melissa worked as an analytical chemist for Pfizer, Inc., (Kalamazoo, MI) validating compounds for use in pharmaceutical manufacturing. Melissa also worked as a clinical research scientist at BioSafe Laboratories, Inc., (Chicago, IL) where she led a research team to develop novel testing protocols employing clinical chemistry instrumentation for analysis of human whole blood samples. In August of 2006, Melissa joined the Neuroscience Program at Loyola

University Medical Center (Maywood, IL). She became a member the laboratory of Dr. Kathryn J. Jones in August of 2008, where she studied motoneuron survival after facial nerve injury in a mouse model of Amyotrophic lateral sclerosis (ALS). Melissa's research has been presented at the Society for Neuroscience meetings (2009, 2010, 2011), and at the Experimental Biology meetings (2009, 2010, 2011). Melissa was the recipient of three travel awards to attend the Experimental Biology meetings.

During Melissa's undergraduate career, she was a teaching assistant in the Radiology Department's Division of Human Anatomy's Advanced Neuroanatomy course (2003) at Michigan State University. Melissa has also been a teaching assistant in the Stritch School of Medicine's Medical Neuroscience course (2008) at Loyola University Chicago. In addition, Melissa has lectured on the neurobiology portion for the Department of Oral Biology's Molecular Cell Biology course (2011) at Indiana University's School of Dentistry.

After completing her Ph.D., Melissa will remain in the laboratory of Dr. Kathryn J. Jones and continue her research as a post-doctoral appointee at Indiana University School of Medicine (Indianapolis, IN).